

Artificial Intelligence for Solar Photovoltaic Systems

Approaches, Methodologies,
and Technologies

EXPLAINABLE AI (XAI) FOR ENGINEERING APPLICATIONS



Edited by
Bhavnesk Kumar
Bhanu Pratap
Vivek Shrivastava

VISIT...

LANZAROTE
Caliente.COM

Artificial Intelligence for Solar Photovoltaic Systems

This book provides a clear explanation of how to apply artificial intelligence (AI) to solve the challenges in solar photovoltaic technology. It introduces readers to new AI-based approaches and technologies that help manage and operate solar photovoltaic systems effectively. It also motivates readers to find new AI-based solutions for these challenges by providing a comprehensive collection of findings on AI techniques.

It covers important topics including solar irradiance variability, solar power forecasting, solar irradiance forecasting, maximum power point tracking, hybrid algorithms, swarm optimization, evolutionary optimization, sensor-based sun-tracking systems, single-axis and dual-axis sun-tracking systems, smart metering, frequency regulation using AI, emerging multilevel inverter topologies, and voltage and reactive power control using AI.

This book is useful for senior undergraduate students, graduate students, and academic researchers in areas such as electrical engineering, electronics and communication engineering, computer science, and renewable energy.

Explainable AI (XAI) for Engineering Applications

Series Editors:

Aditya Khamparia and Deepak Gupta

Explainable AI (XAI) has developed as a subfield of Artificial Intelligence (AI), focusing on exposing complex AI models to humans in a systematic and interpretable manner. This area explores and discusses the steps and models involved in making intelligent decisions. This series covers the working behavior and explains the ability of powerful algorithms such as neural networks, ensemble methods including random forests, and other similar algorithms to sacrifice transparency and explainability for power, performance, and accuracy in different engineering applications related to the real world. Aimed at graduate students, academic researchers, and professionals, the proposed series will focus on key topics including XAI techniques for engineering applications, XAI for deep neural network predictions, XAI for machine learning predictions, XAI-driven recommendation systems for Automobile and Manufacturing Industries, and XAI for Autonomous Vehicles.

Deep Learning in Gaming and Animations: Principles and Applications

Vikas Chaudhary, Moolchand Sharma, Prerna Sharma, and Deevyankar Agarwal

Artificial Intelligence for Solar Photovoltaic Systems: Approaches,
Methodologies, and Technologies

Bhavnes Kumar, Bhanu Pratap, and Vivek Shrivastava

For more information about this series, please visit: <https://www.routledge.com/Explainable-AI-XAI-for-Engineering-Applications/book-series/CRCEAIFEA>

Artificial Intelligence for Solar Photovoltaic Systems

Approaches, Methodologies, and Technologies

Edited by
Bhavnesk Kumar, Bhanu Pratap,
and Vivek Shrivastava



CRC Press

Taylor & Francis Group

Boca Raton London New York

CRC Press is an imprint of the
Taylor & Francis Group, an **informa** business

MATLAB® and Simulink® are trademarks of The MathWorks, Inc. and are used with permission. The MathWorks does not warrant the accuracy of the text or exercises in this book. This book's use or discussion of MATLAB® and Simulink® software or related products does not constitute endorsement or sponsorship by The MathWorks of a particular pedagogical approach or particular use of the MATLAB® and Simulink® software.

First edition published 2023

by CRC Press

6000 Broken Sound Parkway NW, Suite 300, Boca Raton, FL 33487-2742

and by CRC Press

4 Park Square, Milton Park, Abingdon, Oxon, OX14 4RN

CRC Press is an imprint of Taylor & Francis Group, LLC

© 2023 selection and editorial matter, Bhavnesh Kumar, Bhanu Pratap and Vivek Shrivastava; individual chapters, the contributors

Reasonable efforts have been made to publish reliable data and information, but the author and publisher cannot assume responsibility for the validity of all materials or the consequences of their use. The authors and publishers have attempted to trace the copyright holders of all material reproduced in this publication and apologize to copyright holders if permission to publish in this form has not been obtained. If any copyright material has not been acknowledged please write and let us know so we may rectify in any future reprint.

Except as permitted under U.S. Copyright Law, no part of this book may be reprinted, reproduced, transmitted, or utilized in any form by any electronic, mechanical, or other means, now known or hereafter invented, including photocopying, microfilming, and recording, or in any information storage or retrieval system, without written permission from the publishers.

For permission to photocopy or use material electronically from this work, access www.copyright.com or contact the Copyright Clearance Center, Inc. (CCC), 222 Rosewood Drive, Danvers, MA 01923, 978-750-8400. For works that are not available on CCC please contact mpkbookspermissions@tandf.co.uk

Trademark notice: Product or corporate names may be trademarks or registered trademarks and are used only for identification and explanation without intent to infringe.

ISBN: 978-1-032-05441-4 (hbk)

ISBN: 978-1-032-11947-2 (pbk)

ISBN: 978-1-003-22228-6 (ebk)

DOI: 10.1201/9781003222286

Typeset in Palatino

by codeMantra

I would like to dedicate this book to my father, Mr. Kali Charan Singh, my mother, Mrs. Chameli Devi, my family members including my wife Mrs. Rajrani, my daughter Aradhya Kumar, and my son Parikshit Kumar for their constant support and motivation. I would also like to specially thank the publisher and the other coeditors for having faith in my abilities. Before all and after all, a man should always thank the Almighty.

Dr. Bhavnesh Kumar

I would like to dedicate this book to my parents and my family members for their constant support and motivation. No words can adequately express my gratitude to my friends whose unflinching support, constant encouragement, and thoughtfulness have been a stable source of strength and upliftment. I would also like to give my special thanks to the publisher and my other coeditors for having faith in my abilities. Any comments/suggestions/criticisms toward the eminence enhancement of the book are most welcome.

Dr. Bhanu Pratap

I would like to dedicate this book to God Almighty and my creator, my strong pillar, my source of inspiration, wisdom, knowledge, my understanding parents, Dr. Awadh Bihari Shrivastava and Mrs. Snehlata Shrivastava. I also dedicate this work to my loving wife, Mrs. Radha Shrivastava, who has encouraged me all the way and whose encouragement has made sure that I give it all it takes to finish what I have started. Thanks to my children Tejas (Yash) and Tanay (Madhav) who have been affected in every way possible by this quest. This work could not have been completed without the tremendous efforts of coeditor Dr. Bhavnesh Kumar and Dr. Bhanu Pratap. I also like to give my special thanks to the publisher.

Dr. Vivek Shrivastava

Contents

Preface.....	ix
About the Book.....	xi
Editors.....	xiii
Contributors.....	xvii
1. History and Application of Solar PV System	1
<i>Vinaya Rana, Arjun Tyagi, Krishan Kumar, and Himanshu Grover</i>	
2. Solar Power Forecasting.....	23
<i>Agrim Khurana, Ankit Dabas, Vaibhav Dhand, Rahul Kumar, Bhavnesh Kumar, and Arjun Tyagi</i>	
3. Comprehensive Technique for Modeling of PV Module	43
<i>Vandana Jha</i>	
4. Conventional Techniques for Maximum Power Point Tracking	79
<i>Shilpi Yadav, Kamlesh K. Bharti, Vijay Kumar Tewari, Santosh Kumar Tripathi, and Rajesh Kumar</i>	
5. Intelligent Techniques for Maximum Power Point Tracking.....	105
<i>Dilip Yadav and Nidhi Singh</i>	
6. Analysis of Multijunction Solar Cell-Based PV System with MPPT Schemes	129
<i>Omveer Singh and Mukul Singh</i>	
7. Emerging Techniques of Shade Dispersion.....	159
<i>Md. Faizan Nomani, Bhavnesh Kumar, and Bhanu Pratap</i>	
8. Solar Tracking Technology to Harness the Green Energy.....	189
<i>Ram Krishan, K. Anil Naik, and R. David Amar Raj</i>	
9. Development of Solar Panel Models in Different Countries/Regions.....	213
<i>Isa S. Qamber</i>	
10. Performance Degradation in Solar Modules	231
<i>Shabbir S. Bohra</i>	

**11. Performance and Reliability Investigation of Practical
Microgrid with Photovoltaic Units 255**
*Burhan U Din Abdullah, Shiva Pujan Jaiswal, Suman Lata,
Suman Dulal, and Vivek Shrivastava*

Index 289

Preface

Harvesting energy worldwide on the scale of economic and sustainability is a challenging task. In the current circumstances, solar energy is acting as a vital role, being the fastest-growing energy source in the world. Economic sustainability for a long period is still to be accomplished. This requires improving significant technical and economic practices to reduce the cost of solar energy with its efficient performance. The objective of this book is to present the newest development in the field of artificial intelligence applications to solar photovoltaic systems and to stimulate further research. Another objective of this book is to overpass the research gap between the available literature and recent research. The book is especially useful as it combines hard-to-find industrial knowledge of solar photovoltaic systems modeling and design in a summarizing document from the viewpoint of the researcher/engineer. The solar system design standards and the simulation results included in this book will be crucial to anyone entering the industry. The design and MPPT control portion of the book guides the reader through new approaches and reliable ideas successfully.

This book *Artificial Intelligence for Solar Photovoltaic Systems: Approaches, Methodologies, and Technologies* consists of eleven chapters. The major contributions of this book are (1) solar power forecasting, (2) modeling of the solar system, (3) maximum power point tracking with conventional and intelligent techniques, (4) shade dispersion, (5) harness of the green energy, (6) solar panels development, (7) integration of solar with microgrid, etc.

Today's modern world is currently under a significant influence on innovative technologies such as Artificial Intelligence, Deep Learning, Machine Learning, and IoT. This book aims to present the various approaches, techniques, and applications that are available in the field of gaming and animations. It is a valuable source of knowledge for researchers, engineers, practitioners, and graduate and doctoral students working in the same field. It will also be helpful for faculty members of graduate schools and universities.

We would also like to thank the authors of the published chapters for adhering to the schedule and incorporating the review comments. We wish to extend our heartfelt acknowledgment to the authors, peer-reviewers, committee members, and production staff whose diligent work shaped this volume. We especially want to thank our dedicated team of peer-reviewers who volunteered for the arduous and tedious step of quality checking and critique on the submitted chapters.

**Editor(s): Bhavnesh Kumar
Bhanu Pratap
Vivek Shrivastava**

MATLAB® is a registered trademark of The MathWorks, Inc. For product information, Please contact:

The MathWorks, Inc.

3 Apple Hill Drive

Natick, MA 01760-2098 USA

Tel: 508-647-7000

Fax: 508-647-7001

E-mail: info@mathworks.com

Web: www.mathworks.com

About the Book

Solar photovoltaic technology is now considered to be a prominent energy generation source from the future perspective. It is well known that deteriorating environmental conditions are adversely affecting human lives. Therefore, alternate energy sources with clean energy conversion are a need of time. Recently, artificial intelligence (AI) techniques have also been applied in the field of solar photovoltaic to address the issues related to solar forecasting, power extraction, system optimization, sun-tracking systems, etc.

This book makes an enormous contribution to this beautiful, vibrant area of study: an area that is developing rapidly in both breadth and depth. This book lays a good foundation for the core concepts and principles of applying AI techniques to solar photovoltaic systems, walking the reader through the fundamental ideas with expert ease. The book progresses on the topics in a step-by-step manner. It reinforces theory with a full-fledged pedagogy designed to enhance students' understanding and offer them a practical insight into its applications. Also, some chapters introduce and cover novel ideas about how AI has changed the world in the renewable energy sector.

It gives us the motivation that AI can also be applied in solar photovoltaics, and there are limited textbooks in this area. This book comprehensively addressed all the aspects of solar photovoltaic systems. Also, each chapter follows a similar structure so that students, teachers, and industry experts can orientate themselves within the text. Our book teaches you how to apply the power of AI to build an efficient solar photovoltaic system. After exposing the readers to the foundations of solar photovoltaic, program codes written in Python/MATLAB[®] software are presented. We also focus on how different meteorological, geographical, and operating conditions affect the performance of solar photovoltaic systems. Multiple illustrations are presented to give a clear understanding of the processes.

Editors



Dr. Bhavnesh Kumar is an assistant professor in the area of power electronics and drives at the Division of Instrumentation & Control Engineering, NSIT Delhi. He holds a Bachelor of Technology degree in Electrical & Electronics Engineering from Uttar Pradesh Technical University, Lucknow, and a Master of Technology degree in Control & Instrumentation from Motilal Nehru National Institute of Technology, Allahabad. He holds a Ph.D. from Gautam Buddha University, Greater

Noida in the area of artificial intelligent controllers for induction motor drives. With a teaching experience of more than ten years, he had served GBU, Greater Noida, Airports Authority of India, KNGD Modi Engineering College, Modinagar. He has published various research papers in journals and conferences. He has presented his research work at many international conferences. He is a member of various professional bodies such as the Institute of Electrical and Electronics Engineers (IEEE) and International Association of Computer Science and Information Technology (IACSIT).



Dr. Bhanu Pratap has more than 10 years of experience in teaching and research. Presently, he is working as an assistant professor in the Department of Electrical Engineering, National Institute of Technology Kurukshetra, India. Before his academic assignments, he has worked as senior research fellow under the project funded by the Department of Science & Technology, Govt. of India, New Delhi at Motilal Nehru National Institute of Technology Allahabad, India. He has also worked at the National Institute of Technology Silchar, India. Dr. Pratap has extensive experience in academics and assignments such

as Warden of hostel and prof.-in-charge of various Laboratories at NIT Kurukshetra. Also, he has initiated the development of an Advanced Control Systems Laboratory at the National Institute of Technology Kurukshetra. He has published over 50 papers in various journals/conferences and book chapters. He has supervised one Ph.D. thesis and 16 M.Tech. dissertations,

and currently supervising four Ph.D. theses and four M.Tech. dissertations. Also, he is serving as the principal investigator of an R&D project funded by the Indian Navy. His research interests are in the areas of intelligent control of nonlinear systems, robust and adaptive control, control of renewable energy systems, and control of hybrid electric vehicles.



Dr. Vivek Shrivastava has more than 18 years of diversified experience in the scholarship of teaching and learning, accreditation, research, industrial, and academic leadership in India, China, and United States. Presently, he is holding the position of dean (Research & Consultancy) at the National Institute of Technology Delhi. Previously, he has worked as an associate professor in the Department of Electrical Engineering at Rajasthan Technical University Kota, associate professor at NIT Delhi, assistant professor at Gautam Buddha

University Greater Noida, UP India. Prior to his academic assignments, he has worked as system reliability engineer at SanDisk Semiconductors in Shanghai, China, and United States.

Dr. Shrivastava has significant industrial experience of collaborating with industry and governmental organizations. At SanDisk Semiconductors, he has made a significant contribution to the design and development of memory products. At GBU Greater Noida, he has contributed to the development and delivery of the Five-Year Integrated B. Tech–M. Tech Program (Electrical Engineering) and Master's Program (Power Systems). He has extensive experience in academic administration in the various capacity of dean (Research & Consultancy), dean (Student Welfare), faculty-in-charge (Training & Placement), faculty-in-charge (Library), nodal officer (Academics, TEQIP-III), nodal officer RUSA, Experts in various committees in AICTE, UGC, etc. Dr. Shrivastava has carried out research and consultancy, and attracted significant funding projects from the Ministry of Human Resources & Development, Government of India, and Board of Research in Nuclear Sciences (BRNS) subsidiary organization of Bhabha Atomic Research Organization.

Dr. Shrivastava has published over 80 journal articles, presented papers at conferences, and published several chapters in books. He has supervised 4 Ph.D. and 14 Master's students, and is currently supervising several Ph.D. students. His diversified research interests are in the areas of reliability engineering, renewable energy, and conventional power systems which include wind, photovoltaics (PV), hybrid power systems, distributed generation, grid integration of renewable energy, power systems analysis, and smart grid.

Dr. Shrivastava is an editor/associate editor of the journals *International Journal of Swarm Intelligence (IJSI)* and *International Journal of System Assurance Engineering and Management*. He is a fellow of the Institution of Engineers (India) and a senior member of the Institute of Electrical and Electronics Engineers (IEEE). Presently, he is also a member of the Board of Governors NIT Delhi and AICTE nominee in BoG of Engineering College Bikaner.

Contributors

Burhan U din Abdullah

Electrical Engineering Department
Sharda University
Greater Noida, India

K. Anil Naik

Electrical Engineering Department
National Institute of Technology
Warangal
Telangana, India

Kamlesh K. Bharti

Rajkiya Engineering College
Kannauj, India

Shabbir S. Bohra

Sarvajanik College of Engineering &
Technology
Sarvajanik University
Surat, India

Ankit Dabas

Instrumentation & Control
Engineering Department
Netaji Subhas University of
Technology
Delhi, India

R. David Amar Raj

Electrical Engineering Department
National Institute of Technology
Warangal
Warangal, India

Vaibhav Dhand

Instrumentation & Control
Engineering Department
Netaji Subhas University of
Technology Delhi
New Delhi, India

Suman Dulal

Electrical Engineering Department
Sharda University
Greater Noida, India

Himanshu Grover

Department of Energy Science and
Engineering
Indian Institute of Technology Delhi
New Delhi, India

Shiva Pujan Jaiswal

Electrical Engineering Department
Sharda University
Greater Noida, India

Vandana Jha

CV Raman Global University
Bhubaneswar, India

Agrim Khurana

Instrumentation & Control
Engineering Department
Netaji Subhas University of
Technology
Delhi, India

Ram Krishan

Electrical Engineering Department
National Institute of Technology
Warangal
Warangal, India

Krishan Kumar

Department of Electrical Engineering
Gautam Buddha University
Greater Noida, India

Rahul Kumar

Instrumentation & Control
Engineering Department
Netaji Subhas University of
Technology Delhi
New Delhi, India

Rajesh Kumar

Rajkiya Engineering College
Kannauj, India

Suman Lata

Electrical Engineering Department
Sharda University
Greater Noida, India

Md. Faizan Nomani

Instrumentation & Control
Engineering Department
Netaji Subhas University of
Technology
Delhi, India

Isa S. Qamber

Department of Electrical and
Electronics Engineering
University of Bahrain
Isa Town, Kingdom of Bahrain

Vinaya Rana

Department of Electrical Engineering
Gautam Buddha University
Greater Noida, India

Mukul Singh

Department of Electrical Engineering
Gautam Buddha University
Greater Noida, India

Nidhi Singh

Department of Electrical Engineering
Gautam Buddha University
Greater Noida, India

Omveer Singh

Department of Electrical Engineering
Gautam Buddha University
Greater Noida, India

Vijay Kumar Tewari

Rajkiya Engineering College
Kannauj, India

Santosh Kumar Tripathi

Rajkiya Engineering College
Kannauj, India

Arjun Tyagi

Department of Electrical Engineering
Netaji Subhas University of Technology
Delhi, India

Dilip Yadav

Department of Electrical Engineering
Gautam Buddha University
Greater Noida, India

Shilpi Yadav

Rajkiya Engineering College
Kannauj, India

1

History and Application of Solar PV System

Vinaya Rana

Gautam Buddha University

Arjun Tyagi

Netaji Subhas University of Technology

Krishan Kumar

Gautam Buddha University

Himanshu Grover

Indian Institute of Delhi

CONTENTS

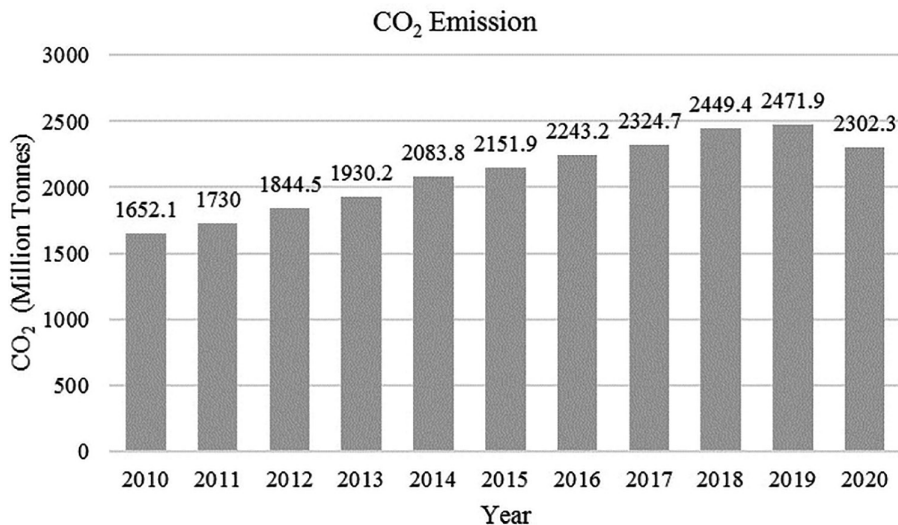
1.1	Introduction: Solar PV System	2
1.2	Historical Background of Solar Cell.....	5
1.2.1	Historical Development of Solar PV System in India.....	10
1.3	Application of Solar Energy	11
1.3.1	Residential Application.....	11
1.3.2	Industrial Application.....	11
1.3.3	Transportation.....	11
1.3.4	Solar Water Heating	12
1.3.5	Solar Desalination.....	12
1.3.6	Solar Cooking.....	13
1.3.7	Solar Energy of Industry Process/Heating.....	14
1.3.8	Solar Pumps for Agriculture.....	14
1.3.9	Some Recent Advance Application	15
1.3.9.1	Solar Energy in Electric Vehicle.....	15
1.3.9.2	Solar-Powered Airplanes and Railways	15
1.3.9.3	Solar Energy used in Space Applications.....	16
1.4	Basic Components of Solar PV System	16
1.4.1	Solar Panels.....	16
1.4.2	Controller	17
1.4.3	Solar Performance Monitoring Equipment.....	17
1.4.4	Solar Storage.....	17

1.4.5	Solar Inverter	17
1.4.6	AC and DC Distribution	18
1.4.7	Mounting Support	18
References.....		18

1.1 Introduction: Solar PV System

Energy is an essential part of our lives and is used in various fields such as agricultural land, transportation, domestic, and industrial applications. It is found in various forms such as electrical, nuclear, heat, light, and chemical energy (Panwar, Kaushik, and Kothari 2011). Coal, gas, and petrol are the main sources of energy in the early stages of industrialization. The electricity demand is increasing expeditiously due to industrialization and modernization. With the rising demand for electricity, it is necessary to increase the generation capacity to meet the increasing demand. Fossil fuel-based conventional energy sources are used to generate electricity, but they lead to environmental impacts like rise in pollution and climatic change. Therefore, alternative energy sources are used to meet the increasing demand for energy with less environmental impact (Dincer 1998). Renewable energy (RE) sources (RESs) are becoming more popular nowadays due to the usage of limited fossil fuels and being more eco-friendly (Basit et al. 2020). The RESs produce energy from natural sources that replace themselves again in a short period. These sources incorporate solar, wind, biogas, geothermal, small hydro and tidal energy, etc. The key advantages of RESs are that they are freely available, pollution free, inexhaustible, and can be used for electricity generation and for other applications as well as for air and water heating (Hayat et al. 2019). According to the information available from Carbon Dioxide Information Analysis (CDIAC), India, the idea of using RESs is to reduce the level of CO₂ and increase the value of the life of mankind (Prasad et al. 2020). India ranks 3rd (7.2%) in CO₂ emissions worldwide (BP plc. 2021). The growth of CO₂ emission in India is shown in Figure 1.1.

Since RESs are environmentally friendly, utilization of RE-based sources tends to make the system more useful and efficient. Keeping in concern the benefits in the integration of RESs, the Government of India and various other private sector companies are showing great interest by participating in this sector (Sharma, Tyagi, and Rana 2019). The total energy generated from RESs is 95656.25 MW, i.e., 24.95% of the total installed energy as of 31 May 2021 (CEA 2021). In recent years, solar energy has been considered one of the major RESs for power generation. Solar energy is a huge and freely available resource in India, which covers 43% of total RE generation (CEA 2021). It has a major impact on power generation, including alternative resources, due to the relationship between energy and the Sun and its major links with environmental and sustainability-related problems. The Sun is the ultimate

**FIGURE 1.1**CO₂ emission of India.

source of energy and mainly consists of direct and diffused radiations, which can be utilized by solar thermal and solar photovoltaics (PVs). The photosynthetic process is the root in the development of all fossil fuels such as coal, gas, wood, and oil (A. Kumar et al. 2010). Wind energy and tidal energy are also indirectly produced by solar energy due to variations in atmospheric temperature. Solar PV system, wind energy, biogas, etc. are used as alternative energy sources that are renewable in nature and have no harmful effect on the environment. India's total energy production and total RE production (CEA 2021) are shown in Figures 1.2 and 1.3, respectively.

Solar energy is the most increasing RES because of its various advantages such as pollution free, low maintenance, long lifespan, low cost, no moving part, direct electricity conversion, etc. Hence, such a source is very reliable and congenial to use. Solar photon energy or Sun radiation is converted into electrical energy with the help of PV cell, which is a photosensitive p-n semiconductor junction. PV cells use semiconductor materials for the conversion of sunlight into electricity (Rakesh Tej Kumar, Ramakrishna, and Durga Sukumar 2018). Silicon (Si) is available more abundantly on the earth and is used as a semiconductor material for PV cells. Most of the PV modules use Si-wafer-based semiconductors for power generation. "Si" can be used as Si wafer or thin film for PV cells. When sunlight strikes over the surface of the PV cell, electron and hole pairs are generated. As a result, the positive and negative charges are accumulated across the p-n junction, which causes the potential difference across the junction. Mainly three types of solar cell technologies, viz. thin film/amorphous, polycrystalline, and multicrystalline (Pal et al. 2021), are used and shown in Figure 1.4.

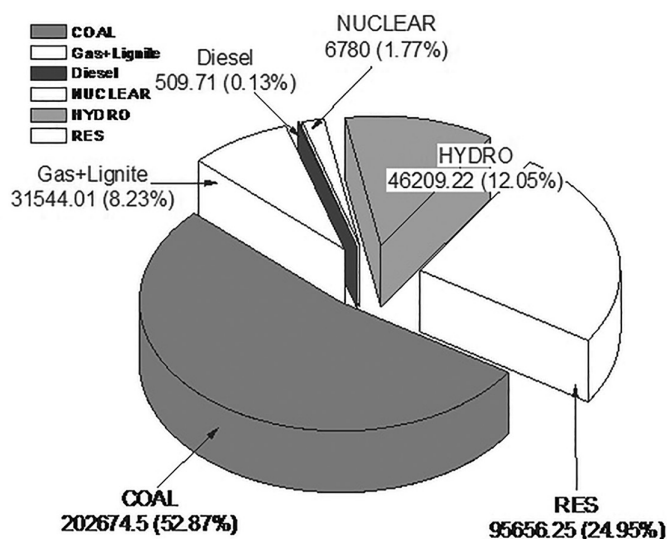


FIGURE 1.2

Total installed energy.

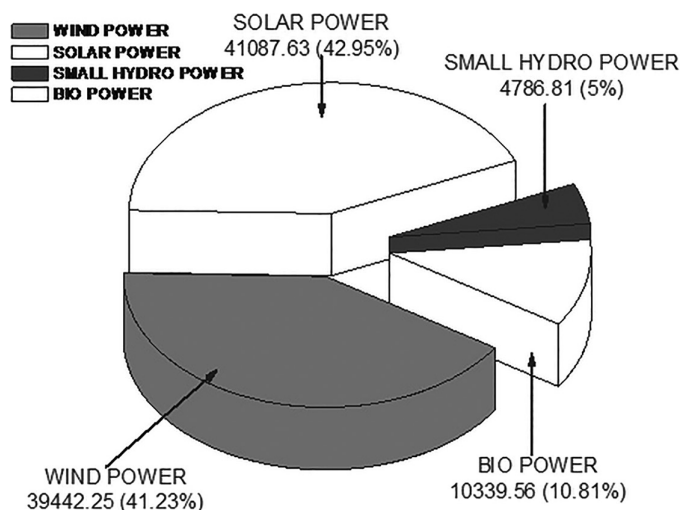
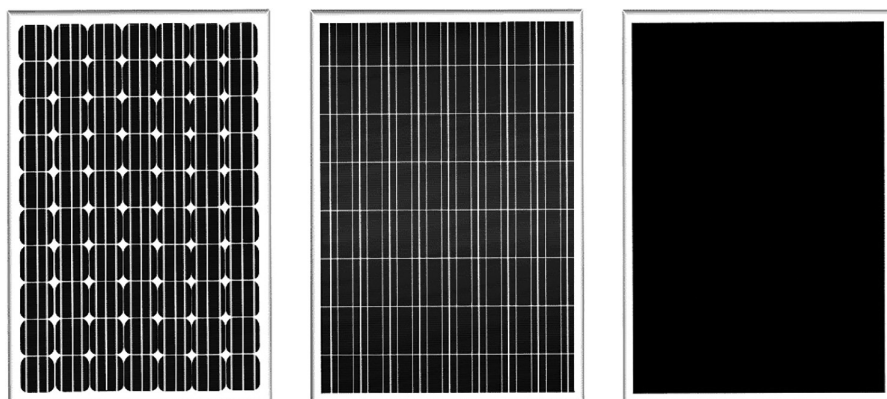


FIGURE 1.3

Total installed RE.

Solar energy may be transformed into different forms of energy like electrical energy, thermal energy, or chemical energy. The demand for electricity is rising day by day, and fossil fuels are depleting. It cannot be replenished in human life span, so the RE-based sources play an important role to fulfill the energy demand (Hayat et al. 2019). The PV-based RE system is more

**FIGURE 1.4**

Types of solar PV system.

commonly used with various advantages. The PV output depends on the irradiation level and other environmental conditions such as temperature, shading, and dust, etc. In the shading condition, the irradiation level is uneven over the surface of the panel, and a hotspot is created in the panel; this problem can be addressed using a bypass diode. The solar cell efficiency is very less, because of the effects of some environmental factors like shading effects and cloudy condition, etc. Different maximum power point tracking (MPPT) methods are considered to track the maximum power and efficiency (Rana, Ansari, and Chauhan 2020). Solar PV panel efficiency is dependent on solar irradiation level and atmospheric temperature. As the irradiation level is decreased, the efficiency is also decreased, and if the irradiation level is increased, then the temperature of the panel is also increased, which reduces the efficiency (B. Kumar, Chauhan, and Shrivastava 2014). So, the irradiation level should be within the permissible limit for maximum efficiency. The different types of shading are also reducing the radiation level on the surface of the panel, i.e., the overall efficiency of the panel is decreased (K. Kumar, Ansari, Varshney, et al. 2018). The temperature of the PV panel should minimize for high power generation. So, the cooling methods are applied to the panel surface to minimize the temperature effect, and then the PV panel can operate on the maximum power and efficiency.

1.2 Historical Background of Solar Cell

The PV effect has a long history. The era of the development of the first phase of electricity from sunlight through the PV effect was described from 1839 to 1904 (Akinyele, Rayudu, and Nair 2015).

The first PV effect was observed in 1839 by A.E. Becquerel, when a current was passed through an electrode immersed in a conductive solution when sunlight was illuminated (Spanggaard and Krebs 2004). Later, the PV effect in selenium was discovered by W. Smith, W.G. Adams, and R.E. Day in the late 1870s (Adams and Day 1877). The first amorphous selenium-based PV cell with a thin gold film was made in 1883 by C. Fritts, although the efficiency of the cell developed was less than 1% (Pallavolu et al. 2020). The second phase of development of the PV cell was described between 1905 and 1950 with some improvements and operational features.

In 1905, the PV effect based on quantum theory was published in a research paper by A. Einstein (Pais 1979). In 1918, Jan Czochralski developed a single crystal on the metal (Tomaszewski 2002). Later, this method was used for the growth of single-crystal silicon (Si). The band theory based on single crystals was introduced in 1928 by F. Bloch (Hoddeson, Baym, and Eckert 1987). In 1931, the high purity semiconductor theory was developed. It was proposed and developed by A.H. Wilson (G. Pearson and Brattain 1955). In 1948, a single-crystalline germanium was developed by G. Teal and John based on the Czochralski invention (Uecker 2014). A single-crystalline silicon was also developed later. The development of the first and second stages of PV cells is summarized in Table 1.1.

The third stage of PV cell development was from 1950 to 1959. In 1950, the solar cell was developed for space at Bell Laboratories (Green et al. 1999). In 1953, research on lithium-silicon PV cells was carried out by G. Pearson (Malhotra and Singh 2020). History was made in 1954 by manufacturing single-crystal PV cells with 6% efficiency at Bell Laboratories (Goetzberger and Hebling 2000). In 1955, the first commercial solar cell was introduced by Hoffman Electronics semiconductor division having 2% efficiency (Shah et al. 2004). G. Pearson, D.M. Chapin, and C.S. Fuller received patent on a solar energy converting apparatus in 1957 (G. L. Pearson, Chapin, and Fuller 1957). Hoffman Electronics also developed another solar cell with 8% efficiency.

TABLE 1.1
Summary of First- and Second-Stage Development of PV Cell

S. No.	Year	Scientist Name	Innovation/Development
1	1839	A. E. Becquerel	When illuminated, current passes through an electrode immersed in a conductive solution
2	1870	W. Smith, W.G. Adams & R.E. Day	PV effect in selenium
3	1883	C. Fritts	Amorphous selenium-based PV cell
4	1905	A. Einstein	PV effect based on quantum theory
5	1918	J. Czochralski	Development of a single crystal on the metal
6	1928	F. Bloch	Single crystals-based band theory
7	1931	A. H. Wilson	Development of high purity semiconductor theory
8	1948	G. Teal & John	Single-crystalline germanium (Ge) and silicon (Si)

In 1958, T. Mandelkorn developed n–p silicon solar cells suitable for space applications. Hoffman Electronics also developed another solar cell with 9% efficiency (Miles, Hynes, and Forbes 2005). The first solar-based satellite was launched by Vanguard I in 1958 (Joshi, Dincer, and Reddy 2009). The first grid contact and low cell resistance-based commercial solar cell with 10% efficiency was developed by Hoffman Electronics in 1959 (Loferski 1993). The summary of the third stage of PV cell is shown in Table 1.2.

The development of the fourth phase in the solar PV cell took place from 1960 to 1979. This development was also of great importance for the solar industries and space applications. Solar PV cell was developed by Hoffman Electronics in 1960 with 14% efficiency (Petrova-Koch 2009). In 1961, the first introductory conference on solar energy for the developing world was held at the United Nations. History was made in 1962 with the launch of the first Telstar communication satellite based on solar power (Bray 1995). In 1963, a PV array of 242 W was installed at a lighthouse in Japan (Miles, Hynes, and Forbes 2005) which was the world's largest PV array at that time. The spacecraft Nimbus was launched by NASA in 1964 (Bray 1995). Soyuz 1, the first solar PV cell-based manned spacecraft, was launched in 1967. In 1970, Gallium arsenide (GaAs)-based solar PV cells were made in the USSR by Z. Alferov.

The world's first space station, named Salyut 1, was launched in 1971 by the USSR powered by solar PV cells (Vallerani 1988). In 1972, J.M. Woodall and H.J. Hovel developed GaAlAs-based, heterojunction-based solar PV cells with 16%–20% depending on air mass values (Kressel 1981). The Skylab space station developed by NASA was powered by solar PV cells launched in 1973 (Kaplan 1983). The first amorphous Si-based PV cells were developed in 1976 by D. Carlson and C. Wronski with an efficiency of 2.4% (Carlson and Wronski 1976). For research and development, the Solar Energy Research Institute was first established in 1977 in Colorado, United States. The first solar calculator based on amorphous Si PV cells was developed in 1978 (Kuwano and Ohnishi 1981). A 3.5kW PV system installed in Southern Arizona was used between

TABLE 1.2

Summary of Third Phase (1950–1959) Development of PV Cell

S. No.	Year	Scientist Name/Lab/ Event	Innovation/Development
1	1950	Bell Lab	Solar cells for space
2	1953	G. Pearson	Lithium-silicon PV cells
3	1954	Bell Lab	Single-crystal PV cells with 6% efficiency
4	1955	Hoffman Electronics	First commercial solar cell with 2% efficiency
5	1957	G. Pearson, D.M. Chapin & C.S. Fuller Hoffman Electronics	Patent on a solar energy converting apparatus Solar cell with 8% efficiency
6	1958	T. Mandelkorn Hoffman Electronics Vanguard I	Developed n-p silicon solar cells for space application Solar cell with 8% efficiency First solar-based satellite
7	1959	Hoffman Electronics	Commercial solar cell with 10% efficiency

1978 and 1983 to electrify and pump water for a village (Ramakumar et al. 1993). The PV cell developments of the fourth stage are summarized in Table 1.3.

The next step in the development of solar PV systems has a greater impact on power generation through RESs, especially PV systems. The time frame for the development of the 5th phase was from 1980 to 1999. The first thin-film solar cell was developed in 1980 at the University of Delaware (Bragagnolo et al. 1980). In 1981, the mass production of bifacial PV cells was done in Isofoton based on the development by A. Luque and his team in Madrid (Edmonds 1990). The first Fresnel lens-based concentrating PV system was in operation in 1981 with a joint venture between the US and Saudi Arabia. The worldwide total energy generation through the solar PV system reached 21.3 MW in 1983. Silicon cells were developed in 1985 by the Centre for Photovoltaic Engineering at the University of New South Wales with the efficiency of 20% (Green 1987). The reflector was used with solar cells for efficiency improvement in 1989.

In 1991, the Solar Energy Research Institute was renamed the National Renewable Energy Laboratory (NERL) on the instructions of President George H.W. Bush. Thin-film PV cells were developed at the University of South

TABLE 1.3

Summary of Fourth-Phase (1960–1979) Development of PV Cell

S. No.	Year	Scientist Name/Lab/ Event	Innovation/Development
1	1960	Hoffman Electronics	PV cell with 14% efficiency
2	1961	Conference	Solar energy in the developing world at the United Nations
3	1962	Communication Satellite	First Telstar communication satellite based on solar power was launched
4	1963	PV Installation in Japan	242 W PV array was installed at a lighthouse in Japan
5	1964	Nimbus	The spacecraft Nimbus was launched by NASA
6	1967	Soyuz	First solar PV cell-based manned spacecraft was launched
7	1970	Z. Alferov	GaAs-based solar PV cells were developed
8	1971	Salyut	The world's first space station was launched
9	1972	J.M. Woodall & H.J. Hovel	GaAlAs-based heterojunction-based solar PV cells were developed
10	1973	Skylab	Skylab space station developed by NASA was launched based on solar power
11	1976	D. Carlson & C. Wronski	The first amorphous Si-based PV cells were developed with an efficiency of 2.4%.
12	1977	Research Institute, Colorado	First Solar Energy Research Institute was established
13	1978	Solar Calculator	The first solar calculator based on amorphous Si PV cell was developed
14	1978	World's first PV village	3.5 kW was used for electrification and water pumping between 1978 and 1983

Florida in 1992 with 15.9% efficiency made from cadmium telluride (CdTe) (Kazmerski, Emery, and DeBlasio 1994). NERL has developed various material solar PV cells, i.e., InGaP and GaAs, the first solar cell with monolithic junction having conversion efficiency of more than 30% in 1994 (Takamoto et al. 1994). The worldwide solar energy reached 1,000 MW in 1999. The summary of the fifth-phase development of solar PV cell is shown in Table 1.4.

The development of the sixth phase is an important factor for various reforms in the field of solar energy era. The time frame for the sixth phase is between 2000 and 2021. Polysilicon was first used to manufacture PV cells in 2006. In the same year, the newly developed solar cell was found to be 40% more efficient than conventional PV cells (Tyagi, Kaushik, and Tyagi 2012). In 2007, a 15 MW plant was developed which was named Nellis Solar Power Plant. NREL has developed a triple-junction solar PV cell which converts 40.8% of the light into electricity in the laboratory environment (El Chaar, Lamont, and El Zein 2011). In 2011, the manufacturing cost of PV cells had come down drastically due to the high manufacture of cells in China. The CdTe-based solar cell was developed by the first solar in 2016, converting 22.1% of the light into electricity (Polman et al. 2016). In 2018, GaAs-based PV cell was developed by Alta Devices with a conversion efficiency of 29.1%, and this cell was verified in ISE lab. The first recycled solar plant was also developed in 2018. In 2019, the highest efficiency was achieved by NREL. The multijunction solar cell was developed with a record efficiency of 47.1% compared to polycrystalline or thin-film PV cell (Kong et al. 2020). With single junction, the efficiency of perovskite solar cells is increased from 3% to 25% in a short time, i.e., 2009 to 2020. The efficiency of silicon tandem cells also reached 29.1% compared to single-junction silicon solar cells. A prototype was developed for a bifacial PV system with a conversion efficiency of 26% in 2021 (De Bastiani et al. 2021).

TABLE 1.4

Summary of Fifth-Phase (1980–1999) Development of PV Cell

S. No.	Year	Scientist Name/Lab/Event	Innovation/Development
1	1980	University of Delaware	First thin-film solar cell was developed
2	1981	A. Luque	Development of bifacial PV cells
		Joint venture of USA & UAE	Frist Fresnel lens-based concentrating PV system
3	1983	–	Total energy PV generation reached 21.3 MW
4	1985	Centre for PV Engineering	Silicon cells were developed with 20% efficiency
5	1989	–	Reflectors are used for efficiency improvement
6	1991	–	SERI was renamed the NERL
7	1992	University of South Florida	Thin-film PV cells were developed with 15.9% efficiency made from CdTe
8	1994	NERL	Various material solar PV cells i.e. InGaP & GaAs, the first monolithic junction solar cell with 30% efficiency
9	1999	–	Worldwide solar energy reached 1000 MW

1.2.1 Historical Development of Solar PV System in India

Solar energy is the highest growing energy in the field of RE. Many developed and developing countries focus on solar energy more than other RE. The Commission for Additional Sources of Energy (CASE) was established in 1981 under the Department of Science and Technology. The main objective of CASE was to reduce the energy crisis with the implementation of new schemes and to enhance the research program for new and RE. In 1982, the Department of Non-Conventional Energy Sources was created under CASE to look after new and RESs (Kapoor et al. 2014; K. Kumar, Ansari, Rana, et al. 2018). The newly dedicated ministry was established in 1992 as the Ministry of Non-Conventional Energy Sources, which was renamed as the Ministry of New and Renewable Energy (MNRE) in 2006. The Government of India has always focused on the energy sector for both conventional and nonconventional energy sources. Various incentive schemes have been launched to support the energy sector from time to time (Prasad et al. 2020; Verma 2017).

Solar PV system is the most emerging energy source among all RES. The total solar power installed capacity in India as of 31 May 2021 is 41.08 GW (CEA 2021). The total installed capacity in March 2010 is 161 MW, which has grown rapidly to reach 40.08 GW in March 2021 (CEA 2021). The growth of solar PV system in India since 2010 is shown in Figure 1.5.

The National Solar Mission is one of the major incentives of the Government of India. As per the incentive, the total solar power targeted for 2022 was 20 GW, which was achieved in 2018. A new target of 100 GW in 2022 has been set

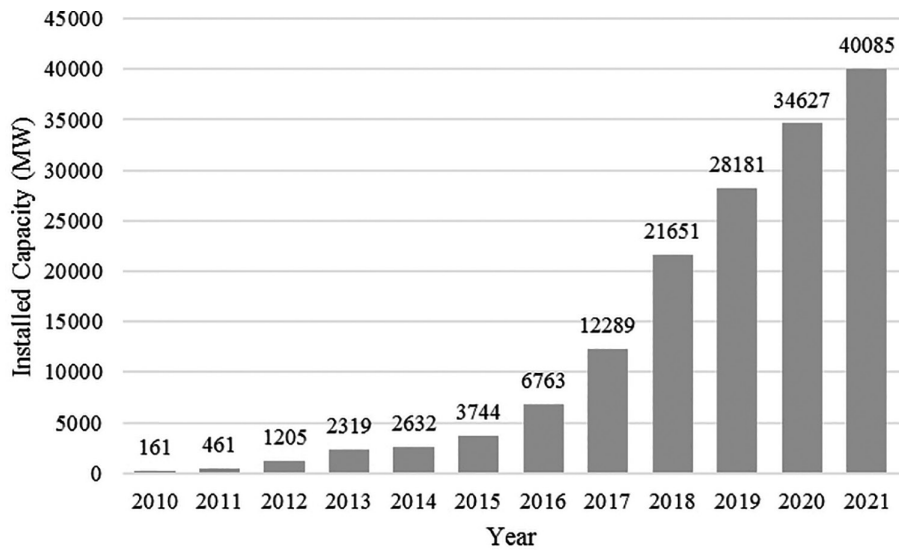


FIGURE 1.5
Installed capacity of solar PV system.

through various means like rooftops and solar parks. India has the world's largest solar park, Bhadla Solar Park, Rajasthan, and the second largest solar park, Pavagada Solar Park, Karnataka. An International Solar Alliance (ISA) with the concept of One Sun, One World, and One Grid has also been proposed by India and a founding member of the ISA.

1.3 Application of Solar Energy

The uses of solar energy can broadly be of three categories.

1.3.1 Residential Application

The rooftop solar panels installed in a residential area can be mainly used as solar electricity and heating the water at individual or bulk level as heating of pools, etc. Solar energy can be used to charge the batteries that may be utilized in the absence of sunlight or grid supply for residential loads. Moreover, solar energy can also be used in remotely located load/islanded systems such as remote villages and hospitals.

1.3.2 Industrial Application

Solar energy can be used in various industrial applications, some of which are industrial power supply warning light indicators for lighthouse, aircraft, etc.

1.3.3 Transportation

The transport sector is a major part of power consumption. A major part of fossil fuels is spent on transportation only. The depleting fossil fuels and the pollution generated due to their consumption is a warning to both the future and the environment. Hence, for a stable future, we have to focus on RE, and in this area, solar energy can be a better option.

Nowadays, electric vehicles (EVs) have emerged as a better option for similar reasons. Various researches are going on in the field of EVs, but the source of charging the EV will have to be decided with great care. If we charge the EV with conventionally generated electric power, then it may not be an as good option for the environment. Better results may come when RE will be used in charging EVs. Based on the above discussion, the classification of PV application is shown in Figure 1.6.

Other than these broad categorizations, solar energy is used in various fields as discussed below.

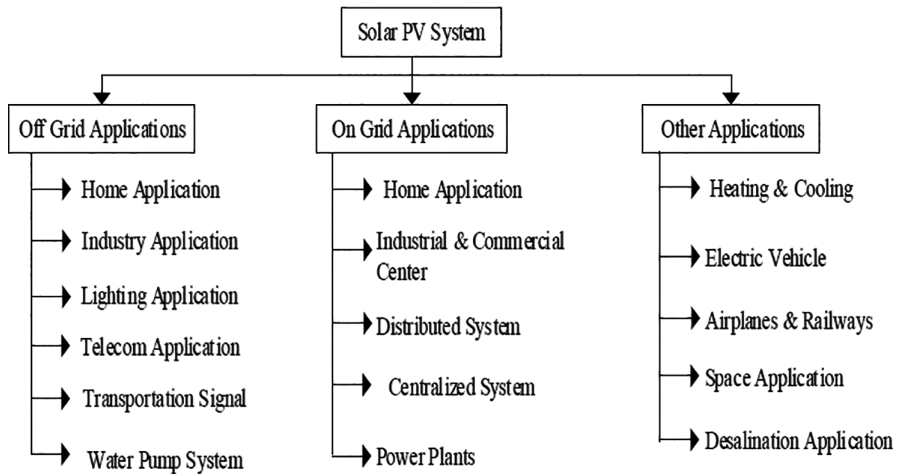


FIGURE 1.6
Classification of PV application.

1.3.4 Solar Water Heating

All over the world, electricity consumption is growing very fast. In simple words, the development of any country is directly proportional to its energy consumption. Among the various loads, water heating has a significant part. For water heating applications, solar energy system is an environment friendly and cost-effective solution. A solar water heating system can have a payback period of 2–4 years, depending on the different technology and systems (Shukla et al. 2013). The schematic diagram of solar water heating system is shown in Figure 1.7.

Its main part is the solar collector plat, which converts solar energy into heat. This heat goes from flat plate collector to cold water storage tank through hot water pipeline. Water storage tank is an insulated storage tank in which utility inlet and outlet points are connected. In some systems, electric heater road is also connected for emergency backup. There are mainly two types of solar water heating systems, the first is Passive Solar Water Heating System and the second is Active Solar Water Heating System. A passive solar water heating system depends on the heat driving convention to circulate the water/heating fluid (Schmidt and Goetzberger 1990; Jaisankar et al. 2009). However, in active power, active solar heating system is used to circulate the heating fluid using one or more pumps (Xu, Zhang, and Deng 2006).

1.3.5 Solar Desalination

Freshwater has reached an alarming situation due to the increasing population and excess use of water around the world. Today, a huge part of the world's population is deprived of clean water (Chauhan et al. 2021; Rodell et al. 2018).

The solar desalination system could be a vital and environment friendly solution to this problem. Solar desalination is a process of elimination of salts from saline water using solar energy (Thakkar et al. 2020). The evaporation and condensation processes are used for solar desalination. This process includes the falling of solar radiation on the top surface of the cover plate and reached to the water carrying basin. In this process, both convective heat and radiative heat play an important role (Rashidi, Bovand, and Esfahani 2016).

1.3.6 Solar Cooking

Residential sector is the second largest energy consumption sector (Aramesh et al. 2019; International Energy Agency 2017).

In Europe, 36% of CO₂ emissions are due to energy consumed in building (Harter, Weiler, and Eicker 2017). Moreover, in the residential sector, most of the energy is consumed in cooking only. In India, around 36% of total energy is consumed for cooking only (Pillai and Banerjee 2009), and this percentage is around 90%–100% in various rural dense areas of Sub-Saharan Africa (Karekezi and Kithyoma 2002). In the United States, the energy used for cooking is around 37%–53% of total energy consumption (Subbiah et al. 2017). For minimization of this significant part of energy consumption, solar cooking is a cleaner and sustainable solution. In solar cooking, solar radiation is used to cook the food with the help of solar cooker. According to the

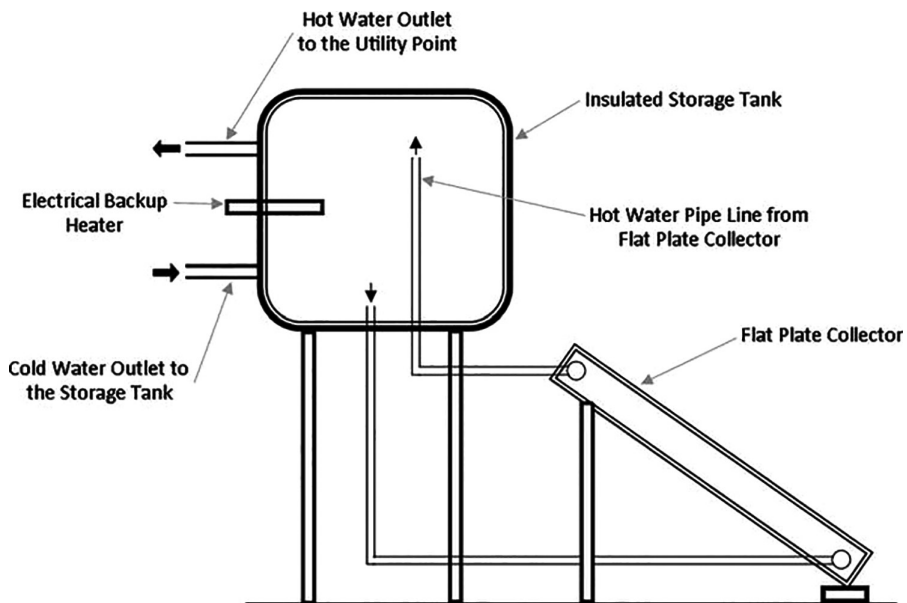


FIGURE 1.7
Schematic diagram of solar water heating system.

Solar Cookers International Association, globally more than 4 million solar cookers have been installed and these are impacting around 14.3 million people (Association, n.d.).

1.3.7 Solar Energy of Industry Process/Heating

In industry, most of the energy is consumed for heating purpose at low and medium temperatures (up to 250°C) (A. K. Sharma et al. 2017). The heating system may be combustion and electrical based. Traditionally, liquid fuel, natural gas, coal, and electricity are utilized in the production of heat. This can be replaced by solar thermal collectors. In state-of-the-art, researchers have developed efficient solar concentrator technology to generate heat up to 300°C (A. K. Sharma et al. 2017). Nowadays, a lot of industries are also using solar process heating systems. Some of these are food processing industry, textile and paper industry, chemical process and pharmaceutical industry, many automobiles equipment manufacturing industry, etc.

1.3.8 Solar Pumps for Agriculture

In developing countries, electricity demand is becoming terrible with growth. In an agricultural country like India, electricity used in the agriculture sector is around one-fourth of the total demand (Korpale, Kokate, and Deshmukh 2016). In the agriculture sector, most of the electricity is utilized for water pumping system. Therefore, solar water pumping systems for irrigation is one of the best options. Solar energy is used at large to operate the irrigation water pumps. Nowadays, integrated models are used to increase

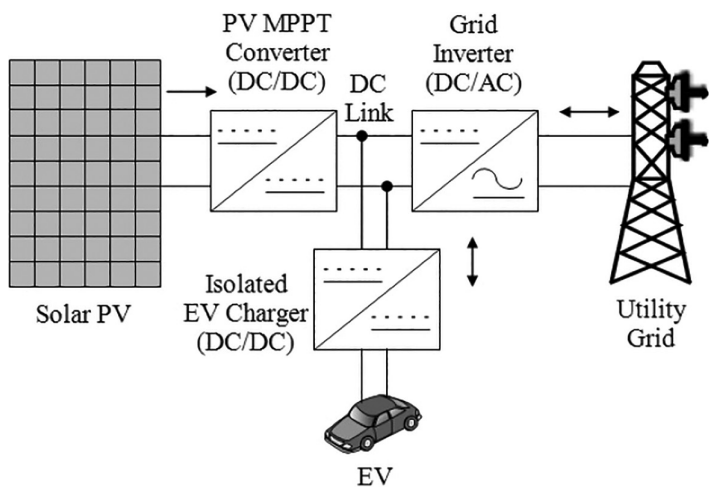


FIGURE 1.8
Solar PV-based electric vehicle.

their utilization further. In this, solar energy is not only used for running water pumps, rather in ideal time of pumps, the generated energy is fed to electric grid.

1.3.9 Some Recent Advance Application

1.3.9.1 Solar Energy in Electric Vehicle

As we know, the whole world is focusing and promoting EVs. Solar energy can be used in the EV sector in two different ways: first is the direct use in which solar panels are installed on the vehicle itself to increase the overall performance. Another is the use of solar energy at charging stations (Chandra Mouli, Bauer, and Zeman 2016). The use of solar-based charging stations increases the purpose and effectiveness of EVs at large. A prototype of a solar PV-based EV is shown in Figure 1.8, where the vehicle is charged through a separate charger that is connected to a grid-connected PV system.

1.3.9.2 Solar-Powered Airplanes and Railways

All over the world, many airports and railway stations are already powered by solar energy. In India, Puducherry airport is fully powered by solar energy only. Moreover, Indian Railways has announced that 960 railway stations are powered by solar panels. Apart from this, solar-powered airplane is also underdeveloped under the Swiss project *Solar Impulse*. Right now, it is being tested on a small scale as a low passenger plane. The solar power aircraft Helios (Gibbs 2015) is shown in Figure 1.9.



FIGURE 1.9
Solar power aircraft Helios.

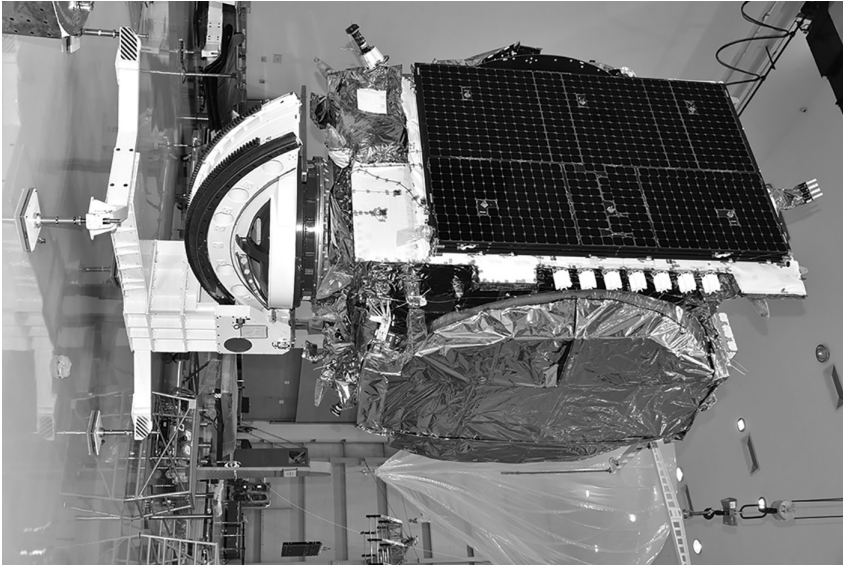


FIGURE 1.10
Communication satellite with PV system.

1.3.9.3 Solar Energy used in Space Applications

Solar energy is available as a better fuel option in the space. Nowadays, solar energy is used in satellite to give power to the spacecraft. In solar power satellites, solar energy makes a big contribution to the energy used in radio frequency of laser transmission systems. Figure 1.10 shows the communication satellite ('ISRO – Government of India' 2016) with the solar PV system.

1.4 Basic Components of Solar PV System

The main components of solar energy system are shown in Figure 1.11, which are discussed below.

1.4.1 Solar Panels

Solar energy panels are the first and basic component of the solar energy system. Solar panels are series and parallel combinations of solar cells made up of silicon material. Solar panels convert the energy received from the Sun into DC electricity. The output of a solar panel is measured in Watts.

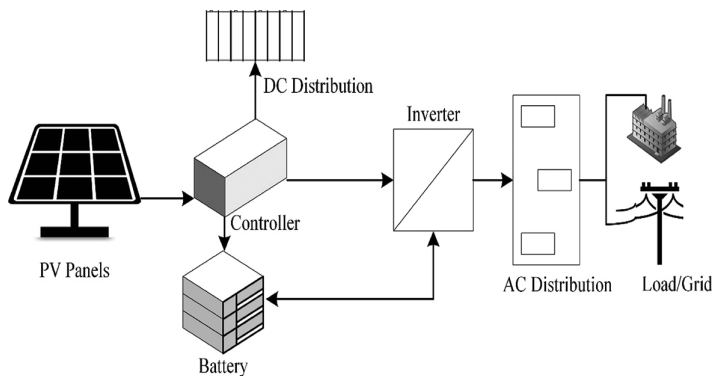


FIGURE 1.11
Components of solar energy system.

1.4.2 Controller

The basic function of the controller is to protect the storage system from over-current charging/damage. The controller is also known as a charge controller. It provides suitable current to charge the battery.

1.4.3 Solar Performance Monitoring Equipment

Performance monitor systems are not an essential part of many isolated domestic solar energy systems. But these devices are necessary to monitor the overall efficiency and performance of solar energy systems. Its main function is to monitor the continuous energy generated from which the performance change over time can be calculated.

1.4.4 Solar Storage

Solar energy storage is mainly a battery bank that is used to keep the electricity supply continuous, even in the absence of sunlight. These batteries are charged during day time and supply electricity during night time in the absence of the sun. The batteries used are generally lead acid batteries and lithium batteries.

1.4.5 Solar Inverter

The main function of solar inverter is to convert DC power generated from solar panels into AC power. A solar inverter works continuously in the solar system, which is why it can also be called the heart of the solar energy system. Solar inverter not only converts the energy but also synchronizes the generator power with the connected load. There are different inverters available in the market for grid-connected and isolated solar energy systems. In the solar energy system, inverters can be string connected or centrally connected.

1.4.6 AC and DC Distribution

Depending on the type of load, AC and DC distribution panels connect the load to the generated solar energy system. The various measuring instrument and energy consumption meters are the part of AC distribution box. In these distribution boxes, many protective systems like surge protector, circuit breaker, etc. are installed. So that the entire solar energy system can be protected in case of any fault at load side and vice versa.

1.4.7 Mounting Support

Mounting of solar PV panels is an important factor for maximum power generation and support. Panels can be mounted on roof, pole, ground, canal, etc. with or without a tracking system.

References

- Adams, W.G., and R.E. Day. 1877. 'The action of light on selenium'. *Proceedings of the Royal Society of London* 25 (171–178): 113–17. <https://doi.org/10.1098/rspl.1876.0024>.
- Akinyele, D.O., R.K. Rayudu, and N.K.C. Nair. 2015. 'Global progress in photovoltaic technologies and the scenario of development of solar panel plant and module performance estimation—application in Nigeria'. *Renewable and Sustainable Energy Reviews* 48: 112–39. <https://doi.org/10.1016/j.rser.2015.03.021>.
- Aramesh, M., M. Ghalebani, A. Kasaeian, H. Zamani, G. Lorenzini, O. Mahian, and S. Wongwises. 2019. 'A review of recent advances in solar cooking technology'. *Renewable Energy* 140: 419–35. <https://doi.org/10.1016/j.renene.2019.03.021>.
- Basit, M.A., S. Dilshad, R. Badar, and S.M. Sami ur Rehman. 2020. 'Limitations, challenges, and solution approaches in grid-connected renewable energy systems'. *International Journal of Energy Research* 44 (6): 4132–62. <https://doi.org/10.1002/er.5033>.
- BP plc. 2021. 'Statistical Review of World Energy 2021'.
- Bragagnolo, J.A., A.M. Barnett, J.E. Phillips, R.B. Hall, A. Rothwarf, and J.D. Meakin. 1980. 'The design and fabrication of thin-film CdS/Cu₂S cells of 9.15-percent conversion efficiency'. *IEEE Transactions on Electron Devices* 27 (4): 645–51. <https://doi.org/10.1109/T-ED.1980.19917>.
- Bray, J. 1995. 'The first satellite communication engineers'. In *The Communications Miracle*, 237–56. Boston, MA: Springer. https://doi.org/10.1007/978-1-4899-6038-2_15.
- Carlson, D.E., and C.R. Wronski. 1976. 'Amorphous silicon solar cell'. *Applied Physics Letters* 28 (11): 671–73. <https://doi.org/10.1063/1.88617>.
- CEA. 2021. 'Ministry of Power, Government of India'.
- Chandra Mouli, G.R., P. Bauer, and M. Zeman. 2016. 'System design for a solar powered electric vehicle charging station for workplaces'. *Applied Energy* 168: 434–43. <https://doi.org/10.1016/j.apenergy.2016.01.110>.

- Chauhan, V.K., S.K. Shukla, J.V. Tirkey, and P.K.S. Rathore. 2021. A comprehensive review of direct solar desalination techniques and its advancements. *Journal of Cleaner Production* 284. Elsevier Ltd. <https://doi.org/10.1016/j.jclepro.2020.124719>.
- De Bastiani, M., A.J. Mirabelli, Y. Hou, F. Gota, E. Aydin, T.G. Allen, J. Troughton, et al. 2021. 'Efficient bifacial monolithic perovskite/silicon tandem solar cells via bandgap engineering'. *Nature Energy* 6 (2): 167–75. <https://doi.org/10.1038/s41560-020-00756-8>.
- Dincer, I. 1998. 'Energy and environmental impacts: Present and future perspectives'. *Energy Sources* 20 (4–5): 427–53. <https://doi.org/10.1080/00908319808970070>.
- Edmonds, I.R. 1990. 'The performance of bifacial solar cells in static solar concentrators'. *Solar Energy Materials* 21 (2–3): 173–90. [https://doi.org/10.1016/0165-1633\(90\)90052-3](https://doi.org/10.1016/0165-1633(90)90052-3).
- El Chaar, L., L.A. Lamont, and N. El Zein. 2011. 'Review of photovoltaic technologies'. *Renewable and Sustainable Energy Reviews* 15 (5): 2165–75. <https://doi.org/10.1016/j.rser.2011.01.004>.
- Gibbs, Y. 2015. 'NASA Dryden Fact Sheet - Solar-Power Research'. <http://www.nasa.gov/centers/armstrong/news/FactSheets/FS-054-DFRC.html>.
- Goetzberger, A., and C. Hebling. 2000. 'Photovoltaic materials, past, present, future'. *Solar Energy Materials and Solar Cells* 62 (1–2): 1–19. [https://doi.org/10.1016/S0927-0248\(99\)00131-2](https://doi.org/10.1016/S0927-0248(99)00131-2).
- Green, M.A. 1987. 'High efficiency silicon solar cells'. In *Seventh E.C. Photovoltaic Solar Energy Conference*, 681–87. Dordrecht: Springer. https://doi.org/10.1007/978-94-009-3817-5_121.
- Green, M.A., J. Zhao, A. Wang, and S.R. Wenham. 1999. 'Very high efficiency silicon solar cells-science and technology'. *IEEE Transactions on Electron Devices* 46 (10): 1940–47. <https://doi.org/10.1109/16.791982>.
- Harter, H., V. Weiler, and U. Eicker. 2017. 'Developing a roadmap for the modernisation of city quarters – comparing the primary energy demand and greenhouse gas emissions'. *Building and Environment* 112: 166–76. <https://doi.org/10.1016/j.buildenv.2016.11.031>.
- Hayat, M.B., D. Ali, K.C. Monyake, L. Alagha, and N. Ahmed. 2019. 'Solar energy-a look into power generation, challenges, and a solar-powered future'. *International Journal of Energy Research* 43 (3): 1049–67. <https://doi.org/10.1002/er.4252>.
- Hoddeson, L., G. Baym, and M. Eckert. 1987. 'The development of the quantum-mechanical electron theory of metals: 1928–1933'. *Reviews of Modern Physics* 59 (1): 287–327. <https://doi.org/10.1103/RevModPhys.59.287>.
- International Energy Agency. 2017. 'World Energy Outlook Iea.Org/Weo'.
- 'ISRO - Government of India'. 2016. <https://www.isro.gov.in/>.
- Jaisankar, S., T.K. Radhakrishnan, K.N. Sheeba, and S. Suresh. 2009. 'Experimental investigation of heat transfer and friction factor characteristics of thermosyphon solar water heater system fitted with spacer at the trailing edge of left-right twisted tapes'. *Energy Conversion and Management* 50 (10): 2638–49.
- Joshi, A.S., Ibrahim Dincer, and B.V. Reddy. 2009. 'Performance analysis of photovoltaic systems: A review'. *Renewable and Sustainable Energy Reviews* 13 (8): 1884–97. <https://doi.org/10.1016/j.rser.2009.01.009>.
- Kaplan, G. 1983. 'Reliable power: Approaching perfection'. *IEEE Spectrum* 20 (9): 64–65. <https://doi.org/10.1109/MSPEC.1983.6501458>.
- Kapoor, K., K.K. Pandey, A.K. Jain, and A. Nandan. 2014. 'Evolution of solar energy in India: A review'. *Renewable and Sustainable Energy Reviews* 40: 475–87. <https://doi.org/10.1016/j.rser.2014.07.118>.

- Karekezi, S., and W. Kithyoma. 2002. 'Renewable energy strategies for rural Africa: Is a PV-led renewable energy strategy the right approach for providing modern energy to the rural poor to Sub-Saharan Africa?' *Energy Policy* 30 (11–12): 1071–86. [https://doi.org/10.1016/S0301-4215\(02\)00059-9](https://doi.org/10.1016/S0301-4215(02)00059-9).
- Kazmerski, L.L., K.A. Emery, and R. DeBlasio. 1994. 'Evaluation and directions of the photovoltaic technologies'. *Renewable Energy* 5 (1–4): 252–67. [https://doi.org/10.1016/0960-1481\(94\)90381-6](https://doi.org/10.1016/0960-1481(94)90381-6).
- Kong, M., C.H. Kang, O. Alkhazragi, X. Sun, Y. Guo, M. Sait, J.A. Holguin-Lerma, T.K. Ng, and B.S. Ooi. 2020. 'Survey of energy-autonomous solar cell receivers for satellite–air–ground–ocean optical wireless communication'. *Progress in Quantum Electronics* 74: 100300. <https://doi.org/10.1016/j.pquantelec.2020.100300>.
- Korpale, V.S., D.H. Kokate, and S.P. Deshmukh. 2016. 'Performance assessment of solar agricultural water pumping system'. *Energy Procedia* 90: 518–24. <https://doi.org/10.1016/j.egypro.2016.11.219>.
- Kressel, H. 1981. 'Chapter 1 the effect of crystal defects on optoelectronic devices'. In *Semiconductors and Semimetals*, 16:1–52. [https://doi.org/10.1016/S0080-8784\(08\)60128-3](https://doi.org/10.1016/S0080-8784(08)60128-3).
- Kumar, A., K. Kumar, N. Kaushik, S. Sharma, and S. Mishra. 2010. 'Renewable energy in India: Current status and future potentials'. *Renewable and Sustainable Energy Reviews* 14 (8): 2434–42. <https://doi.org/10.1016/j.rser.2010.04.003>.
- Kumar, B., Y.K. Chauhan, and V. Shrivastava. 2014. 'A comparative study of maximum power point tracking methods for a photovoltaic-based water pumping system'. *International Journal of Sustainable Energy* 33 (4): 797–810. <https://doi.org/10.1080/14786451.2013.769990>.
- Kumar, K., M.A. Ansari, S.K. Varshney, V. Rana, and A. Tyagi. 2018. 'An efficient technique for power management in hybrid solar PV and fuel cell system'. *Smart Science* 6 (3): 1–11. <https://doi.org/10.1080/23080477.2018.1494974>.
- Kumar, K., M A Ansari, V. Rana, and R. Singh. 2018. 'Simulation based solar PV system: A cost-effective study'. *International Journal of Applied Engineering Research* 13 (11): 8894–98. <http://www.ripublication.com>.
- Kuwano, Y., and M. Ohnishi. 1981. 'Development of amorphous Si solar cells in Japan'. In Palz, W. (ed.) *Photovoltaic Solar Energy Conference*, 309–16. Dordrecht: Springer. https://doi.org/10.1007/978-94-009-8423-3_44.
- Loferski, J.J. 1993. 'The first forty years: A brief history of the modern photovoltaic age'. *Progress in Photovoltaics: Research and Applications* 1 (1): 67–78. <https://doi.org/10.1002/pip.4670010109>.
- Malhotra, R., and B. Singh. 2020. 'Design and construction of solar shed'. In *AIP Conference Proceedings*, vol. 2220, 140061. AIP Publishing LLC AIP Publishing. <https://doi.org/10.1063/5.0001157>.
- Miles, R.W., K.M. Hynes, and I. Forbes. 2005. 'Photovoltaic solar cells: An overview of state-of-the-art cell development and environmental issues'. *Progress in Crystal Growth and Characterization of Materials* 51 (1–3): 1–42. <https://doi.org/10.1016/j.pcrysgrow.2005.10.002>.
- Pais, A. 1979. 'Einstein and the quantum theory'. *Reviews of Modern Physics* 51 (4): 863–914. <https://doi.org/10.1103/RevModPhys.51.863>.
- Pal, P., V. Mukherjee, P. Kumar, and M.E. Makhatha. 2021. 'Pre-feasibility analysis and performance assessment of solar photovoltaic (PV) modules for the application of renewable power generation'. *Materials Today: Proceedings* 39: 1813–19. <https://doi.org/10.1016/j.matpr.2020.10.557>.

- Pallavolu, M.R., A.N. Banerjee, V. Reddy M. Reddy, S.W. Joo, H.R. Barai, and C. Park. 2020. 'Status review on the Cu₂SnSe₃ (CTSe) thin films for photovoltaic applications'. *Solar Energy* 208: 1001–30. <https://doi.org/10.1016/j.solener.2020.07.095>.
- Panwar, N.L., S.C. Kaushik, and S. Kothari. 2011. 'Role of renewable energy sources in environmental protection: A review'. *Renewable and Sustainable Energy Reviews* 15 (3): 1513–24. <https://doi.org/10.1016/j.rser.2010.11.037>.
- Pearson, G., and W. Brattain. 1955. 'History of semiconductor research'. *Proceedings of the IRE* 43 (12): 1794–1806. <https://doi.org/10.1109/JRPROC.1955.278042>.
- Pearson, G.L., D.M. Chapin, and C.S. Fuller. 1957. 'US2780765A, "Solar Energy Converting Apparatus"'. <https://patents.google.com/patent/US2780765A/en>.
- Petrova-Koch, V. 2009. 'Milestones of solar conversion and photovoltaics'. In *High-Efficient Low-Cost Photovoltaics*, 1–5. Berlin: Springer. https://doi.org/10.1007/978-3-540-79359-5_1.
- Pillai, I.R., and R. Banerjee. 2009. 'Renewable energy in India: Status and potential'. *Energy* 34 (8): 970–80. <https://doi.org/10.1016/j.energy.2008.10.016>.
- Polman, A., M. Knight, E.C. Garnett, B. Ehrler, and W.C. Sinke. 2016. 'Photovoltaic materials: Present efficiencies and future challenges'. *Science* 352 (6283): aad4424. <https://doi.org/10.1126/science.aad4424>.
- Prasad, S., S. Kumar, K.R. Sheetal, and V. Venkatramanan. 2020. 'Global climate change and biofuels policy: Indian perspectives'. In *Global Climate Change and Environmental Policy*, 207–26. Singapore: Springer. https://doi.org/10.1007/978-981-13-9570-3_6.
- Rakesh Tej Kumar, K., M. Ramakrishna, and G. Durga Sukumar. 2018. 'A review on PV cells and nanocomposite-coated PV systems'. *International Journal of Energy Research* 42 (7): 2305–19. <https://doi.org/10.1002/er.4002>.
- Ramakumar, R., N.G. Butler, A.P. Rodriguez, and S.S. Venkata. 1993. 'Economic aspects of advanced energy technologies'. *Proceedings of the IEEE* 81 (3): 318–32. <https://doi.org/10.1109/5.241495>.
- Rana, V., M.A. Ansari, and Y.K. Chauhan. 2020. 'Investigation of partial shading effect on PV array configuration'. *International Journal of Digital Signals and Smart Systems* 4 (1/2/3): 184. <https://doi.org/10.1504/IJDSS.2020.106082>.
- Rashidi, S., M. Bovand, and J. Abolfazli Esfahani. 2016. 'Optimization of partitioning inside a single slope solar still for performance improvement'. *Desalination* 395: 79–91. <https://doi.org/10.1016/j.desal.2016.05.026>.
- Rodell, M., J.S. Famiglietti, D.N. Wiese, J.T. Reager, H.K. Beaudoin, F.W. Landerer, and M.H. Lo. 2018. 'Emerging trends in global freshwater availability'. *Nature* 557 (7707): 651–59. <https://doi.org/10.1038/s41586-018-0123-1>.
- Schmidt, C., and A. Goetzberger. 1990. 'Single-tube integrated collector storage systems with transparent insulation and involute reflector'. *Solar Energy* 45 (2): 93–100. [https://doi.org/10.1016/0038-092X\(90\)90033-9](https://doi.org/10.1016/0038-092X(90)90033-9).
- SCI Association. n.d. <https://www.Solarcookers.Org/Partners/Distribution-Solar-Cookers>. Solar Cooker Distribution (Accessed on 05 August 2021).
- Shah, A.V., H. Schade, M. Vanecek, J. Meier, E. Vallat-Sauvain, N. Wyrsch, U. Kroll, C. Droz, and J. Bailat. 2004. 'Thin-film silicon solar cell technology'. *Progress in Photovoltaics: Research and Applications* 12 (23): 113–42. <https://doi.org/10.1002/pip.533>.
- Sharma, A.K., C. Sharma, S.C. Mullick, and T.C. Kandpal. 2017. 'Solar industrial process heating: A review'. *Renewable and Sustainable Energy Reviews* 78: 124–37. <https://doi.org/10.1016/j.rser.2017.04.079>.

- Sharma, N.K., N. Tyagi, and V. Rana. 2019. 'Renewable energy scenario in India: A current status'. *International Journal of Applied Engineering Research* 14 (10): 150–54.
- Shukla, R., K. Sumathy, P. Erickson, and J. Gong. 2013. 'Recent advances in the solar water heating systems: A review'. *Renewable and Sustainable Energy Reviews* 19: 173–90. <https://doi.org/10.1016/j.rser.2012.10.048>.
- Spanggaard, H., and F.C. Krebs. 2004. 'A brief history of the development of organic and polymeric photovoltaics'. *Solar Energy Materials and Solar Cells* 83 (2–3): 125–46. <https://doi.org/10.1016/j.solmat.2004.02.021>.
- Subbiah, R., A. Pal, E.K. Nordberg, A. Marathe, and M.V. Marathe. 2017. 'Energy demand model for residential sector: A first principles approach'. *IEEE Transactions on Sustainable Energy* 8 (3): 1215–24. <https://doi.org/10.1109/TSTE.2017.2669990>.
- Takamoto, T., E. Ikeda, H. Kurita, and M. Ohmori. 1994. 'High efficiency InGaP solar cells for InGaP/GaAs tandem cell application'. In *Proceedings of 1994 IEEE 1st World Conference on Photovoltaic Energy Conversion - WCPEC (A Joint Conference of PVSC, PVSEC and PSEC)*, vol. 2, 1729–32 IEEE. <https://doi.org/10.1109/WCPEC.1994.520552>.
- Thakkar, H., A. Sankhala, P.V. Ramana, and H. Panchal. 2020. 'A detailed review on solar desalination techniques'. *International Journal of Ambient Energy* 41 (9): 1066–87. <https://doi.org/10.1080/01430750.2018.1490351>.
- Tomaszewski, P.E. 2002. 'Jan czochralski—Father of the Czochralski method'. *Journal of Crystal Growth* 236 (1–3): 1–4. [https://doi.org/10.1016/S0022-0248\(01\)02195-9](https://doi.org/10.1016/S0022-0248(01)02195-9).
- Tyagi, V.V., S.C. Kaushik, and S.K. Tyagi. 2012. 'Advancement in solar photovoltaic/thermal (PV/T) hybrid collector technology'. *Renewable and Sustainable Energy Reviews* 16 (3): 1383–98. <https://doi.org/10.1016/j.rser.2011.12.013>.
- Uecker, R. 2014. 'The historical development of the Czochralski method'. *Journal of Crystal Growth* 401: 7–24. <https://doi.org/10.1016/j.jcrysgro.2013.11.095>.
- Vallerani, E. 1988. 'The space station'. *Interdisciplinary Science Reviews* 13 (2): 156–65. <https://doi.org/10.1179/isr.1988.13.2.156>.
- Verma, A., A. Tyagi, and R. Krishan, 2017. 'Optimal allocation of distributed solar photovoltaic generation in electrical distribution system under uncertainties'. *Journal of Electrical Engineering and Technology* 12 (4): 1386–96. <https://doi.org/10.5370/JEET.2017.12.4.1386>.
- Xu, G., X. Zhang, and S. Deng. 2006. 'A simulation study on the operating performance of a solar-air source heat pump water heater'. *Applied Thermal Engineering* 26 (11–12): 1257–65. <https://doi.org/10.1016/j.applthermaleng.2005.10.033>.

Solar Power Forecasting

**Agrim Khurana, Ankit Dabas, Vaibhav Dhand,
Rahul Kumar, Bhavnesh Kumar, and Arjun Tyagi**

Netaji Subhas Institute of Technology

CONTENTS

2.1	Introduction	23
2.2	Tools and Techniques for Solar Forecasting	24
2.2.1	Tools	24
2.2.2	Techniques for Solar Forecasting	25
2.3	Solar Spectrum	25
2.4	Solar Radiation Geometry	28
2.5	Solar Power Prediction Techniques	30
2.5.1	Support Vector Regression (SVR)	30
2.5.2	XG BOOST	31
2.5.3	Random Forest	32
2.5.4	Artificial Neural Network	33
2.5.5	Long-Short Term Memory (LSTM) Model	34
2.6	Results and Discussion	34
2.7	Conclusion	39
	References	41

2.1 Introduction

The need for energy generation is skyrocketing with the increasing population and elevating industrial, urban, and domestic standards. The pressure on our nonrenewable energy resources has been at its apex which has eventually diminished their numbers. This has led the world to switch to their renewable counterpart and use them for energy generation. Although various developments have been made in the production of solar cells and panels, the losses due to intermittent weather conditions and other factors still make up for a huge problem (Kim et al., 2019). The solar industry is now working on the concept of solar prediction. The prediction of weather conditions and grid systems can greatly help in increasing solar power utilization as one has the data for the future conditions on which the output of the solar photovoltaic system depends significantly (Voyant et al., 2017).

Incorporation of artificial intelligence (AI) in the field of renewable energy can help the grid operators to a greater extent (Izgi et al., 2012). Intelligent grid systems can choose between various promising energy-generating assets and make the best choice as per the current demand. Other factors that are greatly impacted by this relationship between the renewable industry and AI is that it can help improve the safety and reliability of the solar photovoltaic system. AI can help detect the leakages, shaded areas, health, and keep track of the losses while the panels are operated. This real-time data can help curb many possible defects and also take timely measures, which can prove fatal for the panels' life if ignored for long times.

Several researchers have proposed different prediction mechanisms. However, there are two major areas of improvement in this domain: the first is the better and more efficient design of algorithms used for prediction (Voyant et al., 2017), and the second is the identification and quantification of the effect of the parameters on the prediction (Jawaid and NazirJunejo, 2016). The approach here is to focus on the improvement of the state of the art in both impertinent areas. First, there is an evaluation of the prediction of solar power using different machine learning regression algorithms and deep learning algorithms. Second, there is the use of different parameters that affect the solar power output in conjunction with the weather data to improve the accuracy and precision of the predicted photo voltaic (PV) output (Jawaid and NazirJunejo, 2016; Khandakar et al., 2019).

2.2 Tools and Techniques for Solar Forecasting

2.2.1 Tools

a. PYTHON

Python is considered one of the most popular programming languages. It is a general-purpose high-level language. In 1991, Guido van Rossum created Python. Python's design philosophy emphasizes code readability. As a result, it is widely used in the scientific world. Python 2.7 and 3.6 are extensively used for production environments, with the latter mainly being used for the high-end latest purposes like AI, ML, and DL.

b. PANDAS

The PANDAS provides flexible, fast, and expressive data structures designed to make working with time-series data easy. It also provides fast working with structured data such as tabular, multidimensional, and potentially heterogeneous.

c. Grid Search

It is a function in the library that is a part of the sklearn model selection package. Its function is to help the user to loop through the predefined hyperparameters and fit their model (estimator) on their training values/set.

It is a library function that is a member of the sklearn model selection package. It helps to loop through predefined hyperparameters and fit estimator (model) on training set. So, in the end, select the best parameters from the listed hyperparameters.

d. SKLEARN

Scikit-learn is the handiest library for machine learning in Python. It contains a lot of efficient tools for machine learning and statistical modeling, including classification, regression, and clustering and dimensionality reduction.

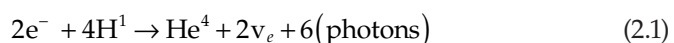
Components of scikit-learn: Scikit-learn is loaded with a lot of helpful and useful features including Supervised-Learning Algorithms. Ranging from Generalized linear models (e.g., Linear Regression), Support Vector Machines (SVM) (Zeng and Qiao, 2013), Decision Trees to Bayesian methods—all of them are part of the scikit-learn toolbox. The diversity of machine learning algorithms present in it is one of the big reasons for the high usage of scikit-learn.

2.2.2 Techniques for Solar Forecasting

- a. Important techniques used for solar forecasting include the weather prediction model. As mentioned before, if one has the data on the weather conditions of a few days, he/she is already a step ahead. The weather model can help decide the cloud patterns that substantially influence the irradiance that is the amount of solar energy falling over a horizontal surface at a particular location (Dise, 2017).
- b. Another technique is PV simulation of photovoltaic simulation. These simulation techniques can help figure out the performance of a particular solar power plant over certain weather conditions, thus enabling us to jot down and analyze the performance of the plant. This greatly helps in understanding the behavior of the plant and also computes the best tilt angle over the coming days (Dise, 2017).

2.3 Solar Spectrum

Solar energy is available in the form of solar radiation is given in eq. (2.1).



where e^- is the charge on electron, H^1 is hydrogen atom, He^4 is helium atom, and ν_e is electron neutrino.

The solar radiation travels in the form of discrete packets of energy called photons. The energy associated with them is termed photon energy and is directly proportional to their frequency.

$$E = h\mu \tag{2.2}$$

where E , h , and μ are the energy of a single photon, Planck’s constant, and frequency, respectively.

The intensity of solar radiation (J/sec or W/m²) is known as radiant flux density (RFD), often referred to as Irradiance or Insolation. It is measured in J/sec or W/m².

Photons or electromagnetic waves are characterized by their frequency or by their wavelength. The energy of the photon is given in electron volts (eV). The sun emits energy in a wide range of wavelengths (0.15 and 120mm), but the wavelength between 0.15 and 4mm is applicable for solar energy application. The categorization of different wavelengths and the energy carried by them is shown in Table 2.1.

Solar irradiance is the power density of sunlight received at a location on the earth and is measured in Watt/m². It is generally denoted by H . The solar radiation incident on the outer atmosphere of the earth is known as Extraterrestrial Radiation. The Extraterrestrial solar radiation received by the earth is essentially constant throughout the year because the medium between the Earth and the Sun (vacuum) does not change with time and the distance between the two remains nearly constant. The solar radiation which reaches the surface of the earth is known as terrestrial radiation. Moreover, the solar radiation received on a flat horizontal surface on the earth is known as solar insolation or incident solar radiation.

Different molecules are suspended in the air, which leads to attenuation of the solar radiation reaching the earth’s surface. The amount of attenuation of solar radiation is a function of the distance that the solar radiation travels through the earth’s air mass (AM). The thickness of the earth’s atmosphere is referred to as AM. The solar energy reaching the earth’s surface is shown in Table 2.2.

TABLE 2.1
The Categorization of Solar Spectrum (Khan, TMH)

Name	Range of Wavelength (μm)	% of Energy Carried
UV radiation	0.15–0.38	7.6
Visible radiation	0.38–0.72	48.4
IR radiation	0.72–4.0	43
Other radiation	>4.0	1

TABLE 2.2
Solar Energy Reaching Earth Surface at Sun’s Different Positions (Khan, TMH)

AM ₀ radiation (Extraterrestrial region)	1,376 W/m ²
AM ₁ (Sun at overhead)	1,105 W/m ²
AM ₂ (Sun at about 60° from overhead)	894 W/m ²

During the journey of solar radiation toward the earth’s surface as it passes through the atmosphere, the radiation is subjected to absorption and scattering, which reduces the amount of solar radiation reaching the surface. Scattering and absorption occur due to the presence of the ozone layer, water vapors, CO₂, O₂, dust particles, etc. The various processes of attenuation are

- a. Absorption
 - Different molecules of different sizes absorb different wavelengths of radiation (selective radiation).
 - i. Ozone absorbs a significant amount of ultraviolet radiation coming from the sun in the range ($\lambda < 0.38 \mu\text{m}$).
 - ii. Most of the infrared radiation in the range ($\lambda > 2.3 \mu\text{m}$) is absorbed by water molecules and carbon dioxide, while most of it below this range is almost depleted.
 - iii. Dust particles and air molecules absorb some of the radiation irrespective of wavelength.
 - iv. Extreme ultraviolet radiation in terrestrial radiation is absorbed by Nitrogen, Oxygen, and other atmospheric gases.
- b. Scattering
 - Dust particles and other particles and air molecules scatter the incident radiation in various directions. Some of the radiation is reflected in space, while some of it is not reflected at all, called direct or beam radiation. The radiation is scattered in different directions, and it is this phenomenon of scattering that makes the sky appear blue.

In a cloudy atmosphere, a major part is reflected to space by clouds and another part is absorbed. The radiation reaching the earth’s surface includes direct radiation; a part of it is reflected again to space by the ground. This is known as ground albedo which is almost 30% of the incoming solar radiation. Thus, on the surface total radiation or Global radiation is the sum of diffuse radiation, that is the radiation reaching the earth’s surface after scattering and absorption and direct or beam radiation that is the radiation that reaches the earth’s surface directly (Khan, TMH).

2.4 Solar Radiation Geometry

The earth revolves elliptically around the sun; therefore, the solar radiation varies in different locations on the earth. In this phenomenon, the various introduced factors are shown in Figure 2.1.

- a. Latitude (Φ): It is the angle subtended by the radial line joining the place to the center of the earth with the projection of the line on the equatorial plane. The latitude is positive for the northern hemisphere and negative for the southern hemisphere.
- b. Declination (δ): It is the angular displacement of the sun from the plane of earth's equator. It is positive when measured from the equatorial plane in the northern hemisphere. It is the angle subtended by a line joining the center of the Earth and the Sun with its projection on the earth's equatorial plane. The declination angle can be calculated as

$$\delta = 23.45 \sin \left(\frac{360}{365} (284 + n) \right) \text{degrees} \quad (2.3)$$

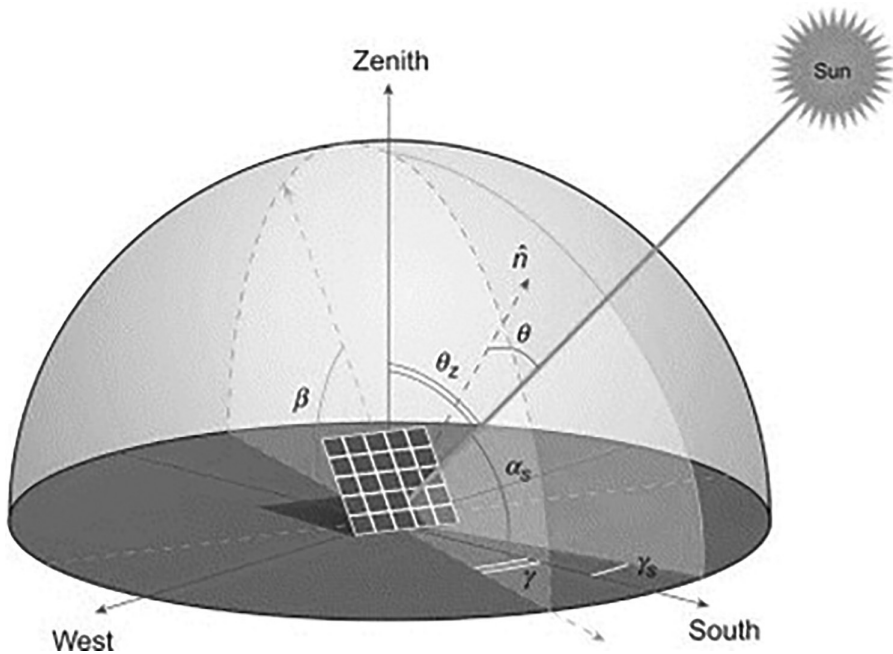
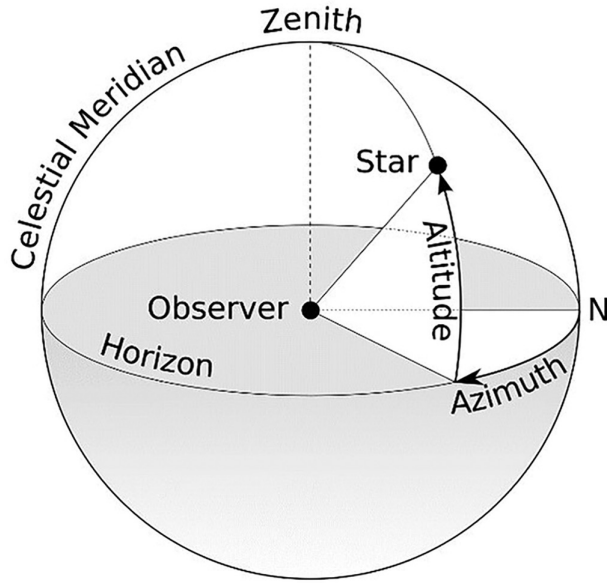


FIGURE 2.1

The solar Zenith, azimuth, and hour angle (Rosa-Clot and Tina 2018).

**FIGURE 2.2**

Formation of Inclination Angle (Carlson, 2020).

where δ is Declination Angle and “ n ” is the n th day of the year, i.e., January 1 is 1st day.

- c. Hour Angle (ω): It is the angle through which the earth must rotate to bring the Meridian of the observed point directly under the sun.
- d. The Inclination or Altitude Angle (α): Inclination is the vertical angle between the direction of the sun rays passing through the point and its projection on the horizontal plane as shown in Figure 2.2.
- e. Zenith Angle (Θ_z): It is the angle between the sun rays and the perpendicular to the horizontal plane. It is the complementary angle of the sun’s altitude angle, i.e.,

$$\theta_z + \alpha = \frac{\pi}{2} \quad (2.4)$$

where Θ_z is Zenith Angle and α is Inclination Angle.

- f. Solar Azimuthal Angle (γ_s): It is the angle in the horizontal plane between the line due to the south and the projection of beam radiation on the horizontal plane. It is considered positive if the projection of the sunbeams is west of south and negative if east of south.

- g. Surface Azimuthal Angle (γ): It is the angle in the horizontal plane between the line due to the south and the horizontal projection of the normal to the inclined plane surface or collector. It is taken as positive when measured from west of south and negative when measured from east of south.
- h. Slope or Tilt Angle (β): It is the angle made by the inclined plane surface or collector under consideration and the horizontal surface. The angle is taken as positive for a surface sloping toward the south and negative for a surface sloping toward the north (Khan, TMH).

2.5 Solar Power Prediction Techniques

The solar energy power output data was obtained from a publicly available repository of the Australian PV Institute for Katherine, Australia (Report: Australian PV Institute). The weather data along with irradiance data was obtained from solcast.com (Report: Solcast), also for Katherine, Australia. There are various machine learning and deep learning techniques that can be used for solar power prediction. These techniques can give an insight into the output of a particular solar power plant under certain weather conditions. This information provides a great advantage to the solar industry as they can make favorable changes in the orientation of the panels in order to elevate the solar output. Some of the techniques that have been used are explained below.

2.5.1 Support Vector Regression (SVR)

SVR is defined by the use of kernels, sparse solutions and margin control of VCs and the sum of support vectors. Though less common than SVM, SVR has proven its efficiency in estimating real-value functions. SVR uses symmetrical loss function as a supervised-learning strategy, which often penalizes high and low estimates. In linear regression, one tries to minimize the error, while SVR tries to match the error according to a certain threshold.

Terms related to SVR:

- a. The kernel is a set of mathematical functions. It takes information as an input and transforms information into the desired prediction form.
- b. Hyper Plane: In SVR, it is the line that predicts the target value.
- c. Boundary line: In SVR, other than Hyperplane, two lines are present that produce a margin. The help vectors may be either on or outside the boundary lines. The boundary line differentiates two classes.
- d. Support vectors: Data points that are close to the boundary line. Distance of the points needs to be least.

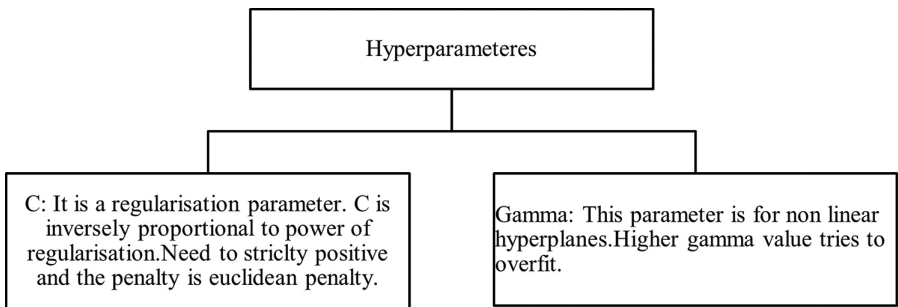


FIGURE 2.3
The hyperparameters for support vector regression.

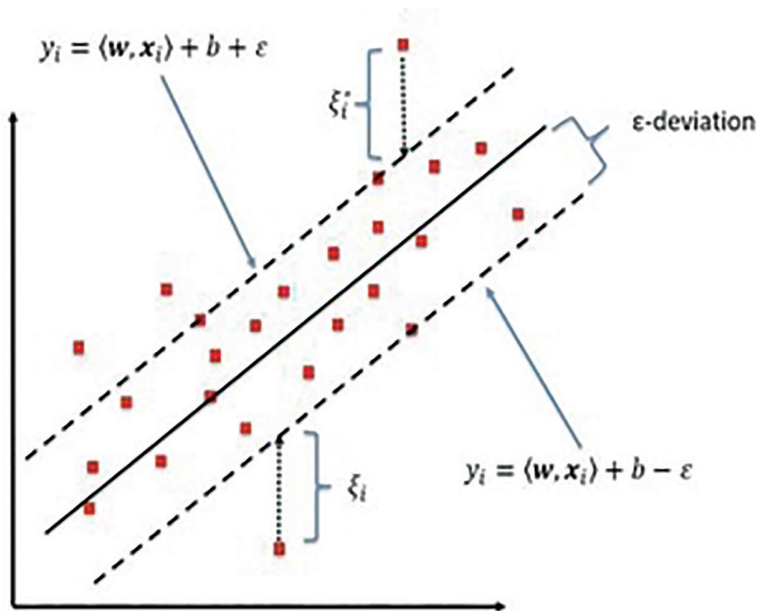


FIGURE 2.4
Working of support vector regression algorithm (Parbat and Chakraborty, 2020).

The hyperparameters and working of SVR algorithm are shown in Figures 2.3 and 2.4, respectively.

2.5.2 XG BOOST

XGBoost is one of the quickest gradients boosted tree implementations. This is achieved by fixing one of the key inefficiencies of gradient-boosted trees: taking account of the loss potential to build a new industry with all potential

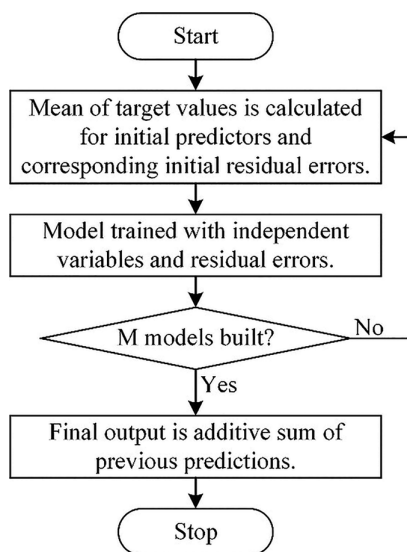


FIGURE 2.5
Schematic diagram of working of XGBoost.

splits (especially if you consider the case where there are thousands of features, and therefore thousands of possible splits). XGBoost resolved this inefficiency by scrutinizing the distribution of features across all data points in a leaf to reduce the spectrum of the quest for future splits of features.

Even if XGBoost brings a few regularization tricks, it is by far the most useful function in the library, which allows for quick investigation of several hyperparameter settings. The flow chart of the working of XGBoost is shown in Figure 2.5.

2.5.3 Random Forest

Decision trees are one of such models that have low bias but high variance. We have studied that decision trees tend to overfit the data. So, the bagging technique becomes a very good solution for decreasing the variance in a decision tree. Instead of using a bagging model with the underlying model as a decision tree, we can also use Random Forest which is more convenient and well optimized for decision trees. The main issue with bagging is that there is not much independence among the sampled datasets, i.e., there is a correlation. The advantage of Random Forests over bagging models is that the Random Forests make a tweak in the working algorithm of the bagging model to decrease the correlation in trees. The idea is to introduce more randomness while creating trees that will help in reducing correlation.

The presence of high variance in decision trees led to the introduction of bagging, which was a suitable idea to reduce variance. But another convenient

method instead of using decision trees along with bagging is to use Random Forests. The advantage of Random Forests over our conventional method of decision trees was decreased amounts of correlation. The idea was the introduction of more randomness, thereby reducing correlation. Let's understand how the algorithm works for a random forest model:

- i. Different samples are collected using bootstrapping.
- ii. The tree is trained on each sample and they are allowed to grow in depths.

The smartness in Random Forests lies in the tree forming part. Every time a split is about to happen in the decision tree, a random sample of " m " predictors is chosen from the total " p " predictors. Only these " m " predictors are used for splitting. Most of the predictors are not allowed to be considered for the split. Generally, the value of " m " is taken as $m \approx \sqrt{p}$, where " p " is the number of predictors in the sample. When $m=p$, the random forest model becomes a bagging model.

Once the trees are formed, a prediction is made by the random forest by aggregating the predictions of all the models. For the regression model, the mean of all the predictions is the final prediction and for classification mode, the mode of all the predictions is considered the final predictions.

Random forest predicts by taking the mode of all the predictions made by all the models since this is the case of classification. This process is also known as "Majority voting." We can also use prediction probability to make the final prediction. We can use the predict probability method, which will predict a probability from 0 to 1 that a given class is the right one for a row. For a problem with the output being only 0 and 1, we'll get a matrix with as many rows as there is in the data and two columns.

2.5.4 Artificial Neural Network

The Artificial Neural Networks (ANNs) are inspired by the biological neural system. A complex structure of an ANN is composed of a basic processing unit, called neurons, which are linked together by weighted, directed connections between them. The input to a neuron is accelerated or retarded by these weighted connections. Analogous to a biological neural system, an artificial neuron receives input from a given number of sources. These inputs are excited or inhibited according to the value of weights and output is generated after passing the weighted sum of inputs through a transfer function.

The complexity of this network can be increased:

- i. Add backward connections, so that output neurons feedback to input nodes, resulting in a recurrent network.
- ii. Add neurons between the input nodes and the outputs, creating an additional ("hidden") layer to the network, resulting in a multilayer perceptron.

The latter approach is more common in applications of Neural Networks. Propagating the inputs forward over two layers is straightforward since the outputs from the hidden layer can be used as inputs for the output layer. However, the process for updating the weights based on the prediction error is less clear, since it is difficult to know whether to change the weights on the input layer or the hidden layer to improve the prediction (Krawczak 2013; Mishra and Ram, 2019).

Updating a multilayer perceptron (MLP) is a matter of

- i. Moving forward through the network, calculating outputs of the given inputs and current weight estimates.
- ii. Moving backward updating weights according to the resulting error from forwarding propagation.

2.5.5 Long-Short Term Memory (LSTM) Model

The long-short term memory (LSTM) model is a special Recurrent Neural Networks (RNN) model, which is proposed to solve the problem of gradient dispersion of RNN models. In traditional RNN, the training algorithm uses BPTT (backpropagation through time). For a long time, the residuals that need to be transmitted will decrease exponentially, causing the network weights to update slowly and fail to reflect the long-term memory effect of the RNN. Therefore, a storage unit is required to store the memory, so the LSTM model is proposed. LSTM network is a special network structure with three “gates,” which are “forget gate,” “input gate,” and “output gate” in this order.

2.6 Results and Discussion

The models have been trained using the data obtained from solcast.com and PVInst.com of Katherine, Australia. The data includes 12 independent parameters and one dependent variable that is PV output. Table 2.3 represents the data used.

The raw data obtained from these sites was preprocessed to make it fit for training. The codes for all the training techniques have been written in Python. A correlation matrix was obtained to derive a statistical relation among the parameters to prevent the overfitting of data. The matrix values have been obtained using the Pearson Correlation Coefficient.¹ The parameters correlating greater than 0.7 were removed to prevent overfitting. This

¹ This test statistic measures the statistical relationship and finds the association between different continuous variables. It uses the formula of covariance. It measures linear correlation between two variables, say M and N and its range is -1 to +1.

TABLE 2.3
Details of Sample Data Used

Air Temp.	Daily Albedo	Azimuth	Dewpoint Temp.	DHI	DNI	GHI	Relative Humidity	Surface Pressure	Wind Direction	Wind Speed	Zenith	Yield Output (KWh)
24.1	0.13	110	23.0	53	0	53	94.0	974.0	265	4.4	75	0.196
24.1	0.13	113	23.2	8	0	8	94.5	974.1	264	3.7	88	0.694
24.1	0.13	118	23.3	0	0	0	95.1	974.3	258	2.9	101	0.787
24.1	0.13	124	23.4	0	0	0	95.8	974.5	249	2.1	114	0.776
24.0	0.13	133	23.3	0	0	0	96.2	974.8	243	1.5	125	1.802
23.7	0.13	146	23.1	0	0	0	95.5	975.0	251	1.1	135	2.194
23.4	0.13	164	22.9	0	0	0	96.9	975.2	266	0.8	141	2.363
23.3	0.13	-174	22.8	0	0	0	97.2	975.1	281	0.6	142	2.022
23.2	0.13	-153	22.9	0	0	0	97.6	974.7	285	0.5	138	2.985
23.2	0.13	-138	22.9	0	0	0	98.0	974.3	289	0.5	130	2.074

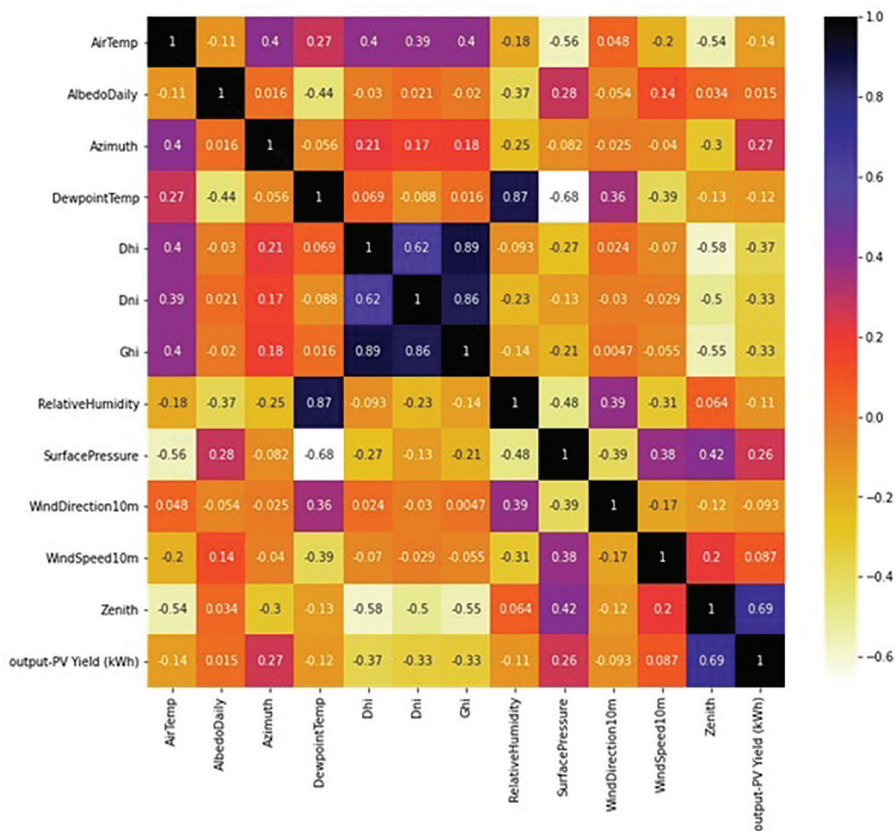


FIGURE 2.6

The correlation of parameters with one another (correlation matrix).

value of 0.7 was chosen arbitrarily keeping in mind the values obtained in the matrix.

The following results were obtained after running the code of various algorithms and the results have been compared based on the weightage of the absolute error obtained, also called Mean Absolute Error (MAE). MAE is the mean value of error in predicted data without considering direction. It can attain values between 0 and ∞ .

The correlation matrix, shown in Figure 2.6, depicts the interrelation of various parameters over one another. This can be used to study the correlation of parameters with one another and overfitting of data can be prevented.

The results were obtained by training the model using SVR Technique, Random Forest Technique, XG Boost Technique, Neural Network Technique, and LSTM Technique and are shown in Figures 2.7, 2.8, 2.9, 2.10, and 2.11, respectively. The absolute error by all these techniques is shown in Table 2.4.

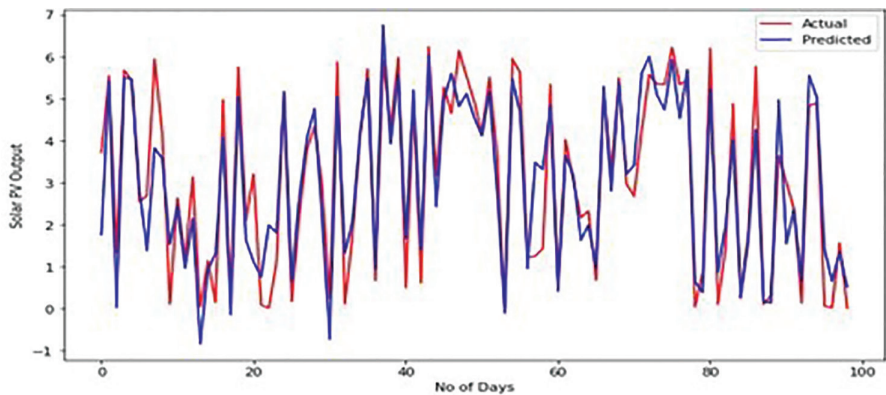


FIGURE 2.7
Predicted solar power generation with SVR.

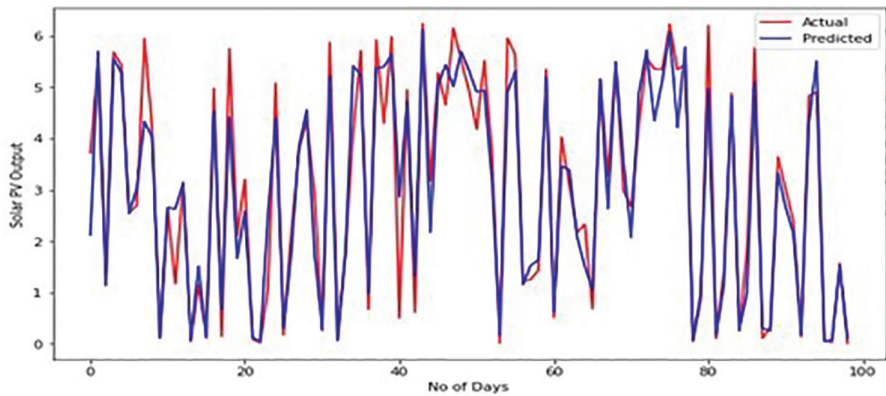


FIGURE 2.8
Predicted solar power generation with random forest.

From the values of absolute error obtained, it can be computed that the Neural Network is the most efficient technique for solar power output prediction. It is also visible from the output graphs that Neural Network matches the output most effectively.

Furthermore, we have analyzed the impact of parameters on solar power prediction. Figure 2.12 shows the percentage contribution of parameters on the solar output power. Based on the results obtained, we analyzed these results experimentally by excluding one of the most contributing parameters while training our most efficient model, that is, Neural Network.

The following plots depict the influence of different parameters (Zenith Angle and Air Temperature) on the accuracy of the outputs predicted.

Figure 2.13 was obtained after removing the highest contributing parameter that is Zenith Angle while training the Neural Network Model.

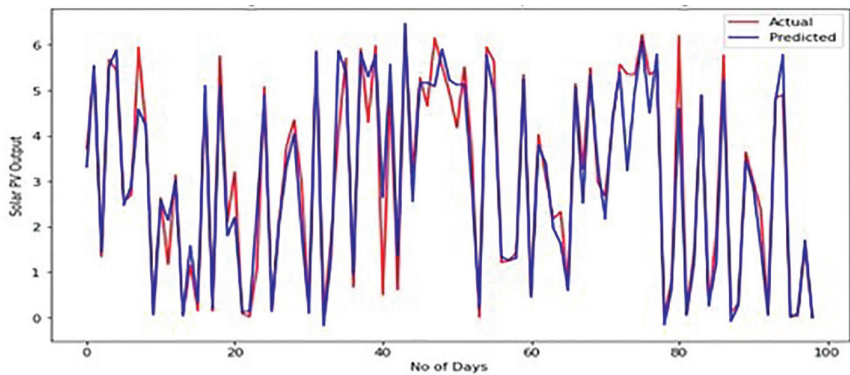


FIGURE 2.9
Predicted solar power generation with XGBoost.

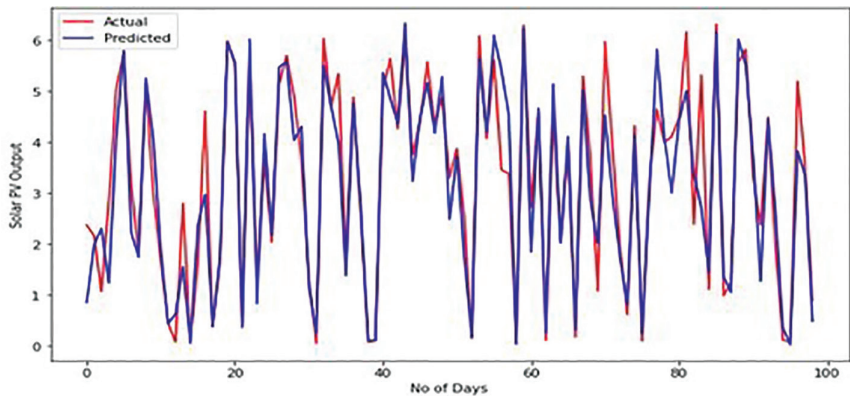


FIGURE 2.10
Predicted solar power generation with Neural Network.

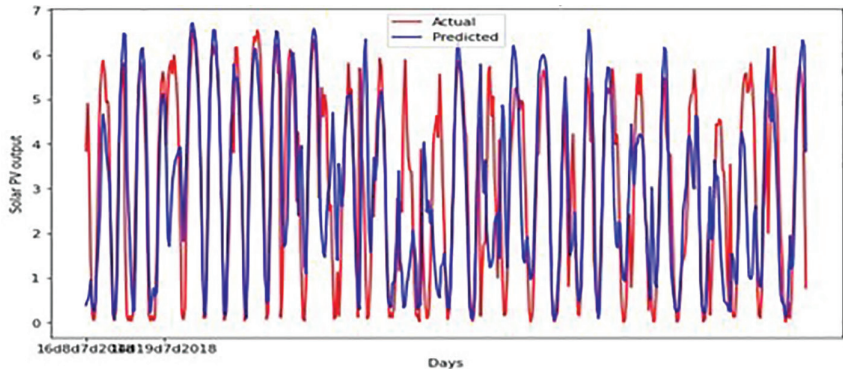


FIGURE 2.11
Predicted solar power generation with LSTM.

TABLE 2.4
Absolute Error in Different Techniques

Training Model Used	Absolute Error
SVR technique	0.39
Random forest technique	0.44
XG boost technique	0.42
Neural Network technique	0.34
LSTM technique	0.55

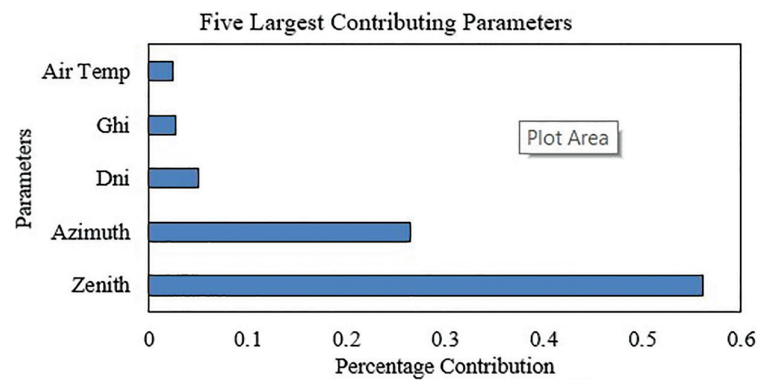


FIGURE 2.12
Top five most contributing parameters.

The results obtained showed a drastic downfall in the accuracy and high levels of error. Without Zenith Angle, the Neural Network shows an error of 0.70 in its performance.

Herein, the influence of Air Temperature is also depicted in Figure 2.14, showing its effect to be about 2.5%–5% on the accuracy which can be used to increase the output of the solar photovoltaic system. This is one interesting result as the air surrounding the solar panel can be cooled down using some techniques, and thus, it can be used to increase the efficiency of solar output.

2.7 Conclusion

The correlation matrix obtained gives an insight into the interdependency of various parameters with one another and this information is useful to prevent overfitting of data. Analysis of the plots obtained by keeping all the parameters while training the models gave high accuracy results but Neural Network held the crown of the highest accuracy. The results obtained after

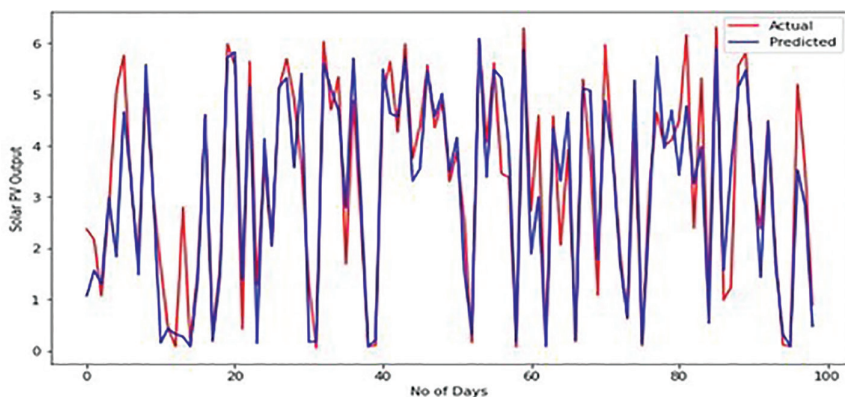


FIGURE 2.13

Predicted solar power generation with Neural Network without Zenith Angle.

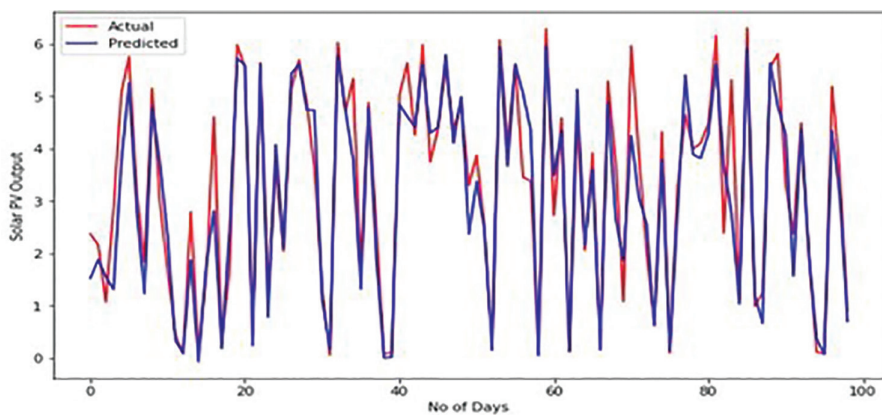


FIGURE 2.14

Predicted solar power generation with Neural Network without Air Temperature.

removing Zenith Angle showed drastic deviation from the one obtained before, pointing out that the Zenith Angle contributes at a high scale. The most interesting result as mentioned above was the one obtained after omitting Air Temperature during the training process. This result draws attention toward increasing solar panel's efficiency as Air Temperature around the panel can be decreased and thus performance can be increased. One such idea is being implemented in Vadodara, Gujarat where solar panels are being set up on canals. The idea is to keep the panels surrounding temperature low to increase their working efficiency. The canal on the other hand gets a symbiotic benefit of having its water prevented from evaporation, hence reducing water loss due to evaporation.

References

- T. W. Carlson, A schematic diagram of the terms “Azimuth” and “Altitude” as they relate to the viewing of celestial objects, Wikipedia, 2020.
- S. Dise, “What is the value of accurate solar forecasting for utility-scale PV plants?,” solaranywhere, 2017. [Online]. Available: <https://www.solaranywhere.com/2017/accurate-solar-forecasting-value/>. (Accessed 12-07-2021).
- E. Izgi, A. Öztöpal, B. Yerli, M. K. Kaymak and A. D. Şahin, “Short-mid-term solar power prediction by using artificial neural networks,” *Solar Energy*, vol. 86, no. 2, pp. 725–733, 2012.
- F. Jawaid and K. NazirJunejo, “Predicting daily mean solar power using machine learning regression techniques,” in *2016 Sixth International Conference on Innovative Computing Technology*, Dublin, Ireland, 2016.
- B. H. Khan, *Non Conventional Energy Resources*. Tata McGraw Education Private Limited, New Delhi, 2009.
- A. Khandakar, M. E. Chowdhury, M. K. Kazi, K. Benhmed, F. Touati, M. A. Hitmi and A. J. S. Gonzales, “Machine learning based photovoltaics (PV) power prediction using different environmental parameters of Qatar,” *Energies*, vol. 12, no. 14, p. 2782, 2019.
- S.-G. Kim, J.-Y. Jung and M. Sim, “A two step approach to solar power generation prediction based on weather data using machine learning,” in *BigDAS2018*, Zhengzhou, China, 2019.
- M. Krawczak, “Introduction to multilayer neural networks,” in *Multilayer Neural Networks*. Springer, Heidelberg, 2013, pp. 1–14.
- S. K. Mishra and B. Ram, “Steepest descent method,” in *Introduction to Unconstrained Optimization with R*. Springer, Singapore, 2019, pp. 131–173.
- D. Parbat and M. Chakraborty, “A python based support vector regression model for prediction of COVID19 cases in India,” *Chaos, Solitons & Fractals*, vol. 138, p. 109942, 2020.
- M. Rosa-Clot and G. M. Tina, “Chapter 2: Photovoltaic electricity,” in *Submerged and Floating Photovoltaic Systems*. Academic Press, Washington, DC, 2017, pp. 13–32.
- Solcast, [Online]. Available: <https://solcast.com/>.
- C. Voyant, G. Notton, S. Kalogirou, M. Nivet, C. Paoli, F. Motte and A. Foulliy, “Machine learning methods for solar radiation forecasting: A review,” *Renewable Energy*, vol. 105, no. 1, pp. 569–582, 2017.
- J. Zeng and W. Qiao, “Short-term solar power prediction using a support vector machine,” *Renewable Energy*, vol. 52, pp. 118–127, 2013.

3

Comprehensive Technique for Modeling of PV Module

Vandana Jha

C.V. Raman Global University

CONTENTS

Nomenclature	44
3.1 Introduction	44
3.2 Mathematical Modeling of Two-Diode Model of PV Module.....	47
3.3 Fundamental Calculation of the Parameters	49
3.3.1 Calculation of Photovoltaic Current.....	49
3.3.2 Calculation of Diode Ideality Constants	49
3.3.3 Calculation of Diode Reverse Saturation Currents.....	52
3.3.4 Calculation of Series and Parallel Resistances	52
3.3.4.1 Fitness Function	53
3.3.4.2 Initialization of Population.....	53
3.3.4.3 Constraints on Series and Parallel Resistances	54
3.3.4.4 Selection.....	54
3.3.4.5 Crossover.....	55
3.3.4.6 Mutation	55
3.4 Upgrading the Model.....	55
3.4.1 First Degree of Upgradation.....	55
3.4.1.1 Calculation of Upgraded Photovoltaic Current.....	55
3.4.1.2 Calculation of Upgraded Diode Ideality Constants.....	56
3.4.1.3 Calculation of Upgraded Diode Reverse Saturation Currents	57
3.4.1.4 Calculation of Upgraded Series and Parallel Resistances ...	57
3.4.2 Second Degree of Upgradation.....	57
3.5 Dependence of Parameters of the Characteristic Equation of PV Module on Irradiance and Temperature	58
3.6 Calculation of Parameters of the Characteristic Equation of PV Module at STC	58
3.7 Calculation of Parameters of the Characteristic Equation of PV Module at NOCTC	61
3.8 Validation of the Proposed Model.....	63
3.9 Conclusion	67
References.....	76

Nomenclature

- I_{PV} : Photovoltaic current of the PV module (A)
 I_{O1} : Reverse saturation or leakage current of diode 1 (A)
 I_{O2} : Reverse saturation or leakage current of diode 2 (A)
 A_1 : Ideality constant of diode 1
 A_2 : Ideality constant of diode 2
 R_S : Equivalent series resistance of the PV module (Ω)
 R_P : Equivalent parallel resistance of the PV module (Ω)
 V_T : Thermal voltage of the PV module (V)
 q : Electron charge ($1.60217646 \times 10^{-19}$ C)
 k : Boltzmann constant ($1.3806503 \times 10^{-23}$ J/K)
 G : Irradiance (W/m^2)
 T : Temperature of the PV module (K)
 N_S : Number of cells connected in series in the PV module
 P_{MPP} : Power of the PV module at the maximum power point (W)
 V_{MPP} : Voltage of the PV module at the maximum power point (V)
 I_{MPP} : Current of the PV module at the maximum power point (A)
 V_{OC} : Open-circuit voltage of the PV module (V)
 I_{SC} : Short-circuit current of the PV module (A)
 $K_{P_{MPP}}^G$: Irradiance coefficient of P_{MPP}
 $K_{P_{MPP}}^T$: Temperature coefficient of P_{MPP} (W/K)
 $K_{V_{MPP}}^G$: Irradiance coefficient of V_{MPP}
 $K_{V_{MPP}}^T$: Temperature coefficient of V_{MPP} (V/K)
 $K_{I_{MPP}}^T$: Temperature coefficient of I_{MPP} (A/K)
 $K_{V_{OC}}^G$: Irradiance coefficient of V_{OC}
 $K_{V_{OC}}^T$: Temperature coefficient of V_{OC} (V/K)
 $K_{I_{SC}}^T$: Temperature coefficient of I_{SC} (A/K)
 STC: Standard test condition
 NOCTC: Nominal operating cell temperature condition
-

3.1 Introduction

Global warming has directly or indirectly impacted almost every life form on the earth. In order to minimize the hazardous consequences of global warming which is majorly caused due to the pollution generated by fossil fuels, widespread utilization of renewable energy (clean energy) has come

into picture (Chennoufi et al., 2021; Meng et al., 2020). Out of all the renewable energy sources, solar photovoltaics (PVs) is the most popular form of renewable energy source because of many attractive qualities associated with its usefulness (AbuHussein and Sadi, 2020; Kumaresan and Govindaraju, 2020; Jha and Triar, 2019; Jha, 2021). First, solar PV system does not involve any movable component that makes it more or less maintenance free. Second, the PV module, which is the core element of the system, is composed of semiconductor material that can be manufactured with comparatively lesser resources. Lastly, the rapid advancement in the technologies of power electronic devices (which act as an interface between the modules and the grid or batteries) has led to the fall in manufacturing expenditure. The increasing demand and optimum utilization of solar PV energy have compelled the researchers to formulate various models and algorithms so as to estimate the performance of the PV system under different ambient conditions (Villalva et al., 2009; Jha and Triar, 2018). The accurate modeling of PV module is of great importance because it ensures the utility to take full advantage of the available solar energy and costly PV modules (Ishaque et al., 2011).

The modeling of PV module principally deals with the extraction of the unknown parameters and estimation of the curves of transcendental I - V and P - V equations of the PV module. Previously, analysts have proposed several techniques of parameter evaluation with different levels of complexity and accuracy based mostly on single-diode model of PV module. The single-diode model is the simplest model of the PV module in which a current source is connected in parallel to a diode (Tan et al., 2004; Kajihara and Harakawa, 2005). For improving the accuracy of the single-diode model, a series resistance and a parallel resistance have been added in the circuit, thus increasing the number of unknown parameters to five (Xiao et al., 2004; Walker, 2001; Khouzam et al., 1994). The simplicity of single-diode model lies in the fact that the recombination loss in the space charge region of the PV cell has been neglected. But, in actual practice, there is a considerable amount of recombination loss that cannot be overlooked. As a result, the single-diode model suffers from inaccuracy deficiency. For improvising the model's accuracy and precision, the recombination loss has been taken into account by including second diode in the circuit, which gives rise to the two-diode model (Gow and Manning, 1999; Chowdhury et al., 2007; Hovinen, 1994). The addition of an extra diode in the circuit increases the number of unknown parameters to seven. The key confrontation now is to evaluate the unknown parameters of the two-diode model while upholding a rational computational attempt.

Various numerical techniques, namely, iterative programming technique (Xiao et al., 2004; Walker, 2001), interpolation technique (Khouzam et al., 1994), resistive companion method (Liu and Dougal, 2002), nonlinear least square optimization method (Chegaar et al., 2001), and differential evolution technique (Ishaque and Salam, 2011), have been proposed in the literature to model the I - V equation of the single-diode model of PV module. The backbone of the concepts applied in these techniques is based on the truth that the generated I - V and P - V curves have to fit in to the manufacturer's catalog

curves particularly at three significant points, i.e., open-circuit voltage (V_{OC}), short-circuit current (I_{SC}), and maximum power point (P_{MPP}). The numerical techniques proposed in (Liu and Dougal, 2002; Chegaar et al., 2001; Ishaque and Salam, 2011) involved the implementation of many intricate and interrelated equations that have been solved either by long calculations or by making certain approximations due to which compromise has to be made between the computational time, effort, and accuracy of the proposed techniques.

Several techniques have been applied for extracting the unknown parameters of the two-diode model of PV module, viz. levenberg/merquardt curve fitting technique (Gow and Manning, 1999), the venin's theorem (Chowdhury et al., 2007), computational method (Hovinen, 1994), hybrid solution based on differential evolution technique (Chin et al., 2016), blended analytical and hybrid method (Chennoufi et al., 2021), iterative technique (Babu and Gurjar, 2014), explicit method based on Lambert W-function (Lun et al., 2015), advanced onlooker-ranking-based adaptive differential evolution technique (Muangkote et al., 2019) to name a few. But, many of the mentioned techniques undergo the disadvantage of unnecessary introduction of many new additional coefficients, which makes the process of extraction of parameters unnecessarily cumbersome.

Several authors have applied artificial intelligence (AI) techniques such as artificial neural network (ANN) (Mellit et al., 2007; Almonacid et al., 2010) and fuzzy logic (Lalouni and Rekioua, 2009) to extract the parameters of the PV module model. Intelligent and metaheuristic algorithms, for example, particle swarm optimization (PSO) (Bana and Saini, 2017), cat swarm optimization (Guo et al., 2016), evolutionary and hybrid evolutionary (Siddiqui and Abido, 2013; Muhsen et al., 2015), bacterial foraging (Rajasekar et al., 2013), pattern search (AlHajri et al., 2012), flower pollination (Alam et al., 2015), chaotic whale optimization (Oliva et al., 2017), teaching learning-based (Li et al., 2019), and simplex simplified swarm optimization (Yeh et al., 2018) algorithms have also been illustrated in the literature to model the I - V characteristics. Even though these methods produce accurate results and are having the merit of escaping the numerical complexity, they experience several limitations such as extensive computation due to huge population, data training, determination, and sensitivity of initial value and convergence unpredictability.

Keeping all the preceding discussion into consideration, this chapter presents an upgraded comprehensive technique for the calculation of parameters and modeling of the two-diode model of PV module. The major contribution of this work is the attainment of a high level of accuracy in calculating the seven unknown parameters of the nonlinear I - V equation of PV module taking just the manufacturer's specified data at standard test condition (STC) as input. The attainment of high level of accuracy has been accomplished due to the fact that the proposed technique does not consider any assumption and is based on the clean application of the versatile genetic algorithm theory on the mathematical equations of the PV module. Furthermore, a novel idea "degree of upgradation" has been introduced

that improves the accuracy of the calculated parameters up to the required degree. The accuracy of the proposed model has been authenticated for seven different economically existing PV modules of different types from a range of manufacturers. The experimental validation of the output characteristics of PV module at different ambient conditions generated by the proposed technique has also been done for SPM30 and ZONHAN PV modules. In addition, the accuracy of the proposed technique has been compared against three popular modeling techniques (Villalva et al., 2009; Ishaque et al., 2011; Walker, 2001) and the superiority of the proposed technique has been confirmed.

The flow of the chapter goes like this. The chapter begins with the illustration of the mathematical modeling of a two-diode model of PV module in Section 3.2. Section 3.3 deals with the concept of fundamental calculation of the parameters of PV module by the proposed technique. Section 3.4 describes the upgradation procedure of the proposed modeling technique. Section 3.5 explains the dependence of parameters of the characteristic equation of PV module on ambient conditions. The parameters of the characteristic equation of the PV module at STC and NOCTC are calculated in Sections 3.6 and 3.7, respectively. The procedure and results of datasheets (theoretical) and experimental validation of the proposed technique and the comparison of the proposed technique with three popular modeling techniques (Villalva et al., 2009; Ishaque et al., 2011; Walker, 2001) are described in Section 3.8. The chapter ends by providing concluding remarks in Section 3.9.

3.2 Mathematical Modeling of Two-Diode Model of PV Module

Figure 3.1 depicts the two-diode equivalent circuit of a PV module (Ishaque et al., 2011).

The I - V characteristic of a PV module is illustrated mathematically by eq. (3.1).

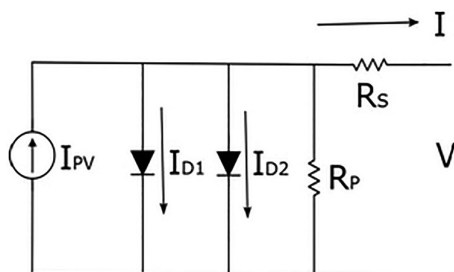


FIGURE 3.1

Two-diode equivalent circuit of a PV module.

$$I = I_{PV} - I_{O1} \left[\exp \left(\frac{V + R_S I}{V_T A_1} \right) - 1 \right] - I_{O2} \left[\exp \left(\frac{V + R_S I}{V_T A_2} \right) - 1 \right] - \left(\frac{V + R_S I}{R_p} \right) \quad (3.1)$$

$$V_T = N_s k T / q \quad (3.2)$$

The P - V characteristic of a PV module is expressed mathematically by eq. (3.3).

$$P = V \left[I_{PV} - I_{O1} \left\{ \exp \left(\frac{V + R_S I}{V_T A_1} \right) - 1 \right\} - I_{O2} \left\{ \exp \left(\frac{V + R_S I}{V_T A_2} \right) - 1 \right\} - \left(\frac{V + R_S I}{R_p} \right) \right] \quad (3.3)$$

The calculation of all the parameters of eq. (3.1) is a requisite for the analysis of the performance of the PV module (Villalva et al., 2009).

Manufacturer's catalogs usually furnish information concerning the parameters and characteristics of PV modules at STC, which is taken as 1,000 W/m² solar irradiance and 25°C module temperature. Several datasheets also provide information regarding PV modules at nominal operating cell temperature condition (NOCTC), which is normally considered 800 W/m² irradiance and 25°C ambient temperature.

Table 3.1 presents the values of the parameters of seven different economically existing PV modules at STC furnished by the manufacturers.

The values of the parameters mentioned in the manufacturer's catalogs are utilized for evaluating the vital parameters (I_{PV} , A_1 , A_2 , I_{O1} , I_{O2} , R_S and R_p) of eq. (3.3), so as to study the characteristics and performance of a PV module.

TABLE 3.1

Parameters of Seven Different Economically Existing PV Modules at STC Furnished by the Manufacturers

Parameter	Thin-Film		Monocrystalline		Multicrystalline		
	Power Foil						EVVO
	165	FS-280	SPM-30	BIL-325M	ND-AK275	GSP6 250	72GN 320
$R_{MPP\ STC}$ (W)	165	80	30	325	275	250	320
$V_{MPP\ STC}$ (V)	28	71.2	17.80	37.4	31.4	30.10	36.90
$I_{MPP\ STC}$ (A)	5.9	1.12	1.686	8.69	8.76	8.31	8.68
$V_{OC\ STC}$ (V)	38.1	91.5	22.2	45.8	38.5	37.5	45.70
$I_{SC\ STC}$ (A)	6.5	1.22	1.801	9.21	9.38	8.85	9.05
K_{MPP}^T (%/°C)	-0.25	-0.25	-0.48	-0.41	-0.41	-0.43	-0.38
K_{VOC}^T (%/°C)	-0.30	-0.25	-0.34	-0.31	-0.32	-0.33	-0.30
K_{ISC}^T (%/°C)	0.10	0.04	0.037	0.053	0.055	0.05	0.05
N_s	28	116	36	72	60	60	72

3.3 Fundamental Calculation of the Parameters

The proposed methodology efforts to extract the seven unknown parameters (I_{PV} , A_1 , A_2 , I_{O1} , I_{O2} , R_s and R_p) of a PV module.

Since the value of R_p is usually very high, $\left(\frac{V + R_s I}{R_p}\right)$ term of eq. (3.1) can be approximated to zero.

$$\left(\frac{V + R_s I}{R_p}\right) \approx 0 \quad (3.4)$$

From eqs. (3.1) and (3.4), eq. (3.5) is obtained.

$$I = I_{PV} - I_{O1} \left[\exp\left(\frac{V + R_s I}{V_T A_1}\right) - 1 \right] - I_{O2} \quad (3.5)$$

3.3.1 Calculation of Photovoltaic Current

Under short-circuit condition ($I = I_{SC}$ and $V = 0$), eq. (3.5) gets transformed into eq. (3.6).

$$I_{SC} = I_{PV} - I_{O1} \left[\exp\left(\frac{I_{SC} R_s}{V_T A_1}\right) - 1 \right] - I_{O2} \left[\exp\left(\frac{V + R_s I}{V_T A_2}\right) - 1 \right] \quad (3.6)$$

Since $\left(I_{O1} \left[\exp\left(\frac{I_{SC} R_s}{V_T A_1}\right) - 1 \right] \approx 0\right)$ and $\left(I_{O2} \left[\exp\left(\frac{I_{SC} R_s}{V_T A_2}\right) - 1 \right] \approx 0\right)$, eq. (3.6) can be expressed as

$$I_{PV} \approx I_{SC} \quad (3.7)$$

The photovoltaic current of a PV module is approximately equal to the short-circuit current at any ambient condition.

3.3.2 Calculation of Diode Ideality Constants

Under open-circuit condition ($I = 0$ and $V = V_{OC}$), eq. (3.5) gets transformed into eq. (3.8).

$$0 = I_{PV} - I_{O1} \left[\exp\left(\frac{V_{OC}}{V_T A_1}\right) - 1 \right] - I_{O2} \left[\exp\left(\frac{V_{OC}}{V_T A_2}\right) - 1 \right] \quad (3.8)$$

Approximating $I_{O1} \approx I_{O2} \approx I_O$ and $A_1 \approx A_2 \approx A$, eq. (3.8) can be written as

$$I_O = \frac{I_{PV}}{2 \left[\exp \left(\frac{V_{OC}}{V_{T^A}} \right) - 1 \right]} \quad (3.9)$$

$$P = VI \quad (3.10)$$

$$\frac{1}{V} \frac{dP}{dV} = \frac{dI}{dV} + \frac{I}{V} \quad (3.11)$$

According to the property of P - V characteristic of a PV module, at maximum power point (MPP), $dP/dV = 0$.

Applying MPP condition to eq. (3.11), eq. (3.12) is obtained.

$$\frac{dI}{dV} \Big|_{MPP} + \frac{I_{MPP}}{V_{MPP}} = 0 \quad (3.12)$$

Differentiating eq. (3.5) and applying MPP condition, eq. (3.13) is obtained.

$$\frac{dI}{dV} \Big|_{MPP} = \frac{-\frac{I_{O1}}{V_T A_1} \exp \left(\frac{V_{MPP} + I_{MPP} R_S}{V_T A_1} \right) - \frac{I_{O2}}{V_T A_2} \exp \left(\frac{V_{MPP} + I_{MPP} R_S}{V_T A_2} \right)}{1 + \frac{I_{O1}}{V_T A_1} R_S \exp \left(\frac{V_{MPP} + I_{MPP} R_S}{V_T A_1} \right) + \frac{I_{O2}}{V_T A_2} R_S \exp \left(\frac{V_{MPP} + I_{MPP} R_S}{V_T A_2} \right)} \quad (3.13)$$

Substituting eq. (3.13) in eq. (3.12), eq. (3.14) is obtained.

$$\begin{aligned} & I_{MPP} + (I_{MPP} R_S - V_{MPP}) \frac{I_{O1}}{V_T A_1} \exp \left(\frac{V_{MPP} + I_{MPP} R_S}{V_T A_1} \right) \\ & + (I_{MPP} R_S - V_{MPP}) \frac{I_{O2}}{V_T A_2} \exp \left(\frac{V_{MPP} + I_{MPP} R_S}{V_T A_2} \right) \\ & \left[1 + \frac{I_{O1}}{V_T A_1} R_S \exp \left(\frac{V_{MPP} + I_{MPP} R_S}{V_T A_1} \right) + \frac{I_{O2}}{V_T A_2} R_S \exp \left(\frac{V_{MPP} + I_{MPP} R_S}{V_T A_2} \right) \right] V_{MPP} = 0 \end{aligned} \quad (3.14)$$

For eq. (3.14) to be valid, the numerator of eq. (3.14) must be zero as the denominator is finite.

$$\begin{aligned} & I_{MPP} + (I_{MPP} R_S - V_{MPP}) \frac{I_{O1}}{V_T A_1} \exp \left(\frac{V_{MPP} + I_{MPP} R_S}{V_T A_1} \right) \\ & + (I_{MPP} R_S - V_{MPP}) \frac{I_{O2}}{V_T A_2} \exp \left(\frac{V_{MPP} + I_{MPP} R_S}{V_T A_2} \right) = 0 \end{aligned} \quad (3.15)$$

Approximating $I_{O1} \approx I_{O2} \approx I_O$ and $A_1 \approx A_2 \approx A$, eq. (3.15) can be written as

$$I_{MPP} + (I_{MPP}R_S - V_{MPP}) \frac{2I_O}{V_TA} \exp\left(\frac{V_{MPP} + I_{MPP}R_S}{V_TA}\right) = 0 \quad (3.16)$$

Applying MPP condition to eq. (3.5), approximating $I_{O1} \approx I_{O2} \approx I_O$, $A_1 \approx A_2 \approx A$ and rearranging terms, eqs. (3.17) and (3.18) are obtained.

$$\exp\left(\frac{V_{MPP} + I_{MPP}R_S}{V_TA}\right) = \frac{I_{PV} - I_{MPP} + 2I_O}{2I_O} \quad (3.17)$$

$$R_S = \frac{V_TA}{I_{MPP}} \ln\left(\frac{I_{PV} - I_{MPP} + 2I_O}{2I_O}\right) - \frac{V_{MPP}}{I_{MPP}} \quad (3.18)$$

Combining eqs. (3.17) and (3.18), eq. (3.19) is obtained.

$$(I_{PV} - I_{MPP} + 2I_O) \left\{ V_TA \ln\left(\frac{I_{PV} - I_{MPP} + 2I_O}{2I_O}\right) - 2V_{MPP} \right\} + V_TA I_{MPP} = 0 \quad (3.19)$$

Substituting eqs. (3.7) and (3.9) in eq. (3.19), eq. (3.20) is obtained.

$$f(A) = \left(I_{SC} - I_{MPP} + \frac{I_{SC}}{\left[\exp\left(\frac{V_{OC}}{V_TA}\right) - 1 \right]} \right) \left\{ V_TA \ln\left(\frac{I_{SC} - I_{MPP} + \frac{I_{SC}}{\left[\exp\left(\frac{V_{OC}}{V_TA}\right) - 1 \right]}}{I_{SC}} \right) - 2V_{MPP} \right\} + V_TA I_{MPP} = 0 \quad (3.20)$$

Putting the values of the parameters provided in the manufacturer's catalogs, the left-hand side of eq. (3.20) transforms into a function of "A" and it is denoted by $f(A)$.

$$f(A) = \left(I_{SC} - I_{MPP} + \frac{I_{SC}}{\left[\exp\left(\frac{V_{OC}}{V_T A}\right) - 1 \right]} \right) \left\{ V_T A \ln \left(\frac{I_{SC} - I_{MPP} + \frac{I_{SC}}{\left[\exp\left(\frac{V_{OC}}{V_T A}\right) - 1 \right]}}{I_{SC}} \right) - 2V_{MPP} \right\} + V_T A I_{MPP} \quad (3.21)$$

Thus, “ A ” is calculated by solving $f(A) = 0$ at any ambient condition.

It is evident that $\left(\frac{A_1 + A_2}{2}\right) \approx A$, where A_1 symbolizes diode ideality constant for diffusion current and A_2 symbolizes diode ideality constant for recombination current. According to Shockley’s diffusion theory, A_1 should be equal to unity. However, the value of A_2 is flexible (Ishaque et al., 2011).

3.3.3 Calculation of Diode Reverse Saturation Currents

With reference to eq. (3.9),

$$I_{O1} = \frac{I_{PV}}{2 \left[\exp\left(\frac{V_{OC}}{V_T A_1}\right) - 1 \right]} \quad (3.22)$$

$$I_{O2} = \frac{I_{PV}}{2 \left[\exp\left(\frac{V_{OC}}{V_T A_2}\right) - 1 \right]} \quad (3.23)$$

The reverse saturation currents of diodes 1 and 2 at any ambient condition can be evaluated by eqs. (3.22) and (3.23), respectively.

3.3.4 Calculation of Series and Parallel Resistances

The steps involved in the calculation of series resistance and parallel resistance are given next.

3.3.4.1 Fitness Function

The genetic algorithm requires a particular function called the fitness function to solve the equations. The property of P - V characteristic of a PV module that at maximum power point (MPP), $dP/dV = 0$, provides a perfect option for the fitness function. For expressing F as the fitness value to be minimized, eq. (3.12) can be rewritten as

$$\text{Minimize } F = \frac{-\frac{I_{O1}}{V_T A_1} \exp\left(\frac{V_{MPP} + I_{MPP} R_S}{V_T A_1}\right) - \frac{I_{O2}}{V_T A_2} \exp\left(\frac{V_{MPP} + I_{MPP} R_S}{V_T A_2}\right)}{1 + \frac{I_{O1}}{V_T A_1} R_S \exp\left(\frac{V_{MPP} + I_{MPP} R_S}{V_T A_1}\right) + \frac{I_{O2}}{V_T A_2} R_S \exp\left(\frac{V_{MPP} + I_{MPP} R_S}{V_T A_2}\right)} + \frac{I_{MPP}}{V_{MPP}} \quad (3.24)$$

$$\text{Minimize } F = I_{MPP} + (I_{MPP} R_S - V_{MPP}) \frac{I_{O1}}{V_T A_1} \exp\left(\frac{V_{MPP} + I_{MPP} R_S}{V_T A_1}\right) + (I_{MPP} R_S - V_{MPP}) \frac{I_{O2}}{V_T A_2} \exp\left(\frac{V_{MPP} + I_{MPP} R_S}{V_T A_2}\right) \left[1 + \frac{I_{O1}}{V_T A_1} R_S \exp\left(\frac{V_{MPP} + I_{MPP} R_S}{V_T A_1}\right) + \frac{I_{O2}}{V_T A_2} R_S \exp\left(\frac{V_{MPP} + I_{MPP} R_S}{V_T A_2}\right) \right] V_{MPP} \quad (3.25)$$

3.3.4.2 Initialization of Population

With reference to eq. (3.3) at MPP,

$$V_{MPP} I_{MPP} = P_{MPP} \quad (3.26)$$

$$V_{MPP} \left[I_{PV} - I_{O1} \left\{ \exp\left(\frac{V_{MPP} + R_S I_{MPP}}{V_T A_1}\right) - 1 \right\} - I_{O2} \left\{ \exp\left(\frac{V_{MPP} + R_S I_{MPP}}{V_T A_2}\right) - 1 \right\} - \left(\frac{V_{MPP} + R_S I_{MPP}}{R_p} \right) \right] = P_{MPP} \quad (3.27)$$

$$R_p = \frac{V_{MPP} (V_{MPP} + I_{MPP} R_s)}{V_{MPP} I_{PV} - V_{MPP} I_{O1} \exp\left(\frac{V_{MPP} + R_s I_{MPP}}{V_T A_1}\right) - V_{MPP} I_{O2} \exp\left(\frac{V_{MPP} + R_s I_{MPP}}{V_T A_2}\right) + V_{MPP} I_{O1} + V_{MPP} I_{O2} - P_{MPP}} \quad (3.28)$$

For every value of R_s , there is a value of R_p that satisfies eq. (3.28). The aim is to find an only pair of R_s and R_p for the specified ambient condition that fits the manufacturer's model most precisely.

3.3.4.3 Constraints on Series and Parallel Resistances

In order to confirm that the calculated values of R_s and R_p fall within a permissible range, constraints on the values of R_s and R_p should be imposed, that is,

$$R_s > 0 \quad \text{and} \quad R_s < \left[\frac{V_T A}{I_{MPP}} \ln\left(\frac{I_{PV} - I_{MPP} + 2I_O}{2I_O}\right) - \frac{V_{MPP}}{I_{MPP}} \right] \quad \text{and}$$

Putting $R_s = 0$, in eq. (3.28), the minimum possible value of R_p is obtained.

$$R_p \geq \frac{V_{MPP}}{I_{PV} - I_{O1} \exp\left(\frac{V_{MPP}}{V_T A_1}\right) - I_{O2} \exp\left(\frac{V_{MPP}}{V_T A_2}\right) + I_{O1} + I_{O2} - \frac{P_{MPP}}{V_{MPP}}}$$

3.3.4.4 Selection

Selection is the procedure of choosing two parents from the population to perform crossing. The probability of selection is computed as

$$\text{Prob}_i = \frac{f(x)_i}{\sum_{i=1}^n f(x)_i} \quad (3.29)$$

where n is the number of populations, $f(x)$ is the fitness value corresponding to a particular individual in the population, and $\sum f(x)$ is the summation of all the fitness value of the entire population.

The next step is to evaluate the expected count, which is expressed as

$$\text{Expected count} = \frac{f(x)_i}{[\text{Avg } f(x)]_i} \quad (3.30)$$

where

$$(\text{Avg } f(x))_i = \left[\frac{\sum_{i=1}^n f(x)_i}{n} \right]$$

The expected count for the entire population is calculated. The expected count suggests which population can be selected for further processing in the mating pool. After that, the actual count is obtained. On the basis of the actual count, the individuals are selected who would participate in the cross-over cycle using roulette wheel selection.

3.3.4.5 Crossover

Crossover operation is performed to produce new offspring. The crossover points are marked and on the basis of the crossover points, the multipoint crossover is executed, and new offspring are generated. The fitness values of the new offspring produced after crossover operations are calculated.

3.3.4.6 Mutation

Mutation flipping operation is performed to produce new offspring after the crossover operation. The fitness values of the new offspring produced after mutation operations are computed.

After the completion of selection, crossover and mutation operations, one generation is completed and the new population becomes all set to be tested. The average performances improve in the successive cycles of new population. Thus, an optimal pair of R_s and R_p is found for the specified ambient condition that fits the manufacturer's model accurately.

3.4 Upgrading the Model

The accuracy of the values of calculated parameters (I_{PV} , A_1 , A_2 , I_{O1} , I_{O2} , R_s and R_p) is upgraded up to the requisite degree by means of a novel idea "degree of upgradation."

3.4.1 First Degree of Upgradation

3.4.1.1 Calculation of Upgraded Photovoltaic Current

Under short-circuit condition ($I = I_{SC}$ and $V = 0$), eq. (3.1) gets transformed into eq. (3.31).

$$I_{SC} = I_{PV1st} - I_{O11st} \left[\exp\left(\frac{I_{SC}R_S}{V_T A_{11st}}\right) - 1 \right] - I_{O21st} \left[\exp\left(\frac{I_{SC}R_S}{V_T A_{21st}}\right) - 1 \right] - \frac{R_S I_{SC}}{R_P} \quad (3.31)$$

$$\text{Since } \left(I_{O11st} \left[\exp\left(\frac{I_{SC}R_S}{V_T A_{11st}}\right) - 1 \right] \approx 0 \right) \quad \text{and} \quad \left(I_{O21st} \left[\exp\left(\frac{I_{SC}R_S}{V_T A_{21st}}\right) - 1 \right] \approx 0 \right),$$

eq. (3.31) can be written as

$$I_{PV1st} \approx I_{SC} \left(1 + \frac{R_S}{R_P} \right) \quad (3.32)$$

Eq. (3.32) gives the first degree of upgraded value of photovoltaic current of a PV module (I_{PV1st}) at any ambient condition.

3.4.1.2 Calculation of Upgraded Diode Ideality Constants

Under open-circuit condition ($I = 0$ and $V = V_{OC}$), eq. (3.1) gets transformed into eq. (3.33).

$$0 = I_{PV1st} - I_{O11st} \left[\exp\left(\frac{V_{OC}}{V_T A_{11st}}\right) - 1 \right] - I_{O21st} \left[\exp\left(\frac{V_{OC}}{V_T A_{21st}}\right) - 1 \right] - \frac{V_{OC}}{R_P} \quad (3.33)$$

Approximating $I_{O11st} \approx I_{O21st} \approx I_{O1st}$ and $A_{11st} \approx A_{21st} \approx A_{1st}$, eq. (3.33) can be written as

$$I_{O1st} = \frac{I_{PV1st} - \frac{V_{OC}}{R_P}}{2 \left[\exp\left(\frac{V_{OC}}{V_T A_{1st}}\right) - 1 \right]} \quad (3.34)$$

Applying the same technique on eq. (3.1), as has been applied on eq. (3.5) to evaluate the diode ideality constant, an upgraded and more precise value of diode ideality constant is attained, because both R_S and R_P are taken into consideration.

The function $f(A_{1st})$, where A_{1st} is the first degree of upgraded value of diode ideality constant, transforms into,

$$f(A_{1st}) = \left\{ R_p \left[I_{SC} \left(1 + \frac{R_S}{R_p} \right) - I_{MPP} + \frac{I_{SC} \left(1 + \frac{R_S}{R_p} \right) - \frac{V_{OC}}{R_p}}{\exp \left(\frac{V_{OC}}{V_T A_{1st}} \right) - 1} \right] - (V_{MPP} + R_S I_{MPP}) \right\} \\ \times (-V_{MPP} + R_S I_{MPP}) - V_T A_{1st} (V_{MPP} - R_p I_{MPP} - R_S I_{MPP}) \quad (3.35)$$

Thus, “ A_{1st} ” is calculated by solving $f(A_{1st}) = 0$ at any ambient condition.

Again, it is evident that $\left(\frac{A_{11st} + A_{21st}}{2} \right) \approx A_{1st}$, A_{11st} should be equal to unity and the value of A_{21st} is flexible (Ishaque et al., 2011).

3.4.1.3 Calculation of Upgraded Diode Reverse Saturation Currents

With reference to eq. (3.34),

$$I_{O11st} = \frac{I_{PV1st} - \frac{V_{OC}}{R_p}}{2 \left[\exp \left(\frac{V_{OC}}{V_T A_{11st}} \right) - 1 \right]} \quad (3.36)$$

$$I_{O21st} = \frac{I_{PV1st} - \frac{V_{OC}}{R_p}}{2 \left[\exp \left(\frac{V_{OC}}{V_T A_{21st}} \right) - 1 \right]} \quad (3.37)$$

The first degree of upgraded value of reverse saturation currents of diodes 1 and 2 at any ambient condition can be evaluated by eqs. (3.36) and (3.37), respectively.

3.4.1.4 Calculation of Upgraded Series and Parallel Resistances

Following the same process as has been followed to calculate R_S and R_p , but with I_{PV1st} , A_{11st} , A_{21st} , I_{O11st} , and I_{O21st} as inputs, the first degree of upgraded values of series resistance (R_{S1st}) and parallel resistance (R_{p1st}) for the specified ambient condition can be evaluated.

3.4.2 Second Degree of Upgradation

Substituting $R_S = R_{S1st}$ and $R_p = R_{p1st}$ in eqs. (3.32) and (3.35), a second degree of upgraded value of photovoltaic current (I_{PV2nd}) and diode ideality constants of diodes 1 and 2 (A_{12nd} and A_{22nd}) can be evaluated. Consequently, a second

degree of upgraded value of reverse saturation currents of diodes 1 and 2 (I_{O12nd} and I_{O22nd}), series resistance (R_{S2nd}), and parallel resistance (R_{P2nd}) can be evaluated. The upgradation can go forward up to i th degree (I_{PVith} , A_{1ith} , A_{2ith} , I_{O1ith} , I_{O2ith} , R_{Sith} , and R_{Pith}), until the percentage error between the values of parameters calculated by the proposed technique and the values of parameters specified in manufacturer's datasheet approaches a minimum specified value inputted by the user (Tolerance (ϵ)).

3.5 Dependence of Parameters of the Characteristic Equation of PV Module on Irradiance and Temperature

The V_{OC} , I_{SC} , V_{MPP} , I_{MPP} and P_{MPP} of the PV module depend strongly on both solar irradiance and temperature which can be expressed as

$$V_{OC} = \left(1 + K_{V_{OC}}^G (\log(G / G_{STC}))\right) (V_{OC_{STC}} + K_{V_{OC}}^T \Delta T) \quad (3.38)$$

$$I_{SC} = \frac{G}{G_{STC}} (I_{SC_{STC}} + K_{I_{SC}}^T \Delta T) \quad (3.39)$$

$$V_{MPP} = \left(1 + K_{V_{MPP}}^G (\log(G / G_{STC}))\right) (V_{MPP_{STC}} + K_{V_{MPP}}^T \Delta T) \quad (3.40)$$

$$I_{MPP} = \frac{G}{G_{STC}} (I_{MPP_{STC}} + K_{I_{MPP}}^T \Delta T) \quad (3.41)$$

$$P_{MPP} = \frac{G}{G_{STC}} \left(1 + K_{P_{MPP}}^G (\log(G / G_{STC}))\right) (P_{MPP_{STC}} + K_{P_{MPP}}^T \Delta T) \quad (3.42)$$

$$\Delta T = T - T_{STC} \quad (3.43)$$

3.6 Calculation of Parameters of the Characteristic Equation of PV Module at STC

The flowchart for the calculation of seven unknown parameters of a PV module at STC ($I_{PV_{STC}}$, $A_{1_{STC}}$, $A_{2_{STC}}$, $I_{O1_{STC}}$, $I_{O2_{STC}}$, $R_{S_{STC}}$ and $R_{P_{STC}}$) is illustrated in Figure 3.2.

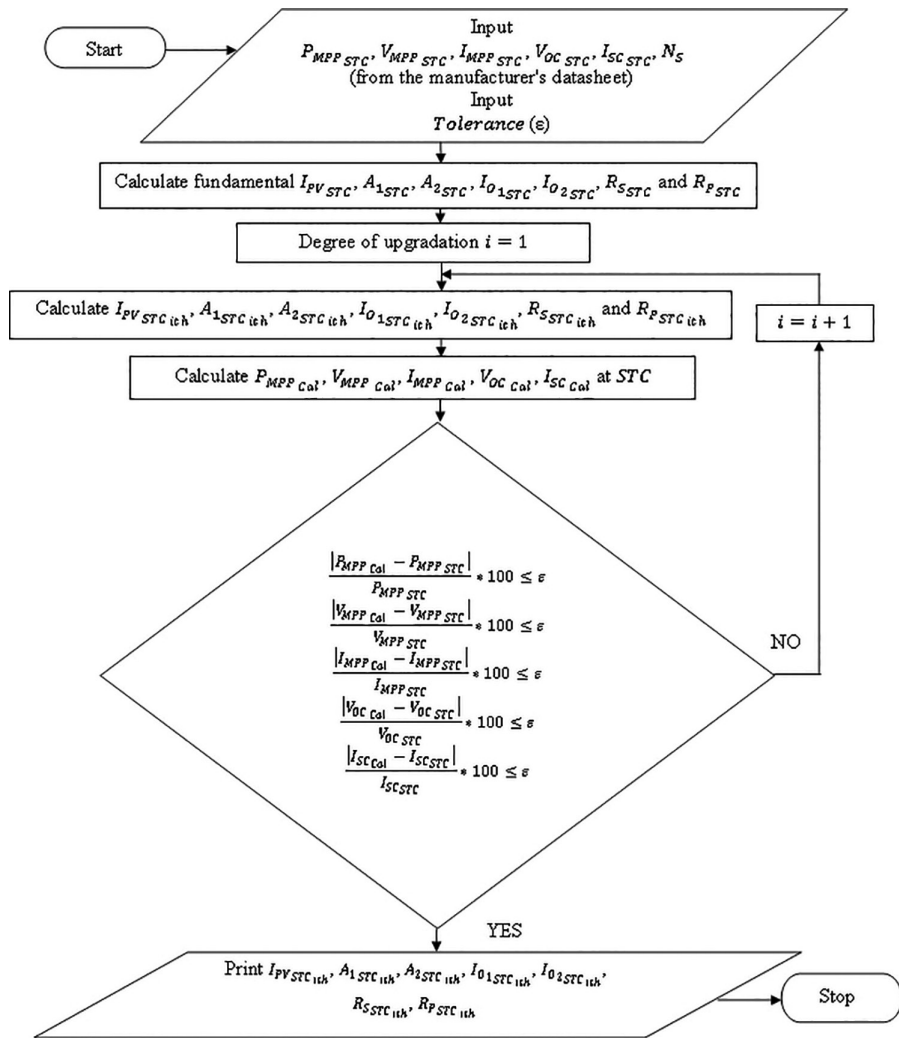


FIGURE 3.2

Flowchart for calculation of seven unknown parameters of a PV module at STC.

Table 3.2 represents the calculated parameters of seven different economically existing PV modules for the proposed model, R_s model (Walker, 2001), $R_s - R_p$ model (Villalva et al., 2009), and conventional two-diode model (Ishaque et al., 2011) at STC by MATLAB® code.

TABLE 3.2
Calculated Parameters of Seven Different Economically Existing PV Modules for the Proposed Model, R_s Model, $R_s - R_p$ Model and Conventional Two-Diode Model at STC

Model	Parameter	Thin-Film			Monocrystalline			Multicrystalline		
		Power Foil 165	FS-280	SPM-30	BIL-325M	ND-AK275	GSP6 250	EVVO 72GN 320		
Proposed model	$I_{PV\ STC}$ (A)	6.5000	1.2200	1.8010	9.2100	9.3800	8.8500	9.0500		
	A_{1STC}	1.0000	1.0000	1.0000	1.0000	1.0000	1.0000	1.0000		
	A_{2STC}	5.6790	2.9266	1.4328	1.2658	1.7625	1.3388	0.4992		
	I_{01STC} (A)	3.2439×10^{-23}	2.8312×10^{-14}	3.3937×10^{-11}	0.8142×10^{-10}	0.668×10^{-10}	1.2057×10^{-10}	0.8445×10^{-10}		
	I_{02STC} (A)	2.8958×10^{-4}	1.6960×10^{-5}	4.7791×10^{-8}	1.4743×10^{-8}	3.2894×10^{-6}	0.5685×10^{-7}	1.4561×10^{-21}		
	R_{SSTC} (Ω)	0.7356	4.3584	0.7606	0.2710	0.1496	0.2817	0.5024		
	R_{PSTC} (Ω)	2,037.9571	8,544.5077	6,728.5016	7,652.7443	9,990.2319	3,463.7967	4,508.7442		
R_s model	A_{11st}	1.0000	1.0000	1.0000	1.0000	1.0000	1.0000	1.0000		
	A_{21st}	5.5512	2.6698	1.3838	1.2470	1.7498	1.3048	0.4676		
	$I_{PV\ STC}$ (A)	6.5000	1.2200	1.8010	9.2100	9.3800	8.8500	9.0500		
	A_{3TC}	2.1609	1.1496	1.0367	1.0230	1.0480	1.0361	1.0047		
	I_{0STC} (A)	1.4764×10^{-10}	3.0834×10^{-12}	1.5909×10^{-10}	2.8433×10^{-10}	4.2021×10^{-10}	5.6295×10^{-10}	1.9000×10^{-10}		
	R_{SSTC} (Ω)	1.0840	10.4722	1.0449	0.3406	0.3094	0.3529	0.3292		
	I_{PVSTC} (A)	6.5000	1.2200	1.8010	9.2100	9.3800	8.8500	9.0500		
$R_s - R_p$ model	A_{3TC}	2.1609	1.1496	1.0367	1.0230	1.0480	1.0361	1.0047		
	I_{0STC} (A)	1.4764×10^{-10}	3.0834×10^{-12}	1.5909×10^{-10}	2.8433×10^{-10}	4.2021×10^{-10}	5.6295×10^{-10}	1.9000×10^{-10}		
	R_{SSTC} (Ω)	0.9620	8.8620	0.8950	0.3100	0.2510	0.3120	0.3300		
	R_{PSTC} (Ω)	151.3759	1,982.3952	724.6910	586.5250	199.5228	315.3556	104,930.794324		
	$I_{PV\ STC}$ (A)	6.5000	1.2200	1.8010	9.2100	9.3800	8.8500	9.0500		
	A_{1STC}	1.0000	1.0000	1.0000	1.0000	1.0000	1.0000	1.0000		
	A_{2STC}	1.2000	1.2000	1.2000	1.2000	1.2000	1.2000	1.2000		
Conventional two-diode model	I_{01STC} (A)	6.4879×10^{-23}	5.6625×10^{-14}	6.7873×10^{-11}	1.6284×10^{-10}	1.3359×10^{-10}	2.4113×10^{-10}	1.6890×10^{-10}		
	I_{02STC} (A)	6.4879×10^{-23}	5.6625×10^{-14}	6.7873×10^{-11}	1.6284×10^{-10}	1.3359×10^{-10}	2.4113×10^{-10}	1.6890×10^{-10}		
	R_{SSTC} (Ω)	1.2800	9.7000	0.9300	0.3200	0.2700	0.3300	0.3800		
	R_{PSTC} (Ω)	86.3506	1,708.5435	688.2362	603.6194	194.1622	340.8771	98.7159		

3.7 Calculation of Parameters of the Characteristic Equation of PV Module at NOCTC

The irradiance coefficients of V_{OC} , V_{MPP} and P_{MPP} ($K_{V_{OC}}^G$, $K_{V_{MPP}}^G$ and $K_{P_{MPP}}^G$) and temperature coefficients of V_{MPP} , I_{MPP} and P_{MPP} ($K_{V_{MPP}}^T$, $K_{I_{MPP}}^T$ and $K_{P_{MPP}}^T$) can be calculated by substituting the manufacturer given data at STC and NOCTC in eqs. (3.38)–(3.43).

Following equations are proposed for evaluating the first degree of upgraded values of seven unknown parameters of a PV module at NOCTC.

$$I_{PV\ NOCTC1st} \approx \left(\frac{G_{NOCTC}}{G_{STC}} (I_{SCSTC} + K_{I_{SC}}^T \Delta T) \right) \left(1 + \frac{R_{S_{NOCTC}}}{R_{P_{NOCTC}}} \right) \quad (3.44)$$

$$\begin{aligned} f(A_{NOCTC1st}) = & \left\{ R_{P_{NOCTC}} \left[\left(\frac{G_{NOCTC}}{G_{STC}} (I_{SCSTC} + K_{I_{SC}}^T \Delta T) \right) \left(1 + \frac{R_{S_{NOCTC}}}{R_{P_{NOCTC}}} \right) - \left(\frac{G_{NOCTC}}{G_{STC}} (I_{MPPSTC} + K_{I_{MPP}}^T \Delta T) \right) \right. \right. \\ & + \frac{\left(\frac{G_{NOCTC}}{G_{STC}} (I_{SCSTC} + K_{I_{SC}}^T \Delta T) \left(1 + \frac{R_{S_{NOCTC}}}{R_{P_{NOCTC}}} \right) - \left(\left(1 + K_{V_{OC}}^G (\log(G_{NOCTC}/G_{STC})) \right) (V_{OCSTC} + K_{V_{OC}}^T \Delta T) \right) \right)}{\left[\exp \left(\frac{\left(\left(1 + K_{V_{OC}}^G (\log(G_{NOCTC}/G_{STC})) \right) (V_{OCSTC} + K_{V_{OC}}^T \Delta T) \right)}{V_{T_{NOCTC}} A_{NOCTC1st}} \right) - 1 \right]} \left. \right] \\ & - \left(\left(\left(1 + K_{V_{MPP}}^G (\log(G_{NOCTC}/G_{STC})) \right) (V_{MPPSTC} + K_{V_{MPP}}^T \Delta T) \right) + R_{S_{NOCTC}} \left(\frac{G_{NOCTC}}{G_{STC}} (I_{MPPSTC} + K_{I_{MPP}}^T \Delta T) \right) \right) \right\} \\ & - V_{T_{NOCTC}} A_{NOCTC1st} \left[\left(\left(1 + K_{V_{MPP}}^G (\log(G_{NOCTC}/G_{STC})) \right) (V_{MPPSTC} + K_{V_{MPP}}^T \Delta T) \right) \right. \\ & \left. - R_{P_{NOCTC}} \left(\frac{G_{NOCTC}}{G_{STC}} (I_{MPPSTC} + K_{I_{MPP}}^T \Delta T) \right) - R_{S_{NOCTC}} \left(\frac{G_{NOCTC}}{G_{STC}} (I_{MPPSTC} + K_{I_{MPP}}^T \Delta T) \right) \right] \end{aligned} \quad (3.45)$$

$$I_{O1_{NOCTC1st}} =$$

$$\frac{\left(\frac{G_{NOCTC}}{G_{STC}} (I_{SCSTC} + K_{I_{SC}}^T \Delta T) \right) \left(1 + \frac{R_{S_{NOCTC}}}{R_{P_{NOCTC}}} \right) - \frac{\left(\left(1 + K_{V_{OC}}^G (\log(G_{NOCTC}/G_{STC})) \right) (V_{OCSTC} + K_{V_{OC}}^T \Delta T) \right)}{R_{P_{NOCTC}}}}{2 \left[\exp \left(\frac{\left(\left(1 + K_{V_{OC}}^G (\log(G_{NOCTC}/G_{STC})) \right) (V_{OCSTC} + K_{V_{OC}}^T \Delta T) \right)}{V_{T_{NOCTC}} A_{NOCTC1st}} \right) - 1 \right]} \quad (3.46)$$

$$I_{O2NOCTC1st} =$$

$$\frac{\left(\frac{G_{NOCTC}}{G_{STC}} (I_{SCSTC} + K_{ISC}^T \Delta T) \right) \left(1 + \frac{R_{SNOCTC}}{R_{PNOCTC}} \right) - \frac{\left((1 + K_{VOC}^G (\log(G_{NOCTC}/G_{STC}))) (V_{OCSTC} + K_{VOC}^T \Delta T) \right)}{R_{PNOCTC}}}{\left[2 \exp \left(\frac{\left((1 + K_{VOC}^G (\log(G_{NOCTC}/G_{STC}))) (V_{OCSTC} + K_{VOC}^T \Delta T) \right)}{V_{TNOCTC} A_{2NOCTC1st}} \right) - 1 \right]} \quad (3.47)$$

$$R_{PNOCTC1st} = \frac{X}{Y} \quad (3.48)$$

$$\begin{aligned} X = & \left((1 + K_{VMPP}^G (\log(G_{NOCTC}/G_{STC}))) (V_{MPPSTC} + K_{VMPP}^T \Delta T) \right) \\ & \left(\left((1 + K_{VMPP}^G (\log(G_{NOCTC}/G_{STC}))) (V_{MPPSTC} + K_{VMPP}^T \Delta T) \right) + \left(\frac{G_{NOCTC}}{G_{STC}} (I_{MPPSTC} + K_{IMPP}^T \Delta T) \right) R_{SNOCTC1st} \right) \\ Y = & \left((1 + K_{VMPP}^G (\log(G_{NOCTC}/G_{STC}))) (V_{MPPSTC} + K_{VMPP}^T \Delta T) \right) \left(\left(\frac{G_{NOCTC}}{G_{STC}} (I_{SCSTC} + K_{ISC}^T \Delta T) \right) \left(1 + \frac{R_{SNOCTC}}{R_{PNOCTC}} \right) \right) \\ & - \left((1 + K_{VMPP}^G (\log(G_{NOCTC}/G_{STC}))) (V_{MPPSTC} + K_{VMPP}^T \Delta T) \right) \\ & \left(\frac{\frac{G_{NOCTC}}{G_{STC}} (I_{SCSTC} + K_{ISC}^T \Delta T) / \left(1 + \frac{R_{SNOCTC}}{R_{PNOCTC}} \right) - \frac{\left((1 + K_{VOC}^G (\log(G_{NOCTC}/G_{STC}))) (V_{OCSTC} + K_{VOC}^T \Delta T) \right)}{R_{PNOCTC}}}{\left[\exp \left(\frac{\left((1 + K_{VOC}^G (\log(G_{NOCTC}/G_{STC}))) (V_{OCSTC} + K_{VOC}^T \Delta T) \right)}{V_{TNOCTC} A_{1NOCTC1st}} \right) - 1 \right]} \right) \\ & \exp \left[\frac{\left(\left((1 + K_{VMPP}^G (\log(G_{NOCTC}/G_{STC}))) (V_{MPPSTC} + K_{VMPP}^T \Delta T) \right) + \left(\frac{G_{NOCTC}}{G_{STC}} (I_{MPPSTC} + K_{IMPP}^T \Delta T) \right) R_{SNOCTC1st} \right)}{V_{TNOCTC} A_{1NOCTC1st}} \right] \\ & - \left((1 + K_{VMPP}^G (\log(G_{NOCTC}/G_{STC}))) (V_{MPPSTC} + K_{VMPP}^T \Delta T) \right) \\ & \left(\frac{\left(\frac{G_{NOCTC}}{G_{STC}} (I_{SCSTC} + K_{ISC}^T \Delta T) \right) \left(1 + \frac{R_{SNOCTC}}{R_{PNOCTC}} \right) - \frac{\left((1 + K_{VOC}^G (\log(G_{NOCTC}/G_{STC}))) (V_{OCSTC} + K_{VOC}^T \Delta T) \right)}{R_{PNOCTC}}}{2 \left[\exp \left(\frac{\left((1 + K_{VOC}^G (\log(G_{NOCTC}/G_{STC}))) (V_{OCSTC} + K_{VOC}^T \Delta T) \right)}{V_{TNOCTC} A_{2NOCTC1st}} \right) - 1 \right]} \right) \\ & \exp \left[\frac{\left(\left((1 + K_{VMPP}^G (\log(G_{NOCTC}/G_{STC}))) (V_{MPPSTC} + K_{VMPP}^T \Delta T) \right) + \left(\frac{G_{NOCTC}}{G_{STC}} (I_{MPPSTC} + K_{IMPP}^T \Delta T) \right) R_{SNOCTC1st} \right)}{V_{TNOCTC} A_{2NOCTC1st}} \right] \end{aligned}$$

$$\begin{aligned}
& \left(\left(1 + K_{V_{MPP}}^G \left(\log(G_{NOCTC}/G_{STC}) \right) \right) \left(V_{MPP_{STC}} + K_{V_{MPP}}^T \Delta T \right) \right) \\
& \left(\frac{\left(\frac{G_{NOCTC}}{G_{STC}} \left(I_{SC_{STC}} + K_{I_{SC}}^T \Delta T \right) \right) \left(1 + \frac{R_{S_{NOCTC}}}{R_{P_{NOCTC}}} \right) - \frac{\left(\left(1 + K_{V_{OC}}^G \left(\log(G_{NOCTC}/G_{STC}) \right) \right) \left(V_{OC_{STC}} + K_{V_{OC}}^T \Delta T \right) \right)}{R_{P_{NOCTC}}}}{2 \left[\exp \left(\frac{\left(\left(1 + K_{V_{OC}}^G \left(\log(G_{NOCTC}/G_{STC}) \right) \right) \left(V_{OC_{STC}} + K_{V_{OC}}^T \Delta T \right) \right)}{V_{NOCTC} A_{1NOCTC1st}} \right) - 1 \right]} \right) \\
& + \left(\left(1 + K_{V_{MPP}}^G \left(\log(G_{NOCTC}/G_{STC}) \right) \right) \left(V_{MPP_{STC}} + K_{V_{MPP}}^T \Delta T \right) \right) \\
& \left(\frac{\left(\frac{G_{NOCTC}}{G_{STC}} \left(I_{SC_{STC}} + K_{I_{SC}}^T \Delta T \right) \right) \left(1 + \frac{R_{S_{NOCTC}}}{R_{P_{NOCTC}}} \right) - \frac{\left(\left(1 + K_{V_{OC}}^G \left(\log(G_{NOCTC}/G_{STC}) \right) \right) \left(V_{OC_{STC}} + K_{V_{OC}}^T \Delta T \right) \right)}{R_{P_{NOCTC}}}}{2 \left[\exp \left(\frac{\left(\left(1 + K_{V_{OC}}^G \left(\log(G_{NOCTC}/G_{STC}) \right) \right) \left(V_{OC_{STC}} + K_{V_{OC}}^T \Delta T \right) \right)}{V_{NOCTC} A_{1NOCTC1st}} \right) - 1 \right]} \right) \\
& - \left(\frac{G_{NOCTC}}{G_{STC}} \left(1 + K_{P_{MPP}}^G \left(\log(G_{NOCTC}/G_{STC}) \right) \right) \left(P_{MPP_{STC}} + K_{P_{MPP}}^T \Delta T \right) \right)
\end{aligned}$$

Table 3.3 represents the calculated parameters of seven different economically existing PV modules for the proposed model at NOCTC by MATLAB code.

It is a truism that the characteristics and performances of a PV module depend strongly on the ambient condition. It can be concluded from Tables 3.2 and 3.3 that the values of all the parameters of the characteristic equation of PV module calculated by the proposed technique vary with irradiance and temperature. As a result, the proposed technique proves to be highly accurate in predicting the characteristics and performances of PV module in comparison to conventional techniques where the parameters are supposed to be constant (Villalva et al., 2009; Ishaque et al., 2011; Walker, 2001).

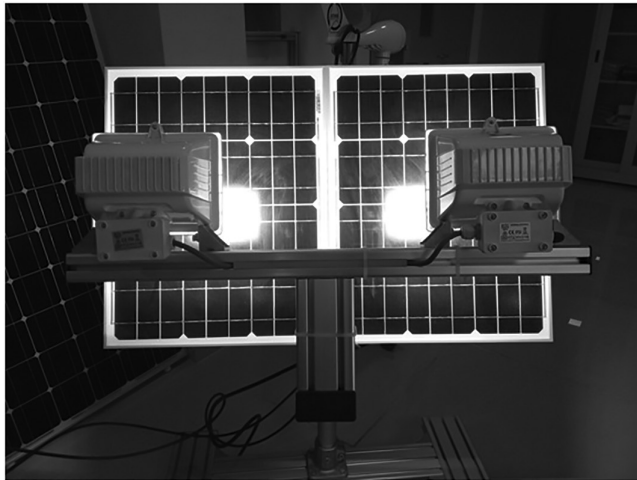
3.8 Validation of the Proposed Model

The I - V and P - V characteristics generated by the MATLAB code of the proposed modeling for SPM30 PV module have been experimentally validated. The irradiance and temperature for the proposed modeling were inputted as 400 W/m² and 35°C, respectively, which are according to the irradiance and temperature of the experimental set up (shown in Figure 3.3) at C.V. Raman Global University, India.

Figure 3.4a and b represents the characteristics of I - V and P - V , respectively, generated by the MATLAB code of the proposed modeling for SPM30 PV

TABLE 3.3
Calculated Parameters of Seven Different Economically Existing PV Modules for the Proposed Model at NOCTC

Parameter	Thin-film			Monocrystalline			Multicrystalline		
	Power Foil 165	FS-280	SPM-30	BIL-325M	ND-AK275	GSP6 250	EVVO 72GN 320		
K_{VMPP}^T	0.0000	-0.2200	-0.0727	-0.1650	-0.1300	-0.0950	-0.1365		
K_{VMPP}^T	-0.0012	0.00025	-0.0003	-0.0045	0.0032	-0.0011	0.0016		
K_{VMPP}^G	-0.2358	0.0589	-0.0533	0.0690	-0.0304	-0.1029	-0.0277		
K_{VOC}^G	-0.0232	0.0940	-0.0000	0.1001	0.0542	0.0671	0.0258		
$I_{PV\ NOCTC}\ (A)$	5.3040	0.9838	1.4514	7.4461	7.5865	7.1508	7.3124		
$A_{1\ NOCTC}$	1.0000	1.0000	1.0000	1.0000	1.0000	1.0000	1.0000		
$A_{2\ NOCTC}$	8.2942	2.6854	1.4812	1.7718	1.4904	1.6334	0.5014		
$I_{01\ NOCTC}\ (A)$	2.2809×10^{-20}	2.3523×10^{-12}	1.1416×10^{-9}	4.2780×10^{-9}	3.0275×10^{-9}	5.5680×10^{-9}	2.9322×10^{-9}		
$I_{02\ NOCTC}\ (A)$	1.86×10^{-2}	4.6270×10^{-5}	1.0357×10^{-6}	4.5343×10^{-5}	3.7472×10^{-6}	1.8961×10^{-5}	1.3268×10^{-18}		
$R_{S\ NOCTC}\ (\Omega)$	0.0351	3.3064	0.7646	0.10876	0.1845	0.0869	0.5771		
$R_{P\ NOCTC}\ (\Omega)$	1,049.5685	5,125.9030	1,482.7873	3,745.7565	3,692.4197	2,739.8060	1,114.3677		

**FIGURE 3.3**

Experimental setup for validation of proposed modeling for SPM30 PV module.

module plotted along with the experimental data at 400 W/m^2 and 35°C . The experimental data are depicted by the circular markers in Figure 3.4. It can be observed that the characteristics generated by the proposed model are adequately matching the experimental points.

The I - V and P - V characteristics generated by the MATLAB code of the proposed modeling for ZONHAN PV module have also been experimentally validated. The values of the parameters of ZONHAN PV module mentioned on the manufacturer's name plate at STC are $P_{\text{MPP}} = 5 \text{ W}$, $V_{\text{MPP}} = 17.5 \text{ V}$, $I_{\text{MPP}} = 0.29 \text{ A}$, $V_{\text{OC}} = 22.0 \text{ V}$ and $I_{\text{SC}} = 0.31 \text{ A}$. The irradiance and temperature for the proposed modeling were inputted according to the irradiance and temperature of the experimental set up (shown in Figure 3.5) at C.V. Raman Global University, India.

Figure 3.6a and b illustrates, respectively, the I - V and P - V characteristics generated by the MATLAB code of the proposed modeling for ZONHAN PV module with varying irradiance from 200 to $1,200 \text{ W/m}^2$ at 25°C . Figure 3.7a and b show the I - V and P - V curves, respectively, for ZONHAN PV module with varying temperature from 0°C to 75°C at $1,000 \text{ W/m}^2$. The experimental points are marked by the asterisk markers in Figures 3.6 and 3.7. It can be inferred that the proposed theoretical curves are accurate as the majority of experimental points are falling along the theoretical curves.

Tables 3.4–3.9 represent the comparison of R_s model, $R_s - R_p$ model, conventional two-diode model, and proposed model outputs with manufacturer's datasheets specified values for six different economically existing PV modules.

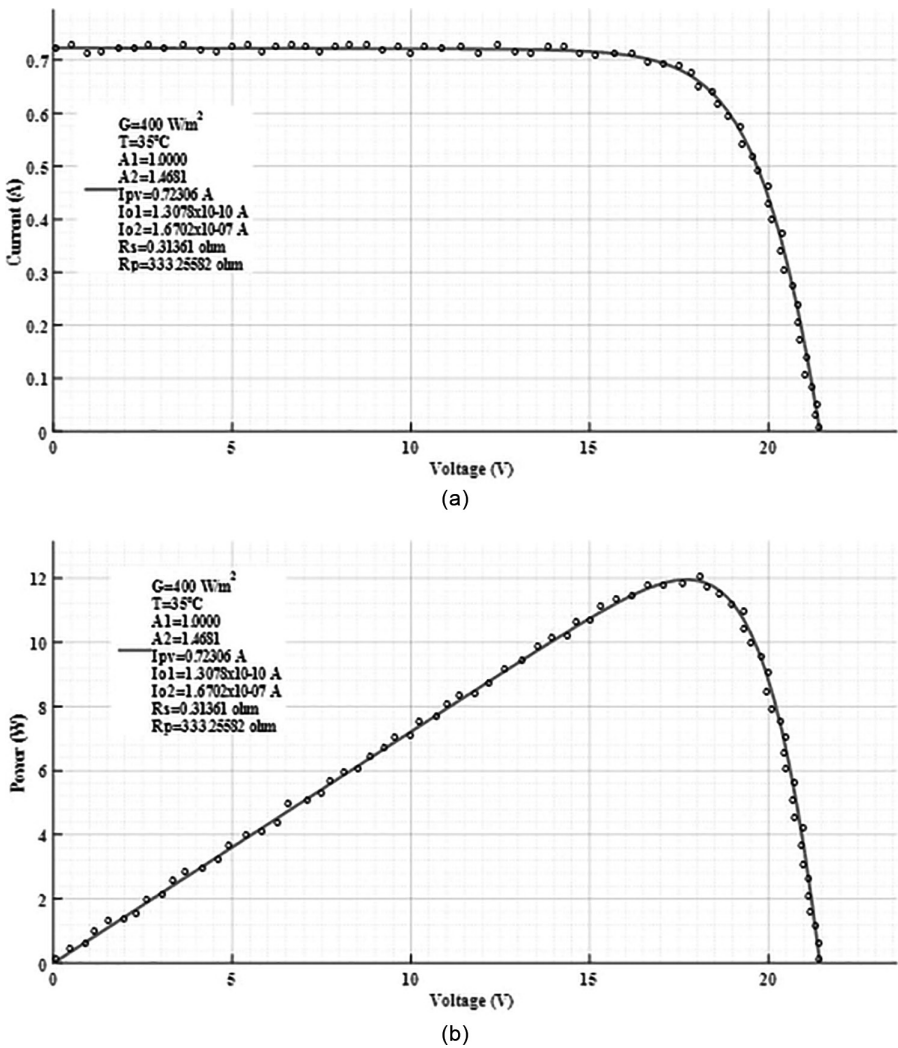
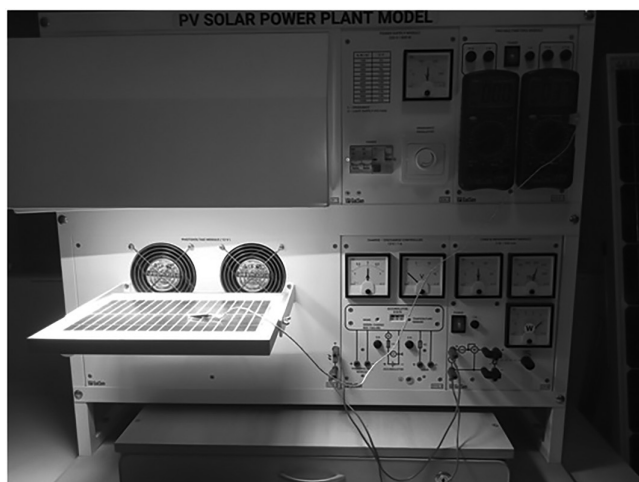


FIGURE 3.4
(a) I – V characteristic and experimental data of SPM30 PV module at 400 W/m^2 and 35°C . (b) P – V characteristic and experimental data of SPM30 PV module at 400 W/m^2 and 35°C .

It can be deduced from Tables 3.4–3.9 that the proposed model is far more accurate in comparison to traditional models (Villalva et al., 2009; Ishaque et al., 2011; Walker, 2001) because the values of percentage errors between the model outputs and datasheet values are very small for the proposed model in comparison to conventional models. The absolute value of percentage error in the case of proposed model falls below 0.5%.

**FIGURE 3.5**

Experimental setup for validation of proposed modeling for ZONHAN PV module.

3.9 Conclusion

In this chapter, an upgraded comprehensive technique for calculation of parameters and modeling of the two-diode model of PV module is presented. The proposed PV module modeling technique outshines the other modeling schemes previously available because the proposed technique does not consider any assumption and is based on the pure application of the versatile genetic algorithm theory on the mathematical equations of the PV module. Additionally, a novel idea “degree of upgradation” has been introduced that improves the accuracy of the calculated parameters of the nonlinear I – V equation of the two-diode model of PV module up to the required degree. The proposed technique characterizes to be very robust due to its capability of calculating the unknown parameters and generating the output curves of the PV module at any ambient condition with great accuracy, taking merely the manufacturer’s specified data at standard test condition as input. The accuracy of the proposed technique has been tested for seven different economically existing PV modules by calculating the percentage error of determinable parameters (power, voltage and current at maximum power point, open circuit voltage, and short circuit current) between the proposed model outputs and the manufacturer’s specified PV module datasheet values at STC and NOCTC. The percentage errors for three other popular modeling techniques have also been calculated. The proposed technique has been found to be highly accurate in comparison to three other existing modeling techniques

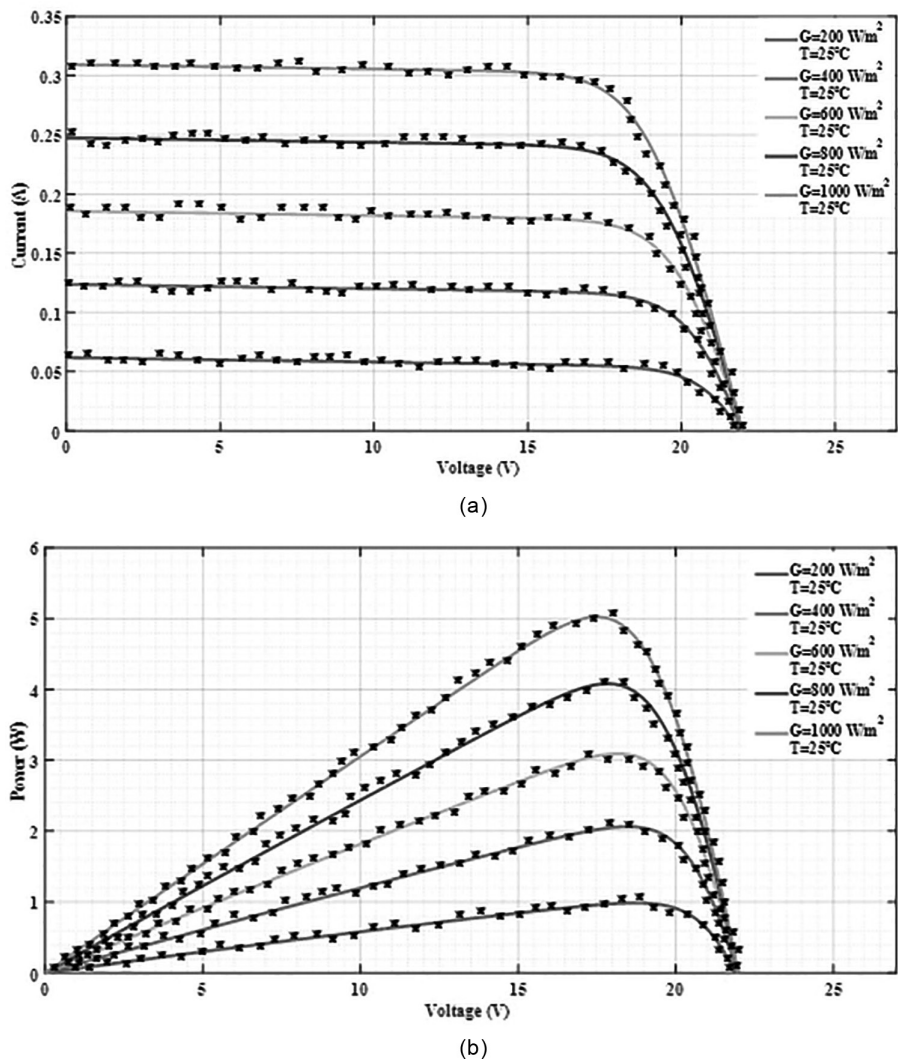


FIGURE 3.6
(a) *I-V* characteristics and experimental data of ZONHAN PV module at different irradiances (temperature constant=25°C). (b) *P-V* characteristics and experimental data of ZONHAN PV module at different irradiances (temperature constant=25°C).

especially when the PV module experiences irradiance and temperature variations. The experimental authentication of the *I-V* and *P-V* characteristics of PV module at different ambient conditions generated by the proposed technique have also been accomplished for SPM30 and ZONHAN PV modules.

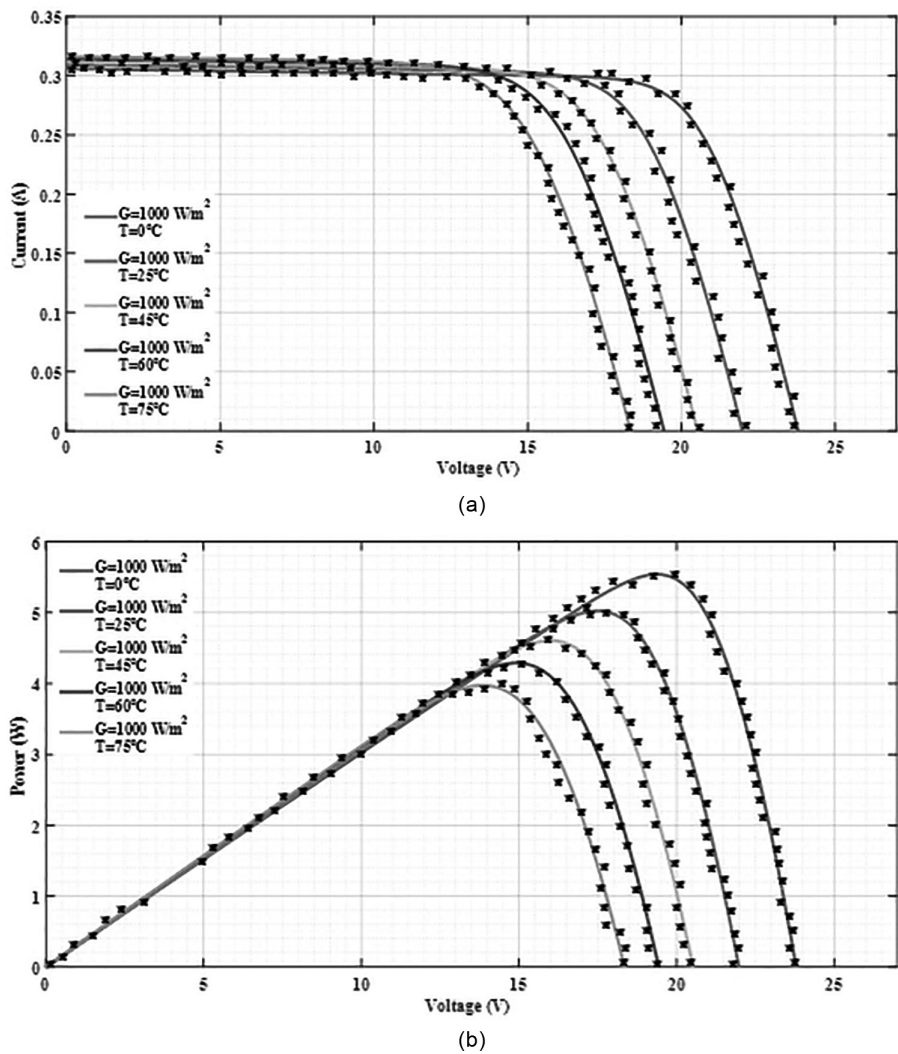


FIGURE 3.7
(a) I - V characteristics and experimental data of ZONHAN PV module at different temperatures (irradiance constant= $1,000 \text{ W/m}^2$). (b) P - V characteristics and experimental data of ZONHAN PV module at different temperatures (irradiance constant= $1,000 \text{ W/m}^2$).

The curves generated by the proposed technique specifically fit very accurately at significant points. The proposed modeling technique because of its accuracy, robustness, and ease of application is predicted to be a highly useful tool for PV power converter designs and circuit simulator synthesis.

TABLE 3.4
Comparison of Conventional Models and Proposed Model Outputs with Manufacturer’s Datasheet for Power Foil 165 PV Module

Ambient Conditions	Parameter	Datasheet Value	R_s		$R_s - R_p$		Conventional Two-Diode Model Value		Proposed Model Value		Error R_s Model (%)		Error Conventional Two-Diode Model (%)		Error Proposed Model (%)	
			Model Value	Model Value	Model Value	Model Value	Model Value	Model Value	Model Value	Model Value	Model (%)	Model (%)	Model (%)	Model (%)	Model (%)	Model (%)
STC (25°C and 1,000 W / m ²)	$R_{MP\ STC}$ (W)	165	165.7088	165.2001	165.1575	165.0009	165.1575	165.0009	165.0009	0.4296	0.1213	0.0955	0.0005	0.0005	0.0005	0.0005
	$V_{MP\ STC}$ (V)	28	27.4320	28.1940	28.1940	28.0995	28.1940	28.0995	28.0995	-2.0286	0.6929	0.6929	0.3554	0.3554	0.3554	0.3554
	$I_{MP\ STC}$ (A)	5.9	6.0407	5.8594	5.8579	5.8723	5.8579	5.8723	5.8723	2.3847	-0.6881	-0.7136	-0.4695	-0.4695	-0.4695	-0.4695
	$V_{OC\ STC}$ (V)	38.1	38.1000	38.1000	38.1000	38.1000	38.1000	38.1000	38.1000	0.0000	0.0000	0.0000	0.0000	0.0000	0.0000	0.0000
	$I_{SC\ STC}$ (A)	6.5	6.5000	6.4590	6.4051	6.5000	6.4051	6.5000	6.5000	0.0000	-0.6308	-1.4600	0.0000	0.0000	0.0000	0.0000
NOCTC (45°C and 800 W / m ²)	$R_{MP\ STC}$ (W)	132	126.7170	125.2055	127.9112	132.0013	127.9112	132.0013	132.0013	-4.0023	-5.1473	-3.0976	0.0010	0.0010	0.0010	0.0010
	$V_{MP\ STC}$ (V)	28.0	25.7861	26.5024	26.8605	28.0800	26.8605	28.0800	28.0800	-7.9068	-5.3486	-4.0696	0.2857	0.2857	0.2857	0.2857
	$I_{MP\ STC}$ (A)	4.7	4.9142	4.7243	4.7621	4.7009	4.7621	4.7009	4.7009	4.5574	0.5170	1.3213	0.0191	0.0191	0.0191	0.0191
	$V_{OC\ STC}$ (V)	36	35.8140	35.8140	35.8140	36.0000	35.8140	36.0000	36.0000	-0.5167	-0.5167	-0.5167	0.0000	0.0000	0.0000	0.0000
	$I_{SC\ STC}$ (A)	5.3	5.3040	5.2705	5.2265	5.3007	5.2265	5.3007	5.3007	0.0755	-0.5566	-1.3868	0.0132	0.0132	0.0132	0.0132

TABLE 3.5
Comparison of Conventional Models and Proposed Model Outputs with Manufacturer's Datasheet for FS-280 PV Module

Ambient Conditions	Parameter	Datasheet Value	R_s		$R_s - R_p$		Conventional Two-Diode Model Value		Proposed Model Value		Error R_s Model (%)		Error Conventional Two-Diode Model (%)		Error Proposed Model (%)	
			Model Value	Model Value	Model Value	Model Value	Model Value	Model Value	Model Value	Model Value	Model (%)	Model (%)	Model (%)	Model (%)	Model (%)	Model (%)
STC (25°C and 1,000 W/m ²)	$P_{MPP\ STC}$ (W)	80	80.1140	79.7450	79.7448	79.7448	80.0010	80.0010	80.0010	80.0010	0.1425	-0.3187	-0.3190	-0.3190	0.0013	0.0013
	$V_{MPP\ STC}$ (V)	71.2	69.5400	71.3700	71.3700	71.3700	71.3700	71.3700	71.3700	71.3700	-2.3315	0.2388	0.2388	0.2388	0.2388	0.2388
	$I_{MPP\ STC}$ (A)	1.12	1.1521	1.1173	1.1173	1.1173	1.1209	1.1209	1.1209	1.1209	2.8661	-0.2411	-0.2411	-0.2411	0.0804	0.0804
	$V_{OC\ STC}$ (V)	91.5	91.5000	91.5000	91.5000	91.5000	91.5000	91.5000	91.5000	91.5000	0.0000	0.0000	0.0000	0.0000	0.0000	0.0000
	$I_{SC\ STC}$ (A)	1.22	1.2200	1.2146	1.2131	1.2131	1.2200	1.2200	1.2200	1.2200	0.0000	-0.4426	-0.5656	-0.5656	0.0000	0.0000
NOCTC (45°C and 800 W/m ²)	$P_{MPP\ STC}$ (W)	60	61.1615	60.2673	60.5103	60.5103	60.0330	60.0330	60.0330	60.0330	1.9358	0.4455	0.8505	0.8505	0.0550	0.0550
	$V_{MPP\ STC}$ (V)	66.8	66.0630	67.8015	67.8015	67.8015	66.7552	66.7552	66.7552	66.7552	-1.1033	1.4993	1.4993	1.4993	-0.0671	-0.0671
	$I_{MPP\ STC}$ (A)	0.9	0.9258	0.8889	0.8925	0.8925	0.8993	0.8993	0.8993	0.8993	2.8667	-1.2333	-0.8333	-0.8333	-0.0778	-0.0778
	$V_{OC\ STC}$ (V)	85.1	86.9250	86.9250	86.9250	86.9250	85.1000	85.1000	85.1000	85.1000	2.1445	2.1445	2.1445	2.1445	0.0000	0.0000
	$I_{SC\ STC}$ (A)	1	0.9838	0.9794	0.9783	0.9783	0.9882	0.9882	0.9882	0.9882	-1.6200	-2.0600	-2.1700	-2.1700	-1.1800	-1.1800

TABLE 3.7
Comparison of Conventional Models and Proposed Model Outputs with Manufacturer's Datasheet for ND-AK275 PV Module

Ambient Conditions	Parameter	Datasheet Value	R_s		$R_s - R_p$		Conventional Two-Diode Model Value		Proposed Model Value		Error R_s Model (%)		Error $R_s - R_p$ Model (%)		Conventional Two-Diode Model (%)		Error Proposed Model (%)	
			Model Value	Model Value	Model Value	Model Value	Model Value	Model Value	Model Value	Model Value	Model (%)	Model (%)	Model (%)	Model (%)	Model (%)	Model (%)	Model (%)	Model (%)
STC (25°C and 1,000 W/m ²)	$P_{MPP\ STC}$ (W)	275	275.3614	275.0621	275.0251	274.9806	275.0251	274.9806	274.9806	274.9806	0.1314	0.0226	0.0226	0.0091	0.0091	0.0091	-0.0071	-0.0071
	$V_{MPP\ STC}$ (V)	31.4	31.1850	31.5700	31.5700	31.4115	31.5700	31.4115	31.4115	31.4115	-0.6847	0.5414	0.5414	0.5414	0.5414	0.5414	0.0366	0.0366
	$I_{MPP\ STC}$ (A)	8.76	8.8299	8.7128	8.7116	8.7541	8.7116	8.7541	8.7541	8.7541	0.7979	-0.5388	-0.5388	-0.5525	-0.5525	-0.5525	-0.0674	-0.0674
	$V_{OC\ STC}$ (V)	38.5	38.5000	38.5000	38.5000	38.5000	38.5000	38.5000	38.5000	38.5000	0.0000	0.0000	0.0000	0.0000	0.0000	0.0000	0.0000	0.0000
	$I_{SC\ STC}$ (A)	9.38	9.3800	9.3682	9.3670	9.3800	9.3670	9.3800	9.3800	9.3800	0.0000	-0.1258	-0.1258	-0.1386	-0.1386	-0.1386	0.0000	0.0000
NOCT (45°C and 800 W/m ²)	$P_{MPP\ STC}$ (W)	203.33	203.8640	202.6561	202.8152	203.3308	202.8152	203.3308	203.3308	203.3308	0.2626	-0.3314	-0.3314	-0.2532	-0.2532	-0.2532	0.0004	0.0004
	$V_{MPP\ STC}$ (V)	28.8	28.4684	28.8288	28.8288	28.8090	28.8288	28.8090	28.8090	28.8090	-1.1514	0.1000	0.1000	0.1000	0.1000	0.1000	0.0313	0.0313
	$I_{MPP\ STC}$ (A)	7.06	7.1611	7.0296	7.0352	7.0579	7.0352	7.0579	7.0579	7.0579	1.4320	-0.4306	-0.4306	-0.3513	-0.3513	-0.3513	-0.0297	-0.0297
	$V_{OC\ STC}$ (V)	35.6	36.0360	36.0360	36.0360	35.6000	36.0360	35.6000	35.6000	35.6000	1.2247	1.2247	1.2247	1.2247	1.2247	1.2247	0.0000	0.0000
	$I_{SC\ STC}$ (A)	7.58	7.5865	7.5770	7.5760	7.5802	7.5760	7.5802	7.5802	7.5802	0.0858	-0.0396	-0.0396	-0.0528	-0.0528	-0.0528	0.0026	0.0026

TABLE 3.8
Comparison of Conventional Models and Proposed Model Outputs with Manufacturer's Datasheet for GSP6 250 PV Module

Ambient Conditions	Parameter	Datasheet Value	R_s		$R_s - R_p$		Conventional Two-Diode Model Value		Proposed Model Value		Error R_s Model (%)		Error $R_s - R_p$ Model (%)		Conventional Two-Diode Model (%)		Error Proposed Model (%)	
			Model Value	Model Value	Model Value	Model Value	Model Value	Model Value	Model Value	Model Value	Model (%)	Model (%)	Model (%)	Model (%)	Model (%)	Model (%)	Model (%)	Model (%)
STC (25°C and 1000W/m ²)	$R_{MPP\ STC}$ (W)	250	250.1838	250.1315	250.0717	249.9882	250.0717	250.0717	249.9882	250.0717	0.0735	0.0526	0.0526	0.0287	0.0287	0.0287	0.0287	-0.0047
	$V_{MPP\ STC}$ (V)	30.10	30.0000	30.3750	30.0000	30.0780	30.0000	30.0000	30.0780	30.0780	-0.3322	0.9136	0.9136	-0.3322	-0.3322	-0.3322	-0.3322	-0.0731
	$I_{MPP\ STC}$ (A)	8.31	8.3395	8.2348	8.3357	8.3113	8.3357	8.3357	8.3113	8.3113	0.3550	-0.9049	-0.9049	0.3093	0.3093	0.3093	0.3093	0.0156
	$V_{OC\ STC}$ (V)	37.5	37.5000	37.5000	37.5000	37.5000	37.5000	37.5000	37.5000	37.5000	0.0000	0.0000	0.0000	0.0000	0.0000	0.0000	0.0000	0.0000
	$I_{SC\ STC}$ (A)	8.85	8.8500	8.8413	8.8414	8.8500	8.8414	8.8414	8.8500	8.8500	0.0000	-0.0983	-0.0983	-0.0972	-0.0972	-0.0972	-0.0972	0.0000
NOCT (45°C and 800W/m ²)	$R_{MPP\ STC}$ (W)	187	184.6959	184.0831	184.1685	186.9969	184.1685	184.1685	186.9969	186.9969	-1.2321	-1.5598	-1.5598	-1.5142	-1.5142	-1.5142	-1.5142	-0.0017
	$V_{MPP\ STC}$ (V)	28.2	27.6698	27.6698	27.6698	28.2200	27.6698	27.6698	28.2200	28.2200	-1.8801	-1.8801	-1.8801	-1.8801	-1.8801	-1.8801	-1.8801	0.0709
	$I_{MPP\ STC}$ (A)	6.63	6.6750	6.6529	6.6560	6.6264	6.6560	6.6560	6.6264	6.6264	0.6787	0.3454	0.3454	0.3922	0.3922	0.3922	0.3922	-0.0543
	$V_{OC\ STC}$ (V)	34.5	35.0250	35.0250	35.0250	34.5000	35.0250	35.0250	34.5000	34.5000	1.5217	1.5217	1.5217	1.5217	1.5217	1.5217	1.5217	0.0000
	$I_{SC\ STC}$ (A)	7.04	7.1508	7.1437	7.1439	7.0416	7.1439	7.1439	7.0416	7.0416	1.5739	1.4730	1.4730	1.4759	1.4759	1.4759	1.4759	0.0227

TABLE 3.9
Comparison of Conventional Models and Proposed Model Outputs with Manufacturer's Datasheet for EVVO 72GN 320 PV Module

Ambient Conditions	Parameter	Datasheet Value	R_s		$R_s - R_p$		Conventional Two-Diode Model Value		Proposed Model Value		Error R_s Model (%)		Error $R_s - R_p$ Model (%)		Conventional Two-Diode Model (%)		Error Proposed Model (%)	
			Model Value	Model Value	Model Value	Model Value	Model Value	Model Value	Model Value	Model Value	Model (%)	Model (%)	Model (%)	Model (%)	Model (%)	Model (%)	Model (%)	Model (%)
STC (25°C and 1,000 W / m ²)	$P_{MPP\ STC}$ (W)	320	320.6647	320.5903	320.2813	320.0010	320.0010	320.0010	320.0010	320.0010	0.2077	0.1845	0.0879	0.0003	0.0879	0.0003	0.0003	0.0003
	$V_{MPP\ STC}$ (V)	36.90	37.4740	37.4740	37.0170	36.9103	36.9103	36.9103	36.9103	36.9103	1.5556	1.5556	0.3171	0.0279	0.3171	0.0279	0.0279	0.0279
	$I_{MPP\ STC}$ (A)	8.68	8.5570	8.5550	8.6523	8.6697	8.6697	8.6697	8.6697	8.6697	-1.4171	-1.4401	-0.3191	-0.1187	-0.3191	-0.1187	-0.1187	-0.1187
	$V_{OC\ STC}$ (V)	45.70	45.7000	45.7000	45.7000	45.7000	45.7000	45.7000	45.7000	45.7000	0.0000	0.0000	0.0000	0.0000	0.0000	0.0000	0.0000	0.0000
	$I_{SC\ STC}$ (A)	9.05	9.0500	9.0500	9.1277	9.0500	9.0500	9.0500	9.0500	9.0500	0.0000	0.0000	0.8586	0.0000	0.8586	0.0000	0.0000	0.0000
NOCTC (45°C and 800 W / m ²)	$P_{MPP\ STC}$ (W)	238.01	238.2641	238.2121	238.5512	238.0186	238.0186	238.0186	238.0186	238.0186	0.1068	0.0849	0.2274	0.0036	0.2274	0.0036	0.0036	0.0036
	$V_{MPP\ STC}$ (V)	34.17	34.7960	34.7960	34.3664	34.1680	34.1680	34.1680	34.1680	34.1680	1.8320	1.8320	0.5748	-0.0059	0.5748	-0.0059	-0.0059	-0.0059
	$I_{MPP\ STC}$ (A)	6.97	6.8475	6.8460	6.9414	6.9661	6.9661	6.9661	6.9661	6.9661	-1.7575	-1.7791	-0.4103	-0.0560	-0.4103	-0.0560	-0.0560	-0.0560
	$V_{OC\ STC}$ (V)	42.71	42.9580	42.9580	42.9580	42.7100	42.7100	42.7100	42.7100	42.7100	0.5807	0.5807	0.5807	0.0000	0.5807	0.0000	0.0000	0.0000
	$I_{SC\ STC}$ (A)	7.30	7.3124	7.3124	7.3803	7.3026	7.3026	7.3026	7.3026	7.3026	0.1699	0.1699	1.1000	0.0356	1.1000	0.0356	0.0356	0.0356

References

- A. AbuHussein, M.A.H. Sadi. (2020). Fault ride-through capability improvement of grid connected PV system using dynamic voltage restorer. *Electric Power Components and Systems*, 48(12–13), 1296–1307. doi: 10.1080/15325008.2020.1854374.
- D.F. Alam, D.A. Yousri, M.B. Eteiba. (2015). Flower pollination algorithm based solar PV parameter estimation. *Energy Conversion and Management*, 101, 410–422.
- M.F. AlHajri, K.M. El-Naggar, M.R. AlRashidi, A.K. Al-Othman. (2012). Optimal extraction of solar cell parameters using pattern search. *Renewable Energy*, 44, 238–245.
- F. Almonacid, C. Rus, L. Hontoria, F.J. Muñoz. (2010). Characterisation of PV CIS module by artificial neural networks: A comparative study with other methods. *Renewable Energy*, 35(5), 973–980.
- B.C. Babu, S. Gurjar. (2014). A novel simplified two-diode model of photovoltaic (PV) module. *IEEE Journal of Photovoltaics*, 4 (4), 1156–1161.
- S. Bana, R.P. Saini. (2017). Identification of unknown parameters of a single diode photovoltaic model using particle swarm optimization with binary constraints. *Renewable Energy*, 101, 1299–1310.
- M. Chegaar, Z. Ouennoughi, A. Hoffmann. (2001). A new method for evaluating illuminated solar cell parameters. *Solid State Electron*, 45, 293–296.
- K. Chennoufi, M. Ferfra, M. Mokhlis. (2021). An accurate modelling of Photovoltaic modules based on two-diode model. *Renewable Energy*, 167, 294–305.
- V.J. Chin, Z. Salam, K. Ishaque. (2016). An accurate modelling of the two-diode model of PV module using a hybrid solution based on differential evolution. *Energy Conversion and Management*, 124, 42–50.
- S. Chowdhury, G.A. Taylor, S.P. Chowdhury, A.K. Saha, Y.H. Song. (2007). Modelling, simulation and performance analysis of a PV array in an embedded environment. *2007 42nd International Universities Power Engineering Conference*, pp. 781–785. doi: 10.1109/UPEC.2007.4469048.
- J.A. Gow, C.D. Manning. (1999). Development of a photovoltaic array model for use in power electronics simulation studies. *IEE Proceedings Electric Power Applications*, Loughborough University of Technology, 146(2), 193–200.
- L. Guo, Z. Meng, Y. Sun, L. Wang. (2016). Parameter identification and sensitivity analysis of solar cell models with cat swarm optimization algorithm. *Energy Conversion and Management*, 108, 520–528.
- A. Hovinen. (1994). Fitting of the solar cell IV-curve to the two diode model. *Physica Scripta*, 54, 175–176.
- K. Ishaque, Z. Salam, H. Taheri. (2011). Simple, fast and accurate two-diode model for photovoltaic modules. *Solar Energy Materials and Solar Cells*, 95 (2), 586–594.
- K. Ishaque, Z. Salam. (2011). An improved modeling method to determine the model parameters of photovoltaic (PV) modules using differential evolution (DE). *Solar Energy*, 85(9), 2349–2359.
- V. Jha. (2021). Performance analysis of hybrid photovoltaic array configurations under randomly distributed shading patterns. *Proceedings of the 7th International Conference on Advances in Energy Research*, Springer Proceedings in Energy. Springer, Singapore, pp. 1287–1296. doi: 10.1007/978-981-15-5955-6_123.

- V. Jha, U.S. Triar. (2018). Effect of varying temperature on different PV array configurations under partial shading condition. *2018 15th IEEE India Council International Conference (INDICON)*, Coimbatore, India, pp. 1–6. doi: 10.1109/INDICON45594.2018.8987049.
- V. Jha, U.S. Triar. (2019). A detailed comparative analysis of different photovoltaic array configurations under partial shading conditions. *International Transactions on Electrical Energy Systems*. doi: 10.1002/2050-7038.12020.
- A. Kajihara, A.T. Harakawa. (2005). Model of photovoltaic cell circuits under partial shading. *2005 IEEE International Conference on Industrial Technology*, pp. 866–870. doi: 10.1109/ICIT.2005.1600757.
- K. Khouzam, C. Ly, C.K. Koh, P.Y. Ng. (1994). Simulation and real-time modelling of space photovoltaic systems. *Proceedings of 1994 IEEE 1st World Conference on Photovoltaic Energy Conversion - WCPEC (A Joint Conference of PVSC, PVSEC and PSEC)*, vol. 2, pp. 2038–2041. doi: 10.1109/WCPEC.1994.520770.
- J. Kumaresan, C. Govindaraju. (2020). Development of a power management algorithm for PV/battery powered plug-in dual drive hybrid electric vehicle (DDHEV). *Electric Power Components and Systems*, 48(1–2), 70–85. doi: 10.1080/15325008.2020.1736212.
- S. Lalouni, D. Rekioua. (2009). Modeling and simulation of a photovoltaic system using fuzzy logic controller. *2009 Second International Conference on Developments in eSystems Engineering*, pp. 23–28. doi: 10.1109/DeSE.2009.17.
- S. Li, W. Gong, X. Yan, C. Hu, D. Bai, L. Wang, L. Gao. (2019). Parameter extraction of photovoltaic models using an improved teaching-learning-based optimization. *Energy Conversion and Management*, 186, 293–305.
- S. Liu, R.A. Dougal. (2002). Dynamic multiphysics model for solar array. *IEEE Transactions on Energy Conversion*, 17 (2), 285–294. doi: 10.1109/TEC.2002.1009482.
- S. Lun, S. Wang, G. Yang, T. Guo. (2015). A new explicit double-diode modeling method based on Lambert W-function for photovoltaic arrays. *Solar Energy*, 116, 69–82.
- A. Mellit, M. Benghanem, S.A. Kalogirou. (2007). Modeling and simulation of a standalone photovoltaic system using an adaptive artificial neural network. *Renewable Energy*, 32, 285–313.
- Z. Meng, Y. Zhao, S. Tang, Y. Sun. (2020). An efficient datasheet-based parameters extraction method for two-diode photovoltaic cell and cells model. *Renewable Energy*, 153, 1174–1182.
- N. Muangkote, K. Sunat, S. Chiewchanwattana, S. Kaiwinit. (2019). An advanced onlooker-ranking-based adaptive differential evolution to extract the parameters of solar cell models. *Renewable Energy*, 134, 1129–1147.
- D.H. Muhsen, A.B. Ghazali, T. Khatib, I.A. Abed. (2015). Parameters extraction of double diode photovoltaic module's model based on hybrid evolutionary algorithm. *Energy Conversion and Management*, 105, 552–561.
- D. Oliva, M.A.E. Aziz, A.E. Hassanien. (2017). Parameter estimation of photovoltaic cells using an improved chaotic whale optimization algorithm. *Applied Energy*, 200, 141–154.
- N. Rajasekar, N.K. Kumar, R. Venugopalan. (2013). Bacterial foraging algorithm based solar PV parameter estimation. *Solar Energy*, 97, 255–265.
- M.U. Siddiqui, M. Abido. (2013). Parameter estimation for five- and seven-parameter photovoltaic electrical models using evolutionary algorithms. *Applied Soft Computing*, 13(12), 4608–4621.

- Y.T. Tan, D.S. Kirschen, N. Jenkins. (2004). A model of PV generation suitable for stability analysis. *IEEE Transactions on Energy Conversion*, 19(4), 748–755.
- M.G. Villalva, J.R. Gazoli, E.R. Filho. (2009). Comprehensive approach to modeling and simulation of photovoltaic arrays. *IEEE Transactions on Power Electronics*, 24(5), 1198–1208. doi: 10.1109/TPEL.2009.2013862.
- G.R. Walker. (2001). Evaluating MPPT converter topologies using a MATLAB PV model. *Journal of Electrical and Electronic Engineering*, 21(1), 49–55.
- W. Xiao, W.G. Dunford, A. Capel. (2004). A novel modeling method for photovoltaic cells. *2004 IEEE 35th Annual Power Electronics Specialists Conference (IEEE Cat. No.04CH37551)*, vol. 3, pp. 1950–1956. doi: 10.1109/PESC.2004.1355416.
- W.C. Yeh, C.L. Huang, P. Lin, Z. Chen, Y. Jiang, B. Sun. (2018). Simplex simplified swarm optimization for the efficient optimization of parameter identification for solar cell models. *IET Renewable Power Generation*, 12(1), 45–51.

4

Conventional Techniques for Maximum Power Point Tracking

**Shilpi Yadav, Kamlesh K. Bharti, Vijay Kumar Tewari,
Santosh Kumar Tripathi, and Rajesh Kumar**

Rajkiya Engineering College

CONTENTS

4.1	Introduction	79
4.1.1	Need for Solar Energy	80
4.2	Solar Energy	81
4.3	Need of MPPT	83
4.4	MPPT	83
4.4.1	MPPT Solar Charge Controller	84
4.5	Conventional MPPT Techniques.....	85
4.5.1	Perturb and Observe (P&O) MPPT Technique.....	86
4.5.2	Variable Step Size (VSS) P&O MPPT Method	89
4.5.3	Modified P&O	89
4.5.4	Simulation Results of P&O MPPT Technique.....	90
4.5.5	Incremental Conductance (I&C) MPPT Technique.....	93
4.6	Conclusion	100
	References.....	101

4.1 Introduction

The advancement of human civilization has resulted in rapid industrialization, which has been accompanied by urbanization and globalization, resulting in increased global energy demand. To begin, this chapter examines the need for unconventional energy sources, because conventional sources are depleted at a faster rate, appearing to be unable to fulfill rising energy demand on their own. Solar Energy (SE) is a pervasive and renewable energy source (RES) that is friendly to the environment and has become one of the most powerful sources of energy used in a variety of fields. The sun is a

RES that can be considered one of the good solutions to the energy crisis (Kermadi & Berkouk, 2017).

In the present era as energy consumption is increasing, efforts have been made toward renewable technology, toward rising energy production from existing ones, and also to decrease reliance on traditional sources of energy and increase dependency on RES like photovoltaic (PV) energy, wind energy (WE), and hydro energy. A contrast to conventional energy sources, SE is an utmost, efficacious and powerful source of renewable energy. It has several significant advantages, such as being pollution-free, quiet in service, high durability, easy to maintain, very low operating cost, and an endless supply of input energy in the form of solar power (Premkumar & Sowmya, 2019). The modules are used in space and on the ground where they are cost-effective compared to other energy sources. The three categories of PV systems are stand-alone, grid-interconnected, and hybrid. Stand-alone PV system networks have been considered a successful solution for areas that are distant from a traditional generation system. These systems are implemented in remote areas where the grid electricity is not completely expanded giving the brilliant and secure fiscal source of electricity (Pakkiraiah & Sukumar, 2016). The International Renewable Energy Agency (IRENA) summarizes accurate and trustworthy data on renewable energy capacity and use around the world. The Renewable Energy Statistics 2020 contains data on the power-generation capacity for 2010–2019, real power generation for 2010–2018, and renewable energy balances for 2017–2018 for over 130 countries and regions. The information was gathered from several sources, including official national statistics, IRENA questionnaire, industry association reports, consultant reports, and news articles (Ishaque et al., 2012).

4.1.1 Need for Solar Energy

Due to increased domestic and industrial demand, the world is currently experiencing an energy crisis and exploring more renewable energy resources has become difficult for researchers. In the generation of electric power, RES has been a significant role. For electrical power generation (EPG), various RESs such as SE, WE, and geothermal energy (GTE) have been used. The RES is the best available solution for satisfying power demand. In comparison to nonrenewable energy (NRE) sources such as oil, natural gas, and fossil fuels (FF), RE sources are acquiring popularity for both residential and commercial applications because of their advantages, such as affordability, consistency, cleanliness, environmentally friendly nature, high durability, and low maintenance. Solar PV (SPV) systems have a low power conversion rate, about 30%–40%. The low cost, high performance, and abundance in nature of the solar power system are now commonly used in every sector. Despite its benefits, the output active power P of a solar power system changes with solar irradiance EE and operating temperature T , especially under hasty changing partial shading conditions (PSC) due to the effects of

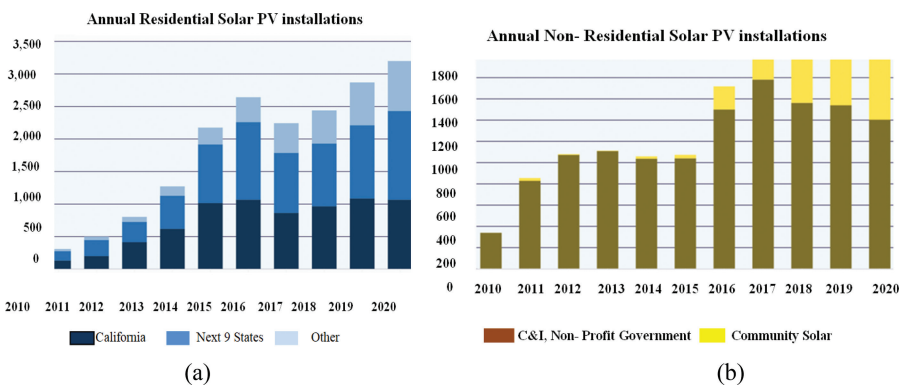


FIGURE 4.1
(a) Residential PV installation and (b) Nonresidential PV installation (Irena, 2012).

the sun, and the nonlinear characteristic of PV cells. The increasing demand for the installation of SPV panels in residential and nonresidential is shown in Figure 4.1, considering data from 2010 to 2020.

4.2 Solar Energy

SE is the electricity produced by SPV modules using solar radiation from the sun. While solar power accounts for a small portion of global energy output, it is used extensively in some countries. The United States and China are the world leaders in SE, while Germany gets a significant portion of its electricity demand from the sun (Salas et al., 2006). The SE output includes many energy sources, both passive and active. It is generated in two ways: by direct conversion of solar power into current by using PV panels (or SPV) or by the accumulation of SE to generate steam and operate turbines (concentrated SE). The SPV system can be mounted on our terrace or in massive “solar farms,” which are simple to comprehend. The SE is received by the solar panel in the form of light, which energizes electrons in the panel and produces an electric current. In the solar panel, DC flows to an inverter box, which transforms it into AC. The majority of homeowners are unaware that their solar panels are connected to the power grid, which means they don’t need a backup battery system via the home’s electric meter; the current of solar panels either flows into the house or the grid. In certain cases, the homeowner has to pay for the extra electricity (Masoum et al., 2002). To increase overall conversion efficiency, the PV technique is being developed in two ways: power conditioner (DC/AC and/or DC/Converters) devices and cell material. Despite advances in solar cell, materials such as polycrystalline, amorphous, thin-film, and monocrystalline, conversion efficiency persists at low cost, but the system costs remain high. As a result, the

power conditioner’s output is critical in improving overall power conversion efficiency and lowering costs. As shown in Figure 4.2, a solar cell can be driven at any position along its typical voltage–current curve. The open-circuit voltage (OCV) and short-circuit current (SCC) are two critical points on this curve (I_{sc}). The greatest voltage at zero current is the OCV, while the highest current at zero voltage is the SCC (Daraban et al., 2014).

A typical PV panel consists of lots of solar cells interconnected in series and parallel to raise the PV’s output voltage and current. Figure 4.3 depicts the ideal and realistic characteristics of a PV panel.

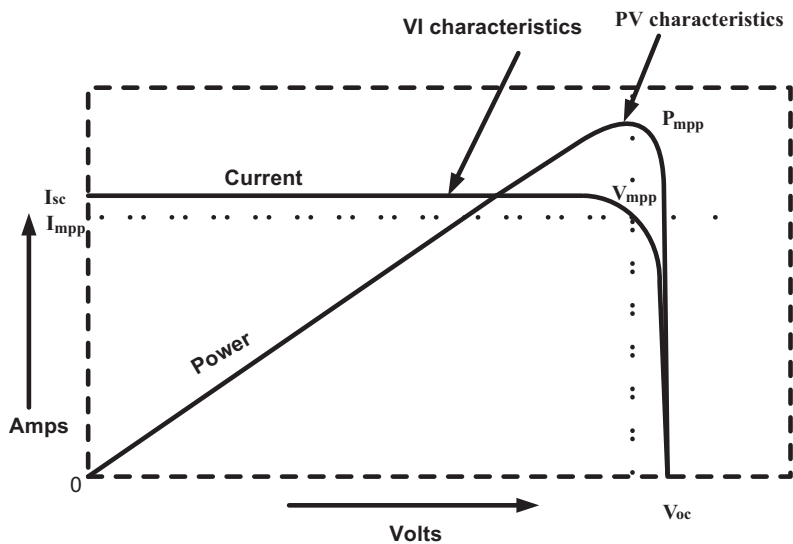


FIGURE 4.2
P–V and I–V characteristics of solar cell.

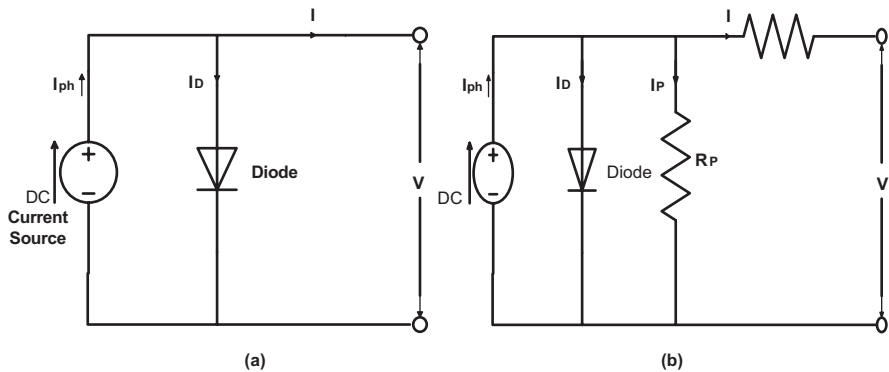


FIGURE 4.3
(a) Ideal PV circuit diagram and (b) Practical PV circuit diagram.

4.3 Need of MPPT

The RES, such as PV energy, play a critical role in electricity generation and have become increasingly important in recent years as a result of traditional fuel shortages and environmental issues. Because of the scarcity of fossil fuels and their consequences for the environment, PV energy will become more relevant in the future. The PV arrays can produce more than 45% of the world's required electricity. The power-generation systems, however, have these flaws: the efficiency of electricity production is poor and the power produced by solar modules varies constantly, depending on climatic conditions (Ali et al., 2018; Bataineh et al., 2018). Furthermore, since PV systems have NL V-I and P-V characteristics, their output power varies with environmental conditions, such as atmospheric temperature, solar radiation, and the type of load associated. Since there is a likely inequality between the Maximum Power Points (MPPs) and load characteristics of the PV module, MPPT is needed to ensure optimum solar module utilization. The use of MPPT lowers the cost of energy produced by solar panels (Bhatnagar & Nema, 2013; Messai et al., 2011). The power excavation is unsatisfactory due to the complex relationship between power output and PV input parameters. The MPPT becomes the research objective to strengthen the performance of the SE system and ensure that the working point is still at MPP to mitigate the aforementioned limitation (Ahmed et al., 2013).

4.4 MPPT

Under certain conditions, the MPPT is a charge controller-based algorithm for deriving the maximum power (MP) available from a PV module. The PV cell MMP is the voltage at which it produces the peak power voltage (or most power). The maximum intensity is affected by ambient temperature, solar radiation, and PV cell temperature. A standard PV array generates power with an MP voltage of almost 17 when determined at a solar module of 25°C; however, on a very hot day, it can lower to about 15 V, and on a very cold day, it can raise to 18 V. The key idea behind MPPT is to have the most power available drawn out from PV modules by running them at the best voltage. The following are the steps for the MPPT algorithm:

- The MPPT analyzes the PV module's output needs to be compared to the voltage of the battery and then calculates the highest power PV cells to generate voltage to charge a battery and then convert it to the best voltage possible to deliver the maximum current to the battery.

- It runs a DC load attached explicitly to the battery. MPPT is most beneficial in the following situations.
- Days of cloudy or hazy skies and cold weather: PV modules conduct much better in colder weather, and MPPT is used to draw out the full power from them.
- Whenever the batteries are completely ejected, MPPT will extract extra current and recharge the batteries if the charge in the battery is smaller.

4.4.1 MPPT Solar Charge Controller

An MPPT Solar Charge Controller is a charge controller that uses the MPPT algorithm to optimize the current that a PV module gives to the battery. The DC/DC MPPT converter draw DC from a PV array and converts it to AC and then transforms it back to DC at distinct voltage values and current to fit the PV cell to the battery exactly (Rezk & Eltamaly, 2014). In the P-V curve, the MPP is the knee where power is at its highest. Since the location of MPP changes with changing atmospheric conditions, MPPT is a method used to acquire the MP available in the PV system. The MPP tracker tracks down the PV working voltage that corresponds to MPP and closes the working point at MPP allowing the PV array to extract full power. In both grid-interconnected PV systems and stand-alone multiple MPPT methods have been suggested for the solar module to supply its MP. The MPPT techniques are typically implemented on DC/DC converters in stand-alone systems and need battery banks to store surplus energy. The power generated by the PV module system can be transferred to the grid by DC/DC converter that serves as an inverter and MPPT controller that transforms the DC bus voltage to the AC grid voltage in grid-interconnected systems. However, only a particular DC/AC inverter can accomplish this (Shaue et al., 2013).

The MPPT model is a mathematical model that calculates the probability of it is important to integrate an MPPT circuit between the load and PV module to implement the PV device to work at MPP according to variations in temperature and solar irradiation, as shown in Figure 4.4. A DC/DC converter and controller circuit can be classified as boost, buck, and buck-boost (Mohanty et al., 2014).

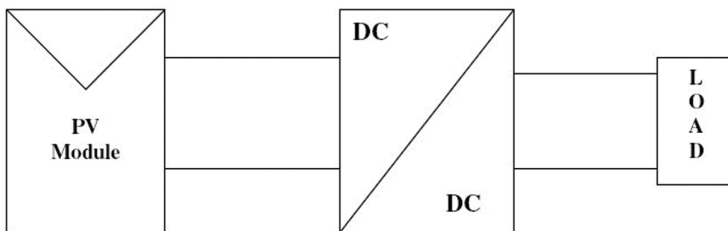


FIGURE 4.4

Block diagram of MPPT based PV system.

4.5 Conventional MPPT Techniques

The direct and indirect techniques are the two major categories of MPPT techniques (Nguyen et al., 2020). The OCV MPPT, set voltage (SV) MPPT and SCC MPPT methods are examples of indirect strategies that involve previous learning of PV cell features or are dependent on statistical correlation and also not suitable for all weather conditions. As a result, they are unable to monitor the MPP of a PV array at any cell temperature or irradiance with precision. Furthermore, utilizing irradiance and temperature as sensed parameters is not suggested since their evaluation necessitates the placement of expensive devices across the PV module to obtain the amounts of such quantities for individual panels or group of panels, resulting in a very expensive measurement, particularly for large PV plants. The direct strategies, on the other hand, operate regardless of the weather. The direct MPPT methods, which calculate voltage, current, and power, are much more reliable and have a quicker response time than indirect MPPT techniques (Belkaid et al., 2017). The Incremental Conductance (I&C) and Perturbation and Observation (P&O) are the popular direct approaches for MPPT. Commercial goods usually employ perturbative MPPT methods, which determine the value of voltage after which the PV array delivers its MP instant-by-instant basis. The P&O and I&C MPPT techniques are commonly used to restrain the reference signal of a DC/DC converter that converts PV cell voltage to DC bus voltage or functions as a battery charger. These methods have the following advantages: they can be used with any solar-based generator, they don't want any knowledge related to PV generators, and they're easy to integrate into a digital controller. Moreover, these methods can be integrated into industrial inverters. The voltage- and current-dependent MPPT, sliding mode control, gradient descent method with variable phase scale, ripple correlation control (RCC), temperature-based method, bisection search theorem-based MPPT, dual tracking-based MPPT, and the hill climbing (HC) MPPT technique are given in the literature (Salman et al., 2018; Azad et al., 2017).

Different methods, as discussed in various literature, have various benefits and drawbacks in terms of various performance indices. In this chapter, we'll look at some of the most widely used MPPT techniques, their working principles, and how they compare in terms of efficiency. The effectiveness of various techniques is compared based on desirable characteristics such as speed, complexity, hardware configuration, essential sensors, price, and usefulness range, dynamic characteristics, steady-state error, system stability, and efficiency are all factors that need to consider. The different types of MPPT techniques are depicted in Figure 4.5.

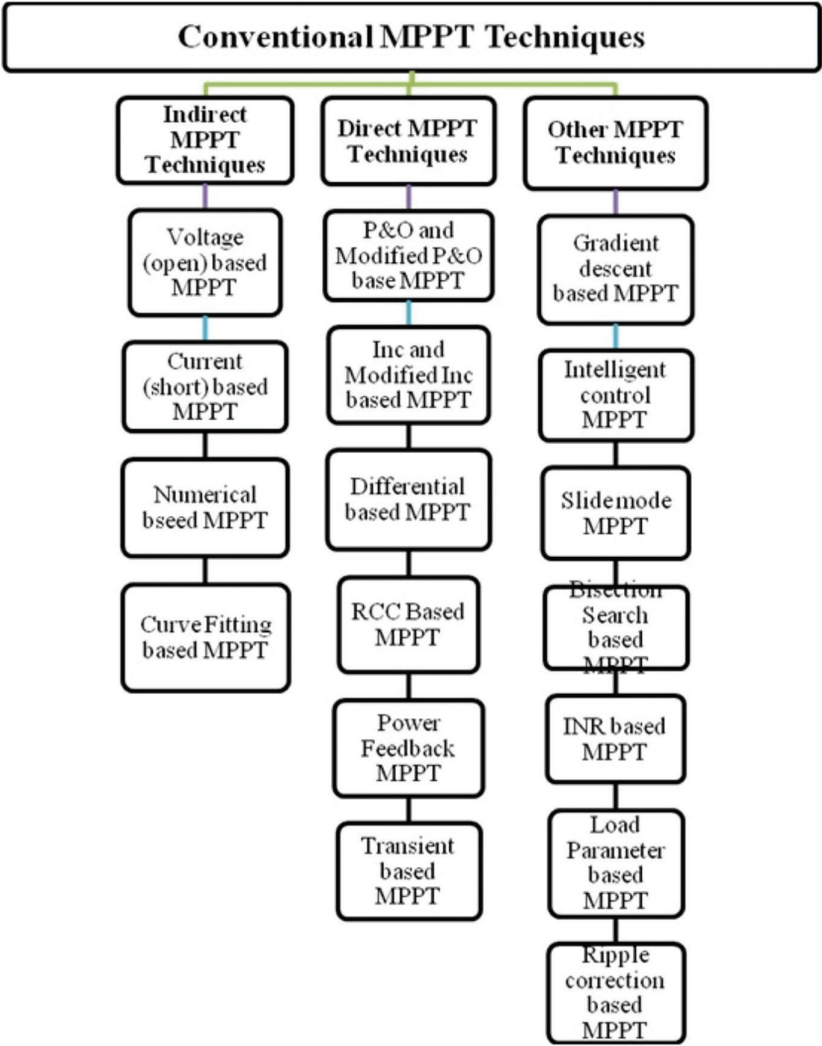


FIGURE 4.5
Classification of all conventional MPPT techniques for PV module.

4.5.1 Perturb and Observe (P&O) MPPT Technique

The popular “P&O” approach is a direct conventional MPPT technique that has been applied in many SE-related fields. The P&O technique is generally used to keep track of the MPP. A slight perturbation is added in this technique to permit the PV module’s power to change. The PV output power is computed regularly and compared to the prior power. A similar mechanism is repeated if the output power rise; otherwise, the perturbation is flipped.

The PV module voltage is perturbed using this algorithm. To see whether the power has risen or decreased, the PV module voltage is decreased or increased. When a rise in voltage results in an increase in power, the PV module's working point has shifted to the left of the MPPT. As a result, further perturbation to the right is needed to hit MPP. If a rise in voltage causes a decline in power, the PV module's working point is to the right of the MPP, requiring more perturbation to the left to achieve MPP. The iterative P&O algorithm requires only two sensors to sense the PV array's current and voltage, and then determine the output power that is the product of these parameters. Its operation is depending on perturbing the array terminal voltage by a less increment and then comparing the array terminal power to that of the prior perturbation cycle. Due to perturbation the panel power increase (decrease), the upcoming perturbation is rendered in the reversal direction. As a result, the MPP tracker is constantly looking for the highest power spot. The DC of the chosen converter is inversely related to its input voltage for a given output voltage, as shown by Basha & Rani (2020).

$$V_0 = V/(1 - d) \quad (4.1)$$

The P&O charge controller's algorithm is depicted in Figure 4.6a, as a flow map. The PV and battery voltages are measured by the charge controller when it is attached between the battery and PV module. After checking the voltage, it decides whether or not the battery is completely charged. If the battery is completely recharged, it inhibits charging to stop the battery from extra charging. However, the battery is not charging, it began charging by initiating the DC/DC converter. The microcontroller (MC) will then use voltage and current measurements to determine the current power P_{new} at the output and compare it to the prior calculated energy P_{old} . If P_{new} is larger than P_{old} , the PWM DC is raised to retrieve MP from the PV module. If P_{new} is far from P_{old} , the DC is decreased to make certain the system retreat to the earlier MP. This MPPT method is very easy, straightforward, low cost, and accurate. To ensure optimal power, this algorithm alters the operating voltage. There are several new and optimized iterations of this algorithm available, a simple P&O MPPT algorithm and their PV characteristic is shown in Figure 4.6b, when PV module output current I_{PV} and output voltage V_{PV} are sensed and then power $P(K)$ is computed and collate with the computing power in the prior sample $P(K - 1)$, To acquire the DP with the sign of DV and DP, the DC of the converter is replaced to track MPP (Aganah & Member, 2011).

A minor perturbation is included in this algorithm. The power of the module varies as a result of the perturbation; if the power grows as a result of the perturbation, the perturbation continues within this direction. After attaining the highest power, the power lowers at the following moment, and the perturbation reverses. When the algorithm reaches a steady state, it oscillates about the peak point. The perturbation size is maintained minimal to keep the power variation small, as seen in Figure 4.6.

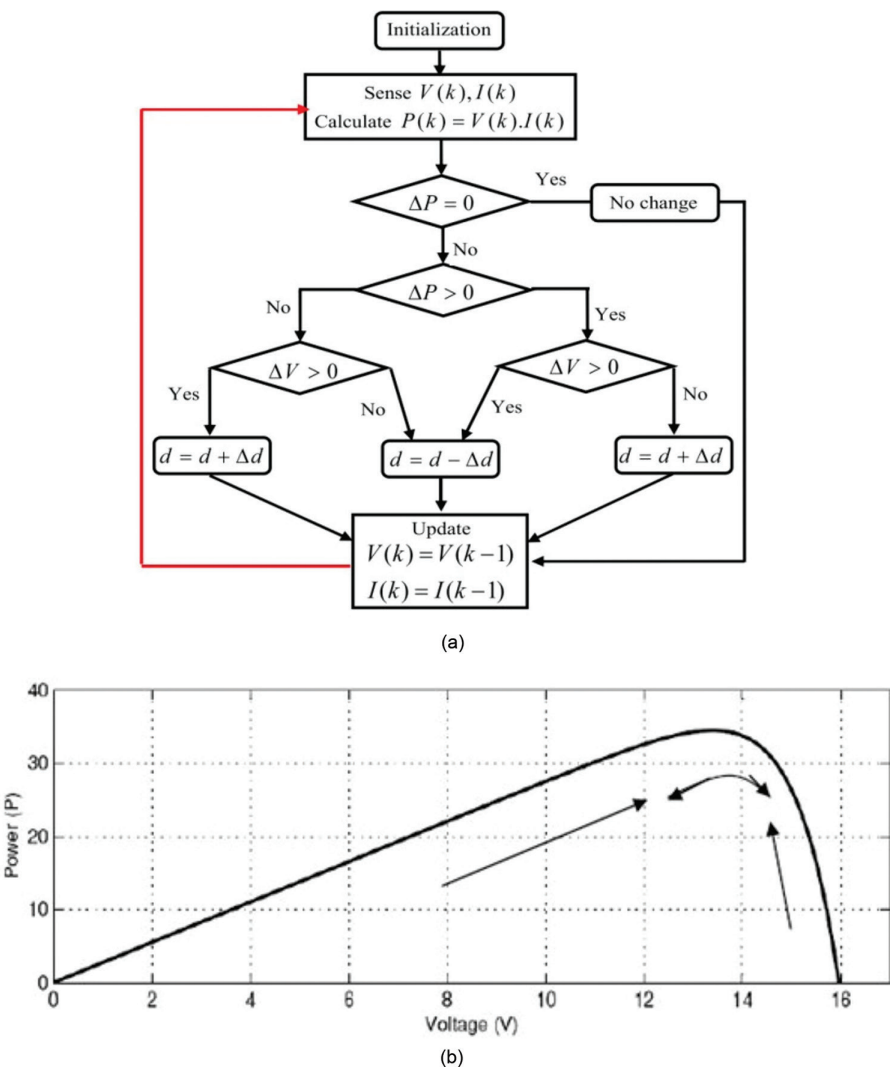


FIGURE 4.6
(a) Basic P&O algorithm and (b) PV curve for P&O algorithm.

The PV curve for the P&O method is shown in Figure 4.6b. The algorithm is designed to set a reference voltage for the module that corresponds to the highest voltage of the module. The working point of the module is then moved to another voltage level by a PI controller. It has been noticed that this disruption causes some power loss, as well as the failure to follow the power under rapidly changing air circumstances. Nonetheless, this algorithm is quite popular and intuitive.

4.5.2 Variable Step Size (VSS) P&O MPPT Method

The P&O technique is the majorly used of all MPPT technologies since it has an easy and reliable steady-state response. However, this approach is limited to the steady-state working conditions of an SPV device. To address the shortcomings of the traditional P&O system, a new version is proposed. The (variable step size) VSS-based P&O MPPT method is used to trace MPP to resolve the limitation of traditional P&O. To increase tracing speed, large step size is used at first, and then the step size is decreased to minimize oscillations around the MPP. The VSS-based P&O MPPT method flow chart is shown in Figure 4.7 (Bendib et al., 2015; Ishaque et al., 2014).

4.5.3 Modified P&O

The direct MPPT techniques, which calculate voltage, current, or power, are most reliable and have a quicker response time than indirect MPPT techniques. The direct MPPT technique P&O is used here with some amendments. To address the shortcomings of the traditional P&O system, a new version is proposed. It starts by measuring the voltage and the current to calculate the power output (refer Figure 4.8).. The present MPPT may present an improvement in the system behavior by the addition of a third variable in its flowchart, which is the alteration in current. As a result, eight types of working point perturbation are identified: Four is the same as the original

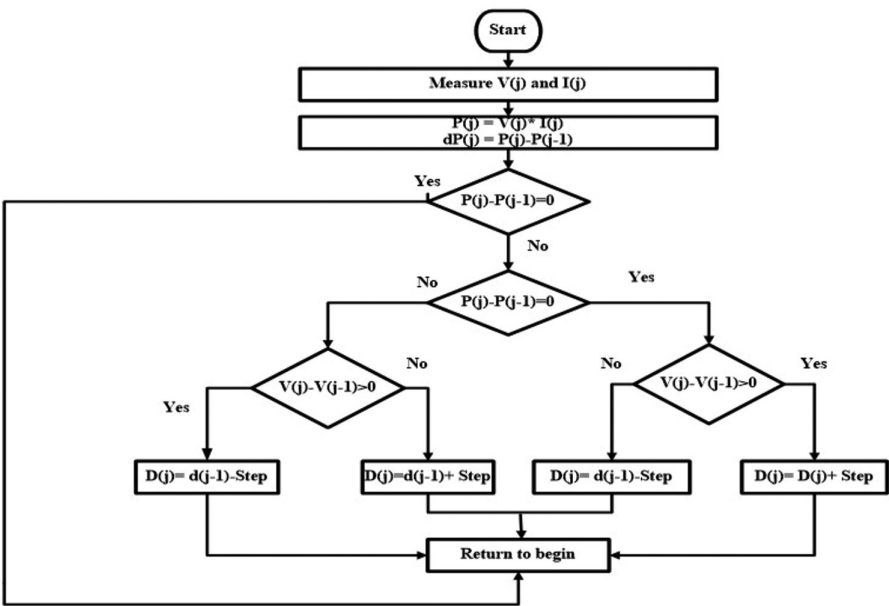


FIGURE 4.7
Modified VSS P&O algorithm.

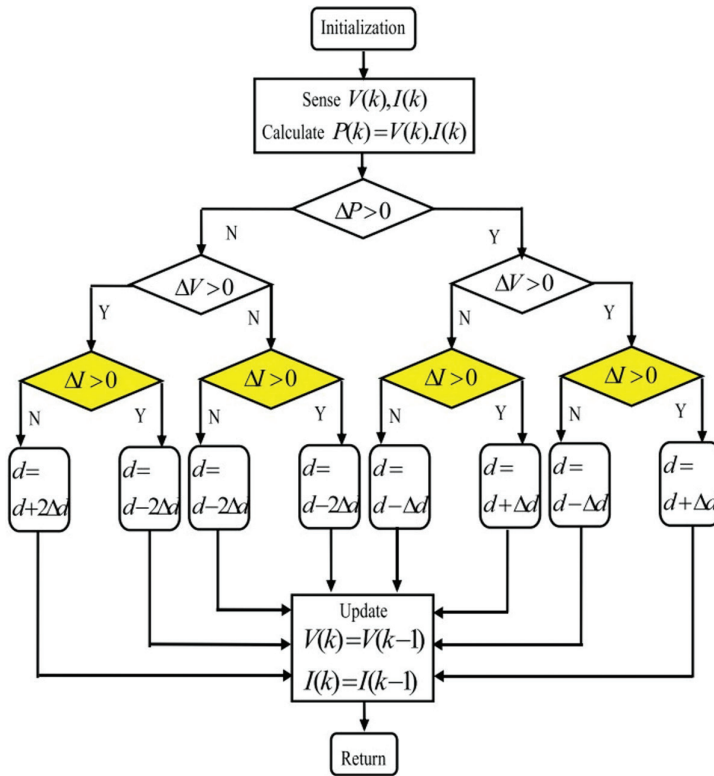


FIGURE 4.8
Modified P&O algorithm.

approach (fixed irradiance), and four more are introduced to show states where the irradiance level is gradually evolving, either increasing or decreasing. If the voltage and current changes have the same symbol, the PV module is under constant illumination; if they don't, the PV module is under varying environmental conditions. The algorithms minimize the old one in fixed illumination; when the illumination change, this algorithm behaves differently than the traditional one. When a bad tracking method is found, the phase size must be doubled to increase tracking speed. The MPPT can distinguish whether the change in power is due to a change in sunlight or a change in reference voltage perturbation using this method, avoiding divergence from the MPP (Bharti et al., 2019).

4.5.4 Simulation Results of P&O MPPT Technique

The MATLAB®/Simulink® is used to simulate SPV cell characteristics, P&O technique of MPPT has been coupled with the PV model and MPP tracking system. Parameters of the SPV module with values are shown in Table 4.1.

TABLE 4.1
Different Components of PV Module

Parameters	Values
Voltage in open-circuit condition	23.23 V
Current in short-circuit condition	5.47 A
Current at maximum power	4.75 A
Voltage at maximum power	16.26 V
Ideality factor(m) for diode	2.0
Thermal voltage (v_T)	$(k.T/e)$
Boltzmann constant (k)	$1.380658 \times 10^{-23} \text{ Jk}^{-1}$
Electron charge (e)	$1.6021733 \times 10^{-19} \text{ As}$
Insolation	800.05 W/M^2

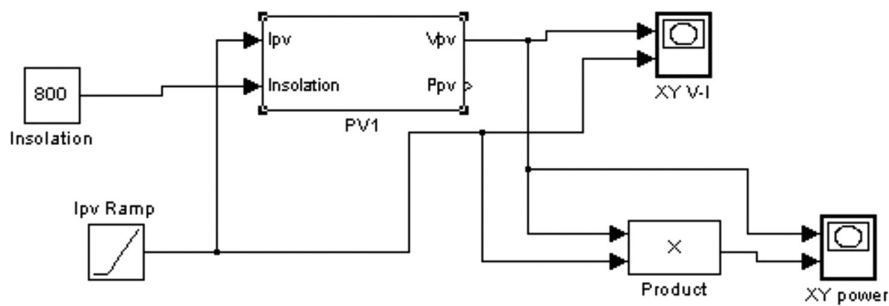


FIGURE 4.9
TATA BP module.

The Simulink setup of the TATA BP module is shown in Figure 4.9, in which output is the power. Figure 4.10 shows the inside module of the TATA PV subsystem. The PV and IV characteristics are represented in Figure 4.11.

Figure 4.12 shows the Simulink setup of the PV module at different insolation levels with the masked subsystem. The PV module characteristics with various insolation are shown in Figure 4.13. Model of the complete system developed in MATLAB/Simulink software is shown in Figure 4.14. The MPPT block sends the current and voltage from the module to the multimeter. The MPPT block houses the algorithm, which is depicted in Figure 4.14. The temperature and the amount of insolation are not changed. Figure 4.15 depicts the algorithm's Simulink implementation. To implement the P&O (perturb and observe) algorithm. Table 4.2 lists the specifications of PV panel elements.

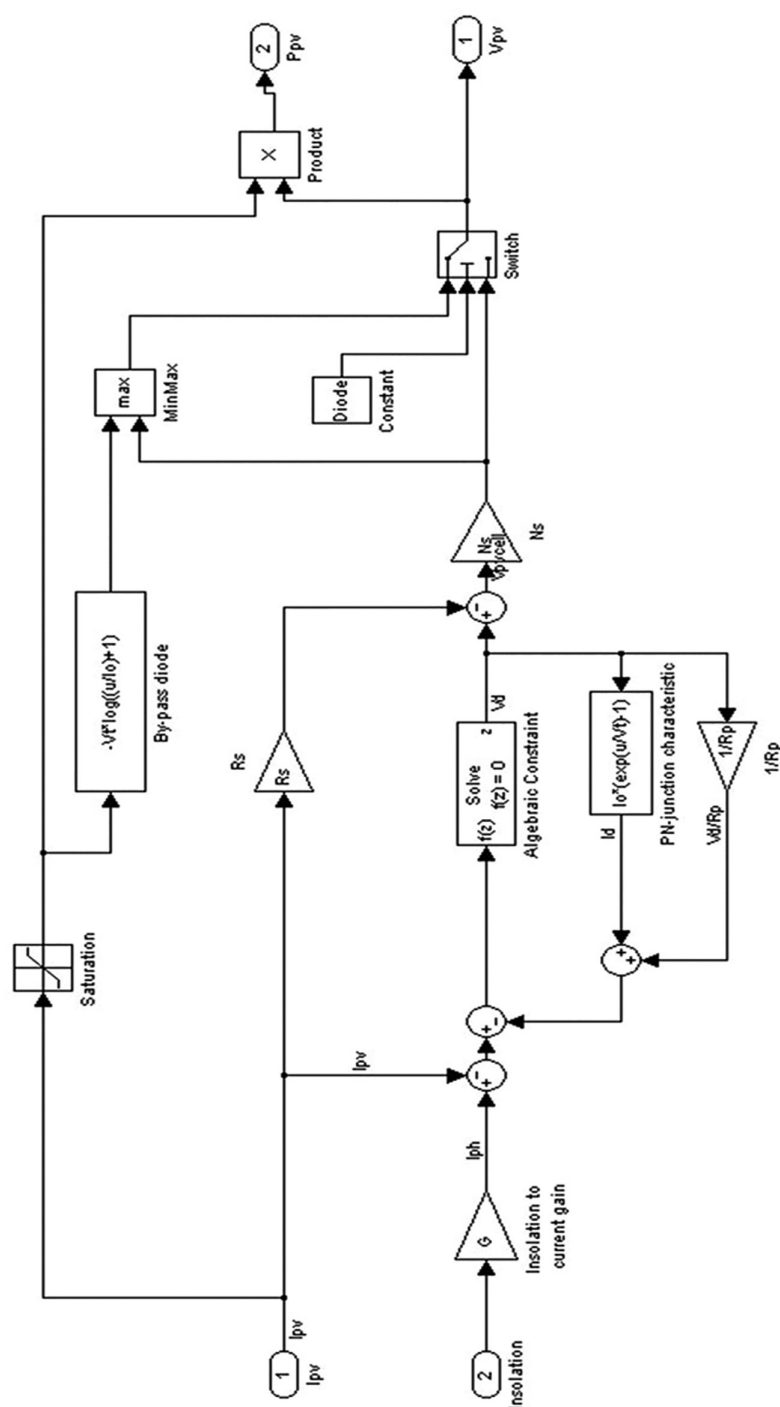
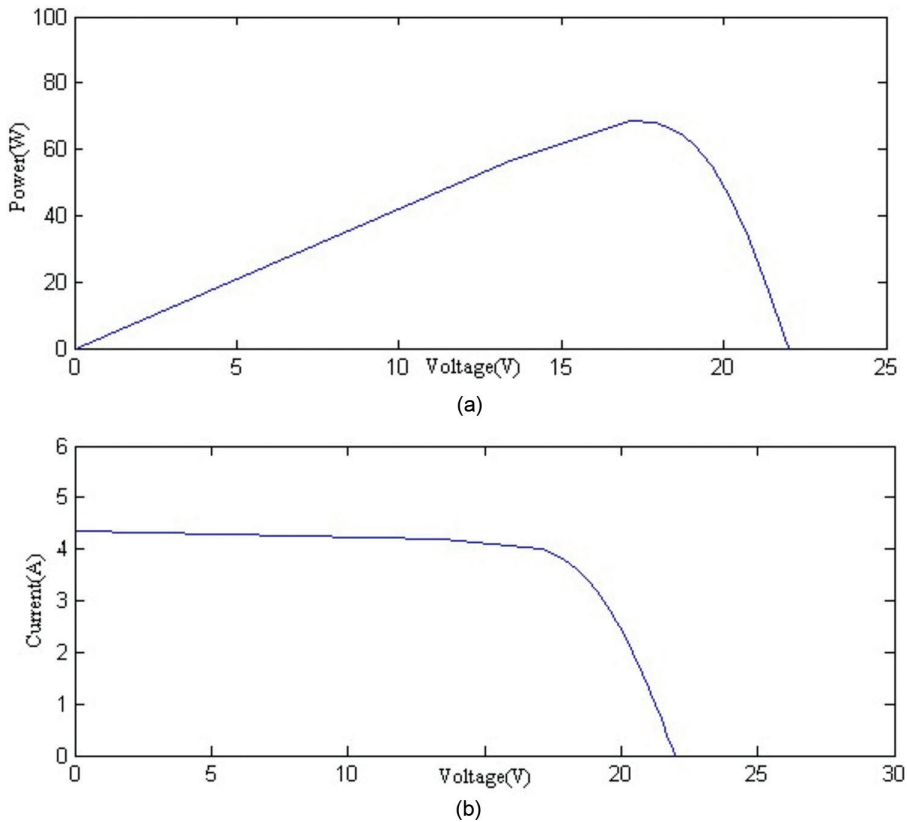


FIGURE 4.10
Inside module of TATA PV subsystems.

**FIGURE 4.11**

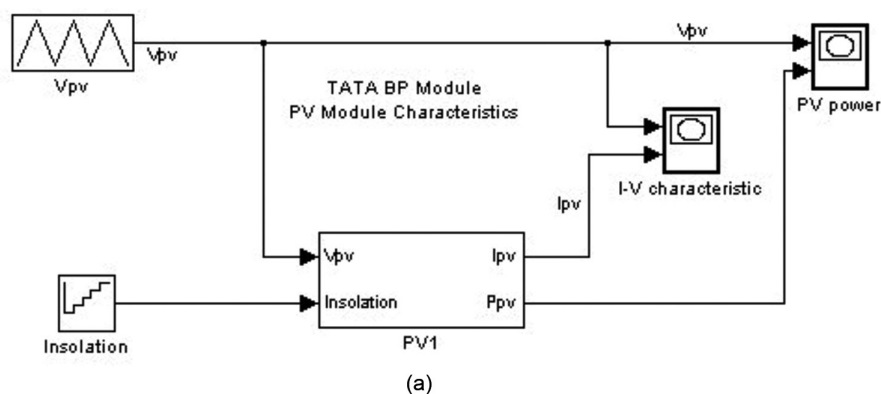
(a) P-V characteristics of PV module and (b) I-V characteristics of PV module.

Power vs. time is shown in Figure 4.16. The amount of power drawn from the solar cell is initially low. After that, the duty ratio is increased using an algorithm. Voltage versus time is depicted in Figure 4.17. Figure 4.18 depicts the current vs. time characteristic. The initial condition is more akin to an open circuit, with a high voltage. As the duty ratio raises, the current drawn (Figure 4.19) from the solar panel rises, resulting in a voltage decrease. Finally, when the power reaches its highest point, the duty ratio is determined, and the power oscillates around it. The highest power available is 82 W.

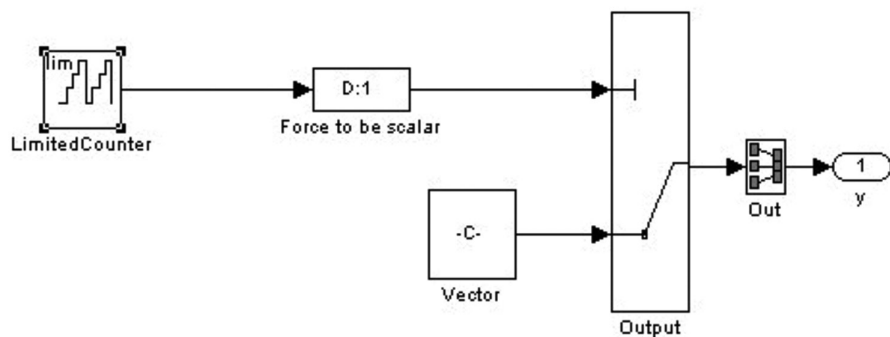
Figure 4.20, depicts the pulses created by the perturb and observes the method of maximum peak PowerPoint, which are utilized to control the switch (MOSFET) of the DC Buck converter to extract the MP from the SPV panel.

4.5.5 Incremental Conductance (I&C) MPPT Technique

The I&C method was developed in 1993, an alternative to the “P&O” method. It is predicated on Eq. (4.2), that is, subtracting the PV power from the voltage



(a)



(b)

FIGURE 4.12

(a) PV module at different insolation and (b) Insolation mask subsystem.

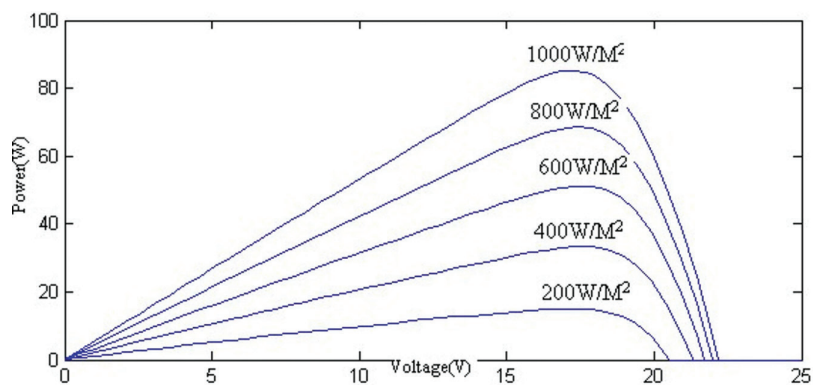


FIGURE 4.13

PV module P-V characteristics at various insolation.

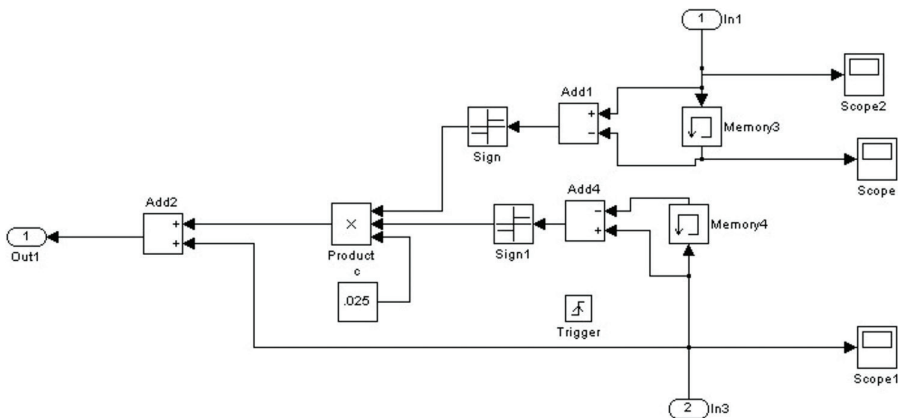


FIGURE 4.15
Duty ratio method implemented in SIMULINK (S1).

TABLE 4.2
PV Panel Components Specification

Components	Values
Current due to light produced	$I_{ph} = 5.56 \text{ A}$
PV module series resistance	$R_s = 0.01 \text{ } \Omega$
PV module parallel resistance	$R_p = 63.513 \text{ } \Omega$
Buck or down converter	$L = 0.01\text{H}$ & $C = 0.00050 \text{ F}$

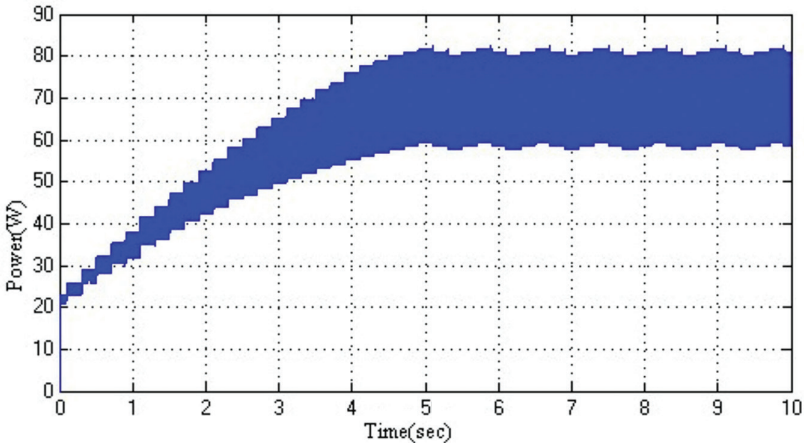


FIGURE 4.16
Power vs time.

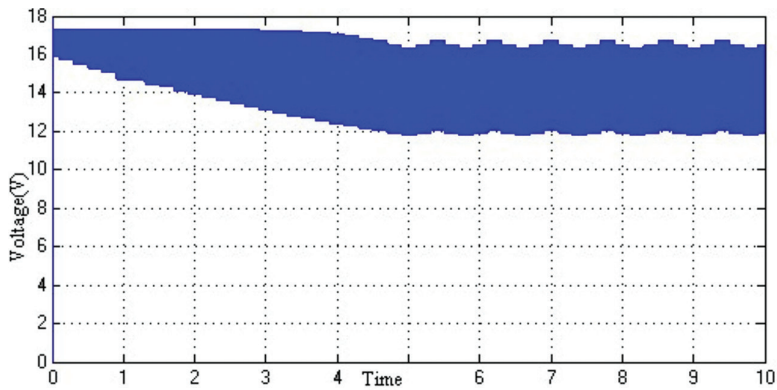


FIGURE 4.17
Voltage vs time.

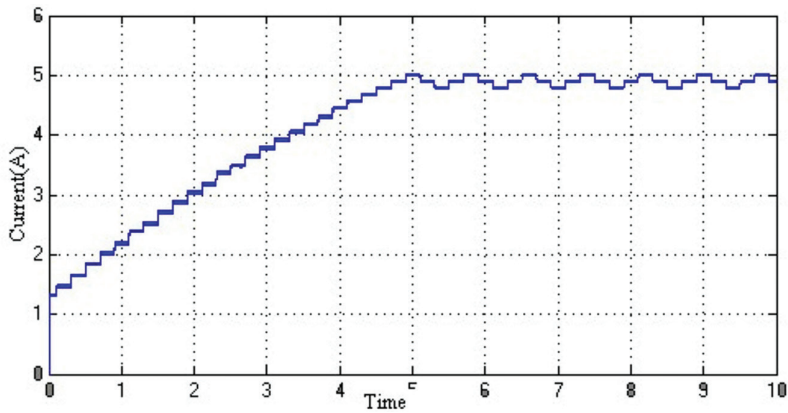


FIGURE 4.18
Current vs time.

and dividing the result by zero. The approach believes in the assumption that at the MPP, the zero slopes between power and voltage ($P-V$). It was suggested that monitoring precision and dynamic performance under rapidly changing conditions be improved. The PV array's current and output voltage are tracked, and the MPPT controller uses this information to measure conductance and $I \& C$, as well as make decisions (to decrease or increase duty ratio output), $P = V^1 \cdot I$ is the formula for calculating the output power of a PV array. The product derivative then yields

$$\frac{dP}{dV^1} = \frac{d(I \cdot V^1)}{dV^1} = V^1 \frac{dI}{dV^1} + I \rightarrow \frac{1}{V^1} * \frac{dP}{dV^1} = \frac{dI}{dV^1} + \frac{I}{V^1} \quad (4.2)$$

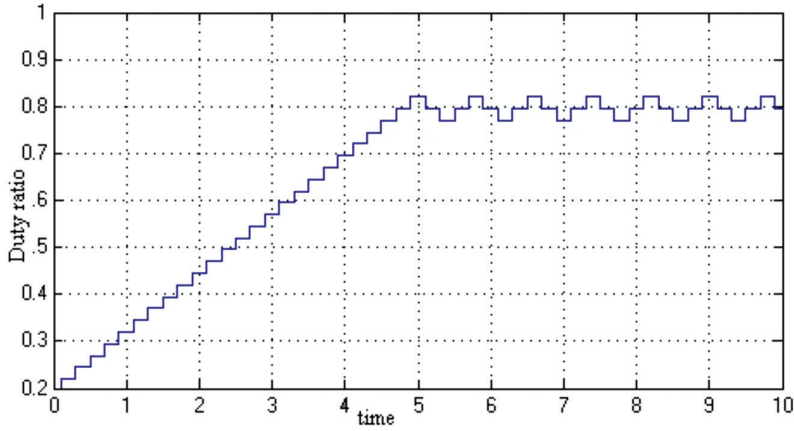


FIGURE 4.19
Duty ratio vs time.

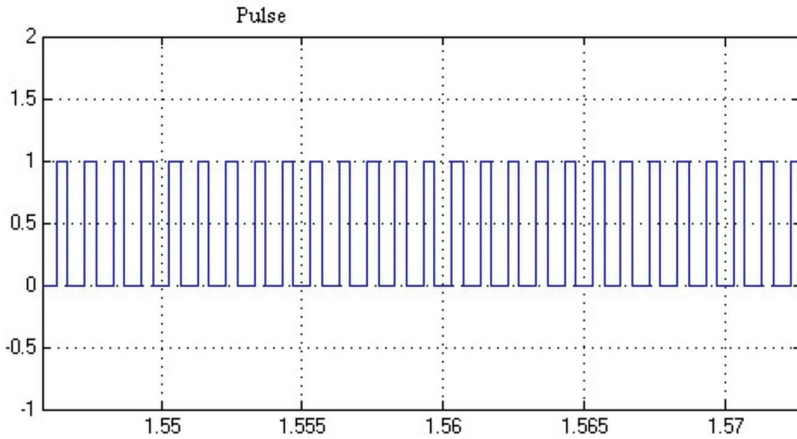


FIGURE 4.20
Transition pulse for the buck chopper switch.

PV array voltage, power, and current are represented by V , P , and I , respectively, as shown in equation (4.2). The goal of this flowchart is to determine the operating point for voltage where the PV array's I&C (dI/dV^1) and instantaneous conductance (I/V^1) are equal. The following equations are used to express this:

$$\frac{dP}{dV^1} = 0, \text{ If } \frac{dI}{dV^1} = -\frac{I}{V^1}, \text{ (at MPPT)} \quad (4.3)$$

$$\frac{dP}{dV^1} > 0, \quad \text{If } \frac{dI}{dV^1} > -\frac{I}{V^1}, \quad (\text{Left of MPPT}) \quad (4.4)$$

$$\frac{dP}{dV^1} < 0, \quad \text{If } \frac{dI}{dV^1} < -\frac{I}{V^1}, \quad (\text{Right of MPPT}) \quad (4.5)$$

The I&C algorithm's flowchart is shown in Figure 4.9. Two sensors are used in this system to evaluate the array's working current I and voltage V . As shown in Figure 4.8, the gradual changes dV^1 and dI can be measured digitally by sampling the PV array current I and voltage V^1 at time intervals $(k-1)$ and (k) .

$$dV^1(k) = V^1(k) - V^1(k-1) \quad (4.6)$$

$$dI(k) = I(k) - I(k-1) \quad (4.7)$$

In Figure 4.21, the reference voltage (V_{ref}) is at a level which the PV system is compelled to work. At the MPPT, V_{ref} equals V_{mppt} . When the MPP is achieved, the PV array continues to operate until a change is detected in dI , signaling a change in MPP and the weather conditions. The algorithm uses a constant adjustment phase width to decrement or increment V_{ref} to monitor the new MPP. The I&C algorithm can determine that direction to perturb the operating point to reach the MPP. As a result, under significant amounts of growth radiation, it would not have gone in the wrong way, as P&O may have. The condition $(I/V^1 = -dI/dV^1)$ is rarely reached due to measurement errors and quantification, so the device oscillates around the MPP under stable environmental conditions. Furthermore, by using a constant adjustment stage distance, it is extremely hard to change V to the exact V_{mppt} . Variable stage size has been proposed as a solution to this problem (Bendib et al., 2015). However, it necessitates complex and expensive control circuits. To solve this problem, apply a smaller marginal error (ϵ) to the highest power condition $(I/V^1 + dI/dV^1 = 0)$, making the MPP equal to

$$\left| \frac{dI}{dV^1} + \frac{I}{V^1} \right| \leq \epsilon \quad (4.8)$$

where ϵ is the marginal error. The sensitivity of the device is determined by the value of this marginal error (ϵ). This error is chosen based on the chance of fluctuating at a similar operating point when switching between steady-state oscillations.

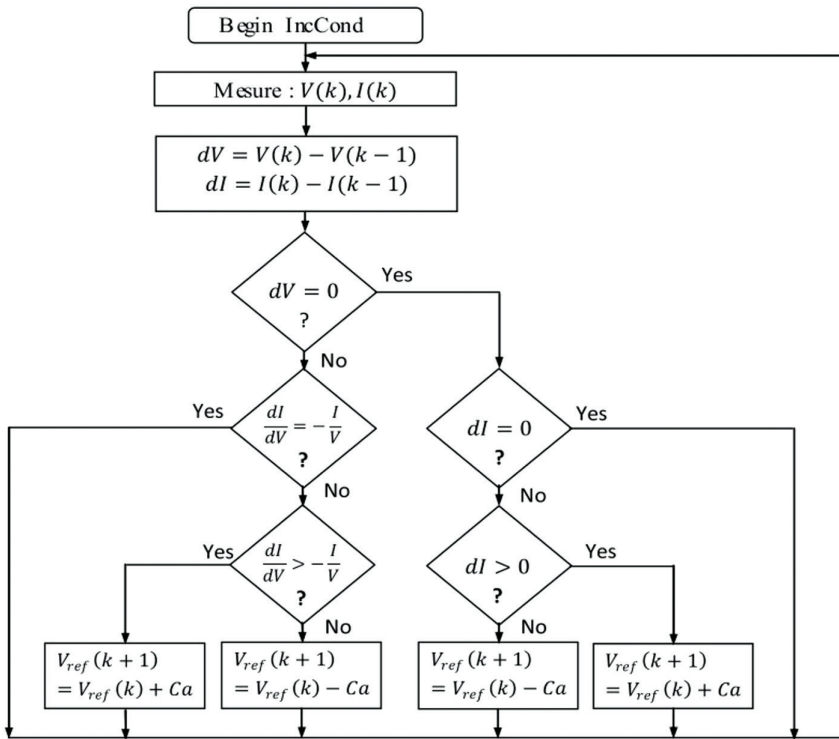


FIGURE 4.21

Algorithm for incremental conductance (I&C) MPPT technique.

4.6 Conclusion

Nonrenewable resources, which face rapid depletion, appear to be unable to meet the rising power demand alone. Solar is a ubiquitous and environmentally beneficial source of RE and has become one of the most widely used kinds of energy generation in a variety of applications.

Because PV cells are typically expensive and unreliable, getting the most power out of them is one of the most essential aspects of SE research. The electricity produced by a PV system varies depending on meteorological factors such as temperature, solar irradiation, and so on. Analyzing the performance of a SPV system under various weather circumstances is critical. It's also crucial to keep track of your MPP. For an MP tracking system with battery storage, an MPPT algorithm is utilized. To enhance the efficiency of a SPV system, it must be operated at maximum MPP with the MPPT algorithm. There have been detailed comparisons of all MPPT approaches, as well as a brief assessment of their benefits and drawbacks.

In addition, an error-based I&C MPPT structure has been developed. Furthermore, this review provides recommendations for SPV system researchers and engineers in selecting the appropriate prediction tool for improving the performance characteristics of SPV systems and maximizing the use of available solar radiation. In this chapter, we first discussed the need for SE and MPPT, with systematic diagrams and their characteristics. Next, this chapter explained the various traditional MPPT techniques, which are intended to support in many fields in the present and future distributed SG, energy storage system integration, including renewable energy integration, home energy management, demand response management, and protection. These approaches are supposed to boost performance even further while simplifying Smart Grid management. There have been several different MPPT conventional methods available in the literature, but the systematic comparison of different strategies with their tracking efficiencies under various weather conditions has not been done. This chapter aims to close the distance. This chapter focuses on the main conventional MPPT techniques, especially the most recent and widely used MPPT methods. Some MPPT techniques use irradiance and temperature to describe MPP. This chapter next explained the simplest and most commonly used traditional MPPT techniques which are P&O and I&C, with the algorithms and characteristics. Next, what are the drawbacks in the basic form of these MPPT techniques discussed in this chapter, and modified versions of these MPPT techniques also have been discussed? The simulation-based work of the P&O MPPT technique with detailed Simulink models and with their graphs is also represented in this chapter.

References

- Aganah, K. A. and S. Member, "A constant voltage maximum power point tracking method for solar powered systems," In *2011 IEEE 43rd Southeastern Symposium on System Theory*, pp. 125–130, 2011.
- Ahmed, J., S. Member, and Z. Salam, "A modified P & O maximum power point tracking method with reduced steady state oscillation and improved tracking efficiency". *IEEE Transactions on Sustainable Energy*, vol. 7, pp. 1–10, 2016. doi: 10.1109/TSTE.2016.2568043.
- Ali, A. I. M., M. A. Sayed, and E. E. M. Mohamed. "Electrical power and energy systems modified efficient perturb and observe maximum power point tracking technique for grid-tied PV system". *Electrical Power and Energy Systems*, vol. 99, pp. 192–202, 2018. doi: 10.1016/j.ijepes.2017.12.029.
- Azad, M. L., S. Das, P. Kumar Sadhu, B. Satpati, A. Gupta, and P. Arvind, "P&O algorithm based MPPT technique for solar PV system under different weather conditions," *Proceedings of IEEE International Conference on Circuit, Power and Computing Technologies, ICCPCT 2017*, 2017. doi: 10.1109/ICCPCT.2017.8074225.

- Basha, C. H. and C. Rani, "Different conventional and soft computing MPPT techniques for solar PV systems with high step-up boost converters: A comprehensive analysis," *Energies*, vol. 13, no. 2, 2020. doi: 10.3390/en13020371.
- Bataineh, K. M., & A. Hamzeh, "Efficient maximum power point tracking algorithm for PV application under rapid changing weather condition". *ISRN Renewable Energy*, vol. 2014, no. 3, pp. 1–13, 2014.
- Belkaid, A., I. Colak, and K. Kayisli, "Implementation of a modified P&O-MPPT algorithm adapted for varying solar radiation conditions," *Electrical Engineering*, vol. 99, no. 3, pp. 839–846, 2017. doi: 10.1007/s00202-016-0457-3.
- Bendib, B., H. Belmili, and F. Krim, "A survey of the most used MPPT methods: Conventional and advanced algorithms applied for photovoltaic systems," *Renewable and Sustainable Energy Reviews*, vol. 45, pp. 637–648, 2015. doi: 10.1016/j.rser.2015.02.009.
- Bharti, K. K., V. P. Singh, R. K. Patel and S. P. Singh, "Algorithm for tracking the maximum power from PV system," In *2019 3rd International Conference on Recent Developments in Control, Automation & Power Engineering (RDCAPE)*, pp. 693–697, 2019. doi: 10.1109/RDCAPE47089.2019.8979024.
- Bhatnagar, P. and R. K. Nema, "Maximum power point tracking control techniques: State-of-the-art in photovoltaic applications," *Renewable and Sustainable Energy Reviews*, vol. 23, pp. 224–241, 2013. doi: 10.1016/j.rser.2013.02.011.
- Daraban, S., D. Petreus, and C. Morel, "A novel MPPT (maximum power point tracking) algorithm based on a modified genetic algorithm specialized on tracking the global maximum power point in photovoltaic systems affected by partial shading," *Energy*, vol. 74, pp. 1–15, 2014. doi: 10.1016/j.energy.2014.07.001.
- "Irena.", 2012 [Online]. Available: <https://www.irena.org/publications/2020/Jul/Renewable-energy-statistics-2020>.
- Ishaque, K., Z. Salam, A. Shamsudin, and M. Amjad, "A direct control based maximum power point tracking method for photovoltaic system under partial shading conditions using particle swarm optimization algorithm". *Applied Energy*, vol. 99, pp. 414–422, 2012. doi: 10.1016/j.apenergy.2012.05.026.
- Ishaque, K., Z. Salam, and G. Lauss, "The performance of perturb and observe and incremental conductance maximum power point tracking method under dynamic weather conditions," *Applied Energy*, vol. 119, pp. 228–236, 2014, doi: 10.1016/j.apenergy.2013.12.054.
- Kermadi, M. and E. M. Berkouk, "Photovoltaic systems: Comparative study cross-mark," *Renewable and Sustainable Energy Reviews*, vol. 69, pp. 369–386, 2017. doi: 10.1016/j.rser.2016.11.125.
- Masoum, M. A. S., H. Dehbonei, and E. F. Fuchs, "Theoretical and experimental analyses of photovoltaic systems with voltage- and current-based maximum power-point tracking," vol. 17, no. 4, pp. 514–522, 2002.
- Messai, A., A. Mellit, A. Guessoum, and S. A. Kalogirou, "Maximum power point tracking using a GA optimized fuzzy logic controller and its FPGA implementation," *Solar Energy*, vol. 85, no. 2, pp. 265–277, 2011, doi: 10.1016/j.solener.2010.12.004.
- Mohanty, P., G. Bhuvaneswari, R. Balasubramanian, and N. Kaur, "MATLAB based modeling to study the performance of different MPPT techniques used for solar PV system under various operating conditions," *Renewable and Sustainable Energy Reviews*, vol. 38, pp. 581–593, 2014. doi: 10.1016/j.rser.2014.06.001.

- Nguyen, B. N., V. T. Nguyen, M. Q. Duong, K. H. Le, H. H. Nguyen, and A. T. Doan, "Propose a MPPT algorithm based on thevenin equivalent circuit for improving photovoltaic system operation," *Frontiers in Energy Research*, vol. 8, 2020, doi: 10.3389/fenrg.2020.00014.
- Pakkiraiah, B. and G. D. Sukumar, "Research survey on various MPPT performance issues to improve the solar PV system efficiency," *Journal of Solar Energy*, vol. 2016, pp. 1–20, 2016, doi: 10.1155/2016/8012432.
- Premkumar, M. and R. Sowmya, "An effective maximum power point tracker for partially shaded solar photovoltaic systems," *Energy Reports*, vol. 5, pp. 1445–1462, 2019. doi: 10.1016/j.egyr.2019.10.006.
- Rezk, H. and A. M. Eltamaly, "ScienceDirect a comprehensive comparison of different MPPT techniques for photovoltaic systems," *Solar Energy*, vol. 112, pp. 1–11, 2015. doi: 10.1016/j.solener.2014.11.010.
- Salas, V. Á., E. Oli, A. Barrado, and A. La, "Review of the maximum power point tracking algorithms for stand-alone photovoltaic systems," *Solar Energy Materials and Solar Cells*, vol. 90, pp. 1555–1578, 2006, doi: 10.1016/j.solmat.2005.10.023.
- Salman, S., X. Ai, and Z. Wu, "Design of a P-&-O algorithm based MPPT charge controller for a stand-alone 200W PV system," *Protection and Control of Modern Power Systems*, vol. 3, no. 1, 2018, doi: 10.1186/s41601-018-0099-8.
- Shaque, K., Z. Salam, and G. Lauss, "The performance of perturb and observe and incremental conductance maximum power point tracking method under dynamic weather conditions". *Applied Energy*, vol. 119, pp. 228–236, 2014. doi:10.1016/j.apenergy.2013.12.054.

Intelligent Techniques for Maximum Power Point Tracking

Dilip Yadav and Nidhi Singh

Gautam Buddha University

CONTENTS

5.1	Introduction.....	105
5.2	Different MPPT Techniques Used in PV System	106
5.3	Intelligent MPPT Techniques and Algorithms.....	108
5.3.1	Artificial Intelligence–Based MPPT	108
5.3.2	Bioinspired/Nature-Inspired Algorithm (Optimization).....	111
5.3.3	Hybrid-Based MPPT.....	122
5.4	Conclusion	124
	References.....	125

5.1 Introduction

Renewable energy (RE) sources derive their energy from natural processes, such as solar radiation, blowing wind, flowing water, biological processes, and other sources. Renewable energies are clean, inexhaustible sources, widely available, and do not pollute the greenhouse gases that cause climate change. In 173 countries, RE targets are in operation, and 146 countries have policies to support RE. Many countries aim to generate 30% of their energy from renewables by 2030; India has set a target of 40% power from RE resources by 2030. According to the recent report of the International Energy Agency (IEA), India is the fourth-largest producer of electricity in November 2020 by utilizing RE resources.

The solar cell is the unit cell connected in series and parallel connections to form an array and modules to increase their wattage rating. In 1968, the first MPPT-based PV system was introduced for space application; after that, many improvements were made to improve its quality, weight, tracking speed, efficiency, and applications. The I–V and P–V characteristics of the solar cell/array or module entirely depend on the value of irradiance and temperature. For silicon-based solar panels, the best efficiency is 29% theoretically and less than 27% in practice, and a fill factor of more than 70% is required for a high-quality

PV module, which differs based on the kind of solar cell and temperature coefficient. As per Vidyanandan (2017), factors like cable thickness, shading, temperature, irradiation, material, PID and accumulation of dust, degradation, tilt angle, and connections affect the efficiency of the solar panel.

The parameters that help in tracking the MPP are P_m , V_{mp} , V_{oc} , I_{mp} , and I_{sc} . According to Mohamed (2020), photovoltaic modules create electricity that may be utilized in both grid-connected and stand-alone systems. For the foreseeable future, PV technologies will be the dominant source of solar energy generation. Furthermore, future demand for off-grid solar systems remains untapped because of supporting policies and organizations. MPP is performed by varying the converter's duty cycle such that the load impedance gets matched with the source impedance.

PV modeling, MPPT techniques, the architecture of DC-DC converters, switching signal, duty control, concentrating solar power, and performance enhancement have all been investigated in solar research. As per Yadav and Singh (2020), improvement in the solar cell can also be one option for improving the performance of PV systems by using advanced optimization techniques. Several researchers have categorized MPPT techniques into traditional and evolutionary-based. According to Baba et al. (2020), Mao et al. (2020), Bollipo et al. (2020), Hussaian Basha and Rani (2020), Chen et al. (2017), and Karami et al. (2017), MPPT techniques can be classified as classical, intelligent, or AI-based, and hybrid-based technique. The concept of global maximum point (GMP) and local maximum point (LMC) with its disadvantages for different MPPT is discussed by Chen et al. (2017). There are some advantages and disadvantages of using different MPPT while using Global Maximum Power Point (GMPP). Although the performance of artificial intelligence (AI) and bioinspired (BI) optimization algorithms are complex, they are more reliable, efficient, and more stable than the classical-based MPPT. The characteristics method of PV model can reduce the error handling of the PV curve, at the same time the soft-computing and intelligent optimization algorithm is independent of PV curves. It can update the algorithm as per the objective function constraints, which helps to find the GMPP of the PV panel. While using the optimization method, objective functions and constraints should be defined. As per Chen et al. (2017), many algorithms suffer from slow global search speed, optimality inside the local environment, and over-reliance, which reduces the system's performance.

5.2 Different MPPT Techniques Used in PV System

Figure 5.1 represents a few MPPT techniques used earlier with the new techniques present nowadays, after reviewing different MPPT techniques and optimization papers, MPPT has been classified into three broad methods:

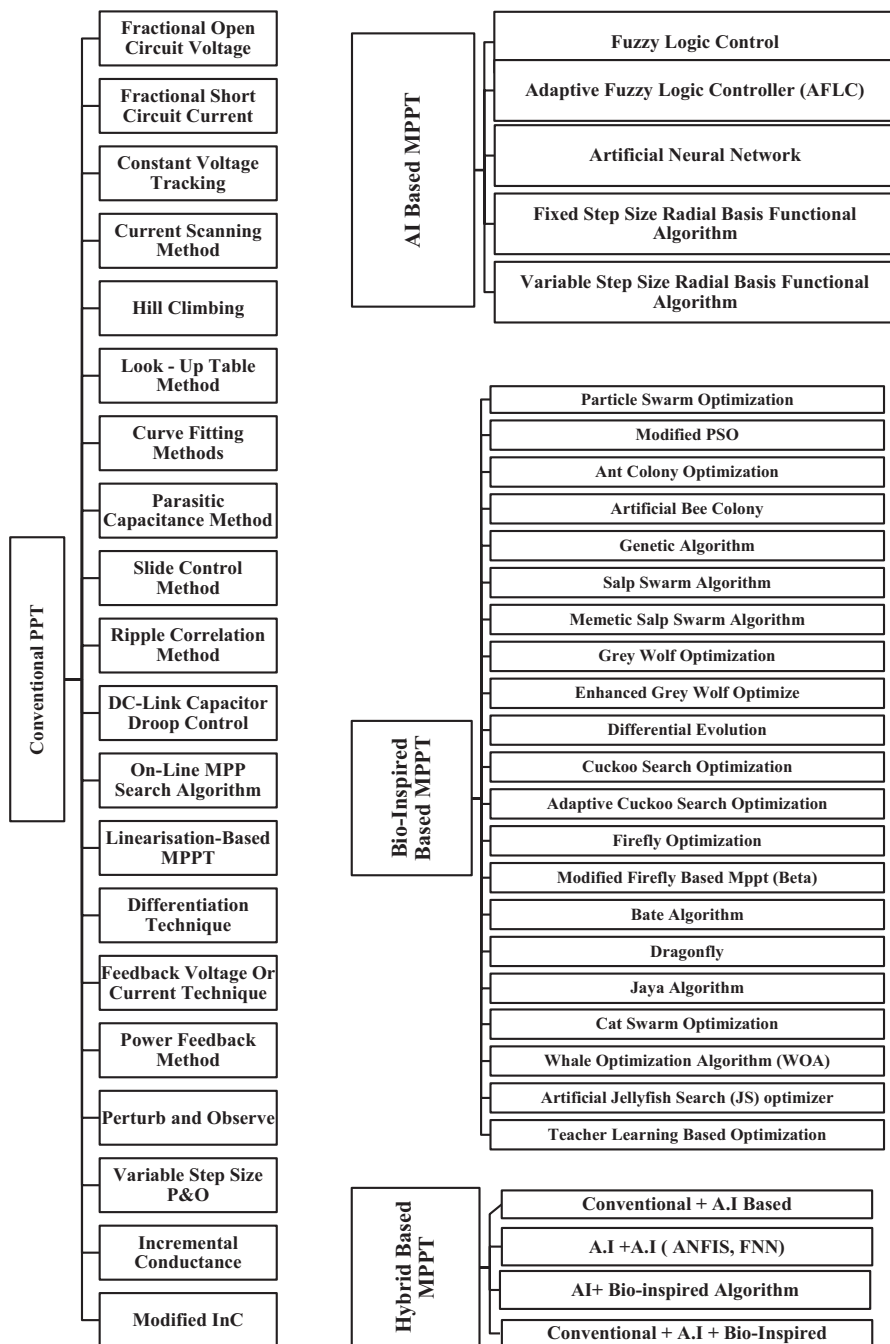


FIGURE 5.1

Classification of different PPT techniques used in PV system.

classical methods, soft computing, and hybrid methods. The most widely used MPPT in classical methods are hill climbing (easy and cost-effective technique method), look-up table (faster than other standard techniques), slide control method (removes steady-state error to a great extent), perturb and observe (implementation is quick, inexpensive, and straightforward), incremental conductance (have better noise rejection), and modified incremental conductance (high tracking speed).

Every MPPT technique has sensors (voltage, current, irradiation, and temperature) that adjust the duty cycle according to the environmental condition. Hu et al. (2014) suggested the new idea of using thermography cameras to assist the MPPT for the PV system. Different approaches have different operation mechanisms for tracking the MPP. In this chapter, intelligent-based (soft-computing and hybrid) MPPT is reviewed with its working, advantages, and disadvantages.

5.3 Intelligent MPPT Techniques and Algorithms

Intelligent controller approaches improve classical controller techniques in terms of tracking the Maximum Power Point Tracking (MPPT) during the dynamic condition. Furthermore, they are efficient, dynamic, fast convergence, output voltage fluctuations are low, can track GMM for all PV curves, and have robust search techniques that provide near-optimum results and feature a high level of implicit redundancy. This intelligent MPPT (soft-computing) technique can be further classified as Artificial Intelligent (AI)-based MPPT technique and BI-based MPPT algorithm. Intelligent MPPT techniques' short reviews are given below.

5.3.1 Artificial Intelligence–Based MPPT

AI-based systems have self-learning capability, solving the nonlinear complex equations with higher accuracy and tracking capability in minimum time. As per Baba et al. (2020), Mao et al. (2020), Bollipo et al. (2020), Hussaian Basha and Rani (2020), and Mellit and Kalogirou (2008), the advantages of different MPPT techniques have uplifted many researchers in utilizing the MPPT technique in different areas and applications. Constant efforts are going on to improve self-learning and problem-solving skills. As per Chen et al. (2017), without a higher degree of mathematical manipulation, fully trained AI-based systems can solve complex problems quickly under partial shading conditions. Recent papers of Garud et al. (2021), Seyedmahmoudian et al. (2016), Zhang et al. (2020), and Yadav and Singh (2021) concluded that AI solution has now established itself as a viable alternative to numerous classical problem-solving approaches. The classical MPPT controller was

nonefficient to track the MPP as the PV module's characteristic is nonlinear and changes with temperature and irradiance. So, to overcome the challenge of classical MPPT techniques, AI was introduced. A few of the AI-based MPPT techniques that are widely used are discussed below.

Fuzzy Logic Control (FLC): According to Baba et al. (2020), fuzzy logic is a logical structure that is an extension of multivalued logic or a theory of fuzzy sets. Fuzzy logic is based on the concept of logic that is easy to understand. As per Hussaian Basha and Rani (2020) and Mellit and Kalogirou (2008), FLC can be used for nonlinear functions that are based on the experience of expert knowledge and on natural language, which is easy to understand. Fuzzy logic MPPT is considered an intelligent technique because it tracks the MPP even if the sources of knowledge are unclear (PV curve). Fuzzification, rulebase–database table (fuzzy rules), and defuzzification are the three important steps of the fuzzy technique. As per Bollipo et al. (2020), fuzzification is a process of converting the input of the PV parameter into a fuzzy set. Garud et al. (2021) and Baba et al. (2020) stated that rules are set by using “IF” and “THEN” statements with “AND,” “OR” or “NOR,” Boolean conditions, which gives the relationship between the input to output parameters. Defuzzification is the inversion of fuzzification in which the center of gravity is mainly used for the computation process. FLCs in the PV system vary the duty ratio in the converter that is based on the knowledge over a change in error and error, intending to reach the panel voltage equal to the maximum value (V_{mpp}). An error E and a change in error ΔE are usually the inputs to an MPPT fuzzy logic controller. Expression is given by eqs. (5.1) and (5.2).

$$E(n) = \frac{V_{pv}(n) * I_{pv}(n) - V_{pv}(n-1) * I_{pv}(n-1)}{V_{pn}(n) - V_p(n-1)}. \quad (5.1)$$

$$\Delta E(n) = E(n) - E(n-1). \quad (5.2)$$

where $V_{pv}(n) * I_{pv}(n)$ and $V_{pv}(n-1) * I_{pv}(n-1)$ represent the instantaneous output powers and photovoltaic generator output voltage, respectively. $\Delta E(k)$ is a global dynamic error, $E(n)$ and $E(n-1)$ are two consecutive sampling values, and “ n ” is the sampling counter. Many users have compared its performance using different input and utilizing it in different applications. The fuzzy inference is performed by using *Mamdani's* tool, and for defuzzification, the *center of gravity* method is used to calculate the output (duty ratio) of this fuzzy logic-based MPPT. As per Baba et al. (2020) and Mao et al. (2020), the FLC controller has a better performance compared to many MPPT techniques. Determining the fuzzy sets and membership functions, and setting the proper rule-based tables are necessary for FLC as these factors affect the performance of MPPT.

Adaptive Fuzzy Logic Controller (AFLC): FLC controllers consist of rules-based and membership functions; challenging situations arise when a wide range of data or conditions exist or specialist expertise is unavailable

or unreliable. To investigate this issue, AFLC is used, which can readjust the parameter to achieve the best results. As per Patcharaprakiti and Premrudeepreechacharn (2002), AFLC has a faster response time and better efficiency. A fuzzy inference base control and a learning mechanism are the two aspects of this system. Seyedmahmoudian et al. (2016) and Patcharaprakiti and Premrudeepreechacharn (2002) compared AFLC with another controller with the same environmental conditions and concluded that the AFLC controller is better in terms of low oscillation around the MPP during the nonuniform condition, but Baba et al. (2020) and Mao et al. (2020) stated that the cost of operation is much higher than the FLC.

Artificial Neural Network (ANN): According to Garud et al. (2021) and Zhang et al. (2020), ANN is inspired by biological algorithms applied in various applications to recreate information processing like in the human brain. The most often utilized topology of the neural network consists of three layers: input, hidden, and output layers. ANN can be classified according to the controller structure embedded in the MPPT process as (1) stand-alone controllers and (2) hybrid controllers. Bollipo et al. (2020) stated that due to the inherent structure of the learning mechanism and the biological nature of neurons, ANN is the intelligence-based advanced MPPT technique. According to Garud et al. (2021) and Saravanan and Babu (2016), the way neurons are linked to one another produces distinct primary types of ANN structure, i.e., Feedforward Neural Network (FNN), Recurrent Neural Network (RNN), and Radial Base Function Network (RBFN). Application of RBFN-based MPPT algorithm for PV system with the high step-up converter is given by Saravanan and Babu (2016). In Zhang et al.'s (2020) research paper, the precision of the model is calculated by using the root mean squared error (RMSE) and the normalized RMSE (NRMSE) between the expected and measured I-V curves. The DC/DC controller uses ANN output as the reference power, and the duty cycle is changed in terms of parameter adjustment to accomplish the MPP. A section of the data is randomly divided into training data, testing data, and validation data to find the regression curve and error in the data, that can be utilized for energy and reliability prediction. In ANN, the activation function is used, which is taken from Bollipo et al. (2020) shown in eq. (5.3).

$$\sum_{m=1}^M X_m + W_m a \quad (5.3)$$

where X_m is the incoming signal, W_m is weighted and a is the biased parameter. As per Garud et al. (2021), the activation function's main work is to convert the linear function to a nonlinear function that consists of a hyperbolic tangent, Tan sigmoid, and Log-sigmoid, etc., function. To predict the best-targeted value, the weights and bias are continuously computed. The number

of neurons in the hidden layer significantly impacts the network's training time and accuracy, given by eq. (5.4)

$$\text{Number of hidden layers} = \frac{\text{Number of input + output neurons}}{2 + \sqrt{\text{number of training data points}}} \quad (5.4)$$

Fixed Step Size Radial Basis Functional Algorithm (FSSRFA): According to Hussaian Basha and Rani (2020), FSSRFA consists of highly interconnected neurons and the hidden layer is chosen by using the empirical process. The output of the duty cycle is either 0 or 1. PV voltage (dV) and power (dP) error values are the first layer's inputs. The duty cycle varies as per the dP/dV sign. If dV_{pv} and dP_{pv} are negative, then dP_{pv}/dV_{pv} is positive, and the change in the duty cycle increases with the step input. If any of dV_{pv}/dP_{pv} is negative, then there is a decrement in the step size. This is how the FSSRFA works. However, this approach has disadvantages such as slow convergence, high oscillations, and poor MPP tracking performance during nonlinear irradiation and temperature condition.

Variable Step Size Radial Basis Functional Algorithm–Based NN MPPT Technique (VSSRBFA): To resolve this issue like slow tracking speed, convergence speed, and oscillations in ANN, VSSRBFA-based NN can be used. As per Hussaian Basha and Rani (2020), VSSRBFA-based NN operates in two stages in the first step, the input layer's control variables are calculated using an unsupervised learning approach, and the output layer weights are adjusted in the second stage. The switching pulses to the DC-DC converter are generated by the NN MPPT controller. The duty cycle is modified in this process using eq. (5.5).

$$D(j) = D(j - 1) \pm (\text{Step} + N * dP). \quad (5.5)$$

where D is the duty value, N is the scaling factor that changes the controller's step scale, and dP is the difference in PV power.

The advantages and disadvantages of widely used AI techniques are given in Table 5.1. Many researchers have analyzed its performance and have given the comparison between them in terms of cost (Baba et al., 2020), efficiency (Mao et al., 2020 and Baba et al., 2020), tracking speed and error detection (Hussaian Basha and Rani, 2020), complexity and hardware implementation (Hu et al., 2014). Other important parameters like tracking time, applications, tuning parameters, dynamic response, dependency on a cure are given in Karami et al.'s (2017) research paper.

5.2.2 Bioinspired/Nature-Inspired Algorithm (Optimization)

Nowadays, BI methods are grabbing great attention as they are based on the movement of nature and can find the best solution or GMPP or the best optimal solution to complicated functions, which are nonlinear in operation and

TABLE 5.1

Advantages and Disadvantages of Different Artificial Intelligence-Based MPPTs

MPPT Technique	Advantage	Disadvantage
Fuzzy logic control	Can adjust the duty cycle when dynamic changing atmospheric condition arises.	When irradiance varies, it causes a drift condition that makes the system more complex.
Adaptive fuzzy logic controller	With a low oscillate around the MPP, AFLC performs better in terms of efficiency and tracking speed.	This device will supply energy to the utility by adjusting its parameter; sometimes, it makes the system complex.
Artificial neural network	Easy to use, low cost and the performance convergence rate is high.	Accuracy depends on data sets numbers.
Fixed step size radial basis functional algorithm	Reduce the system cost and size and make it efficient.	MPP tracking has a slower convergence rate at dynamic irradiation environments, higher steady-state oscillations, and lower precision.
Variable step size radial basis functional algorithm-based NN	MPP tracking at dynamic irradiation conditions provides a robust convergence speed, low steady-state oscillations, and high precision.	The scaling factor should be appropriately selected as it adjusts the step size of the controller.

complicated problems like multimodal objective functions. As per Baba et al. (2020), the search function of these algorithms is simple, and they have a high degree of optimization efficiency. When multiple peaks occur under shade circumstances, the effectiveness of traditional MPPT algorithms is decreased, so to track the GMPP, a two-stage system is suggested in which the LMP's operating point is shifted to the area of the GMPP in the first stage by using the load line, that converges to the GMPP in the second stage. The BI method has numerous advantages like it can eliminate the need for prior knowledge of basic system parameters, reduces computational process, and gives a brief solution to the variables. According to Baba et al. (2020), Mao et al. (2020), Bollipo et al. (2020), Hussaian Basha and Rani (2020), Garud et al. (2021), Saravanan and Babu (2016), and Hu et al. (2019), BI methods can be utilized for tracking the GMM for partial shading conditions with higher efficiency and tracking time. A few of the widely used BI-based MPPT techniques are given below.

Particle swarm optimization (PSO) algorithm: It was structured in 1995 and was inspired by bird flocking and fish schooling, stated by Hu et al. (2019). By using search optimization, the MPP of any kind of P-V curve can be determined. Several collective agents are used in this algorithm, following the most consistent particle and step toward an optimal solution. $P(d_i^k) > P(d_i^{k-1})$ denotes the objective function given in Bollipo et al.'s (2020) paper. The general formula is given by eq. (5.6):

$$x_i^{k+1} = x_i^k + V_i^{k+1} \quad (5.6)$$

where V_i is velocity factor, calculated by given by eq. (5.7)

$$V_i^{k+1} = W * V_i^k + C_1 * r_1 * (P_{best_i} + x_i^k) + C_2 * r_2 * (G_{best_i} - x_i^k) \quad (5.7)$$

where W is the inertia weight, and C_1 and C_2 are acceleration constants whose values are kept up to 2. The initial particle for these voltage samples is x_i , with each iteration, all of the particles travel toward the local best position, just with one value representing the global best position. The particles begin to move to the G_{best} value with each iteration from the local best location. As a result, the P_{best} (personal best) and G_{best} (global best) variables in the velocity term approach zero, and the voltage direction remains almost constant. As per Baba et al. (2020) and Garud et al. (2021), PSO controls the GMPP during all conditions, and it has great potential because of its simplest form, quick execution, and quick computation power. PSO approach has a few steps like initialization, fitness analysis values, updated P_{best} and G_{best} value, update velocity and location of each particle, and convergence conditions that must be fulfilled during the PSO approach. PSO suffers from poor dynamic speed as random oscillations are generated due to random numbers selected during the optimization process.

Modified PSO or Improved PSO (IPSO): As PSO depends on the random variable, the working of PSO becomes complicated, which results in controlling the issue, and the solution falls to find the local optimum solution. According to Benyoucef et al. (2015), PSO is related to random variables; if the random values are too small or too high, then the optimal solution falls in the optimum local value, and MPP gets disturbed. The IPSO work in two modes. When the environmental conditions are uniform, algorithm operates in local search mode. If a nonuniform condition arises or partial shading condition occurs, GMPP comes into action. Garud et al. (2021) stated that IPSO averages the peaks and calculates their total peak point. The range of duty cycles is calculated by using eqs. (5.8) and (5.9).

$$d_{min} = \sqrt{\eta b R L_{min}} / \sqrt{R P V_{max}} + \sqrt{\eta b R L_{min}} \quad (5.8)$$

$$d_{max} = \sqrt{\eta b R L_{max}} / \sqrt{R P V_{min}} + \sqrt{\eta b} \quad (5.9)$$

where d_{min} is the minimum duty cycle, η_b is the converter efficiency, d_{max} is the maximum duty cycle, R_{Lmin} and R_{Lmax} are the minimum and maximum values of the load connected at the output, and $R P V_{max}$ and the $R P V_{min}$ denote the reflective impedance of the PV array taken from Baba et al. (2020). The IPSO algorithm immediately changes to local searching mode once the approximate position of the maximum power point is found. The algorithm is especially suitable for tracking local minima; the performance of the IPSO in the GMPP under the PSC can be improved significantly. The number of iterations is reduced, but the system's complexity rises in this method.

Ant Colony Optimization (ACO): The ACO algorithm uses a similar search theory to the PSO algorithm. Parameters like the number of ants (M), solution size (K), convergence speed constant (A), and location of the search procedure (Q) are considered during the process. For each voltage value V_i , the corresponding value of the duty cycle d_i is calculated as $d_i(t) = 1 - \frac{V_i(t)}{V_{ref}}$.

More ants mean finding the GMPP under varying irradiance conditions is simpler, although transferring all the ants into the MPP takes more time. Its voltage value determines each ant's fitness, and fewer ants offer less convergence level. However, in one of the local power peaks, they will easily get trapped, which reduces its efficiency. The main benefit is that it will respond to changes in real-time and function constantly. It is built on the normal behavior of individual worker ants in ant colonies. Baba et al. (2020), Mao et al. (2020), and Bollipo et al. (2020) compared ACO to genetic algorithm (GA) and concluded that ACO has better performance than GA. It offers remarkable tracking capabilities with high precision, zero oscillations, rapid convergence, and extremely high robustness with less computation time are seen in Baba et al.'s (2020) paper.

Artificial BEE Colony (ABC) Optimization: Benyousef et al. (2015) suggested that ABC is based on the features of the bee foraging behavior, learning, memory, and knowledge exchange. As per Baba et al. (2020) and Yang et al. (2019), ABC uses very few regulated variables. The bees are divided into three groups: employed bees (extracting food source), on-looker bees (choosing the best food source), and scouts bees (improved solution by a variety of tests). The equation used to produce each solution is given by $x_i^j = x_{max}^j + \text{rand}[0, 1](x_{max}^j - x_{min}^j)$, where x_{min}^j and x_{max}^j represent the parameters' minimum and maximum values. It has quick convergence, improved robustness, low computing expense, and high precision, but ABC has a high settle time and oscillation at the output.

The Salp Swarm Algorithm (SSA): SSA is a novel BI approach created in 2017. According to Baba et al. (2020) and Mao et al. (2020), SSA has a primary search function and high optimization performance. The primary motivation for SSA is the swarming activity of salps when navigating and foraging in the ocean. Salps often form a swarm known as a salp chain in deep oceans; these aggregated organisms are often known as *blastozooids*. During swimming and feeding, they remain attached to one another, and each individual grows in size. During iterations of SSA, the leading salp shifts its location around the food supply, and follower salps eventually pursue it. This approach efficiently boosts initial random solutions and converges to the optimum solution. Since SSA can only save one solution as the best solution, it cannot save multiple solutions as the best solution in the case of a multiobjective problem which is a disadvantage of using it.

Genetic Algorithm (GA): It is a common evolutionary computational technique aimed at maximizing fitness function. Selection, crossover, and

mutation are GA's three primary fundamental stages. A chromosome is chosen randomly to participate in the following region based on its fitness value in the first cycle. During the crossover process, two chromosomes became a single chromosome. The mutation stage causes genetic variation. GA is excellent at partial shading since searching for the optimum is carried out on an individual population rather than on a step-by-step basis, resulting in a global optimum as per Baba et al. (2020). Mao et al. (2020) stated that GA is extremely reliable and has a wide range of applications, especially for real-time nonlinear and multimodal objective function problems. At each population size point, the objective function value is evaluated. GA produces new populations before finding a suitable fitness alternative. Maximum terms, fitness limit, generations, feature resistance, and limit sensitivity are some of GA's stopping factors as per Chen et al. (2017). GA and PSO have been found to control the GMMP with good performance and lower installation costs, but implementation is complex. GA has a slow tracking speed as it uses a series format for each particle in the population.

Memetic salp swarm algorithm (MSSA): As per Yang et al. (2019), SSA only uses a single swarm of individuals with a search function, so a better algorithm was required. The MSSA is chosen by using multiple individual slap chains to enforce exploration and exploitation simultaneously. The MSSA algorithm first sets the limit for upper value and lower value of variables for the population of salps. The objective values for each salp are then calculated, and the nondominated ones are found using this algorithm. The position of leading/follower salps is updated using $x_{in} = \frac{1}{2}(x_{ij} + x_i - 1_j)$

where $i \geq 2$ and x_{ij} is the position of i th follower salp in j th dimension. If a salp drifts outside of the boundaries during the upgrading location process, it will be taken back into the boundaries. Finally, except for initialization, all of the preceding steps are repeated until an end condition is satisfied. MSSA algorithm is quick and fast to execute since it only has two key controlling parameters.

Grey Wolf Optimization (GWO): As per Eshak et al. (2020), GWO is a metaheuristic approach that is based on maximizing the assaulting style of grey wolves while stalking. Four groups of grey wolves show the configuration of GWO parameters: *alpha* (α), *beta* (β), *delta* (δ), and *omega* (ω). In mathematical modeling, the optimal solution follows α and then β and after that δ and ω . The main steps in this method are to hunt, chase, and track the prey by forming a ring, then encircle the prey, and then attack the prey. According to Eshak et al. (2020), the grey wolf's hunting system is led by α groups that act as leaders and are accompanied by other groups. P_{pv} is determined with the condition that $P(i) > P(i - 1)$ and if the condition is fulfilled, P_{max} is modified until $G_{max} > P_{max}$ to keep the service cycle stable at MPP and minimize steady-state oscillations. $A = 2 * a * r_1 a$ and $C = 2 * r_2$ are coefficient vectors that have to be updated, " a " values decrease linearly from 2 to 0, and r_1 and r_2 values are chosen at random from 0 to 1. $d_i(k + 1) = d_i(k) A * d$ is

used to measure GWO duty cycle, and fitness is calculated as $P(d_i^k) > P(d_i^{k-1})$, where P represents power, d represents duty cycle, i represents the number grey wolves, and k represents iteration count. It has higher monitoring performance, but in traditional GWO, *delta* (δ) and *omega* (ω) wolves do not engage much in prey hunting, which requires a more significant number of search agents, which takes a long time to find the best solution.

Enhanced Grey Wolf Optimizer (EGWO)-based MPPT: As per Cherukuri and Rayapudi (2017), the main idea behind this enhanced GWO is to use δ and ω wolves phase so that the extra time taken by GWO can be improved. In EGWO α is supposed to be the preferred method, followed by β . The fitness function is modified by using d_α and d_β , i.e., the first and second-best populations with the highest PV power were $D_\alpha = C_1 * d_\alpha - d_i$; $D_\beta = C_2 * d_\beta - d_i$, where D_α and D_β are a distance of d_α and d_β from the maximum power. The EGWO algorithm is found to track global MPP with greater precision and have less processing time.

Differential Evolution Algorithm (DEA): They are used to solve nondifferentiable, noncontinuous, nonlinear, noisy, flat, or multidimensional problems, as well as problems with numerous local minima, constraints, and stochasticity. The DE method is based on the GA principle. The four steps of the algorithm are initialization, mutation, crossover, and selection as suggested by Baba et al. (2020) and Mao et al. (2020). In the DE-based MPP tracking method, the duty cycle is the goal vector, because the DEA method is based on a static objective function, it is ineffective for real-time MPPT applications. To improve the stochastic structure, the parameters are randomly chosen and recombined. A model's function for parameter selection is essential. After crossover, the trial vectors are created and the output power of the DE-based MPPT is evaluated. DE's strengths include a worldwide tracking technique and ease of application. The drawbacks of DE are dependent on the algorithm's control parameters.

Cuckoo Search (CS) Optimization: It is based on the principle of brood parasitism, in which the parasite lays its eggs in the nests of other birds. They are used to solve problems of several dimensions. Three laws govern the operation of CS: (1) each cuckoo lays an egg and places it in a host residence that is chosen at random, (2) the highest-quality eggs in that nest would be passed down to the next generation, and (3) the number of usable host homes is determined, and the host bird discovers the cuckoo's egg with a probability of [0,1]. As per Mesa et al. (2018), the search for a host nest is accomplished by using a mathematical model called *Lévy flight*, which employs random step sizes ruled by the following power-law distribution. $Y = l^\lambda$, where λ and l are variance and flight length, $1 < \lambda < 3$, implies that Y has infinite variance. CS Lévy flight is performed by utilizing the following equation $x_i^{t+1} = x_i^t + \alpha \oplus \text{Levy}(\lambda)$, the sample number is given by i , maximum iteration by t , and α ($\alpha > 0$) is the step size. In this case, the host bird has two options: destroy the egg or create a new one. When a bird recognizes the egg isn't its own, it uses Lévy flight to destroy it. Compared to PSO and DE approaches,

CS has a random step, and in low-power, high-power, and regular zones, the power is differentiated.

Adaptive Cuckoo Search Algorithm (ACA): The fixed switching parameter is involved because undesired and unexpected shifts in the duty cycle trigger oscillations and produce undesired glitches in the output power. The following modified switching parameter technique can be used to increase the performance of the CS, and it is defined as $P_{aci} = (P_{max}) * (C_i)/T_i$, where C_i is the present iteration and T_i is the total number of iterations as suggested by Baba et al. (2020). The sufficient number of initial populations helps in faster convergence and increases its tracking efficiency.

Firefly Based MPPT Algorithm (FB): In some of the publications such as Baba et al. (2020), Garud et al. (2021), and Chaurasia et al. (2017), FB is used for MPPT. This optimization algorithm is based on the principle of firefly movement. The two most crucial roles of such flashes are to attract mating mates and potential prey. As per Baba et al. (2020), the objective function has an effect of brightness on a firefly (optimization problem is directly proportional to an objective function). β , i.e., a coefficient to track MPPP is updated that helps in fast convergence and to obtain an accurate result, which increases the tracking time. If $p < q$, the following equation gives the current location of firefly p .

$x_p^{t+1} = x_p^t + \beta(r)(X_p - X_t) + \alpha \left(\text{rand} - \frac{1}{2} \right)$, where " α " is constant with the value

of 0–1, random number (r) lies from 0 to 1 as per Chaurasia et al. (2017). The algorithm is implemented in the following steps: parameter setting, firefly initialization, brightness evaluation, updating firefly location, and terminating the process. The benefit of using FB is that it has easy procedural steps and quicker convergence.

Bat algorithm (BA). As per AS Oshaba et al. (2018), the behavior of bats was the inspiration for this algorithm. It can be formulated by following these steps: all bats use echolocation to determine the distance between themselves and their prey. Each bat flies at a given frequency f_{min} with a velocity v_i at point x_i . The frequency of the bat is changed based on its distance to the prey, and the frequency of the bat varies from A_0 to a minimum fixed value A_{min} . The basic equations used are (5.10–5.12):

$$f_1 = f_{min} + (f_{max} - f_{min}) * \beta \quad (5.10)$$

$$v_i^t = v_i^{t-1} + (x_i^{t-1} - x') * f_i \quad (5.11)$$

$$x_i^t = x_i^{t-1} + v_i^t \quad (5.12)$$

where β is defined as a vector for uniform distribution and chosen between 0 and 1. x' is the global best position, the minimum and maximum frequency of i th bat is given by f_{min} , and f_{max} is, and β is a random value between [0, 1]. Under atmospheric conditions, BA is used to increase the system's performance and provide peak power to SRM.

Cat Swarm Optimization (CSO): CSO is focused on the foraging and living habits of cats. According to Chu and Tsai (2007), each cat in the swarm has a unique location in this algorithm, which means the solution group, velocity for each spot, and fitness value. It has two modes. In the 1st mode (scanning mode), cats remain alert and advance slowly and in the 2nd mode (tracking mode), cats follow the target after detection. Scanning Mode (SM) is in favor of one, while Tracking Mode TM is in charge of the other. The combination ratio determines the ratio of the two sets Mix Ratio (MR). In TM mode, cats need to hunt targets and foods, and they move quickly to a new position during the chasing process, given by eq. (5.13).

$$V_{i,d} = w \times V_{i,d} + r_1 \times c_1 \times (X_{\text{best},d} - X_{i,d}) \quad (5.13)$$

where X_{best} gives the best position among all cats, c_1 is an acceleration constant, w is the inertia weight, and r_1 is the random number that varies from 0 to 1. The position is updated by using eq. (5.14):

$$X_{i,d} = X'_{i,d} + V_{i,d} \quad (5.14)$$

The algorithm is system-independent, has good tracking precision and convergence speed, and has a high ability to obtain global MPP while eliminating power fluctuations around MPP.

Jaya Algorithm (JA): According to Huang et al. (2018), the JA's key idea is to prevent the worse solutions. As per Baba et al. (2020), the weakest solution is obtained first, and then all other solutions are discarded, and, from the worse solutions, the worst solution is revised. As a result, every successive solution is superior to the preceding worst answer. Huang et al. (2018) and Baba et al. (2020) stated that the primary phases of the JA include parameter selection, Jaya initialization, fitness calculation (a higher P signifies a more substantial V), solution corrections, and termination determination.

Dragonfly-Based Optimization (DB): As per Baba et al. (2020), Mao et al. (2020), and Chen et al. (2017), the behavior of DB is inspired by dragonflies. Their mutual knowledge and swarm behavior result in an algorithm that can easily work with global optimization problems. Explorative and exploitative behaviors are utilized for navigating the algorithm. The flight of dragonflies can be described as sudden small jumps, which is referred to as imitating exploitation. A specific direction of motion to travel between two distant locations is referred to as explorative. Separation, alignment, attraction, adversary, and cohesion are five distinct characteristics of DF swarms that are mathematically modeled. The basic equation of DF is given as $X_i = X_i + \Delta X_i$, where ΔX_i is calculated using the following equation $\Delta X_i = sS_i + \alpha S_i + cC_i + fF_i + eE_i + w\Delta X_i$, where "s" represents separation weight, S_i is the separation of i th DF, "a" is alignment weight, A_i is Alignment of i th DF, "c" is cohesion weight, C_i is the cohesion of i th DF, f is food factor constant, F_i is food attraction, e is enemy factor constant, E_i is enemy position

with inertial weight, and ΔXi is the step size of DF movement. Search space is between D_{\min} and D_{\max} , and the objective function is to maximize output power. Chen et al. (2017) concluded that DF efficiency is higher in a smaller population with a greater food and weight ratio than in PSO.

Whale Optimization Algorithm (WOA): The whale optimization method was inspired by humpback whales' bubble-net hunting method as given by Chen et al. (2017). This technique of following is called bubble-net feeding. Humpback whales hunt small fish at the surface by constructing bubble nets around the prey as it rises in a circular motion. This behavior can be mathematically expressed as $D = C * X * (t) - X(t); X(t+1) = X'(t) - A \cdot D$, where t is the number of iterations, A and D are the coefficient vectors, X' is the best solution vector, and X is the position vector. As a better solution is identified, the best Solution X location vector is modified as $A = 2a * r - a$ and $C = 2 * r$, where r is an arbitrary vector between $[0, 1]$. This parameter is chosen at random to strike a balance between the penetration and investigative periods. Two methods are used to humpback whales' air bubble-net behavior: the shrinking circling system and the spiral updating position. After this investigation point, the new position is used to search for prey, updating A , C , and D . The new location is revised until the optimum solution is not obtained. Under dynamic partial shading conditions, this approach is excellent in tracking the GMPP with high accuracy and minimal tracking time. Furthermore, WOA and its derivatives are incapable of solving high-dimensional optimization problems well enough.

Teaching–Learning Based Optimization Technique (TLBO): M. M. Puralachetty et al. (2016) used the concept of *Patel and Reo* in which many students were taken into account in terms of population and presented them in terms of certain subjects. Student outcomes express the exercise feature. The best exercise score student is selected as a community teacher. If “ r ” is the random number between $[0, 1]$ and one learner (dx) tries to enhance his knowledge by the interaction with another randomly one (dy) through the student stage, $d_{\text{new}} = d_x + r(dy - dx)$, if $P_{pv}(dy) > P_{pv}(dx)$; $d_{\text{new}} = d_x + r(dx - dy)$, if $P_{pv}(dx) > P_{pv}(dy)$. Based on all learners' appraisal, the duty cycle has to be changed, and so either two learners are randomly selected to change the duty cycle. These measures are replicated before all students reach the optimum answer, representing the optimum duty interval corresponding to global MPP.

Artificial Jelly Fish Optimization (AJFO): In Chou and Truong (2021), the concept of AJFO is illustrated that is inspired by the ocean jellyfish behavior. Simulating the behavior of jellyfish in searching requires them to follow the oceanic stream and their movements within a jellyfish swarm, a time check method for moving between these movements, and transforming them into jellyfish bloom. Three idealized rules are as follows: (1) Jellyfish either obey the ocean current and the “time balance system” controls the switching between these movement types, and (2) jellyfish explore the ocean for food.

They're more drawn to places where there's more food around, and (3) the quantity of food found shall be calculated by position and objective function. Ocean current can be determined ocean current can be calculated by using the $X_i(t + 1) = X_i(t) + \text{rand}(0, 1) * (X - \beta) * \text{rand}(0, 1) * \mu$, where $\beta > 0$, μ is the mean location of all jellyfish, and β is a distribution coefficient. The updated location of each jellyfish is given in eq. (5.15).

$$X_i(t + 1) = X_i(t) + \gamma * \text{rand}(0,1) * (Ub - Lb)$$

(5.15)

where $\gamma > 0$ is a motion coefficient. Motion direction and a jellyfish's modified position rely on the time regulation system, including a time control feature $c(t)$ and a constant C_o .

Table 5.2 represents the advantages and disadvantages of using a BI algorithm in a PV system to control the duty cycle/power using the MPPT techniques. Baba et al. (2020), Mao et al. (2020), Karami et al. (2017), and Garud et al. (2021) simulated BI MPPT techniques and compared them in terms of efficiency, tracking speed, complexity, cost, accuracy and hardware

TABLE 5.2
Advantages and Disadvantages of Bioinspired Algorithm Used in MPPT

MPPT Technique	Advantage	Disadvantage
Particle swarm optimization	Monitors the GMPP during the condition, and it has a high potential due to its simple structure, quick execution, and quick computing capabilities.	The dynamic response speed is low, the random numbers rooted in the PSO velocity cause random oscillations, dependent on random variables.
Modified particle swarm optimization	Enhanced type of PSO. The number of iterations is reduced, so tuning effort reduces.	The system's complexity is high. The values of w ; Φ should satisfy the convergence of searching particles.
Ant colony optimization	Have low computing time, good tracking accuracy, zero oscillations in output, rapid convergence, and high robustness.	Need extra parameters as compared to PSO, whereas all the ants need to be relocated to the MPP.
Artificial bee colony	Can solve the 2D space global optimization problems. It has fast convergence, better robustness, low computational cost, high accuracy.	Settling time is more, and oscillation are they're in the output.
Genetic algorithm	It is used for real-time nonlinear and multimodal objective function problems, and it tracks the GP with good efficiency at a low implementation cost.	Not stable and often seeks the optimal local solution, complex than PSO, with slow tracking speed.
Salp swarm algorithm	One slap chain is used to boost the initial random solutions and converge toward optimal efficiency.	It saves one solution as the best. It cannot save different solutions as the best for a multiobjective problem.

(Continued)

TABLE 5.2 (Continued)

Advantages and Disadvantages of Bioinspired Algorithm Used in MPPT

MPPT Technique	Advantage	Disadvantage
Memetic salp swarm algorithm	The MSSA algorithm is simple to execute, and several solutions can be saved for a multiobjective problem.	Uncertainty and cost rise in this MSSA than the SSA algorithm
Grey wolf optimization	Have high tracking performance with less transient and steady-state oscillations in the output.	δ and ω do not hunt the prey. So much effort is spent on locating the best option for the problem.
Enhanced grey wolf optimization	Can track the global MPP with greater precision in less time.	Implementation is complex.
Differential evolution algorithm	More effective in terms of precision, tracking speed, convergence, and reliability.	During optimization, one of the most critical responsibilities is parameter selection.
Cuckoo search optimization	CS approach has more efficient randomization, quicker convergence, fewer parameters needed, and is independent of initial conditions.	It suffers from random step size. Because of unwanted and sudden shifts in the duty cycle, oscillations occur, resulting in undesired glitches in power performance.
Adaptive cuckoo search optimization	The modified swapping parameter technique improves CS performance, quicker convergence, so the initial population was increased. Significant steps result in stronger MPP.	The calculation is complicated, and tracking time is determined by the Lévy flight.
Firefly optimization	Have quick computational measures, the coefficient to track MPPP is revised at a fast rate, quick convergence, and accurate results.	Tracking time is higher, which reduces the efficiency.
Modified firefly optimization	A simpler algorithm, faster convergence and tracking speed, high accuracy, and never being trapped into local optimum means no duty cycle ripple exists.	In every iteration, the coefficients are adjusted, giving poor results than previous swam-based algorithms.
Bat algorithm	Compared to the PSO system, it is more stable in practice and has superior efficiency for variations in radiation and temperature.	Every iteration is updated, with a poor outcome and other swam algorithms coefficients are changed.
Dragonfly optimization	It has high tracking precision, convergence speed, and a high advantage of obtaining global MPP and reducing power fluctuation around MPP. DFO is faster than P&O.	Due to its significant searching steps, this algorithm has an overflowing of the search area and interruption.
Jaya algorithm	Have high tracking performance, and dynamical stability is improved.	A random number is generated in the Jaya algorithm, resulting in a possible negative result, reducing MPPT efficiency.

(Continued)

TABLE 5.2 (Continued)

Advantages and Disadvantages of Bioinspired Algorithm Used in MPPT

MPPT Technique	Advantage	Disadvantage
Cat swarm optimization	The algorithm is system-independent, has a high capacity to obtain global MPP, avoids power fluctuations around MPP, and has a high convergence level.	The current best position should be kept as close to GMPP as practicable. In MPP tracking, there is an issue with premature convergence.
Whale optimization algorithm	WOA is better in terms of tracking than the SA method.	If the random numbers are too small or too large, the optimal solution will fall into an optimum local value, disrupting MPP.
Teaching–learning-based optimization	have a high level of precision and consistency while extracting the global MPP.	Trapping into local optimal is a common drawback of a metaheuristic algorithm, which lacks exploration capacity.
Artificial jellyfish optimization	It has better settling time response and provides higher efficiency.	Dependent on the mean location of all jellyfish and a distribution coefficient, that should be appropriately decided.

implementation, oscillation and stability, dynamic response and error detection, efficiency with convergence speed, converter used with BI, tracking accuracy, input parameters, and efficiency with convergence speed.

5.2.3 Hybrid-Based MPPT

Many MPPT algorithms, especially under PS circumstances, fail to monitor GMPP. Therefore, numerous hybrid MPPT techniques were proposed to obtain high performance. These strategies can boost overall performance and resolve partial shading problems. The hybrid MPPT process varies in reliability, performance, efficiency, and speed. Many researchers categorized it as (1) two classical, (2) classical+soft-computing methods, and (3) two soft-computing methodologies. As per Bollipo et al. (2021), the intelligent and classical hybrid system uses both approaches to boost tracking performance. The hybrid technique can also be a hybrid of three intelligent algorithms. The ultimate objective of the strategy is to increase the tracking efficiency of the PV in less time with higher accuracy.

Classical hybridization is a methodology that combines two classical techniques to overcome the constraints of a single classical MPPT to boost the speed, performance, and accuracy of tracking. Yksek and Mete (2017) suggested the combination of *P&O* and *InC*; the main principle was to adjust the step sizes intelligently. As with bigger step sizes, the power value increases, and with small step sizes, the power approaches toward

the MPP. To achieve faster MPP monitoring time and lower steady-state oscillation near MPP than classical-based P&O technique, the combination of InC with the neural network is used to improve the tracking efficiency of the PV system. This strategy was evaluated by Bollipo et al. (2021) by combining different MPPT methods like fractional short-circuit current (FSCC) and perturbation-and-observe approaches. Combining open-circuit voltage and InC technique is used for the offline method to bring the PV array's operational point close to the MPP, and then the InC approach was used to precisely monitor the MPP. ANN can be used to boost computational efficiency and convergence speed in combination with InC to increase the tracking time of GMPP. Some of the authors have integrated P&O with GA to reduce population size and increase response for PV systems under diverse partial shading patterns compared to a standard GA methodology. To boost overall PV system performance, FL can be combined with the P&O model, this strategy is more effective as the PV array reach the MPP faster, providing more reliable computational power. In Bollipo et al. (2021), P&O- and PSO-based MPPT methods work well in which P&O provided the nearest local limit, while GMPP is identified by using PSO. In Yükses and Mete (2017), a hybrid PSO-FLC algorithm was presented to solve partial shading conditions, and results reveal that hybrid GWO-FLC and hybrid PSO-FLC algorithms deal with the partially shaded MPP model issue. Hybrid WOA with simulated annealing in Mafarja and Mirjalili (2017) was compared with WOA, and SA approaches; the findings reveal that the WOSA-based PV system performs efficiently overall performance. While combining MFO and P&O approach gives an excellent speed, accuracy, and reliability to tackle MPPT problems, whereas GWO, with the CSA technique, is used to calculate the ideal duty cycle.

The benefits of each method are combined in the hybrid approach since it is such a strategy that delivers high convergence accuracy, controls optimum local points, and reaches the optimum global point. Pilakkat and Kantha Lakshmi (2019) integrated P&O with the ABC algorithm consisting of two steps: first, monitoring GMPP using the ABC algorithm, and the second step is to update LLP by combining P&O update LLP. The optimum duty cycle should be reached in less time. DE and PSO (DEPSO) can be coupled as DE can seek local optima in search space utilizing differential knowledge. At the same time, PSO can better identify local optima in search space, but this strategy has substantial integration complexity. The Neuro-Fuzzy approach can be utilized to track MPP at a quicker rate in partial shading conditions. FLC performance is determined by selecting the best membership functions and helping neural networks monitor MPP at better efficiency. However, costs are higher due to the positioning of the converter in each array. A combination of GA and ANN, where ANN has two input layers references for climate change and error, ANN employed the GA principle to track weights in less time. To increase the accuracy prediction by eliminating ANN and FLC shortcomings, ANFIS

was illustrated by Bollipo et al. (2021) and Aldair et al. (2018), where ANN inputs were segregated into random training, validation, and training data set. Input values were extracted and calculated based on trained optimal principles. The model is adjusted either by altering membership functions and rules or by increasing the number of epochs. If wrong results are achieved for the training data set, the model is updated by altering membership functions and rules or training algorithm and number of epochs. In Aldair et al.'s (2018) research paper, ANFIS was simulated to track the MPP efficiently and faster; in contrast, its implementation is sophisticated and comprises three sensors (irradiation sensor, temperature sensor, and current sensor). ANN approaches the MPP by decreasing error and maximizing the output of the system.

5.4 Conclusion

This chapter compares artificially intelligent, BI, and hybrid-based MPPT methods, and the advantages and drawbacks of each method have been extensively utilized. The classical method has a good response in uniform radiation, but when the irradiation and temperature change frequently, the MPP position drifts away, reducing system efficiency. Although some modifications were made in the classical method, it increased the complexity and cost of the MPPT controller. AI technologies are used to lessen reliance on PV system characteristics and efficiently track even at low irradiation values with less complexity. AI self-learning approach and its potential have replaced classical MPPT with AI-based MPPT. AI-based MPPT techniques were more efficient than classical methods. Still, some issues arose during implementation, such as high cost, large data requirement (ANN), time-consuming (FLC), less accuracy (FSSRBFA), scaling factor, and step size selection (VSSRBFA), GMPP issues have sifted it to the BI methods. BI methods were able to solve some issues of AI techniques, but they increased the complexity of the problem by increasing the number of parameters during optimization. In BI, some techniques take much time to track the optimal solutions (GWO), unable to perform complex calculations (ACSP), having limited accuracy (BA). Few of them do not provide an exact solution for multiobjective problems (SSA), requiring more time to operate (ACO) and causing premature convergence (CSW) to the GMP. Many MPPT algorithms are unable to track the GMPP, under shading conditions; as a result, numerous hybrid MPPT techniques with high performance have been developed. Hybrid techniques are combinations of classical +AI+BI methods. They are used nowadays to improve the system's tracking time, performance, and accuracy. ANFIS, FNN, PSO+P&O, PSO+FLC, GWO+FLC, DEPO, and others can be used as per applications in the real world.

References

- A.A. Aldair, A.A. Obed, A.F. Halihal (2018), "Design and implementation of ANFIS-reference model controller-based MPPT using FPGA for photovoltaic system," *Renewable and Sustainable Energy Reviews*, Vol. 82, pp. 1–12.
- A.O. Baba, G. Liu, X. Chen (2020), "Classification and evaluation review of maximum power point tracking methods," *Sustainable Futures*, Vol. 2, p. 100020, ISSN 2666-1888.
- A.S. Benyoussef, A. Chowder, K. Kara (2015), "Artificial bee colony-based algorithm for maximum power point tracking (MPPT) for PV systems operating under partially shaded conditions," *Applied Soft Computing*, Vol. 32, pp. 38–48.
- R. B. Bollipo, S. Mikkili, P. K. Bonthagorla (2021), "Hybrid, optimal, intelligent and classical PV MPPT techniques: A review," *CSEE Journal of Power and Energy Systems*, Vol. 7, no. 1, pp. 9–33.
- R.B. Bollipo, S. Mikkili, P.K. Bonthagorla (2020), Critical review on PV MPPT techniques: Classical, intelligent and optimization. *IET Renewable Power Generation*, Vol. 14, pp. 1433–1452.
- G.S. Chaurasia, A.K. Singh, S. Agrawal, N.K. Sharma (2017), "A meta-heuristic firefly algorithm based smart control strategy and analysis of a grid-connected hybrid photovoltaic/wind distributed generation system," *Solar Energy*, Vol. 150, pp. 265–274.
- M. Chen, S. Ma, J. Wu, L. Huang (2017), "Analysis of MPPT failure and development of an augmented nonlinear controller for MPPT of photovoltaic systems under partial shading conditions" *Applied Sciences*, Vol. 7, no. 1, p. 95. <https://doi.org/10.3390/app7010095>.
- S.K. Cherukuri, S.R. Rayapudi (2017), "Enhanced Grey Wolf optimizer based MPPT algorithm of PV system under partially shaded condition," *International Journal of Renewable Energy Development*, Vol. 6(3), pp. 203–212.
- J.-S. Chou, D.-N. Truong (2021), "A novel metaheuristic optimizer inspired by the behavior of jellyfish in the ocean", *Applied Mathematics and Computation*, Vol. 389, p. 125535. ISSN 0096-3003.
- S.C. Chu, P.W. Tsai (2007), "Computational intelligence based on the behavior of cats," *International Journal of Innovative Computing, Information, and Control*, Vol. 3, pp. 163–173.
- M. M. Eshak, M. A. Khafagy, P. Makeen, S. O. Abdellatif (2020), "Optimizing the performance of a stand-alone PV system under non-uniform irradiance using Gray-Wolf and hybrid neural network AI-MPPT algorithms," *2020 2nd Novel Intelligent and Leading Emerging Sciences Conference*, pp. 600–605. doi: 10.1109/NILES50944.2020.9257965.
- K.S. Garud, S. Jayaraj, M.-Y. Lee (2021), "A review on modelling solar photovoltaic systems using artificial neural networks, fuzzy logic, genetic algorithm, and hybrid models." *International Journal of Energy Research*, Vol. 45, pp. 6–35. doi:10.1002/er.5608.
- K. Hu, S. Cao, W. Li, F. Zhu (2019), "An improved particle swarm optimization algorithm suitable for photovoltaic power tracking under partial shading conditions." *IEEE Access*, Vol. 7, pp. 143217–143232.
- Y. Hu, W. Cao, J. Wu, B. Ji, D. Holliday (2014), "Thermography-based virtual MPPT scheme for improving PV energy efficiency under partial shading conditions," *IEEE Transactions on Power Electronics*, Vol. 29(11), pp. 5667–5672.

- C. Huang, L. Wang, R. S. Yeung, Z. Zhang, H. S. Chung, A. Bensoussan (2018), "A prediction model-guided Jaya algorithm for the PV system maximum power point tracking," *IEEE Transactions on Sustainable Energy*, vol. 9, no. 1, pp. 45–55.
- C.H. Hussaian Basha, C. Rani (2020), "Different conventional and soft computing MPPT techniques for solar PV systems with high step-up boost converters: A comprehensive analysis," *Energies*, Vol. 13, pp. 1–18.
- N. Karami, N. Moubayed, R. Outbib (2017), "General review and classification of different MPPT techniques," *Renewable and Sustainable Energy Reviews*, Vol. 68 (1), pp. 1–18.
- M.M. Mafarja, S. Mirjalili (2017), "Hybrid whale optimization algorithm with simulated annealing for feature selection," *Neurocomputing*, Vol. 260, pp. 302–312.
- M. Mao, L. Cui, Q. Zhang, K. Guo, L. Zhou, H. Huang (2020), "Classification and summarization of solar photovoltaic MPPT techniques: A review based on traditional and intelligent control strategies," *Energy Reports*, Vol. 6, pp. 1312–1327. ISSN 2352-4847. doi:10.1016/j.egyr.2020.05.013.
- A. Mellit, S. A. Kalogirou (2008), "Artificial intelligence techniques for photovoltaic applications: A review," *Progress in Energy and Combustion Science*, Vol. 34(5), pp. 574–632.
- A. Mesa, K. Castromayor, C. Garillos-Manliguez (2018), "Cuckoo search via Levy flights applied to uncapacitated facility location problem." *Journal of Industrial Engineering International*, Vol. 17, pp. 585–592.
- A.A.S. Mohamed (2020), "Dynamic modeling analysis of direct-coupled photovoltaic power systems". In: Eltamaly, A., Abdelaziz, A. (eds.) *Modern Maximum Power Point Tracking Techniques for Photovoltaic Energy Systems*. Green Energy and Technology. Springer, Cham. doi:10.1007/978-3-030-05578-3_17.
- A.S. Oshaba, E.S. Ali, S.A. Elazim (2018), "MPPT control design of PV system supplied SRM using BAT search algorithm," *Sustainable Energy, Grids and Networks*, Vol. 2, pp. 51–60.
- N. Patcharaprakiti, S. Premrudeepreechacharn (2002) "Maximum power point tracking using adaptive fuzzy logic control for grid-connected photovoltaic system." *IEEE Power Engineering Society Winter Meeting. Conference Proceedings* (Cat. No.02CH37309), Vol. 1, pp. 372–377. doi: 10.1109/PESW.2002.985022.
- D. Pilakkat, S. Kantha Lakshmi (2019), "An improved P&O algorithm integrated with artificial bee colony for PV system under partial shading conditions," *Solar Energy*, Vol. 178, pp. 37–47.
- M. M. Puralachetty, V. K. Pamula, L. M. Gondela and V. N. B. Akula (2016), "Teaching-learning-based optimization with two-stage initialization," *IEEE Students' Conference on Electrical, Electronics and Computer Science (SCEECS)*, 2016, pp. 1–5. doi: 10.1109/SCEECS.2016.7509340.
- S. Saravanan, N.R. Babu (2016), "RBFN based MPPT algorithm for PV system with high step-up converter." *Energy Conversion and Management*, Vol. 122, pp. 239–251.
- M. Seyedmahmoudian, B. Horan, T.K. Soon, R. Rahmani, A. MuangThan Oo, S. Mekhilef, A. Stojcevski (2016), "State of the art artificial intelligence-based MPPT techniques for mitigating partial shading effects on PV systems—A review", *Renewable and Sustainable Energy Reviews*, Vol. 64, pp. 435–455.
- K.V. Vidyandandan (2017), "An overview of factors affecting the performance of solar PV systems," *Energy Scan (A House Journal of Corporate Planning, NTPC Ltd.)*, Vol. 27, pp. 1–8.

- D. Yadav, N. Singh (2020), "Advanced optimization scheme to improve photon management to increase solar cell efficiency" *EMSME 2020: 1st International Conference on Energy, Materials Sciences & Mechanical Engineering*, National Institute of Technology Delhi, New Delhi, India.
- D. Yadav, N. Singh (2021), "Application of artificial neural network in maximum power point tracking for different radiation & temperature", *Conference on Scientific and Natural Computing*, Gautam Buddha University, Greater Noida. doi: 10.1007/978-981-16-1528-3_7.
- B. Yang, L. Zhong, X. Zhang, H. Shu, T. Yu, H. Li, L. Jiang, L. Sun (2019), "Novel bio-inspired memetic salp swarm algorithm and application to MPPT for PV systems considering partial shading condition", *Journal of Cleaner Production*, Vol. 215, pp.1203–1222.
- G. Yükses, A.N. Mete (2017), "A hybrid variable step size MPPT method based on P&O and INC methods," *10th International Conference on Electrical and Electronics Engineering (ELECO)*, IEEE, pp. 949–953.
- A C. Zhang, Y. Zhang, J. Su, T. Gu, M. Yang (2020), "Performance prediction of PV modules based on artificial neural network and explicit analytical model," *Journal of Renewable and Sustainable Energy*, Vol. 12, p. 013501.

6

Analysis of Multijunction Solar Cell-Based PV System with MPPT Schemes

Omveer Singh and Mukul Singh

Gautam Buddha University

CONTENTS

6.1	Introduction	130
6.2	Literature Review	131
6.3	Modeling of MJSC-Based PV System	133
6.3.1	System Description	134
6.3.2	Mathematical Modeling of MJSC	135
6.3.2.1	Photocurrent Density (J_{phi})	135
6.3.2.2	Diode Current Density (J_d)	137
6.3.2.3	Shunt Current Density (J_{pr})	137
6.3.2.4	Voltage (V)	137
6.3.3	DC–DC Converter	137
6.3.3.1	Generic Boost Converter Arrangement	138
6.3.3.2	Modeling of Boost Converter	138
6.4	Maximum Power Point Tracking Techniques	139
6.4.1	Perturb and Observe (P&O) Technique	139
6.4.1.1	Paces of P&O Technique	139
6.4.2	Incremental Conductance (INC) Technique	140
6.4.3	Teaching Learning-Based Optimization Technique (TLBO)	141
6.5	Enactment Procedure	143
6.5.1	Simulation of MJSC	143
6.5.1.1	Reverse Saturation Current Density of Diode (J_{oi}) Evaluation	144
6.5.1.2	Open-Circuit Voltage (V_{oci}) Evaluation	145
6.5.1.3	Photo Current Density (J_{phi}) Evaluation	145
6.5.1.4	Current Density of Cell (J_i) Evaluation	146
6.5.2	MJSC Implementation	146
6.5.3	Execution of MPPT Techniques with MJSC	146
6.5.3.1	Simulation Model Using P&O Technique	147
6.5.3.2	Simulation Model Using INC Technique	148
6.5.3.3	Simulation Model Using TLBO Technique	148

6.6 Results and Analysis 150

6.6.1 Results of MJSC 150

6.6.2 Results Analysis 152

6.7 Conclusion 155

Appendix: Specifications for MJSC 156

References..... 157

6.1 Introduction

This era of rapid growth in population and the surge in the industrialization sector has led to an increase in the demand for energy. So this issue is of utmost importance to produce ample amounts of energy. Nonrenewable energy is in limited supply. So switching over to renewable energy sources (RESs) is the best option at present. RESs are a natural source of energy [1]. Such sources of energy are naturally replenished. Sunlight, wind, rain, tides, waves, and geothermal heat are some of the examples of RESs.

More than 34.6 GW capacities of RESs units have been installed in India until June 2021 [1]. The energy market of RESs is expected to grow more in the coming years. This will also enhance technical/nontechnical job opportunities for job seekers in India.

Sustainable power source assets exist over wide land territories as opposed to petroleum derivatives, which are gathered in a set number of nations. The speedy transfer of sustainable power sources and vitality productivity advances is bringing about significant vitality, security, environmental change moderation, and financial benefits. Globally, there is solid help for advancing inexhaustible sources, for example sunlight-based force and wind power.

Nowadays, the sunlight-based generation of energy like solar PV is a very fruitful and stable method for electricity production among other RESs-based electricity production techniques. Traditionally, the solar PV cells were made of silicon and the power delivered by the silicon cell was extremely constrained, because its effectiveness was exceptionally low. So, a progressive strategy has to be designed to have multilayer Sun-oriented cells [2].

Multijunction solar cells (MJSCs) are used in the space environment, whereas in all other sectors, single-junction solar cells are used. A Sun-oriented cell is a solitary and essential unit of the solar PV framework that is utilized in the principal activity of power by daylight [3]. The interconnection of listed individual Sun-powered cells in a sealed shut amalgamation to build the utility is known as the Sun-based module or Sun-powered board that is generally used in customary applications. At that point, these modules are set in the arrangement of equal design and associated appropriately to accomplish the required voltage and cluster and are called Sun-powered cluster.

The non-RESs are easily exhausting. Additionally, energy costs are increasing, and a solar PV device is a promising alternative. These are abundant,

free from pollution, spread all over the world, and recyclable. The hindrance aspect is its high cost of establishment and low efficiency of transition. The key point is to increase the framework's efficiency and power yield. A single maximum power point (MPP) tracking (MPPT) controller arranges all the boost converters associated with any autonomous solar PV-based board and duty ratio to each of the establishments. This chapter discusses the methods, circumstances, expectations, and hypotheses. The task slogan is added to consider the application of various MPPT strategies connected to MJSC. The catchphrase is to gather resources by ecologically accepting the interaction of RESs. This chapter focuses on the development of MJSCs and the relative analysis of MPPT strategies. It was conceived with different MPPT strategies following a common objective of extending the yield power of the solar PV system by pursuing the maximum power on each working condition. The perturb and observe (P&O), incremental conductance (INC) blocks and teaching learning-based optimization (TLBO) techniques are used to increase the solar cell's power production. It has been determined that the TLBO algorithm is superior to the other two MPPT techniques, which maximizes efficiency.

6.2 Literature Review

This section consists of a literature survey on the various modules used in this research chapter. A variety of research papers related to single cells and MJSCs modeling/simulation using MATLAB®/Simulink® and various MPPT techniques and approaches are studied. These research papers become the backbone of this research work.

Gupta et al. [2] presented an audit on the single and multiintersection Sun-based cell with MPPT-based modern methods. It incorporated P&O, artificial neural network (ANN), partial open-circuit voltage (POCV), and so on. Maximum power can be extracted from solar cells with the help of these MPPT techniques. Hussain et al. [3] described single and triple intersection Sun-based cells. The current (I)–voltage (V) and power (P)– V bends characterize the greatest P , V , and I . The Clyde space software utilized halide lights to reenact the irradiation conditions with irradiance of half sun, which is identical to 0.05 W/cm^2 . Then, Das et al. [4] presented a study of MJSCs to improve the change proficiency of PV power age frameworks. From the MATLAB/Simulink results, it was discovered that the two diode model is more accurate than the single-diode model. Thus, the two diode model is utilized to reenact double and triple intersection sunlight-based cells. The reenactments were performed under differing temperatures and Sun-powered irradiance. Also, Razykov et al. [5] described the present status and future possibilities of Sun-powered PV. It gave an audit of the specialized advancements made for quite a long time in the territory of mono and polycrystalline PV advances

dependent on silicon. Si and GaAs monocrystalline Sun-oriented cell efficiencies were near the hypothetically anticipated greatest qualities.

Along with this, Babar et al. [6] presented the recreation model of MJSCs. The model mimics the presented attributes of two unique natures of multiintersection Sun-powered cells including indium gallium phosphide (InGaP)/GaAs DJSC with a burrowing layer of InGaP and InGaP/GaAs/Ge TJSC with a burrowing layer of GaAs. Additionally, Mongelli [7] described MJSCs and its various features. The multiintersection Sun-oriented cells use a layered structure of materials to retain various areas of sunlight-based spectra. The presented structures used GaInP, GaAs, and Ge sublayers with band holes of 1.9, 1.4, and 0.6 eV for space application.

Thomas and Nithyanantham [8] described the execution and examination of MPPT calculations on a MATLAB/Simulink condition for solar PV. To maximize the efficiency of solar PV, MPPT is used. The investigation of different calculations used to actualize MPPT has been highlighted.

After that, Halder [9] outlined the INC technique in which the terminal voltage of the solar array is always adjustable with a power converter system and MPPT controller actions to harvest maximum energy as cost-effective and sizeable solutions to power crisis during the load demand. Dhaifallah et al. [10] inclined a straightforward methodology of fractional order control-based INC for optimal parameter design that was implied and was a more efficient technique as compared to the conventional INC technique. A small signal model produced by the system has INC robustness and the accuracy of fractional order that enhanced the overall power tracking performance of the system.

Additionally, Reisi et al. [11] described an audit of the grouping and comparison of MPPT techniques for PV framework. Various MPPT techniques have been used in this work. Furthermore, different MPPT strategies have been disussed as far as the dynamic reaction to the PV framework to varieties in temperature, irradiance, and attainable efficiency. For improvement of others' work, Kandemir et al. [12] gave an overview of MPPT techniques that were used for maximum power extraction from the PV. In the writing, different kinds of MPPT strategies and elective arrangements are utilized to identify valid global MPPs among other local MPPs, and Selmi et al. [13] described a numerical investigation of solar PV cell for the single-diode and double-diode cell arrangements.

Recently, Gouda et al. [14] demonstrated performance analysis for a PV system-based MPPT using advanced techniques. This work presented a productive plan for PV framework control that utilized three methods: PSO, P&O, and INC. PSO appeared to be the best one with minor oscillation. In summation with that, Fathy et al. [15] examined triple-junction solar cells of PV systems with global MPP using P&O and manta ray foraging optimization (MRFO). The investigated MRFO-based MPPT is employed to extract the global MPP (GMPP) from the triple-junction solar-based array operated under shadow conditions.

Chen et al. [16] developed TLBO with a learning enthusiasm mechanism and its application in synthetic engineering. This adaptive algorithm updated the score for each learner in the class through learning and by interaction between teachers and learners. In addition to this work, Koochaki et al. [17] presented an ideal design of solar–wind hybrid systems using TLBO applied in charging stations for electric vehicles. The results exhibited the capacity of the proposed calculation in planning and optimizing the hybrid system. Rao et al. [18] described TLBO as a new proficient method for the development and advancement of mechanical structure issues. This strategy dealt with the impact of an instructor on students. TLBO is additionally a populace-based technique and used a populace of answers preceding the overall solution. The populace is considered a gathering of students or a class of students. Also, the implementation of TLBO as a productive improvement technique was examined for enormous scope nonstraight development issues for finding the optimal solutions. The proposed strategy depends on the impact of an instructor on the yield of students in a class. The fundamental way of thinking about the strategy is clarified in detail [19].

Further, Chen et al. [20] described TLBO with variable populace, its application for ANN and its advancement. The principal objective of this technique was to diminish the processing cost of unique TLBO and expand it for enhancing the features of ANN. Also, Muhammadsharif [21] discussed efficient extraction of solar cells and module parameters.

6.3 Modeling of MJSC-Based PV System

Single intersection Sun-oriented cells have only one p–n intersection, as against multiintersection sunlight-based cells that have more than one p–n intersection. The traditional sunlight-based cells utilized in Sun-oriented power plants are of the single intersection type and generate power utilizing the single p–n intersection.

The cells which have various p–n intersections made of distinct semiconductor materials constitute the MJSC. In response to distinct light wavelengths, each p–n intersection will generate electricity [4]. The utilization of numerous semiconducting materials permits the absorbance of a more extensive scope of wavelengths improving the cell's daylight to electrical vitality change effectiveness. In this work, the semiconductor materials that are used as various subcells are InGaP, indium gallium arsenide (InGaAs), Si, and Ge. However, these subcells are placed in the decreasing order of bandgap energy. This is the basic way for the implementation of MJSCs. Various other semiconductor materials can be used too in the process of making this type of highly advanced cell. Various materials in the MJSC are stacked with tunnel intersections and are likewise furnished with window layers. The tunnel

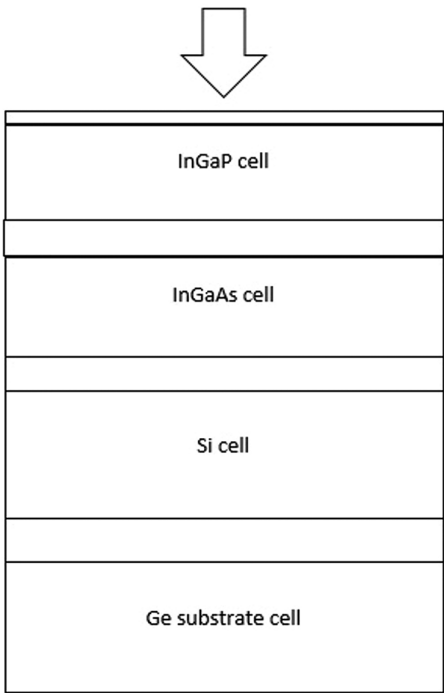


FIGURE 6.1
Four-layer MJSC.

intersection takes care of the issue of interfacing diverse cells although the window layer handles the cross-section consistently. The four-layer MJSC is presented in Figure 6.1.

A solar PV framework is made out of at least one sunlight-based board that is made by MJSC joined with an inverter and other electrical and mechanical equipment that utilizes vitality from the Sun to produce power. Generally, when a solar PV module is directly connected with a load, the working point is dependent on the MPP. The solar PV displays an unregulated DC control source, which must be truly adjusted with an explicit ultimate objective to intermix it into the association. An MPPT is utilized for expelling the greatest power from the Sun-oriented PV module and trading that vitality to the load. A DC–DC converter which is an interface between the load and the module viably moves power from the Sun-powered PV module to the load. All specifications of MJSC are provided in the Appendix.

6.3.1 System Description

The system comprises MJSC, MPPT, DC–DC power converter, and, finally, load as shown in Figure 6.2.

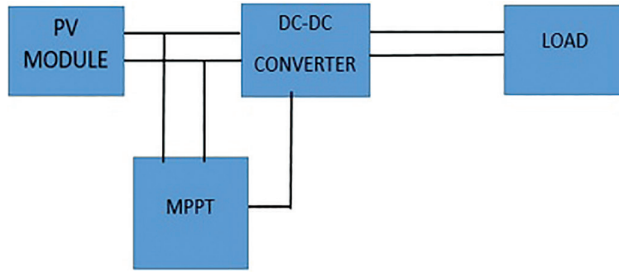


FIGURE 6.2
Fundamental block diagram of solar PV system.

In the initial state, the voltage (V) and current (I) from the MJSC are recognized by the assistance of the current and voltage sensor. This V and I can be the commitment to the MPPT controller. The yield of the MPPT piece is used as the commitment to DC–DC converter, which may be voltage parameter or obligation cycle [12]. The essential inspiration driving DC–DC support converter is to give consistent V or I . It helps in keeping up the working voltage at MPP.

6.3.2 Mathematical Modeling of MJSC

The InGaP as the top layer, InGaAs as the second layer, Si as the third layer, and Ge as the bottom layer are the four junctions or MJSCs which are used here.

In decrementing order of bandgap energy, the subcells are placed [12,3]. The top cell will capture the photons of the highest energy [6]. The next subcell will capture the rest. The equivalent circuit model of a four-junction solar cell is shown in Figure 6.3. Also, elements used in MJSC are listed in Table 6.1.

It is the basic working of MJSC. Further, the equivalent circuit diagram of MJSC is described:

The current density of cell (J_i) is demonstrated using Kirchhoff's law:

$$J_i = J_{\text{phi}} - J_d - J_{pr} \quad (6.1)$$

where J_{phi} = subcell photocurrent density, J_d = subcell diode current density, and J_{pr} = subcell shunt current density.

6.3.2.1 Photocurrent Density (J_{phi})

The standard test condition (STC) of subcell depends on both irradiance and temperature photocurrent density. It is demonstrated as

$$J_{\text{phi}} = G/G_{\text{ref}} (J_{\text{sci}} + \mu_{\text{sc}} \times \Delta T) \quad (6.2)$$

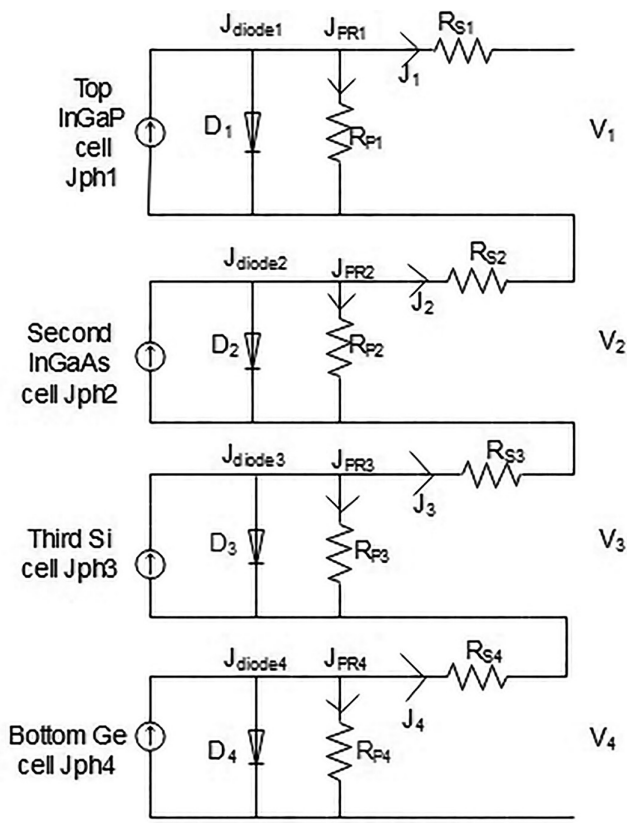


FIGURE 6.3
Equivalent circuit model of a four-junction solar cell.

TABLE 6.1
Elements Used in MJSC

Layers	Cell Materials
Layer 1	InGaP
Layer 2	InGaAs
Layer 3	Si
Layer 4	Ge

where J_{sci} = subcell short circuit current density (STC), G = radiation (watt/m²), G_{ref} = reference irradiance (STC, 1,000 W/m²), and μ_{sc} = temperature short circuit coefficient.

$$\Delta T = T - T_{ref} \tag{6.3}$$

where T = temperature (K) and T_{ref} = reference temperature (298 K, STC).

6.3.2.2 Diode Current Density (J_d)

The current density of diode is demonstrated as

$$J_d = J_{0i} \left(e^{(q(V + J_i \times A \times R_s) / (n_i \times K_b \times T))} - 1 \right) \quad (6.4)$$

where J_{0i} is the diode reverse saturation current density (A/cm²), V = subcell voltage, A is the area of the cell (cm²), n_i = each subcell value is different for this constant, R_s is the resistance which is connected in series, and E_{gi} = cell bandgap energy (eV).

Calculation of reverse saturation current of diode is demonstrated as

$$J_{0i} = K_i \times T^{(3+\gamma_i)/(2)} \times e^{(-E_{gi}) / (n_i \times K_b \times T)} \quad (6.5)$$

For certain materials of subcell, K_i and γ_i have specific constant values.

6.3.2.3 Shunt Current Density (J_{pr})

Solar cell shunt current density is demonstrated as

$$J_{pr} = V + \left((J_i \times A \times R_s) / (A \times R_{sh}) \right) \quad (6.6)$$

where R_{sh} is the shunt resistance.

6.3.2.4 Voltage (V)

The open-circuit voltage per cell of the multiintersection Sun-oriented cell infers a point where reverse saturation current is equivalent to the produced radiation current. The MJSC open-circuit voltage is demonstrated as

$$V_{oci} = \left((n_i \times K_b \times T) / (q) \right) \ln \left((J_{sci} / J_{0i}) + 1 \right) \quad (6.7)$$

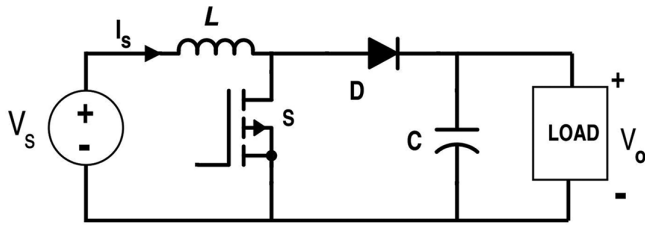
The voltage from the entire four junctions is the total voltage of the MJSC, which can be demonstrated as

$$V = V_1 + V_2 + V_3 + V_4 \quad (6.8)$$

where V_1 = InGaP subcell voltage, V_2 = InGaAs subcell voltage, V_3 = Si subcell voltage, and V_4 = Ge subcell voltage.

6.3.3 DC–DC Converter

A DC–DC converter, i.e., boost converter, steps up the input DC voltage value and provides output. The main components of a boost converter are an inductor, a diode, and a high-frequency switch.

**FIGURE 6.4**

Schematic circuit diagram of boost converter.

The control strategy lies within the manipulation of the duty cycle of the switch that causes the voltage change. The DC–DC converter is the embodiment of the most extreme power point tracker. Nevertheless, a boost converter can generate viability by boosting the voltage. The boost converter ventures up the input voltage centrality to an essential yield voltage measure without the utilization of the transformer. Figure 6.4 depicts the schematic circuit diagram of boost converter.

6.3.3.1 Generic Boost Converter Arrangement

The practical field of the converter can be demonstrated as

$$V_{\text{out}} = V_{\text{in}} / (1 - D) \quad (6.9)$$

where V_{out} = output voltage of the boost converter, V_{in} = input voltage of the boost converter, and D = duty cycle.

6.3.3.2 Modeling of Boost Converter

The DC–DC boost converter circuit contains an inductor, diode, capacitor, load resistor, and control switch.

$$V_{\text{out}} / V_{\text{in}} = 1 / (1 - D) \quad (6.10)$$

The inductor regard of the boost converter is determined using the given equation:

$$L = (V_i \times (V_o - V_i)) / (\Delta I_1 \times f_s \times V_o) \quad (6.11)$$

The capacitor regard of the boost converter is determined using the given equation:

$$C_{\text{out(min)}} = (I_{\text{out(max)}} \times D) / (f_s \times V_o) \quad (6.12)$$

where V_i = typical input voltage of the converter, V_o = desired output voltage, f_s = minimum switching frequency of the converter, ΔI_1 = estimated inductor ripple current, $C_{out (min)}$ = minimum output capacitance, and $I_{out (max)}$ = maximum output current.

6.4 Maximum Power Point Tracking Techniques

A wide variety of MPPT techniques are available in the literature of the concerned area. The prime MPPT techniques are considered among them. So, a detailed discussion is given below.

6.4.1 Perturb and Observe (P&O) Technique

In essence, P&O technique measures the derivatives of the PV cell power dP and the PV cell voltage dV and uses the PV cell voltage and power curve to determine the movement of the operating point [13]. If the dP/dV mark is positive, the real point will be to the left of the MPP; otherwise, dP/dV is negative, the real point is on the right side of the MPP, and this process continues until dP/dV is the same.

$$dP/dV = 0 \text{ at MPP} \quad (6.13)$$

$$dP/dV > 0 \text{ MPP's left side} \quad (6.14)$$

$$dP/dV < 0 \text{ MPP's right side} \quad (6.15)$$

Around MPP, loss of power and motions is seen. This technique is proficient to arrive at the MPP for uniform conditions. In a simple microcontroller, easy execution of this technique is executed. In 2.5 seconds, the MPP can be reached [12]. This method is also eluded as the hill-climbing method. It relies upon the ascent of the bend of intensity against voltage beneath the most extreme force point, and the fall over that point.

6.4.1.1 Paces of P&O Technique

- i. Here a reference voltage V_{ref} is set corresponding to the peak power point of the module.
- ii. Peruse the estimation of I and V from the Sun-oriented PV module.
- iii. The value of P and V at k th instant is stored.
- iv. Then values at $(k+1)$ th instant are measured again and P is calculated from the measured values. V and P at $(k+1)$ th instant are subtracted with the values from k th instant.

- v. In the P - V curve of solar module, if the dP/dV mark is positive, the real point will be to the left of the MPP; otherwise, dP/dV is negative, the real point is on the right side of the MPP and this process continues until dP/dV is the same.
- vi. Likewise, the right side of the curve is for the lower duty cycle, i.e., closer to zero; however, the left side of the curve is for the higher duty cycle, i.e., closer to unification.
- vii. Depending on the sign of $dP [P(k+1) - P(k)]$ and $dV [V(k+1) - V(k)]$, after subtraction, the technique chooses whether to reduce or increase the reference voltage.

6.4.2 Incremental Conductance (INC) Technique

The INC strategy fundamentally utilizes a comparative way; however, it utilizes distinctive relationship of PV curve from P&O to reach MPP [9]. This calculation understands I and V estimations of PV cells and measures the subordinate of PV cell current (dI) and PV cell voltage (dV). In view of its medium multifaceted nature and better execution as per P&O technique, it gives off an impression of being the most famous one for uniform conditions. By examining the INC to the immediate conductance, this technique figures out the most extreme power point. At the point when these two are equivalent, the yield voltage is the MPP voltage. When the INC is equivalent to the negative of the momentary conductance, the most extreme power point is accomplished. The key states of this technique are given below:

$$\Delta I / \Delta V = -I / V_{\text{MPP}} \quad (6.16)$$

$$\Delta I / \Delta V > -I / V_{\text{Left side of MPP}} \quad (6.17)$$

$$\Delta I / \Delta V < -I / V_{\text{Right side of MPP}} \quad (6.18)$$

where dI and dV are the incremental current and voltage, respectively. Loss of power not as much as P&O technique is seen. This procedure can be effectively executed in a straightforward microcontroller and it is important to understand I and V estimations of solar PV cell by utilizing current and voltage sensors for this technique like P&O. This procedure can reach MPP in 2.3 seconds [12]. Undeniably, when the degree of alteration in the yield conductance is relative to the negative yield conductance, the sunlight-based exhibit will achieve at the MPP. In both INC and P&O techniques, MPP has to depend upon the size of the amplification of the reference voltage. The INC strategy offers the fundamental preferred position of giving high proficiency under quickly changing barometrical conditions.

The accompanying technique depends on the observation methodology that originates from

$$P = VI \quad (6.19)$$

As at MPP,

$$dP/dV = 0 \quad (6.20)$$

Utilizing the chain rule as in the given equation:

$$dP/dV = V dI/dV + IV \quad (6.21)$$

The above condition could be created similarly as

$$dI/dV = -I/V \quad (6.22)$$

This calculation has advantages over P&O technique as it doesn't have oscillations around MPP, whereas P&O technique has oscillations around MPP due to which there is loss of power. Additionally, INC technique can stamp rapidly growing and lessening irradiance conditions with more noteworthy accuracy than P&O technique.

6.4.3 Teaching Learning-Based Optimization Technique (TLBO)

The TLBO is a crowd-based metaheuristic search algorithm that mimics a typical educational process lesson [16]. The TLBO considers a group of learners' number of solutions and relevance of solutions treated as a result or comments. Adaptive algorithm updates the score for each learner in the class through learning and by the interaction between teachers and learners. The operation of TLBO process is divided into two basic steps: teaching stage and learning stage.

The teacher is the best solution in the entire populace. This is the teacher phase and also to increase the mean result of the class, the teaching shares his or her knowledge. Taking assumption $x_i = (x_i^1, \dots, x_i^d, \dots, x_i^D)$ i th learner position and x_{teacher} =best fitness learner is teacher. So, the class mean position with number of learners (NP) is

$$x_{\text{mean}} = (1 / \text{NP}) \sum_{i=1}^{\text{NP}} x_i \quad (6.23)$$

Each learner position is updated by

$$x_{i,\text{new}} = x_{i,\text{old}} + \text{rand.} \cdot (x_{\text{teacher}} - T_F \cdot x_{\text{mean}}) \quad (6.24)$$

where $x_{i,\text{new}} = (x_{i,\text{new}}^1, \dots, x_{i,\text{new}}^d, \dots, x_{i,\text{new}}^D)$

and $x_{i,\text{old}} = (x_{i,\text{old}}^1, \dots, x_{i,\text{old}}^d, \dots, x_{i,\text{old}}^D)$

The above two are the new i th learner's and also old one position. The random vector uniformly distributed within $[0,1]^D$ is represented by RAND. Teacher factor is T_F . T_F value is either 1 or 2 which is heuristically set.

The given equation describes the learner phase:

$$x_{i,\text{new}} = x_{i,\text{old}} + \text{rand} \cdot (x_i - x_j), \text{ if } f(x_i) \leq f(x_j) \quad (6.25)$$

$$x_{i,\text{new}} = x_{i,\text{old}} + \text{rand} \cdot (x_j - x_i), \text{ if } f(x_i) > f(x_j) \quad (6.26)$$

$f(x)$ = objective function with D-dimension variables.

$x_{j,\text{old}}$ = old position j th learner.

The same previously mentioned criterion is applied here in the learner phase too. Given below is the basic algorithm for TLBO technique.

1. Initiate
2. Initialization of NP (learner's number) and dimension (D)
3. Learners initialization and evaluating them
4. *While* stopping condition is not met
5. Best learner x_{teacher} is chosen
6. Calculation of mean x_{mean} of all the learners
7. *For* each learner x_i
8. // Teacher Phase//
9. $T_F = \text{round}(1 + \text{rand}(0, 1))$
10. Update the learner according to eq. (6.24)
11. Evaluating the new learner $x_{i,\text{new}}$
12. Accepting $x_{i,\text{new}}$ if it is better than the old one $x_{i,\text{old}}$
13. //Learner phase//
14. Random selection of another learner x_j , which is different from x_i
15. Updating the learner according to eqs. (6.25) & (6.26)
16. Evaluating the new learner $x_{i,\text{new}}$
17. Accepting $x_{i,\text{new}}$ if it is better than the old one $x_{i,\text{old}}$
18. *end for*
19. *end while*
20. *end*

As stated earlier this optimization technique consists of three phases, which are as follows:

- a. Initialization phase
- b. Teacher phase
- c. Learner phase

In the above algorithm, steps 1–6 describe the initialization phase. The dimension D depicts the number of variables. However, the best learner or the best solution, which is calculated according to the fitness function, is the teacher. Further, x_{mean} is calculated for each learner. Steps 8–12 represent the teacher phase. Each learner position is updated according to eq. (6.24). The new learner is evaluated according to the fitness equation. Steps 13–17 represent the last phase that is the learner phase. In this, the learner will randomly interact with various other learners. This is for the improvement of his/her performance. The new learner is again evaluated according to the fitness function. $x_{i,\text{new}}$ is accepted if it is better than the previous one and in the second case it will remain the same as $x_{i,\text{old}}$. Like this, the best solution or optimal solution is found using the above steps. The three phases of TLBO are the initialization phase, teaching phase, and learner phase [16]. On the basis of three phases, the best solution is attained, and, hence, the optimal result is obtained.

6.5 Enactment Procedure

This section deals with MATLAB/Simulink usage of multi intersection Sun-based cell and random MPPT procedures which are P&O, INC, and TLBO applied on it. The conditions that describe the framework steps have been contemplated in the former two sections. This section gives the particularized examination of each subsystem reenactment model and furthermore the explanation of the capacity of each subsystem. The whole model is moreover discussed to summarize things. The proposed system numerical data is provided in the Appendix.

6.5.1 Simulation of MJSC

For simulation, all the equations mentioned should be implemented. The equations will be implemented to all the subcells, i.e., InGaP, InGaAs, Si, and Ge, but the corresponding values of each subcell will be different. The MATLAB/Simulink-based models are specified considering this situation.

The four layers are arranged in decreasing order of bandgap energy and in the same order, the layers are given in Table 6.1. Corresponding bandgap energy of corresponding subcells is given in Table 6.2.

6.5.1.1 Reverse Saturation Current Density of Diode (J_{oi}) Evaluation

Likewise given below is the equation derived for J_{oi} . For certain materials of subcell, the K_i and γ_i values have a specific constant value. E_{gi} is cell bandgap energy (eV). Figure 6.5 presents the execution of J_{oi} for each subcell.

$$J_{oi} = K_i \times T^{(3+\gamma_i)/(2)} \times e^{(-E_{gi})/(n_i \times K_b \times T)}$$

(6.27)

TABLE 6.2
Bandgap Energy of Corresponding Subcells

Subcells	Bandgap Energy
InGaP	2.637 eV
InGaAs	1.874 eV
Si	1.14 eV
Ge	0.6583 eV

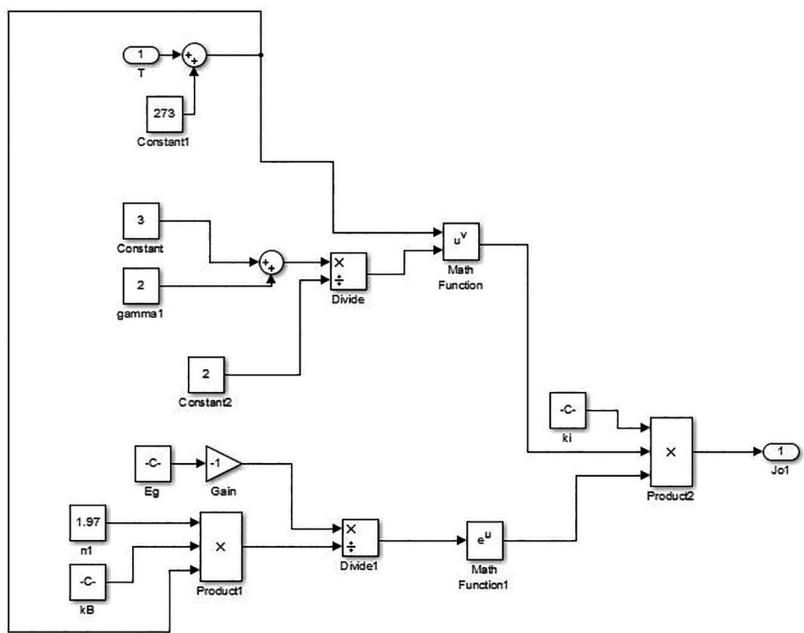


FIGURE 6.5
Execution of J_{oi} for each subcell.

6.5.1.2 Open-Circuit Voltage (V_{oci}) Evaluation

The implemented model can be developed using the respective equation, based on which the model is developed. The execution of V_{oci} for each subcell is reflected in Figure 6.6.

$$V_{oci} = \left((n_i \times K_b \times T) / (q) \right) \ln \left((J_{sci} / J_{0i}) + 1 \right) \quad (6.28)$$

6.5.1.3 Photo Current Density (J_{phi}) Evaluation

Given above is the detailed simulation for the determination of subcell photocurrent density. It is a mimic of eq. (6.2) as mentioned in the earlier section. Figure 6.7 shows the execution of J_{phi} for each subcell.

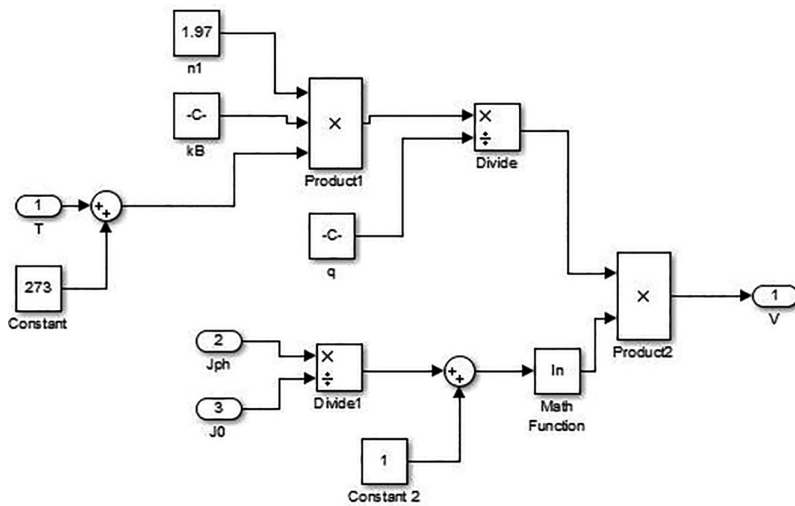


FIGURE 6.6

Execution of V_{oci} for each subcell.

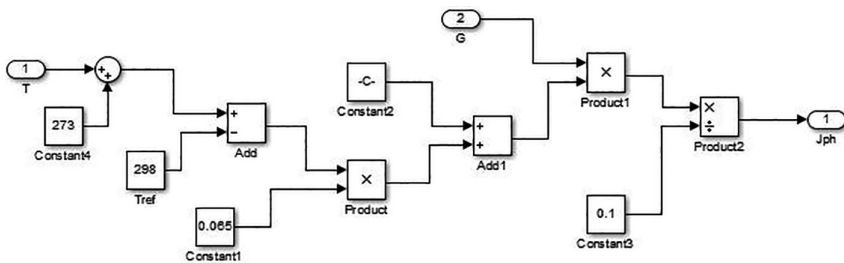


FIGURE 6.7

Execution of J_{phi} for each subcell.

6.5.1.4 Current Density of Cell (J_i) Evaluation

The J_i expression can be used for the model. Figure 6.8 represents the execution of J_i for each subcell.

$$J_i = J_{ph} - J_d - J_{pr} \quad (6.29)$$

6.5.2 MJSC Implementation

The four-layer MJSC in the MATLAB/Simulink interface is depicted in Figure 6.9. This model gives the solar P - V and V - I characteristics at STC. On STC, solar V - I and P - V characteristics are presented. Results are presented for $T=25^\circ\text{C}$ and $G=1,000\text{ W/m}^2$.

6.5.3 Execution of MPPT Techniques with MJSC

In the present work, three sorts of MPPT scheme calculations are utilized for simulation exercise, i.e., P&O, INC, and TLBO techniques. In the upcoming sections, TLBO codes which are used to optimize the power and voltage level, P&O, and INC-dependent MATLAB/Simulink models are given below.

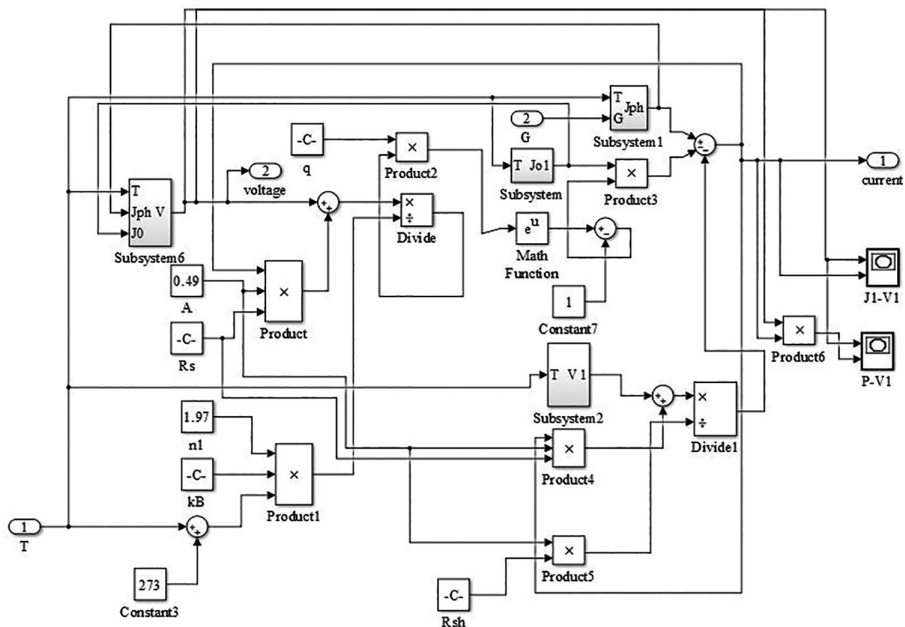


FIGURE 6.8

Execution of J_i for each subcell.

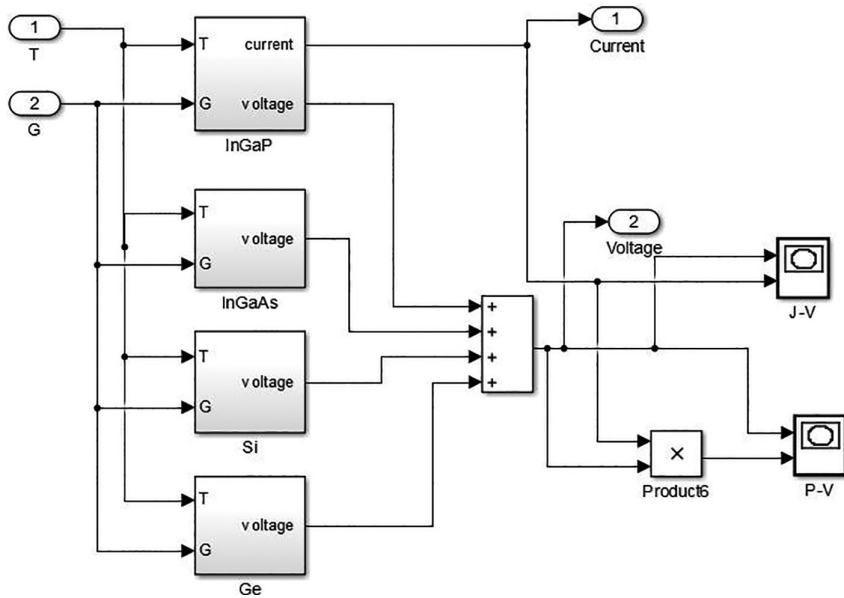


FIGURE 6.9
Implementation of four-layer MJSC.

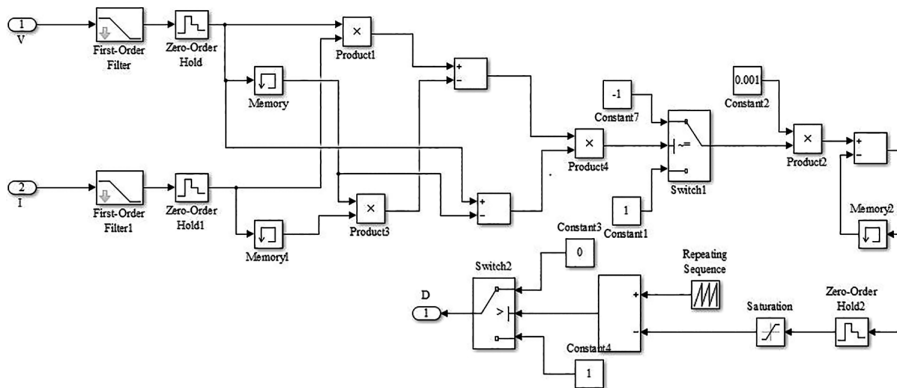


FIGURE 6.10
P&O algorithm implementation using MATLAB/Simulink model.

6.5.3.1 Simulation Model Using P&O Technique

The P&O calculation estimation is shown in the accompanying figure. The referenced model is created in the light of the operating steps that portray the working conditions of the particular calculation after which the most extreme power point is accomplished. On MATLAB/Simulink platform, this calculation is done which is the mimic of the algorithm steps. Figure 6.10 describes the P&O algorithm implementation using MATLAB/Simulink models.

6.5.3.2 Simulation Model Using INC Technique

The INC algorithm calculation is based on the above steps which are reflected in the above INC section. The INC algorithm implementation using MATLAB/Simulink model is shown in Figure 6.11.

6.5.3.3 Simulation Model Using TLBO Technique

The TLBO consists of basically three phases. The first phase is the initialization phase. The second phase is the teacher phase. The last phase is the learner phase. The target function or the fitness function according to which this TLBO optimization procedure will work is

$$\text{fit} = \max(\text{Voltage})$$

$$\text{fit} = \max(\text{Power})$$

Every time the model runs, there is an extraction of maximum P and V . Hence, this is formulated fitness function. In the initialization phase, everything is initialized like the number of variables, lower limit, upper limit, and the number of solutions.

The teacher phase mean of the solution is calculated so that the teacher’s knowledge can increase the mean of the class. On this basic thing, classroom theory works. The best cost or best fitness value will be the teacher. In learner phase, randomly any other learner is chosen and compared until the best cost or best fitness function is achieved. Some of the variables used have a lower limit of 0.001 and an upper limit of 5. The number of population or solution

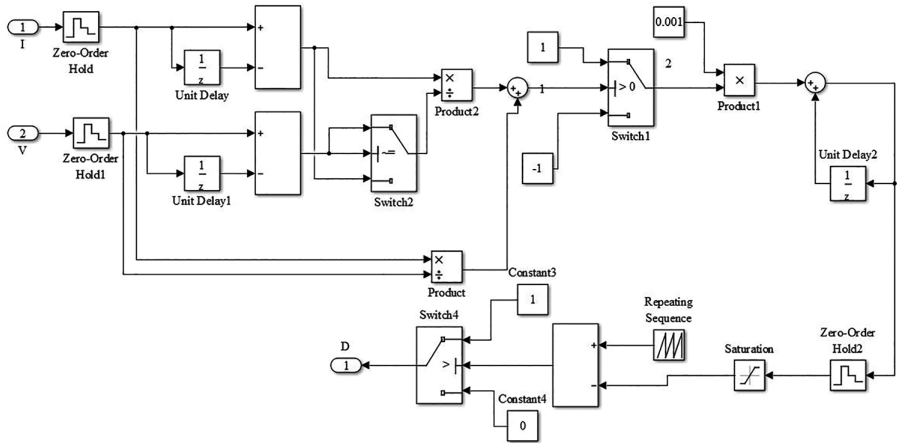


FIGURE 6.11
INC algorithm implementation using MATLAB/Simulink model.

is 5. The number of population can be changed. It can be 10. The simulation time can increase if the population increases. Initially, the best solution value is taken to be zero to see further progress in the loop. Given below are the codes for initialization phase:

```
global JSCI PV
N_Var = 1;
Var_Size = [1 N_Var];
LB = 0.001;
UB = 5;
Max_Iteration = 10;
n_Pop = 5;
Empty_Matrix.Position = [ ];
Empty_Matrix.Cost = [ ];
pop = repmat(Empty_Matrix, n_Pop, 1);
Best_Solution.Cost = 0;
for i=1:n_Pop
pop(i).Position = unifrnd(LB, UB, Var_Size);
pop(i).Cost = fitness(pop(i).Position);
if pop(i).Cost > Best_Solution.Cost
Best_Solution = pop(i);
end
end
```

Implementation of the initialization phase is described in the codes as mentioned. N_Var is the dimension or the number of variables. The lower bound is 0.001 and the upper bound is 5. The number of solutions is 5. The empty_matrix.position will generate an empty matrix for solution. Likewise empty_matrix.cost generates empty matrix for fitness value. The next function generates an empty array. The best solution value is initialized as zero. Table 6.3 describes the parameters initialized in the initialization phase. Each learner position is updated according to eq. (6.24). The new learner is evaluated according to the fitness equation. The basic criterion $x_{i,new}$ is accepted only if $x_{i,new}$ is better than $x_{i,old}$. Either the $x_{i,old}$ is unchanged. Hence best fitness value is evaluated and stored.

This phase is built up according to eqs. (6.25) and (6.26) as mentioned earlier. In this, the learner will randomly interact with various other learners.

TABLE 6.3

Parameters Initialized in Initialization Phase

Parameters of TLBO	Values
N_Var (number of variables)	1
Lower bound (LB)	0.001
Upper bound (UB)	5
Maximum iteration	10
n_Pop (number of population)	5

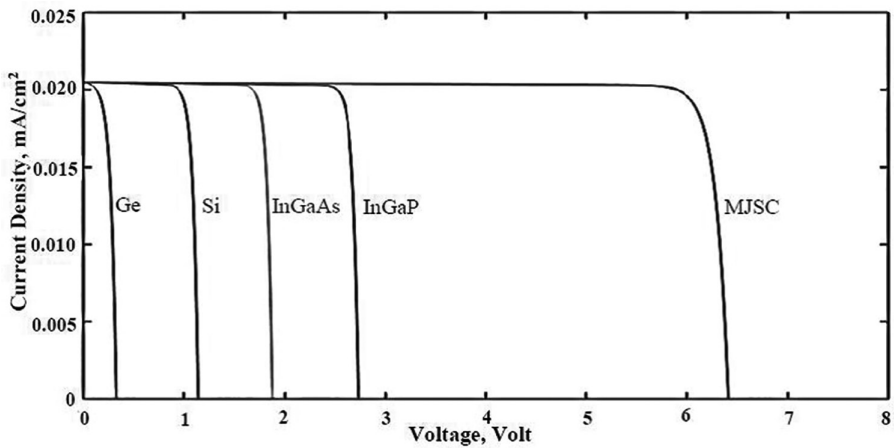


FIGURE 6.13
V-I curve and its subcell of MJSC.

TABLE 6.4

Voltage (V_{oc}) Contribution of Subcells

Subcells	Voltage
Indium gallium phosphide	2.75 V
Indium gallium arsenide	1.82 V
Silicon	1.2 V
Germanium	0.35 V

TABLE 6.5

Power Contribution of Cell

Cells	Power
InGaP, InGaAs, Si, Ge (four-layer MJSC)	0.13 W
InGaP, InGaAs, Ge (three-layer MJSC)	0.09 W

the different layers of V_{oc} contribution, and the power contribution of cells is shown in Table 6.5. Figure 6.14 demonstrates the P - V curve of the MJSC. The maximum power obtained from four-layer MJSC is 0.13 W. The subcell in the three-layer MJSC are InGaP, InGaAs, and Ge. These three layers are used for comparison with the four-layer MJSC. It is also clearly seen that the four-layer MJSC power contribution is more than the three-layer MJSC. The four-layer MJSC is a base work. However, when Si layer is removed, then the three-layer MJSC is compared with the four-layer MJSC. The maximum power obtained from the three-layer MJSC is 0.09 W.

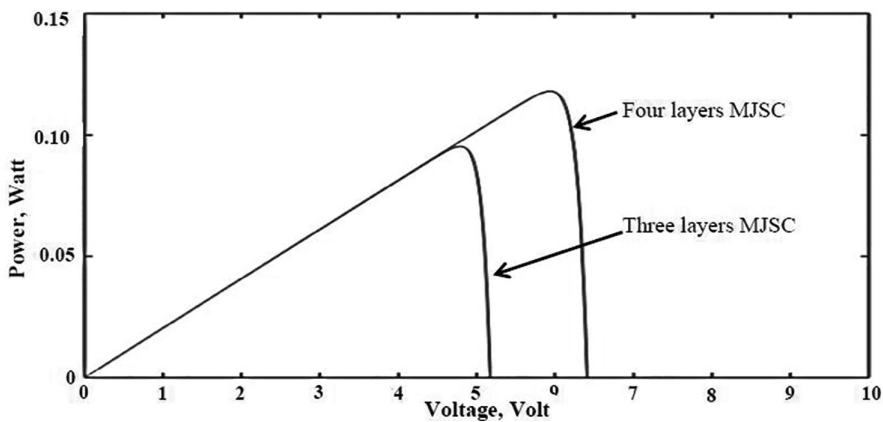


FIGURE 6.14 Comparison between three- and four-layer MJSC.

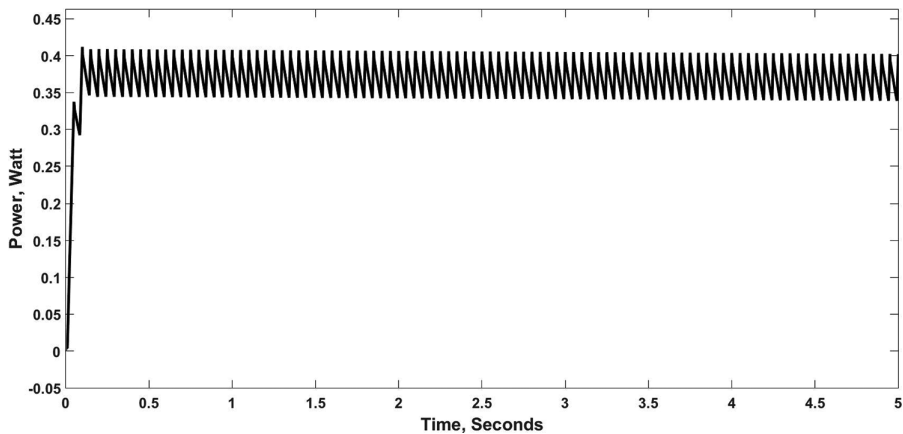
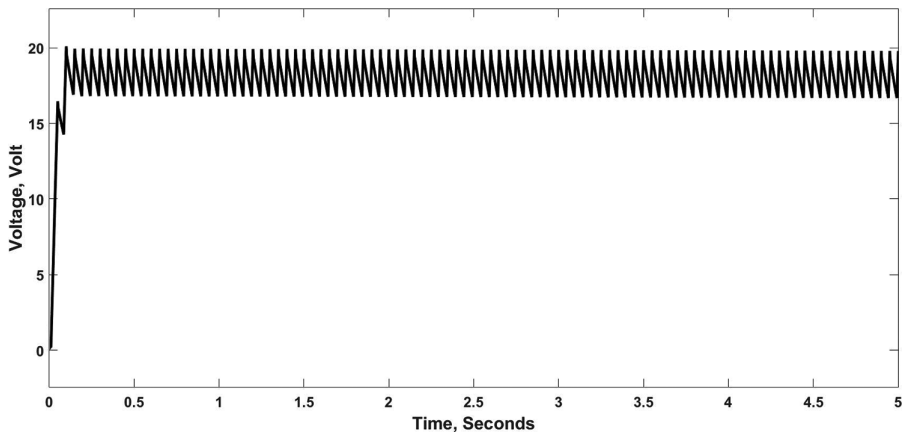


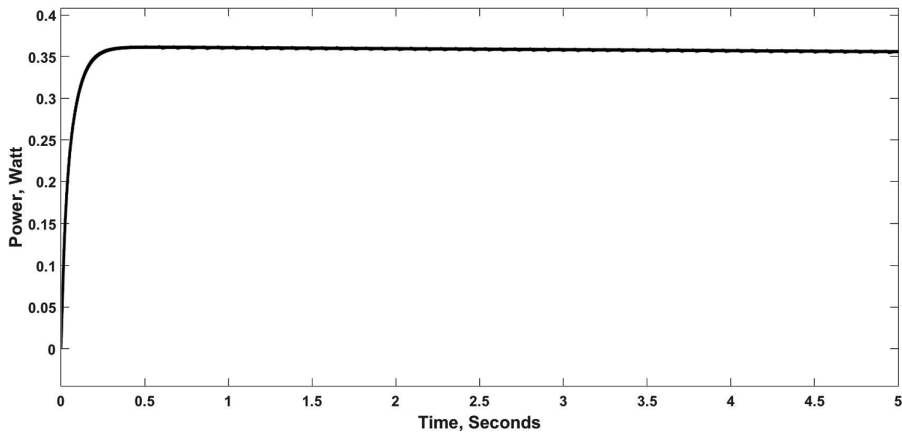
FIGURE 6.15 Power-time curve by P&O technique.

6.6.2 Results Analysis

Figures 6.15 and 6.16 depict power-time and voltage-time curves after the implementation of P&O technique. It is noticed that P&O technique is an effective control method to overcome the nonlinear characteristics of solar PV cell and improve the efficiency of solar PV power generation system but still causes some oscillations and the output produced by the system. This depicts the power-time graph after the implementation of P&O technique. As again it can be seen in this plot that the level of power is incremented as compared to the previous value in Figure 6.14 which was coming out to be 0.13 W.

**FIGURE 6.16**

Voltage–time curve by P&O technique.

**FIGURE 6.17**

Power–time curve by INC technique.

The INC method offers distinctive focal points: good tracking proficiency and good control for the extracted power. This calculation decides when the MPPT has arrived at the MPP, whereas P&O wavers around the MPP. This is a favorable position over the P&O technique.

Additionally, INC can follow quickly, expanding and diminishing irradiance conditions with higher exactness than P&O strategy. Figures 6.17 and 6.18 present power–time and voltage–time graphs after the implementation of the INC technique. This technique is most famous on the conventional technique platform.

The voltage and power obtained from the TLBO technique come out on the basis of fitness function mentioned in the previous section. Every time the

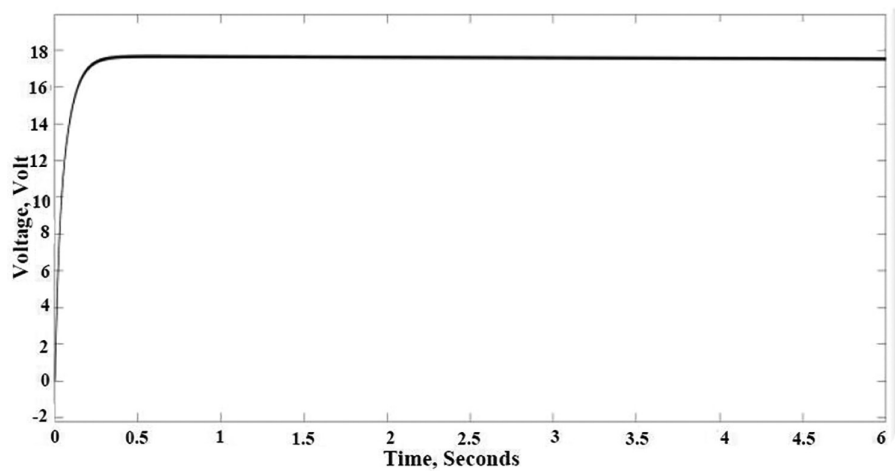


FIGURE 6.18
Voltage–time curve by INC technique.

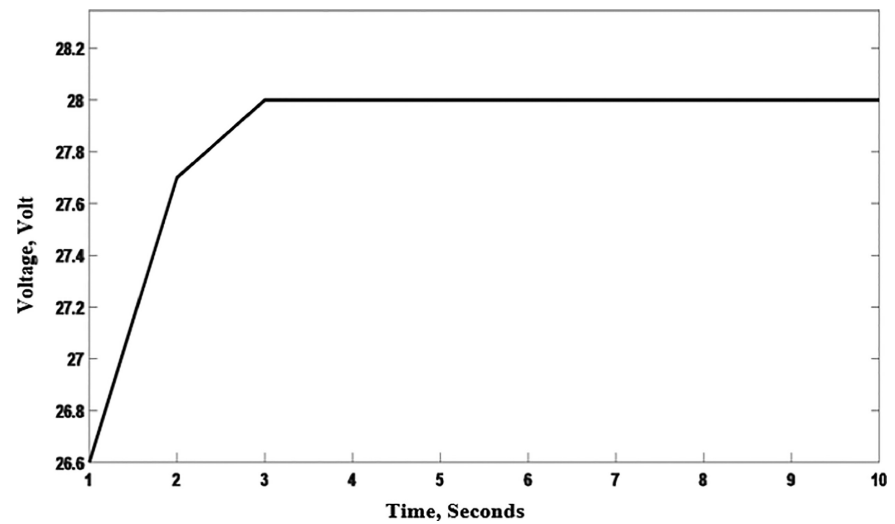


FIGURE 6.19
TLBO technique-based voltage–time curve.

loop will run, it will extract the maximum value of voltage and power, and the best value will be the final value of both parameters.

The optimized value of both voltage and power is depicted in Figures 6.19 and 6.20, which comes out to be 28 V and 6.7699 W by TLBO technique. A comparative study between MPPT techniques-based results is shown in Table 6.6.

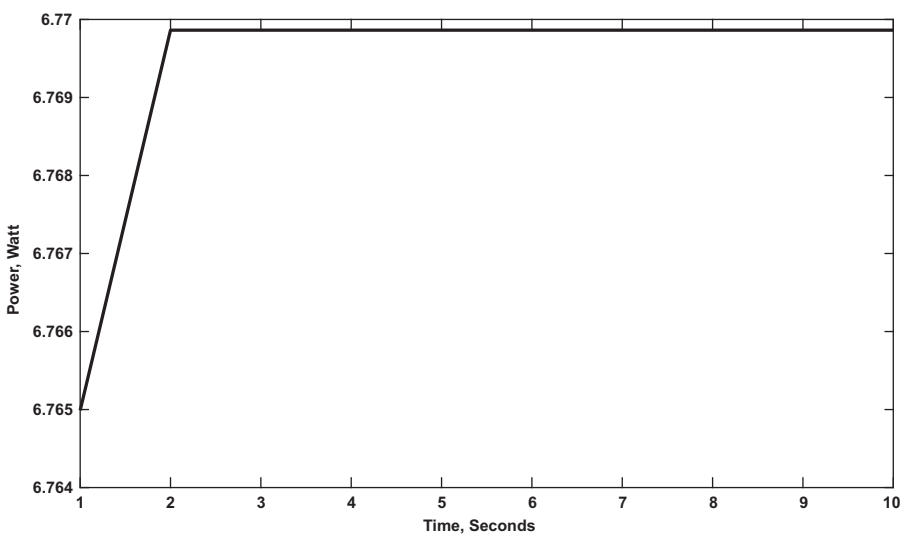


FIGURE 6.20
TLBO technique-based power–time curve.

TABLE 6.6
Comparison between MPPT Techniques

MPPT Techniques	Voltage (Volt)	Power (Watt)
TLBO	28 V	6.7699
P & O	20 V	0.415
INC	17.8 V	0.365

After applying all three techniques, the optimal result was given by the TLBO technique. TLBO is easy and effective and does not require algorithm-specific controlling parameters. The P&O technique falters wherever through MPP’s line, causing loss of vitality despite the fact that in INC lesser swaying occurs. The TLBO gives the steadiest yield.

6.7 Conclusion

The investigation of three diverse MPPT methods has been done in this chapter. There is a difference in power of the three-layer MJSC and four-layer MJSC. From three-layer MJSC, the derived power is 0.09 W and four-layer MJSC 0.13 W. It is clearly visible from this that on an increasing layer of MJSC, power will increase. But the required criteria is that the semiconductor elements should be arranged in the decreasing order of bandgap energy.

The most extreme power at STC in P&O, INC, and TLBO is monitored and discovered palatable. The reenactment was presented remembering the ultimate objective to show the benefit of MPPT and survey the execution and helpfulness of the proposed MPPT strategy. However, after applying all three techniques the optimal result was given by the TLBO technique which provides the maximum power output of 6.7699 W.

A simple, easy, and uncomplicated P&O technique causes it to extraordinarily stretch out to realize in a few activities. The P&O technique falters wherever through MPP’s line that causes loss of vitality despite the fact that lesser swaying occurs in INC. TLBO gives the steadiest yield.

Additionally, INC technique can quickly expand and diminish irradiance conditions with higher exactness than P&O strategy. To sum up, when by and large execution is analyzed, it could be seen that TLBO technique is better and gives ameliorated responses than P&O and INC techniques, as it can adequately improve the wellness or the cost, and it is simple and successful and doesn’t require explicit calculation of controlling parameters.

Appendix: Specifications for MJSC

Specifications	Values
Short circuit current density	20.5mA/cm ²
Irradiance	1,000W/m ²
Temperature	25°C
InGaP bandgap energy	2.637eV
InGaAs bandgap energy	1.874eV
Si bandgap energy	1.14eV
Ge bandgap energy	0.6583eV
Cell area	0.49cm ²
$\gamma_1=\gamma_2=\gamma_3=\gamma_4$	2
Charge q	$1.602\times10^{-19}\text{C}$
Series resistance	0.2190 Ω
k_1 (Cell 1)	1.86×10^{-9}
k_2 (Cell 2)	1.28×10^{-8}
k_3 (Cell 3)	4.5×10^{-7}
k_4 (Cell 4)	10.5×10^{-6}
n_1 (Cell 1)	1.97
n_2 (Cell 2)	1.75
n_3 (Cell 3)	1.56
n_4 (Cell 4)	1.96

References

1. Overview Report, Ministry of New and Renewable Energy, Government of India, June 2021. Online: <https://mnre.gov.in/solar/current-status/>.
2. S. Gupta, O. Singh and S. Urooj, "A review on single and multi-junction solar cell with MPPT techniques," *3rd IEEE International Conference on Nanotechnology for Instrumentation and Measurement*, Gautam Buddha University, India, 2017.
3. A. B. Hussain, A. S. Abdalla, A. S. Mukhtar, M. Elamin, R. Alammari and A. Iqbal, "Modeling and simulation of single and triple junction solar cell using MATLAB/SIMULINK," *International Journal of Ambient Energy*, Vol. 38, pp. 613–621, 2017.
4. N. Das, A. A. Ghadeer and S. Islam, "Modelling of multi-junction photovoltaic cell using MATLAB/Simulink to improve the efficiency," *Renewable Energy*, Vol. 74, pp. 917–924, 2015.
5. T. M. Razykov, C. S. Ferekides, D. Morel, E. Stefanakos, H. S. Ullal and H. M. Upadhyay, "Solar photovoltaic electricity: Current status and future prospects," *Solar Energy*, Vol. 85, pp. 1580–1608, 2011.
6. M. Babar, E. A. Ammar and N. H. Malik, "Numerical simulation model of multi junction solar cell," *Journal of Energy Technologies and Policy*, Vol. 2, pp. 44–53, 2012.
7. G. F. Mongelli, "Multi-junction solar cells: Snapshots from the first decade of the twenty-first century," *Research and Development in Material Science, USA*, Vol. 4, pp. 339–342, 2018.
8. S. Thomas and K. Nithyanantham, "A novel method to implement MPPT algorithms PV panels on a MATLAB/SIMULINK environment," *Journal of Advanced Research in Dynamical and Control Systems*, Vol. 10, pp. 31–40, 2018.
9. T. Halder, "A Maximum Power Point Tracker (MPPT) using the incremental conductance (INC) technique," *7th India International Conference on Power Electronics (IICPE)*, 2016.
10. M. A. Dhaifallah, A. M. Nassefa, H. Rezka and K. S. Nisar, "Optimal parameter design of fractional order control based INC-MPPT for PV system," *Solar Energy*, Vol. 159, pp. 650–664, 2018.
11. R. Reisi, M.H. Moradi and S. Jamasb, "Classification and comparison of maximum power point tracking techniques for photovoltaic system: A review," *Renewable and Sustainable Energy Reviews*, Vol. 19, pp. 433–443, 2013.
12. E. Kandemir, N. S. Cetin and S. Borekci, "A comprehensive overview of maximum power point extraction methods for PV systems," *Renewable and Sustainable Energy Reviews*, Vol. 78, pp. 93–112, 2017.
13. T. Selmi, M. A. Niby, L. Devis and A. Davis, "P&O MPPT Implementation using MATLAB/Simulink," *IEEE 9th International Conference on Ecological Vehicles and Renewable Energy*, Monte-Carlo, Monaco, 2014.
14. E. A. Gouda, M. F. Kotb and D. A. Elalfy, "Modelling and performance analysis for a PV system based MPPT using advanced techniques," *European Journal of Electrical and Computer Engineering (EJECE)*, Vol. 3, pp. 1–7, 2019.
15. A. Fathy, H. Rezk and D. Yousri, "A robust global MPPT to mitigate partial shading of triple-junction solar cell based system using manta ray foraging optimization algorithm," *Solar Energy*, Vol. 207, pp. 305–316, 2020.

16. X. Chen, B. Xu, K. Yu and W. Du, "Teaching-learning-based optimization with learning enthusiasm mechanism and its application in chemical engineering," *Journal of Applied Mathematics, Hindawi*, Vol. 18, pp. 1–19, 2018.
17. A. Koochaki, M. Divandari, E. Amiri and O. Dobzhanskyi, "Optimal design of solar-wind hybrid system using teaching-learning based optimization applied in charging station for electric vehicles," *IEEE Transportation Electrification Conference and Expo (ITEC)*, USA, 2018.
18. R. V. Rao, V. J. Savsani and D. P. Vakharia, "Teaching-learning-based optimization: A novel method for constrained mechanical design optimization problems" *Computer Aided Design*, Vol. 43, No. 3, pp. 303–315, 2011.
19. R. V. Rao, V. J. Savsani and D. P. Vakharia, "Teaching-learning-based optimization: An optimization method for continuous non-linear large scale problems," *Information Science*, Vol. 183, No. 1, pp. 1–15, 2012.
20. D. Chen, R. Lu, F. Zou and S. Li, "Teaching-learning-based optimization with variable-population scheme and its application for ANN and global optimization," *Neuro Computing*, Vol. 173, pp. 1096–1111, 2016.
21. F. F. Muhammadsharif, "A new simplified method for efficient extraction of solar cells and modules parameters from datasheet information," *Silicon*, Vol. 14, pp. 3059–3067, 2022.

Emerging Techniques of Shade Dispersion

Md. Faizan Nomani and Bhavnesk Kumar

Netaji Subhas University of Technology

Bhanu Pratap

National Institute of Technology Kurukshetra

CONTENTS

Nomenclature	159
7.1 Introduction	160
7.2 Recent Developments	161
7.3 Methodology	165
7.3.1 Modeling and Mathematical Description of PV System	165
7.3.1.1 PV Array and Partial Shading Condition (PSC)	167
7.3.2 Simulink Model of Pre-defined PV array Interconnection	169
7.3.2.1 Electrical Interconnection of TCT	169
7.3.2.2 Electrical Interconnection of SP-T	169
7.3.2.3 Electrical Interconnection of BL-T	170
7.3.3 Particle Swarm Optimization (PSO) Implementation	170
7.3.3.1 PSO Code for Rearranging Shade Pattern	173
7.3.4 Genetic Algorithm (GA) Implementation	176
7.3.4.1 GA Code for Rearranging Shade Pattern	177
7.4 Results and Discussion	181
7.4.1 Series Parallel Total Cross Tied (SP-T)	181
7.4.2 Total Cross Tied (TCT)	181
7.4.3 Bridge Link Total Cross Tied (BL-T)	181
References	186

Nomenclature

PSC: Partial Shade Condition
TCT: Total Crossed Tied

SP-T:	Series-Parallel Total Crossed Tied
BL-T:	Bridge Link Total Crossed Tied
MPPT:	Maximum Power Point Tracking
MPP:	Maximum Power-Point
GA:	Genetic Algorithm
PSO:	Particle Swarm Optimization
NS:	Novel Structure
BL-HC:	Bridge Link Honey Comb
RTT:	Ray Tracing Technique

7.1 Introduction

Partial Shading Condition (PSC) of PV array is a very primitive problem, and various solutions to overcome this problem have been suggested before for mitigating it in PV systems. Due to the accumulation of the shade on the modules of a PV array, the condition of partial shading develops, which deteriorates the performance of the PV system steeply (Rao et al., 2018). The reason behind this is the unequal current generation in the series-connected PV modules of an array; therefore, the power generating capability of the PV system gets hammered. The unequal row current not only reduces the power generation but also increases the mismatch losses in the PV system, and it is also noticed that due to this, there are multiple peaks in P-V characteristic of the photovoltaic system, which is a performance measuring parameter of the system (Kirkham, 2014; Vinod et al., 2018). In order to increase the maximum power point (MPP), different predefined interconnections of PV array have been compared under the assumed shade pattern. The predefined interconnection of PV array that has been considered here is Total Cross Tied (TCT), Series-Parallel Total Cross Tied (SP-T), and Bridge-Link Total Cross Tied (BL-T) (Djalab et al., 2018; Mishra et al., 2017). The assumed shade pattern on the PV array needs to be rearranged in order to optimize the power generating capability of the considered PV system. For this, Meta-Heuristic techniques, namely, Particle Swarm Optimization (PSO) and Genetic Algorithm (GA), have been considered. The outcome of the meta-heuristic algorithm is rearranged in shade pattern, which is superimposed on the best performing predefined PV array interconnection amongst the one, which is considered here for the assumed shade pattern. Thus, the methodology implemented to cope with the above-discussed problem is presented in the next sections of this chapter along with the mathematical description and technical specifications of the PV system considered here.

7.2 Recent Developments

In this section, we have taken into account the results and discussions that have been obtained from various works of literature related to this problem. This has been done so that we can get a vivid perspective of the problem and solutions suggested to tackle this problem. After getting insight from the previous research work, we proceeded further and suggested our methodology to reduce the prominence of this problem. In this manner, we tried to make a small contribution in this field. Now, we will discuss briefly the literature that has been used as a reference in pursuance of this work.

Badrul Hasan Khan (2009) gave a basic idea about the principle, construction, and working of the PV cell. The author first discusses the evolution of the PV cell with time. Also, it illustrates the idea of the principle of working with the photovoltaic cell along with the construction of the PV cell. Further, the performance characteristics of PV system with the major problems and design parameters have been discussed in detail. Finally, the author describes the usefulness and place of the utilization of the PV system. Wang et al. (2011) discussed the advantages and disadvantages of the production of energy using a photovoltaic system. The researcher provides a case study of the west region of Gansu, China and elaborately presents the advantages and disadvantages of PV systems in power generation. They also propose an optimal design for utilizing solar energy in the household.

Schmid and Kovach (1996) have suggested the working tool for calculating the energy losses caused due to shading and reflection effect. An I-V characteristic is incorporated to show the effect of the shading on the output. The experiment has been conducted in the laboratory under controlled conditions with commercially available PV cells. The paper also suggests the Ray Tracing Technique (RTT), which gives a matrix of irradiation distribution over PV array for each hour on a day. The result has been presented after analyzing two case studies. Thus, they came up with a guideline, which helps engineers to layout strategies to optimize the power generation by the PV system and reduce the losses caused by shading.

In the work of Gautam and Kaushika (2003), the electrical characteristics of SP-T, BL-T, and TCT for different shade patterns under different array configurations, i.e., 6×6 and 9×4 have been studied, and it has been found that performance of BL-T and TCT is substantially better than that of SP-T interconnection when cost, maximum power, and fill factor are considered the comparing parameters. This paper also deals with the analysis of current at each junction using a computer algorithm to limit it to zero, so that an even distribution of current-voltage in the interconnected array can be presented. In the work by Jiang and Moballegh (2014), three predefined PV array interconnections have been compared for the mismatch losses generated by them when they are exposed to PSC. The considered PV array interconnections

have been compared for different irradiation levels and temperatures. In addition to that, the researcher also suggested the procedure to predict the peak power achievable by the given PV system using the Hill climbing/P&O algorithm and also validated it using a commercially available PV system.

In the work by Yadav et al. (2020), various PV array topologies have been studied; they are TCT, BL-T, SP-T, and Bridge Link Honey Comb (BL-HC). These all topologies are studied under PSC. The comparing parameters considered here are mismatch power loss, performance factor, and fill factor. The effect of variation of temperature on shade dispersion has also been studied. The author also proposed an odd–even configuration to mitigate the effect of PSC on the PV array so that power loss can be reduced and the fill factor can be improved. Hanitscht and Quaschningt (1996) propose the models of PV array and their characteristics were discussed under PSCs. This research work discusses all the voltages and current generated by the proposed model of the solar generator and thus establishes the relationship between current and voltage, which enables the researcher to describe the characteristics of solar cells in the generation region as well as in breakdown at negative and positive voltages. Thus, it provides a complete analysis of current and voltage characteristics under partial shade conditions (PSCs) of the proposed model of PV array.

Salama et al. (2011) propose a novel configuration that results in a considerable reduction in mismatch losses caused by PSC. The mismatch losses cause a reduction in power generation and create a hotspot. The researcher also comes up with the mathematical formula for insolation level mismatch that can be used for comparative evaluation of photovoltaic configuration for a different arrangement. The improvement by implementing the proposed novel configuration has been recorded in this paper. In the work by Nagamani et al. (2013), the losses caused due to PSC have been combated by proposing a new methodology for rearranging the shade on PV array, which is based on the SU-DO-KU theory. The shade pattern obtained by this theory has been realized by altering the electrical connection. The rearrangement of shade done by the SU-DO-KU hypothesis provides a considerable improvement in PV power generation. The performance of the PV system has also been analyzed in this paper; the recorded result shows that the SU-DO-KU pattern of shade dispersion on TCT interconnection of PV array improves the performance of PV system under PSC.

In the work by Larbes and Belhachat (2015), modeling and analysis of performance under PSC of various PV array configurations have been done. The PV array configurations that have been considered here for comparison are Parallel, Series, SP-T, BL-T, TCT, and Honey Comb. They have been exposed to all possible scenarios of shading patterns and the performance parameter that has been chosen for comparison is maximum power and relative power loss under PSC. In most of the cases of PSC, TCT configuration proves to be showing superior results in terms of performance parameters considered. Thus, this paper deals in a comprehensive study of PV array configurations

under possible PSC that occurs in reality. To reduce the partial shading losses and enhance the power generation, a novel scheme had been suggested by Iyer et al. (2016) for rearrangement of the PV module, which is named Zig-Zag scheme. This scheme was implemented on TCT interconnection by taking five different shading patterns under consideration. The simulation result had been compared with the classical TCT interconnection results and been validated by repetitive observations. It had been found that there is a major improvement in the performance and operational characteristics. Another point that had been noted in this research work is that the problem of local maxima in P-V characteristics is lessened due to the implementation of a new scheme, which further simplifies the algorithm utilized for tracking Global MPP (GMPP).

Saravana Ilango et al. (2014) also deal with the reduction of mismatch losses, which are caused by PSCs and enhance the power generation by the photovoltaic system. Till now, different interconnection had been suggested for reducing the effect of PSC, which is realized by electrical rewiring, but in this paper, the researcher suggests that the enhancement of PV power can be done for fixed interconnection by distributing the effect of shading all over the PV array, thus reducing the mismatch losses and enhancing the power generation. A thorough investigation of the effect of PSCs for different shade patterns had been carried out and the result shows how the proposed scheme enhances the power generation capability of the PV system. The result has been validated by the experimental setup of a 5×5 PV array. In the work by Shi et al. (2012), a novel flexible switch array matrix topology had been suggested for the adaptive utility of interactive PV systems. This paper proposes a system, which deals with all the operational problems such as module failure, shading, mismatch, and soiling, and maximizes power generation in real-time. It was also being stated there that the system helps to exclude the power conditioning equipment and demonstrate an improvement of 13% as compared to central topology inverter performance. The results were validated experimentally and it is also been claimed that it benefits a wide range of applications.

In the work by Ahmadi et al. (2016), mathematical analysis and simulation of TCT configuration under PSCs were done. A TCT interconnection in a 2×2 PV array is mathematically analyzed for different partial shade patterns. The effect on output is interpreted through the P-V curve. To prove the superiority of TCT configuration, same shade patterns had been imposed on Series-Parallel, Bridge Link-TCT (BL-TCT), and Honey Comb and their characteristics had been noted in this paper. The input to the PV system had been taken from a standardized photovoltaic cell datasheet. Shi and Eberhart (1998) discuss and analyze the problem-solving capability and usefulness of nature-inspired algorithms. They are implemented on nonlinear optimization problems then their efficiency and adaptability had been recorded here. The two algorithms that have been compared are Differential Evolution (DE) and PSO. This paper mainly compared the accuracy of these two algorithms

in finding the best synaptic weights of the ANN during the learning phase of ANN. The comparison has also been made between the given two algorithms while training an ANN to apply to the nonlinear problem.

Rahmatshamii and Robinson (2004) introduced us to a detailed explanation and conceptual overview of the PSO algorithm and its implementation in electromagnetic optimization. The paper records several results of swarm behavior for engineering optimization. The detailed analyses of PSO implementation in engineering problems and suggestions for parameter value selection have been discussed. Then, it had been implemented for optimization of profile corrugated horn antenna. In the work by Miyatake et al. (2018), a large PV panel interconnected in series and parallel has been assumed which is exposed to PSC, which reduces the power generation capability of the system and introduces multiple peaks in the P-V curve. To abrogate this problem, panels are configured to minimize the losses; this has been done through the SU-DO-KU hypothesis and PSO. The advantage of implementing PSO is recognized here, as there is no requirement of physical movement of the module as required during rearrangement with the SU-DO-KU method, only electrical connections need to be altered with the previous one. Different shade patterns have been imposed on the PV module and extensive simulation had been conducted to generate the I-V and P-V curves, which support the usefulness of the proposed technique over the latter one. Another analysis that has been done here is the performance analysis of the system based on the income generation and energy saving along with the comparison between various electrical array reconfigurations to validate the suitability of the proposed array reconfiguration method.

Deshkar and Dhale (2015) also deal in optimizing the power generation through the PV system, which is under PSC. Here, the reconfiguration of the PV array for maximizing the power production and minimizing the multiple peaks in P-V characteristics has been done using the GA. A 9×9 PV array in TCT interconnection has been considered, which is exposed to the PSC, and rearrangement of shade is carried out using GA. Altering the electrical connection does the realization of obtained shade pattern. It has been validated experimentally that the new electrical interconnection draws maximum power from the assumed PV system.

Thus, after going through all the abovementioned literature, it has concluded that PSC is a very primitive yet very dominant problem in a PV system that still needs to be addressed. Keeping this in mind, we noticed that in all the abovementioned literature, no researcher has made the comparison between two meta-heuristics techniques—either they came with a new rearrangement scheme for the shade pattern to maximize power or they put the comparison between physical relocation scheme and new nature-inspired meta-heuristic algorithm that provides shade rearrangement pattern. Hence, we came up with the idea of comparing two novel meta-heuristic shade rearrangement schemes of PV systems to find out which meta-heuristic technique is performing better in assumed PSCs. In precedence to this, we have also

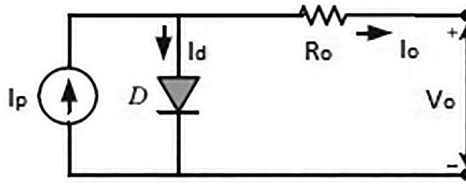
tried to compare the few classical interconnections for the assumed shade pattern in the considered PV array configuration, and best amongst those is selected for further comparison by imposing the rearrange shade pattern obtained through the considered meta-heuristic techniques.

7.3 Methodology

A systematic approach is required to tackle the problem caused by the PSC. First, technical specifications of the components used for designing PV systems have to be noted along with the assumed shade pattern that has been utilized to mark the performance of the system. Afterward, simulation model of the selected PV array interconnection can be developed in the MATLAB® software. Apply the assumed shade pattern on PV panel to note down their performance characteristics, which helps choose the best performing predefined PV array interconnection for the assumed shade pattern. Thereafter, to disperse shading effect optimization using Meta-heuristic algorithm is performed in EDITOR window of MATLAB in order to maximize the power generation through the selected predefined interconnection of PV array. The rearranged shade pattern is superimposed on the Simulink® model of best performing PV array interconnection and their performance is again measured using the P-V characteristics. The result of all these conditions had been recorded and is inscribed under results and discussion.

7.3.1 Modeling and Mathematical Description of PV System

The smallest unit of the PV system is the PV cell, which is a basic element for converting solar directly into electrical energy. PV cell is a current generating device, so when it absorbs light, it knocks out a loose electron, which results in the creation of current due to the flow of electron. The current generated is captured and transferred to the wire. The principle behind the generation of electricity through PV cells is called the photovoltaic effect. The PV cell is made up of semiconductor material usually silicon which knocks loose electrons with the incidence of light. Since, the individual solar cell does not produce enough amount of energy, which can be efficiently utilized for domestic or industrial purposes, so there is a need to arrange them in series and parallel according to the values of current and voltage that need to be generated. Thus, PV cells are arranged to form a PV module and several PV modules are connected to form a PV array. The basic electrical circuit illustration of the PV cell is shown in Figure 7.1. The mathematical equation of PV voltage (V_o) generated through the PV cell, which depends upon the photon current (I_p), is illustrated in eq. 7.1.

**FIGURE 7.1**

Electrical comparable circuit.

$$V_{pv} = \frac{A_i K_c T_c}{e_o} \ln \left(\frac{I_p + I_d + I_o}{I_d} \right) - R_o I_o \quad (7.1)$$

where

 K_c = Boltzmann constant T_c = Cell temperature A_i = Ideality factor $e_o = 1.6 \times 10^{-19}$ coulombs I_d = Diode current

Further, the cell is arranged in series or parallel to form module, if the module is comprised of $N_{se} \times N_{pa}$ PV cells, where N_{se} is the number of cells connected in series and N_{pa} is the number of cells connected in parallel, then the voltage and current generated by the PV module are communicated through eq. 7.2.

$$V_m = N_{se} V_c \quad (7.2a)$$

$$I_m = N_{pa} I_c \quad (7.2b)$$

$$V_{ocm} = N_{se} V_{oc} \quad (7.2c)$$

$$I_{scm} = N_{pa} I_{sc} R_{sm} = \frac{N_{se}}{N_{pa}} R_s \quad (7.2d)$$

where

 V_m, V_c = Module voltage, cell voltage. I_m, I_c = Module current, cell current. V_{ocm}, V_{oc} = Module open-circuit voltage, cell open-circuit voltage. I_{scm}, I_{sc} = Module short circuit current, cell short circuit current. R_{sm}, R_s = Module resistance, cell resistance.

TABLE 7.1

BP-3170-N Characteristic Parameter

Characteristic Parameter	Values
Open circuit voltage (V_{oc})	44.30 Volts
Short circuit current (I_{sc})	5.20 Ampere
Maximum power	177.90 Watt

For our research work, the PV module that we have considered is commercially accessible by the model name BP-3170-N (Mishra et al., 2017). The characteristic parameter of individual cells in the mentioned module is accumulated in Table 7.1.

The value of characteristic parameter of the mentioned PV module is noted for normal irradiation level of $1,000 \text{ W/m}^2$ and at 25°C .

The current generated by the PV cell relies conspicuously upon insolation, which is mathematically observed as shade factor K_f as

$$I_r = K_f I_m = \left(\frac{K_x}{K_c} \right) I_m \quad (7.3)$$

where

K_x = Actual insolation level (Watt/m^2)

K_c = Reference insolation level (Watt/m^2)

The voltage produce through the PV array, V_o , is mathematically depicted as the summation of the voltage produced by each PV module V_{mi} .

$$V_o = \sum_{i=1}^n V_{mi} \quad (7.4)$$

where n is the number of PV modules connected to form PV array.

7.3.1.1 PV Array and Partial Shading Condition (PSC)

The PV array consider here is of 8×4 configuration, i.e., 8 PV modules are connected in column and 4 PV modules are connected in a row. The uneven illumination condition that has been assumed here for 8×4 matrix of PV array is illustrated in Figure 7.2.

This shade pattern comes under the category of short and wide forms. The top four rows are normally illuminated with the insolation level of $1,000 \text{ W/m}^2$. However, the last four rows of the matrix are unevenly illuminated where the first two columns of the matrix are at the insolation level of 600 W/m^2 and the last two columns are illuminated with the insolation level of 400 W/m^2 .

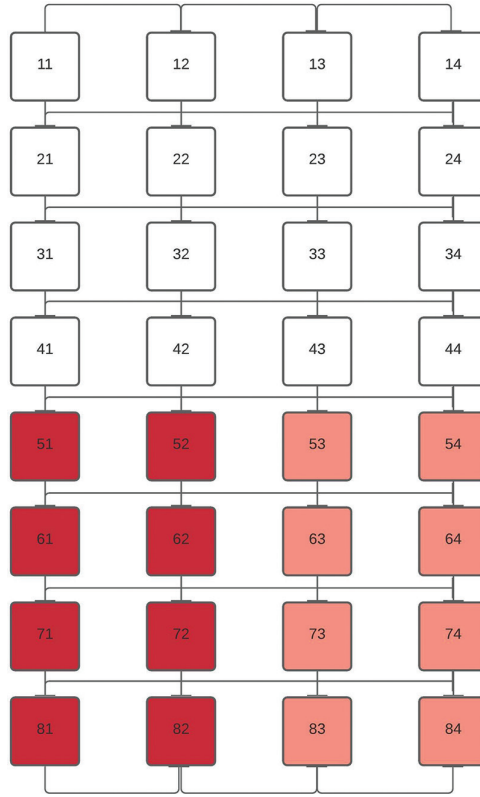


FIGURE 7.2
Assumed shade pattern.

With reference to eq. (7.3), current through each row of the PV array is the summation of current generated by each PV module in the row. So, the assumed shade pattern current generated through each row is given by

$$I_{\text{row}1} = I_{\text{row}2} = I_{\text{row}3} = I_{\text{row}4}$$

$$= \sum_{i=1}^4 I_m = \frac{1,000}{1,000} I_m + \frac{1,000}{1,000} I_m + \frac{1,000}{1,000} I_m + \frac{1,000}{1,000} I_m = 4I_m \quad (7.5)$$

$$I_{\text{row}5} = I_{\text{row}6} = I_{\text{row}7} = I_{\text{row}8}$$

$$= \sum_{i=1}^4 I_m = \frac{600}{1,000} I_m + \frac{600}{1,000} I_m + \frac{400}{1,000} I_m + \frac{400}{1,000} I_m = 2I_m \quad (7.6)$$

Thus, the main objective in order to maximize the power generation of the PV array is to equalize the row current. For this, meta-heuristic algorithm is considered, which is going to be discussed further in this chapter.

7.3.2 Simulink Model of Pre-defined PV array Interconnection

For mitigating the effect of PSC, a few predefined interconnection PV modules have been suggested before. To see the behavior of our assumed shade pattern and further infer which of the predefined interconnection of PV array is giving better results under the assumed shade pattern. Predefined interconnection of PV module to form PV array that has been considered here are mentioned below:

1. TCT
2. SP-T
3. BL-T

In TCT, each PV module in the PV array is connected in series as well as in parallel. Moreover, in SP-T PV modules in each column are connected in series, whereas PV module of alternate rows of PV array is connected in parallel and in BL-T PV module in each column are connected in series, whereas the PV module in alternate rows of middle two columns is connected in parallel. The modeling of the abovementioned predefined interconnection has been done on Simulink window of MATLAB 2017. Then, the shading pattern has been imposed on the PV array interconnections by varying the irradiation input to each PV module according to the assumed shading pattern. Now, the screenshots of connections in Simulink window of considered predefined PV array interconnection are illustrated.

7.3.2.1 Electrical Interconnection of TCT

The modeling of TCT PV array interconnection is illustrated in Figure 7.3.

The load attached to this PV system is 1 k Ω , and all the reading of voltage and current of the PV system is taken across this load. The temperature of the PV module is kept constant to 25°C regardless of the irradiation received by the PV module. All the reading of voltage and current of the Model is imported to EDITOR window of MATLAB for further analysis of the output using the “To Workspace” tool and assigning the variable name.

7.3.2.2 Electrical Interconnection of SP-T

The modeling of SP-T PV array interconnection is illustrated in Figure 7.4.

Here also the load attached to the PV system is 1 k Ω and all the reading of voltage and current of the PV system is taken across this load. The temperature of the PV module remains unchanged and kept constant to 25°C regardless of the irradiation received by the PV module. All the reading of voltage and current of the model is imported to EDITOR window of MATLAB.

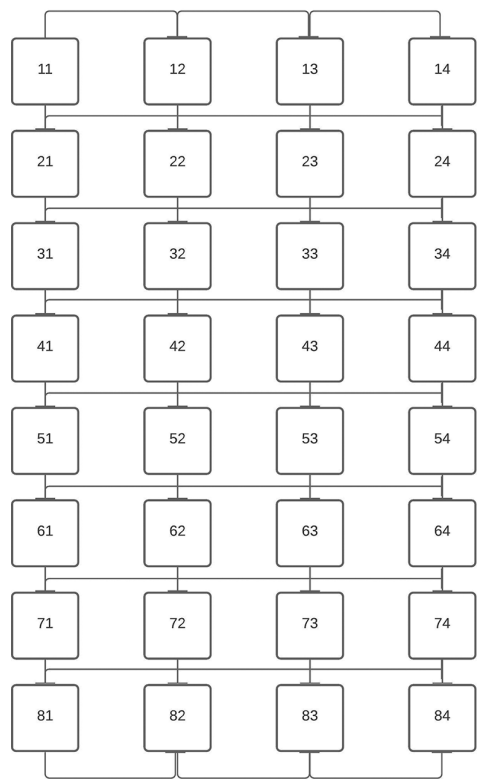


FIGURE 7.3
Electrical interconnection of TCT.

7.3.2.3 Electrical Interconnection of BL-T

The modeling of BL-T PV array is illustrated in Figure 7.5.

In this model also, the load assumed across the PV system is 1 k Ω , and the output values of currents and voltages are taken across this load. The temperature of the PV module remains unchanged and kept constant to 25°C regardless of the irradiation received by the PV module. All the reading of voltage and current of the model is imported to EDITOR window of MATLAB.

Now, we will discuss the implementation of meta-heuristic algorithm that has been utilized to obtain the optimized shade pattern that can be imposed on the best performing predefined interconnection in order to increase the power generation through the PV system.

7.3.3 Particle Swarm Optimization (PSO) Implementation

PSO is a meta-heuristic algorithm, and it has been considered here for rearranging the shade pattern to draw maximum power from the PV system because of the following reasons:

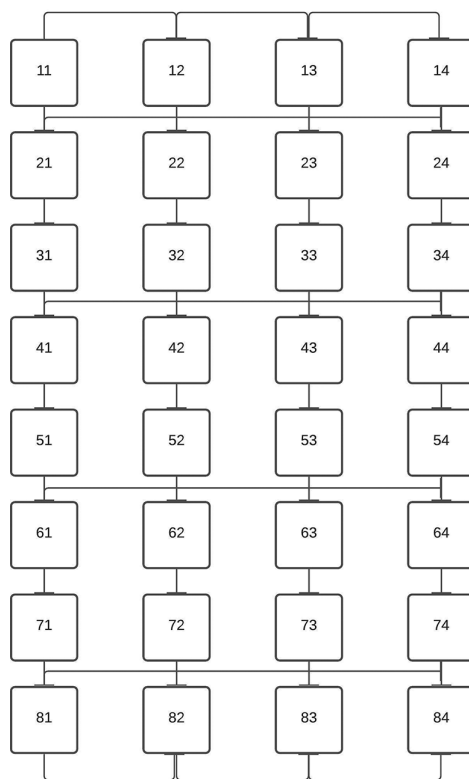


FIGURE 7.4
Electrical interconnection of SP-T.

- It prompts the best result, although it starts with arbitrary solutions.
- The probability of approximate results is diminished to an incredible degree.
- PSO is hearty and has a simple implementation.
- Running simultaneous calculation of parallel equations drastically improves computation time.

The steps followed for implementing PSO in order to rearrange the shade pattern of the assumed PSC to optimize the MPP of the PV system is depicted below (Miyatake et al., 2018):

Value estimation: Various PSO parameters first need to be initialized before carrying out further steps for shade dispersion. Parameters for utility in PSO are social constant (C_c), cognitive constant (C_g), and weight (W). Values of these constants considered here are $C_c=1.20$, $C_g=1.80$, and $W=0.90$. Beginning velocity of each particle is instated utilizing equation:

$$\text{vel}(j) = 1 + \text{round}(\text{rand}() \times 8) \quad (7.7)$$

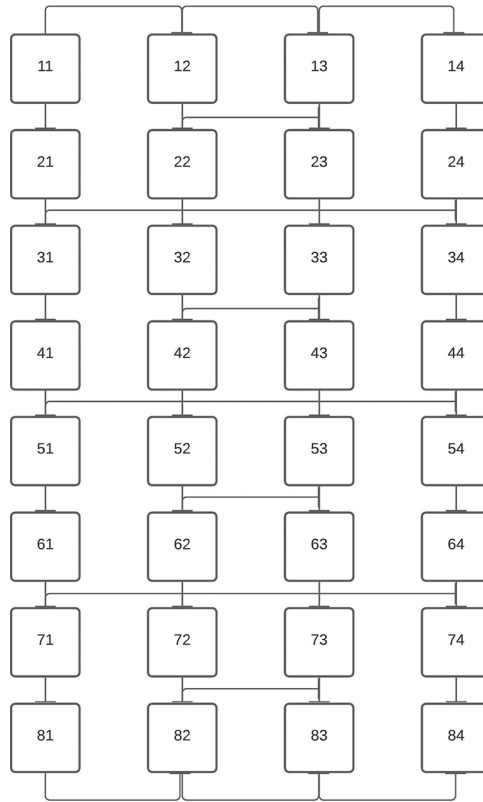


FIGURE 7.5
Electrical interconnection of BL-T interconnection.

Particle Evaluation Phase: Insolation of each cell is either estimated by sensor, else through the information sheet of producer. Insolation allows us to estimate the row current. The goal here is to reduce the difference of row current.

$$G = I_{\text{row}(j)} - I_{\text{row}(j-1)} \quad (7.8)$$

where j represents the row numeration.

Fitness Evaluation: The accuracy towards the sustainable solution of each particle is approximated by

$$\text{Max}(\text{Fitness}(j)) = \text{Sum}(P_o) + \left(\frac{W_{ev}}{E_{ep}} \right) + (W_{po} \times P_{ev}) \quad (7.9)$$

where

E_{ep} = Addition of difference of peak row current to generated row current.

P_o = Power produced through each PV module.

P_{eo} = Power produced through PV array.

W_{eo}, W_{p0} = Weight constants, value assumed here are 10.

Velocity Evaluation: The velocity towards the sustainable solution of each particle is approximated by

$$V_j^{t+1} = W \times V_j^t + \text{rand} \times C_c \times (P_{bst} - X_j^t) + \text{rand} \times C_g \times (G_{bst} - X_j^t) \quad (7.10)$$

where

V_j^t = Velocity of the particle after t th iteration.

X_j^t = Position of the particle after t th iteration.

P_{bst} = Personal best position of the particle.

G_{bst} = Global best position of the particle.

The velocity updation is accountable for obtaining the optimum solution to the problem.

Finishing Phase: The end of calculation happens either when no insolation change is noted and the arrangement has accomplished the most ideal arrangement or when the calculation surpasses the quantity of cycle assigned by the establisher.

The above calculation when implemented transmits the optimum shade pattern. The algorithm has been iterated for 500 turns to get concealing shade. The above-discussed steps for implementation of PSO for rearranging the shade pattern need to be coded in EDITOR window of MATLAB. The code utilized for the implementation of PSO is documented in the next section.

7.3.3.1 PSO Code for Rearranging Shade Pattern

Here, code has been mentioned that is utilized to rearrange the shade pattern of the assumed PSC. The code follows the PSO algorithm whose steps are mentioned in the previous section. Coding has been done in EDITOR window of MATLAB. The detailed implementation of code is as follows:

Objective Function:

```
function[o] = objfcn(Ir1,Ir2,Ir3,Ir4,Ir5,Ir6,Ir7,Ir8)
o1 = Ir1 - Ir2;
o2 = Ir2 - Ir3;
o3 = Ir3 - Ir4;
o4 = Ir4 - Ir5;
o5 = Ir5 - Ir6;
o6 = Ir6 - Ir7;
o7 = Ir7 - Ir8;
o = o1+o2+o3+o4+o5+o6+o7;
```

Fitness Function:

```
function [f] = fitfcn(P,we,Ee,wf,pa)
f = P + (we/Ee) + (wf*pa);
end
```

PSO Main:

```
clear
closeall
clc
c1 = 1.2;
c2 = 1.8;
w = 0.9;
v = zeros(8,4);
v1 = zeros(8,4);
k = zeros(8,4);
Vo = 44.3;
Go = 1000;
pa = 3280;
we = 10;
wf = 10;
A = [1000, 600];
B = [1000, 400];
pbest = zeros(8,4);
gbest = zeros(8,4);
maxitr = 500;
fori = 1:6
for j = 1:4
v(i,j) = 1+round(rand()*8);
end
end
G = [1000,1000,1000,1000; 1000,1000,1000,1000;
1000,1000,1000,1000; 1000,1000,1000,1000; 600,600,400,400; 600,
600,400,400;600,600,400,400;600,600,400,400];
xtl = G;
fori = 1:maxitr
Irl = (xtl(1,1)/Go)*5.2 + (xtl(1,2)/Go)*5.2 + (xtl(1,3)/Go)*5.2
+ (xtl(1,4)/Go)*5.2;
Ir2 = (xtl(2,1)/Go)*5.2 + (xtl(2,2)/Go)*5.2 + (xtl(2,3)/Go)*5.2
+ (xtl(2,4)/Go)*5.2;
Ir3 = (xtl(3,1)/Go)*5.2 + (xtl(3,2)/Go)*5.2 + (xtl(3,3)/Go)*5.2
+ (xtl(3,4)/Go)*5.2;
Ir4 = (xtl(4,1)/Go)*5.2 + (xtl(4,2)/Go)*5.2 + (xtl(4,3)/Go)*5.2
+ (xtl(4,4)/Go)*5.2;
Ir5 = (xtl(5,1)/Go)*5.2 + (xtl(5,2)/Go)*5.2 + (xtl(5,3)/Go)*5.2
+ (xtl(5,4)/Go)*5.2;
Ir6 = (xtl(6,1)/Go)*5.2 + (xtl(6,2)/Go)*5.2 + (xtl(6,3)/Go)*5.2
+ (xtl(6,4)/Go)*5.2;
```

```

Ir7 = (xt1(7,1)/Go)*5.2 + (xt1(7,2)/Go)*5.2 + (xt1(7,3)/Go)*5.2
+ (xt1(7,4)/Go)*5.2;
Ir8 = (xt1(8,1)/Go)*5.2 + (xt1(8,2)/Go)*5.2 + (xt1(8,3)/Go)*5.2
+ (xt1(8,4)/Go)*5.2;
P1 = Vo * Ir1;
P2 = Vo * Ir2;
P3 = Vo * Ir3;
P4 = Vo * Ir4;
P5 = Vo * Ir5;
P6 = Vo * Ir6;
P7 = Vo * Ir7;
P8 = Vo * Ir8;
P = P1+P2+P3+P4+P5+P6+P7+P8;
o = objfcn(Ir1,Ir2,Ir3,Ir4,Ir5,Ir6,Ir7,Ir8);
Ee = (20.8- Ir1)+(20.8- Ir2)+(20.8- Ir3)+(20.8- Ir4)+(20.8-
Ir5)+(20.8 - Ir7)+(20.8- Ir6)+(20.8 - Ir8);
xt = G;
f(i) = fitfcn(P,we,Ee,wf,pa);
for d = 1:8
for j = 1:4
v1(d,j) = w*v(d,j) + rand()*c1*(pbest(d,j)-xt1(d,j)) +
rand()*c2*(gbest(d,j)-xt1(d,j));
end
end
for m = 1:8
for n = 1:2
k(m,n) = randi(length(A));
end
for n = 3:4
k(m,n) = randi(length(B));
end
end

if o~= 0 && f(i)< f(i-1)
for m = 1:8
for n = 1:2
xt1(m,n) = A(k(m,n));
end
for n = 3:4
xt1(m,n) = B(k(m,n));
end
end
else
pbest = xt1;
end
if pbest(i) == pbest(i-1)
gbest = pbest;
end
end
disp(gbest);

```

Thus, by running the above-mentioned code 500 times, we get the desired rearranged shade pattern that optimizes the power generation capability of the considered PV system and equalizes the row current in the PV array. The rearranged shade pattern is stored in variable “gbest.” The obtained rearranged shade pattern is improvised onto the best performing predefined interconnection by changing the irradiation input according to the rearranged shade pattern in the Simulink model. Then the MPP of the model is noted and documented in the result chapter.

7.3.4 Genetic Algorithm (GA) Implementation

GA is also one of the meta-heuristic algorithms inspired by nature, and it also follows the same biological procedure. The steps involved in the implementation of the algorithm are selection, crossover, and mutation. GA is one of the simplest random-based evolutionary algorithms. This is a real-time technique in which outcomes can be tracked after each cycle of the algorithm. The design and implementation of the objective function in GA are comparatively easier, although the parameter estimation in GA appears to be a rigorous exercise because their values need to be precise for convergence. Here, to deal with the problem of uneven illumination of PV array, GA has been invoked as a tool to rearrange the shade on the PV array for evenly distributing the shade over the PV array and allow even current flow among the rows of the PV matrix. The objective function considered here is the same as that of eq. 7.9. The GA steps that have been considered here are illustrated below (Deshkar and Dhale, 2015):

1. A fixed population is accessed for the given problem along with the design of the objective function.
2. Selection among the defined population is carried out by the Roulette wheel method.
3. Mutation followed by crossover is performed among the selected chromosomes from the population. Their respective probability parameters assumed as $P_m=0.10$ and $P_c=0.80$.
4. After each cycle of the algorithm, the population is updated to the newly acquired population.
5. For successive cycles, the algorithm is repeated until a certain limit is set by the user or until there is no further population updation.

The abovementioned procedure is implemented by coding the steps of GA in EDITOR window of MATLAB in order to obtain the rearranged shade pattern of the assumed PSC to maximize the power generation of the PV system. In our case, the above algorithm is repeated for 700 turns to obtain the rearranged shade pattern.

7.3.4.1 GA Code for Rearranging Shade Pattern

Objective Function:

```
function[o] = objfcn(Ir1,Ir2,Ir3,Ir4,Ir5,Ir6,Ir7,Ir8)
o1 = Ir1- Ir2;
o2 = Ir2- Ir3;
o3 = Ir3- Ir4;
o4 = Ir4- Ir5;
o5 = Ir5- Ir6;
o6 = Ir6- Ir7;
o7 = Ir7 - Ir8;
o = o1+o2+o3+o4+o5+o6+o7;
```

Fitness Function:

```
function [f] = fitfcn(P,we,Ee,wf,pa)
f = P + (we/Ee) + (wf*pa);
end
```

Initialization:

```
function [ population ] = initialization(g)
population = g;
end
```

Selection:

```
function [parent1, parent2] = selection(population)
parent 1 = rand(population)
parent 2 = rand(population)
```

Crossover:

```
function [child1, child2] = crossover(parent1, parent2, Pc,
crossoverName)
pa1 = de2bi(parent1);
pa2 = de2bi(parent2);
switch crossoverName
case 'single'
Gene_no = length(pa1);
ub = Gene_no - 1;
lb = 1;
Cross_P = round ((ub - lb) *rand() + lb);
Part1 = pa1(1:Cross_P);
Part2 = pa2(Cross_P + 1 : Gene_no);
child1 = [Part1, Part2];
Part1 = pa2(1:Cross_P);
Part2 = pa1(Cross_P + 1 : Gene_no);
```

```

child2 = [Part1, Part2];

case'double'
Gene_no = length(pa1);
ub = length(pa1) -1;
lb = 1;
    Cross_P1 = round ( (ub - lb) *rand() + lb );
    Cross_P2 = Cross_P1;
while Cross_P2 == Cross_P1
    Cross_P2 = round ( (ub - lb) *rand() + lb );
end

if Cross_P1 > Cross_P2
temp = Cross_P1;
    Cross_P1 = Cross_P2;
    Cross_P2 = temp;
end

    Part1 = pa1(1:Cross_P1);
    Part2 = pa2(Cross_P1 + 1 :Cross_P2);
    Part3 = pa1(Cross_P2+1:end);
child1 = [Part1, Part2, Part3];
    Part1 = pa2(1:Cross_P1);
    Part2 = pa1(Cross_P1 + 1 :Cross_P2);
    Part3 = pa2(Cross_P2+1:end);
child2 = [Part1, Part2, Part3];
end
R1 = rand();
if R1 <= Pc
child1 = bi2de(child1);
else
child1 = bi2de(pa1);
end
R2 = rand();
if R2 <= Pc
child2 = bi2de(child2);
else
child2 = bi2de(pa2);
end
end

```

Mutation:

```

function [child] = mutation(child1,Child2, Pm)
child = rand(child1, child2)
ch = de2bi(child);
Gene_no = length(ch);
for k = 1: Gene_no
    R = rand();

```



```

if R < Pm
ch(k) = ~ ch(k);
end
child = bi2de(ch);
end

```

GA Main:

```

clear
closeall
clc
k = zeros(8,4);
Vo = 44.3;
Go = 1000;
pa = 3280;
we = 10;
wf = 10;
Pc = 0.80;
Pm = 0.10;
A = [1000, 600];
B = [1000, 400];
population = zeros(8,4);
newpopulation = zeros(8,4);
bestsolution = zeros(8,4);
maxitr = 700;
G = [1000,1000,1000,1000; 1000,1000,1000,1000;
1000,1000,1000,1000; 1000,1000,1000,1000; 600,600,400,400; 600,
600,400,400;600,600,400,400;600,600,400,400];
fori = 1:8
for j = 1:4
population(i,j) = Initialization(G(i,j));
end
end
fori = 1:maxitr
xt1 = population;
Ir1 = (xt1(1,1)/Go)*5.2 + (xt1(1,2)/Go)*5.2 + (xt1(1,3)/Go)*5.2
+ (xt1(1,4)/Go)*5.2;
Ir2 = (xt1(2,1)/Go)*5.2 + (xt1(2,2)/Go)*5.2 + (xt1(2,3)/Go)*5.2
+ (xt1(2,4)/Go)*5.2;
Ir3 = (xt1(3,1)/Go)*5.2 + (xt1(3,2)/Go)*5.2 + (xt1(3,3)/Go)*5.2
+ (xt1(3,4)/Go)*5.2;
Ir4 = (xt1(4,1)/Go)*5.2 + (xt1(4,2)/Go)*5.2 + (xt1(4,3)/Go)*5.2
+ (xt1(4,4)/Go)*5.2;
Ir5 = (xt1(5,1)/Go)*5.2 + (xt1(5,2)/Go)*5.2 + (xt1(5,3)/Go)*5.2
+ (xt1(5,4)/Go)*5.2;
Ir6 = (xt1(6,1)/Go)*5.2 + (xt1(6,2)/Go)*5.2 + (xt1(6,3)/Go)*5.2
+ (xt1(6,4)/Go)*5.2;
Ir7 = (xt1(7,1)/Go)*5.2 + (xt1(7,2)/Go)*5.2 + (xt1(7,3)/Go)*5.2
+ (xt1(7,4)/Go)*5.2;

```

```
Ir8 = (xt1(8,1)/Go)*5.2 + (xt1(8,2)/Go)*5.2 + (xt1(8,3)/Go)*5.2
+ (xt1(8,4)/Go)*5.2;
```

```
P1 = Vo * Ir1;
P2 = Vo * Ir2;
P3 = Vo * Ir3;
P4 = Vo * Ir4;
P5 = Vo * Ir5;
P6 = Vo * Ir6;
P7 = Vo * Ir7;
P8 = Vo * Ir8;
P = P1+P2+P3+P4+P5+P6+P7+P8;
o = objfcn(Ir1,Ir2,Ir3,Ir4,Ir5,Ir6,Ir7,Ir8);
Ee = (20.8 - Ir1)+(20.8 - Ir2)+(20.8 - Ir3)+(20.8 - Ir4)+(20.8
- Ir5)+(20.8 - Ir6)+(20.8 - Ir7)+(20.8 - Ir8);
xt = G;
f(i) = fitfcn(P,we,Ee,wf,pa);
for d = 1:8
for j = 1:4
[P1,P2] = selection(population);

    [c1,c2] = crossover(P1,P2,Pc, 'single');

child = mutation(c1,c2,Pm);

newpopulation(d,j) = child;
end
end
for m = 1:8
for n = 1:2
k(m,n) = randi(length(A));
end
for n = 3:4
k(m,n) = randi(length(B));
end
end

if o~= 0 && f(i)< f(i-1)
for m = 1:8
for n = 1:2
xt1(m,n) = A(k(m,n));
end
for n = 3:4
xt1(m,n) = B(k(m,n));
end
end
else
population = newpopulation;
end
```

```

ifnewpopulation(i) == newpopulation(i-1)
bestsolution = newpopulation;
end
end
disp(bestsolution);

```

Thus, by running the abovementioned code 700 times, we get the desired rearranged shade pattern that optimizes the power generation capability of the considered PV system and almost equalizes the row current in the PV array. The rearranged shade pattern is stored in the variable 'best solution'. The obtained rearranged shade pattern is improvised onto the best performing predefined interconnection by changing the irradiation input according to the rearranged shade pattern in the SIMULINK model. Then the MPP of the model is noted and documented in the result chapter.

7.4 Results and Discussion

Results and discussion of the chapter comprises the results obtained by applying the mentioned methodology in the previous chapter and its description. First, the result comprises the comparison among the three considered predefined PV array interconnections under normal insolation level and then under assumed uneven shade pattern. Their respective MPP Tracking (MPPT) portrays their performance. The interconnection showing the maximum peak power generation will be considered to be outperforming the remaining. The MPPT plot of SP-T, TCT, and BL-T under both conditions is illustrated in Figures 7.6, 7.7, and 7.8, respectively. Their peak power generation is clustered in Table 7.2.

7.4.1 Series Parallel Total Cross Tied (SP-T)

The P-V characteristics to track MPP of SP-T interconnection under both normal and assumed PSC are described below.

7.4.2 Total Cross Tied (TCT)

The P-V characteristics in order to track MPP of TCT interconnection under both normal and assumed PSC are inscribed below.

7.4.3 Bridge Link Total Cross Tied (BL-T)

The P-V characteristics in order to track MPP of BL-T interconnection under both normal and assumed PSC are inscribed below.

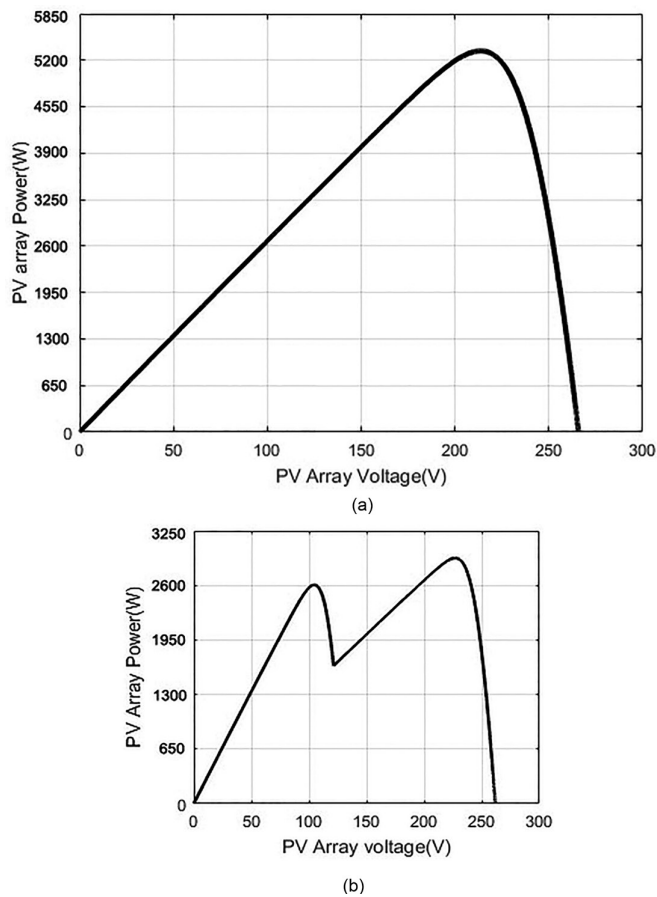
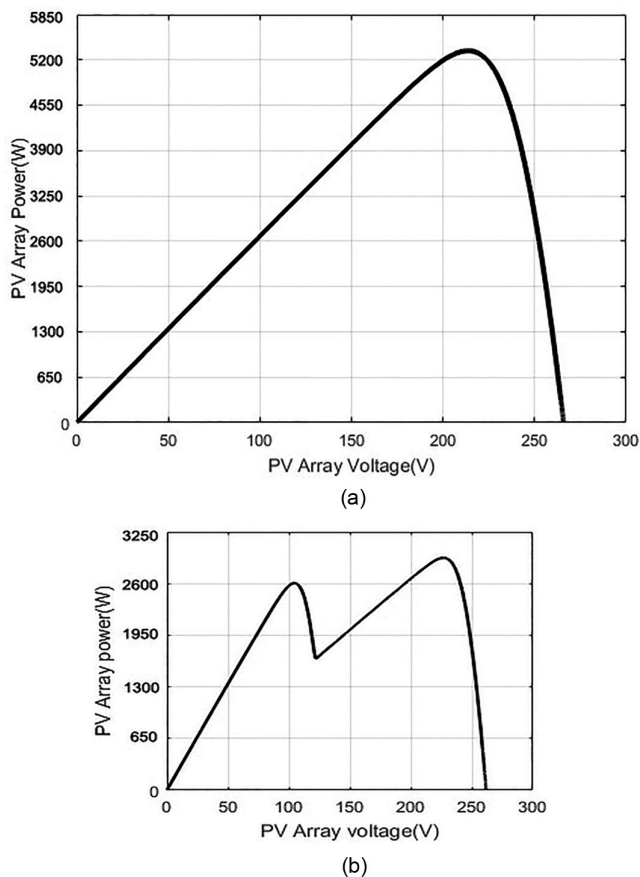


FIGURE 7.6 P–V characteristics of SP-T interconnection under (a) normal irradiation and (b) shade condition.

The result of the P–V characteristics obtained is clustered in Table 7.2 as follows.

The subsequent result shown here is the reconfigured shade pattern that has been obtained by running the algorithm of both the meta-heuristic techniques considered here. Figure 7.9 shows the shade pattern obtained after reconfiguring shade by PSO and GA.

From the acquired outcome, TCT design has demonstrated a better outcome for the assumed shade pattern. Therefore, TCT design has been chosen for implementing the obtained reconfigured shade pattern. The MPPT curves after applying the rearranged shade pattern obtained by GA and PSO on TCT are illustrated in Figure 7.10. The peak power of 4,034 W is observed with GA shade dispersion, which is substantially higher than 2,252 W obtained by

**FIGURE 7.7**

P-V characteristics of TCT interconnection under (a) normal irradiation and (b) shade condition.

TCT connection under the assumed uneven shade pattern, whereas when the rearranged shade pattern obtained by PSO is imposed on the TCT connection, the peak power of 4,110 W was observed, which is considerably higher than TCT connection under assumed uneven shade pattern as well as the peak power observed after shade rearrangement by GA.

The peak power observed after imposing the shade pattern obtained by both the meta-heuristic techniques on TCT connection is accumulated in Table 7.3. The table also accumulates other computational parameters that need to be mentioned in order to complete the analysis of implementing the meta-heuristic techniques to rearrange the shade pattern.

From the observations, it is worth discussing that peak power obtained after imposing shade pattern acquired by meta-heuristic methodology on TCT connection shows drastic improvement. Now, by comparing two

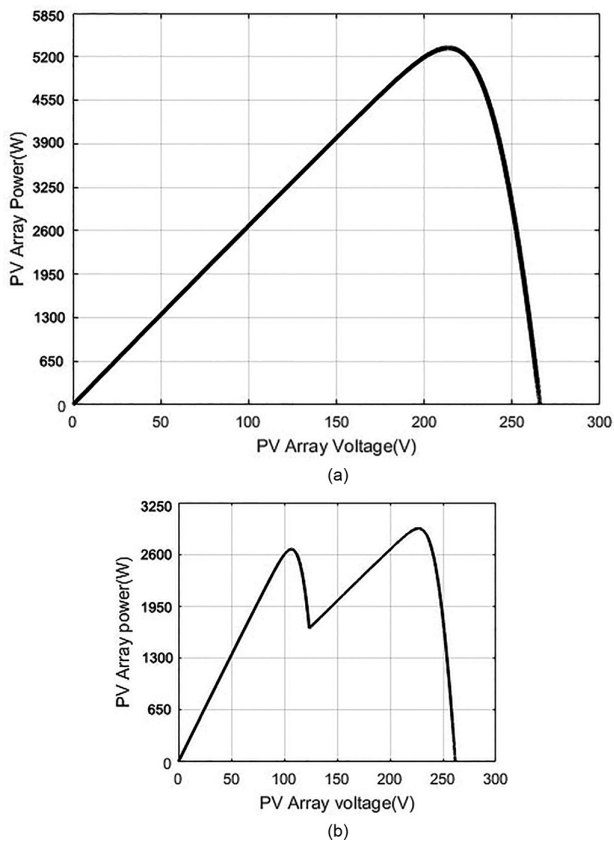
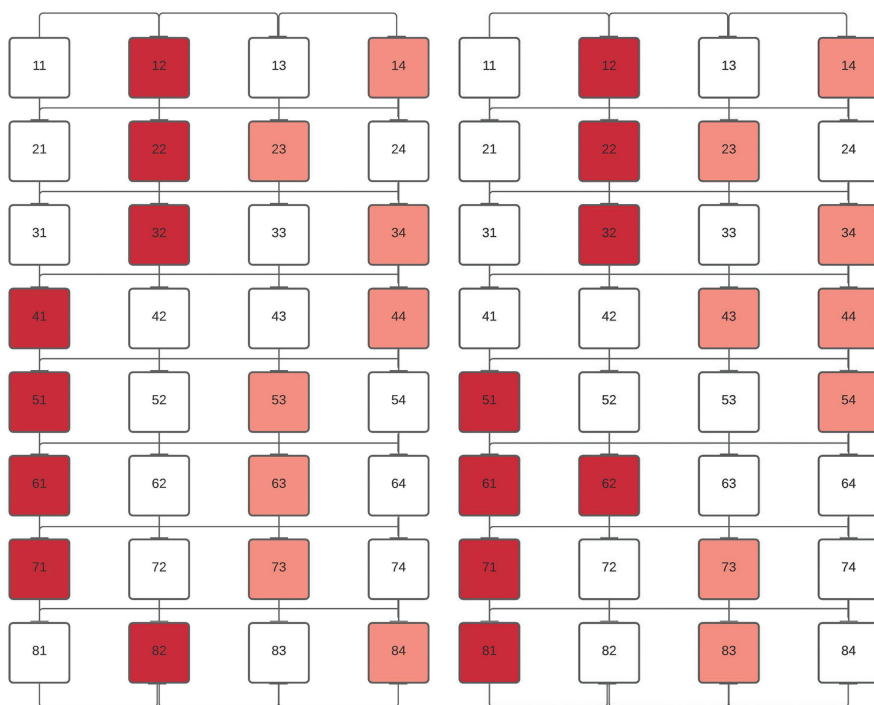


FIGURE 7.8
P–V characteristics of BL-T interconnection under (a) normal irradiation and (b) shade condition.

TABLE 7.2
Comparison of Peak Power Produced Among Predefined Interconnections

Parameter	PV Array Interconnection					
	Series-Parallel Total Cross Tied (SP-T)		Total Cross Tied (TCT)		Bridge Link Total Cross Tied (BL-T)	
	Under Normal irradiation	Under Shade Pattern	Under Normal irradiation	Under Shade Pattern	Under Normal irradiation	Under Shade Pattern
Peak power (Watts)	5,368	3,000	5,368	2,992	5,362	2,986

**FIGURE 7.9**

Rearrangement of shade by (a) PSO and (b) GA.

different methodologies implemented to rearrange the shade pattern, it is observed that PSO outperforms GA. This result has been drawn because the PSO took 500 iterations while GA took 700 iterations to rearrange the shade pattern. In terms of minimum computational required by the algorithm to rearrange the shade pattern, PSO took only 1.36 seconds, whereas GA took 4.86 seconds, which made us draw an inference that PSO is a better meta-heuristic technique than GA when it comes to computational time. The peak power observed by imposing shade patterns obtained by PSO outnumbers the peak power observed by imposing the shade pattern acquired by GA. Thus, PSO reduces the mismatch losses by 1,110 W, whereas the GA reduces the mismatch losses by 1,034 W. Another point that is worth discussing here is that the problem of multiple pinnacles, which occurs due to unequal row current of PV array and is observed in TCT connection under assumed shade pattern shows commendable improvement. When TCT connection is observed with the shaded pattern acquired by GA, it equalizes the row current of PV array to great extent, thus improving the problem of multiple pinnacles. However, PSO completely equalizes the row current of PV array, so it completely removes this problem. Thus, PSO shows better results as compared to GA.

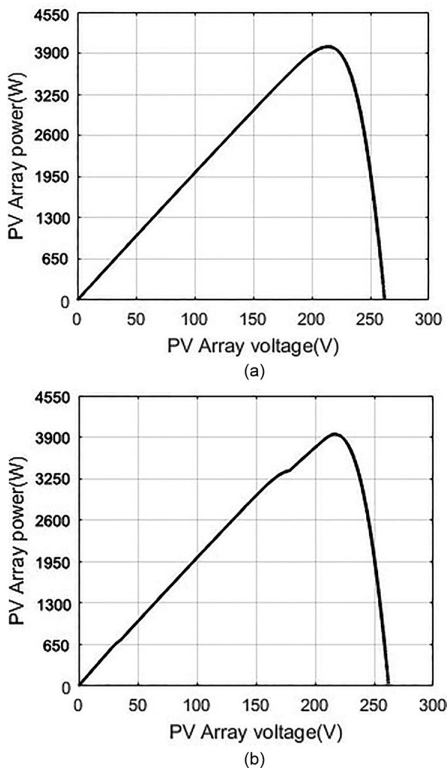


FIGURE 7.10
Peak power curve of TCT after rearrangement of shade using (a) PSO and (b) GA.

TABLE 7.3
Peak Power Achieved by TCT after Imposing Rearrange Shade Pattern and Other Computational Parameters

Meta-heuristic Techniques	Peak Power Achieved	Number of Iteration	Minimum Computational Time
Genetic Algorithm (GA)	4,034 W	700 iterations	4.86 seconds
Particle Swarm Optimization (PSO)	4,110 W	500 iterations	1.36 seconds

References

S.M. Ahmadi, A. Khalafi, S.M. Nejad, "Mathematical Analysis of TCT P.V Array under PSC and it's comparison with other configurations". *Solar Energy*, 2016, vol. 133, pp. 501–511.

- S.N. Deshkar, S.B. Dhale, "Solar PV array reconfiguration under PSCs for maximum power extraction using GA". *Renewable and Sustainable Energy Reviews*, 2015, vol. 43, pp. 102–110.
- A. Djalab, N. Besssous, M.M. Rezaoui, I. Merzouk, "Study of the effect of partial shading on PV array", in *International Conference on Communication and Electrical Engineering*, 2018.
- N.K. Gautam, N.D. Kaushika, "Energy yield simulation of inter-connected solar PV array". *IEEE Transactions on Energy Conversion*, 2003, vol. 18, pp. 127–143.
- V. Hanitscht, V. Quaschnigt, "Numerical simulation of current and voltages of PV system with shaded solar cells". *Solar Energy*, 1996, vol. 56, no. 6, pp. 513–520.
- S.R. Iyer, G.R. Bindu S. Vijayalakshmi, "A novel zig-zag scheme for power enhancement of PS PV array". *Solar Energy*, 2016, vol. 135, pp. 92–102.
- J. Jiang, S. Moballegh, "Prediction, modelling and experimental validation of power peaks of PV Array under PSCs". *IEEE Transactions on Sustainable Energy*, 2014, vol. 5, no. 1, pp. 293–300.
- B.H. Khan, "Solar photovoltaic system", in *Non-conventional Energy Resources*, Tata McGraw Hill, New Delhi, 2009, pp. 118–151.
- M.B. Kirkham, Solar radiation, black bodies and heat budget and radiation balance, in *Principle of Soil and Plant Water Relations*. Academic Press, Cambridge, MA, 2014, pp. 453–472.
- C. Larbes, F. Belhachat, Modelling, analysis and comparison of solar PV array configurations under PSC". *Solar Energy*, 2015, vol. 120, pp. 399–418.
- N. Mishra, A. Singh Yadav, R. Pachauri, Y.K. Chauhan, V.K. Yadav, "Performance enhancement of PV system under proposed array topologies under various shadow pattern". *Solar Energy*, 2017, vol.157, pp.641–656.
- M. Miyatake, F. Blaabjerg, N. Rajasekar, T.S. Babu, J.P. Ram, T. Dragicevic, "PSO based solar PV array reconfiguration of the maximum power extraction under PSCs". *IEEE Transactions on Sustainable Energy*, 2018, vol. 9, pp. 74–85.
- C. Nagamani, G. Saravanallango, B. Indu Rani, "Enhanced power generation from PV array under PSCs by shade dispersion using Su-Do-Ku configuration". *IEEE Transactions on Sustainable Energy*, 2013, vol 4, no. 3, pp. 594–601.
- Y. Rahmatshamii, J. Robinson, "PSO in electro-magnetics". *IEEE Transactions on Antennas and Propagation*, 2004, vol. 52, no.2, pp. 397–407.
- R.R. Rao, M. Mani, P.C. Ramamurthy, "An updated review on factors and their interlinked influences on photovoltaic system performance". *Heliyon*, 2018, vol. 4, pp. 8–15.
- M.M.A. Salama, M. Kazerani, M.Z.S. El-Dein, "Novel configuration for farm to reduce PS losses", in *Proceedings of IEEE International Conference on Energy and Power Society General Meeting*, 2011, pp. 1–5.
- G. Saravana Ilango, C. Nagamani, P.S. Rao, "Maximum power from PV array using a fixed configuration under different shade conditions". *IEEE Journal of Photovoltaics*, 2014, vol. 4, no. 2, pp. 679–686.
- J. Schmid, A. Kovach, "Determination of energy output losses due to shading of building-integrated PV array using a RTT". *Solar Energy*, 1996, vol. 57, no. 2, pp. 117–124.
- J. Shi, J. Neal, S.K. Lau M. Alahmad, M.A. Chaaban, "An adaptive utility interactive PV system based on FSM to optimize performance in real time". *Solar Energy*, 2012, vol. 86, pp. 951–963.
- Y. Shi, R.C. Eberhart, "Evolving ANN", in *Proceeding of International Conference on Neural Network Brain*, 1998, pp. 84–89.

- S.N. Sivanandam, S.N. Deepa "Introduction to genetic algorithm", in *Principles of Soft Computing*. Wiley, Hoboken, NJ, 2005 pp. 385–464.
- R. Vinod, Kumar, S.K. Singh, "Solar Photovoltaic modeling and simulation: As a renewable energy solution". *Energy Reports*, 2018, vol. 4, pp. 701–712.
- Y. Wang, T. Yue, Y. Wang, "Research on the prom. of solar energy house", in *International Conference on Materials for Renewable Energy & Environment*, 2011, pp. 247–250.
- K. Yadav, B. kumar, S. Devaraju, "Mitigation of mismatch power loss of PV array under partial shading condition using novel odd even Configuration". *Energy Reports*, 2020, vol. 6, pp. 427–437.

8

Solar Tracking Technology to Harness the Green Energy

Ram Krishan, K. Anil Naik, and R. David Amar Raj
NIT Warangal

CONTENTS

8.1	Introduction	190
8.2	Electrical Energy from Solar Cell	191
8.2.1	Mathematical Conceptualization of PV Panel	191
8.2.2	Modeling of Ideal Photovoltaic Cell	192
8.2.3	Modeling of Practical/Real-Time Photovoltaic Cell	193
8.2.4	Modeling of a Typical Sun Tracking System.....	194
8.2.5	TLB Optimization-Based-Tuning of PID Controller	196
8.3	Solar Tracker System	197
8.3.1	Components of a Solar Tracker System	197
8.4	Classification of Mechanical Tracking Systems.....	198
8.4.1	Based on Driving Systems Employed.....	199
8.4.1.1	Passive Solar Tracking (PST) System.....	199
8.4.1.2	Active Solar Tracking (AST) System.....	199
8.4.2	Based on the Degree of Freedom.....	199
8.4.2.1	Single-Axis Solar Tracking System.....	202
8.4.2.2	Dual-Axis Solar Tracking System	204
8.4.3	Based on Control Technique	206
8.4.3.1	Open-Loop Solar Tracking (OLST) Systems.....	206
8.4.3.2	Closed-Loop Solar Tracking (CLST) Systems	207
8.4.4	Based on Tracking Approaches	207
8.4.4.1	Using Date and Time	207
8.4.4.2	Employing Sensors, Date, and Time	208
8.4.4.3	Employing Various Microprocessors and Electro-Optical Sensors.....	208
8.4.4.4	AI-Based Solar Tracking Systems	208
8.4.5	Comparison of Solar Tracker Systems	209
8.4.6	Limitations of Solar Tracking Systems	209
8.5	Conclusions.....	210
	References.....	211

8.1 Introduction

Environmental variations and the rapid outgrowth of energy requirements are beckoning for a tremendous augmentation of renewable energy sources (RES) throughout the globe. Presently, the total installed capacity of solar photovoltaic (SPV) systems globally is higher than the aggregate of all the nonconventional energy systems, which is around 103 and 125 GW in 2018 and 2020, respectively (iea-pvps.org, Snapshot report 2020). Solar energy is an unlimited source of electricity and will play a significant role in the future. Nevertheless, solar irradiation changes from place to place and hence, the adoption of solar energy. The application of solar power can be promoted in numerous forms through solar power systems that track the pathway of the sun as shown in Figure 8.1, described as solar tracking systems (Racharla and Rajan, 2017). The central aim of solar tracking systems is to enhance energy yield by almost more than 40% when compared to the static SPV system. Nevertheless, it is additionally dependent on the driver unit, controller system, degrees of freedom, and additional parameters like position and weather (Mousazadeh et al., 2009).

In the last decades, several methods have been developed and implemented to improve tracking systems for tracking the sun throughout the day/seasons. Key methods include optimizing tilt and orientation angles of solar cells by using geographical latitudes information (Awachie, 2003), mathematical models (Canberra, 2004), and tracking algorithms (Suugur, 2007). The robotic arm is designed to enhance the performance of solar tracking systems using information such as atmospheric conditions, climate, geographical characteristics, and solar radiation quantity at a given point of the earth (Ilo et al., 2014).

The produced power from SPV systems is mainly dependent on irradiation hitting the SPV modules, ambient temperature, etc. Nevertheless, the SPV systems are orientated in such a way that the light rays hit perpendicularly to the surface of the SPV array and hence optimize the generation of electrical power. The impact of the temperature of photovoltaic (PV) panels

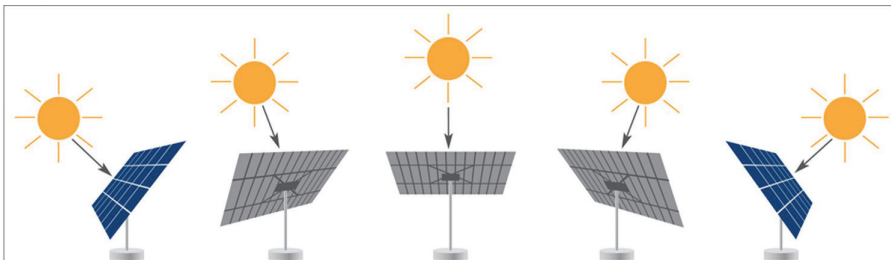


FIGURE 8.1

Tracking of sun's path by the tracking system.

on transformation efficiency is remarkably significant depending on the kinds of PV panels and their application. Besides the kind of technology and additional impacts on PV panels, the conversion efficiency of solar irradiation into electricity is essentially based on impedance regulation, which is known as maximum power point (MPP) tracking (Yatimi and Aroudam, 2018). Optimizing the electrical indices in order to accomplish the maximum generation of electricity from PV systems employing MPPT controllers is additionally remarkably significant. The solar PV tracking systems that track the sun ray's trajectory ensure that the density of solar irradiation is normal to the surface of the module. This tracking is performed by proper regulation and employment of a solar tracking controller drive unit.

8.2 Electrical Energy from Solar Cell

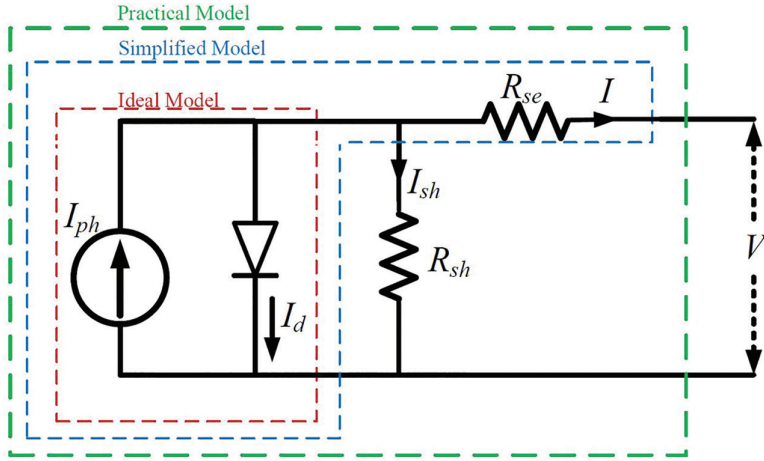
As discussed in the previous section, SPV panels are used to convert solar energy into electrical energy. SPV panels consist of a large number of solar cells that are connected in series and parallel combinations based on the terminal requirement (voltage/current). Solar cells are nothing but a PN junction diode. These days, several types of materials are used in the construction of solar cells and SPV panels, for example, mono-crystalline, polycrystalline, thin-film solar cells, amorphous silicon, biohybrid, and cadmium telluride solar cells.

When a solar photon strikes the SPV panels, some photon energy is transferred to the silicon electrons and makes the electron free from the silicon atom. The free electrons move through the external circuit connected between electrodes and generate the electric current. A mathematical model of the SPV panel is described in brief.

8.2.1 Mathematical Conceptualization of PV Panel

PV cell is a basic element for the transformation of photo-energy into electric power if it is combined in series and parallel manner. Besides building arrays, these PV modules are linked in series and parallel arrangements, which are capable to produce reliable and green power. A single PV cell can be expressed as a segment of electrical circuitry (Modified from Vinod et al., 2018).

It comprises p-n junction diode, photocurrent generator describing the production of current from sunlight, and two resistances, one is provided in series and the other is parallelly connected which represents the losses due to recombination and Joule effect. This arrangement is denominated as a single-diode PV cell model. In order to model the PV panel, a similar methodology is used as specified for PV cell. A simple circuit design of a PV module is demonstrated in Figure 8.2.

**FIGURE 8.2**

Equivalent circuit model of a photovoltaic cell.

8.2.2 Modeling of Ideal Photovoltaic Cell

The PV source can be expressed as an ideal PV cell with the current source connected in parallel to a diode “D” as depicted in Figure 8.2 and by applying the Kirchhoff’s Current Law (KCL), the source current is obtained as

$$I = I_{ph} - I_D \quad (8.1)$$

$$I_D = I_s \times \left[\exp\left(\frac{V_{oc}}{\alpha V_T}\right) - 1 \right] \quad (8.2)$$

$$V_T = \frac{N_s \times A \times T}{q} \quad (8.3)$$

$$I_D = I_s \times \left[\exp\left(\frac{qV_{oc}}{\alpha N_s A T}\right) - 1 \right] \quad (8.4)$$

$$I = I_{ph} - I_s \times \left[\exp\left(\frac{qV_{oc}}{\alpha N_s A T}\right) - 1 \right] \quad (8.5)$$

In an ideal condition, a PV cell produces a photo-generated current which is a direct proportion to the incident illumination and solar irradiation. In this ideal case, few parameters are not considered and that certainly affects the PV cell output in a real-time scenario. Hence, a detailed model of PV cells in realtime is described subsequently.

8.2.3 Modeling of Practical/Real-Time Photovoltaic Cell

A real-time model of PV cell consists of a single diode “D” with series resistance R_{se} and parallel resistance R_{sh} . In ideal conditions, R_{se} and R_{sh} are neglected; however, it is not practicable to neglect the effect of these resistors as the efficiency of solar cells is influenced by these resistances. Therefore, a suitable model is described in Figure 8.2. R_s indicates the losses caused due to the Joule effect, whereas R_{sh} is correlated with leakage current due to the thickness of PV cell and the surface effects (Vinod et al., 2018). The impact of R_{se} is notable due to the addition of PV cells resistance in a module when contrasted to R_{sh} . Only R_{se} is considered and R_{se} is regarded to be infinite, and the equation of diode current (I) is further transformed as

$$I_D = I_s \times \left[\exp \left(\frac{q(V + IR_s)}{\alpha N_s AT} \right) - 1 \right] \quad (8.6)$$

$$I = I_{ph} - I_s \times \left[\exp \left(\frac{q(V + IR_s)}{\alpha N_s AT} \right) - 1 \right] \quad (8.7)$$

By regarding the solar PV cells linked in a series-parallel arrangement, current I is revised and calculated as follows:

$$I = N_p \left(I_{ph} - I_s \left(\exp \left(\frac{V + IR_s}{V_T N_s} \right) - 1 \right) \right) - \left(\frac{V + IR_s}{R_{sh}} \right) \quad (8.8)$$

where “ N_s ” and “ N_p ” denote the cells in series and parallel, respectively; “ T ” is the ambient cell temperature; “ A ” is the Boltzmann constant; I_s and I_D are saturation and diode currents, respectively; and “ q ” is the electron charge. The step-by-step procedure to model a PV cell is given in Table 8.1.

The mathematical model developed in this section is mostly used to test the power electronic-based MPP tracker systems and understudy of solar system dynamics.

TABLE 8.1

Steps to Model a PV Cell

Step 1	Preparation of operating conversion model
Step 2	Develop NskATo product model
Step 3	Model Development for PV photocurrent (I_{ph}) evaluation
Step 4	Model development for PV reverse saturation current (I_{rs}) computation
Step 5	PV saturation current (I_s) model development
Step 6	PV output current model development
Step 7	Sub-models developed in steps 1–6 are integrated for mathematical simulation model
Step 8	Obtained final PV model

8.2.4 Modeling of a Typical Sun Tracking System

A sun-seeker system (SSS) shown in Figure 8.3 is employed to attain the sun’s energy to the highest extent. These kinds of mechanisms are required for employment like rockets and space vehicles. In SSS, the location of the PV panel is constantly adjusted to the axis of the sun. SSS can be executed either to work in an open-loop or closed-loop. The block diagram of SSS system is shown in Figure 8.4.

At the front, the regularly predefined sun’s trajectory is accompanied by it, whereas in closed-loop SSS consistently PV panel is adjusted toward the axis where the sun axis is determined toward the path of the sunrays. Most of the controller problems can be easily controlled by the PID controllers and have a simplistic design providing easy employment. Nevertheless, the determination of proper gains is continually tiresome and complicated. The

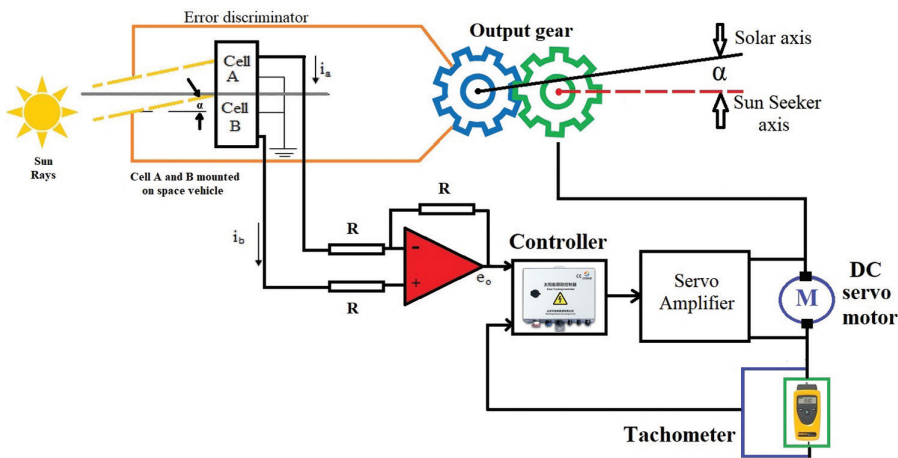


FIGURE 8.3
Schematic of SSS system.

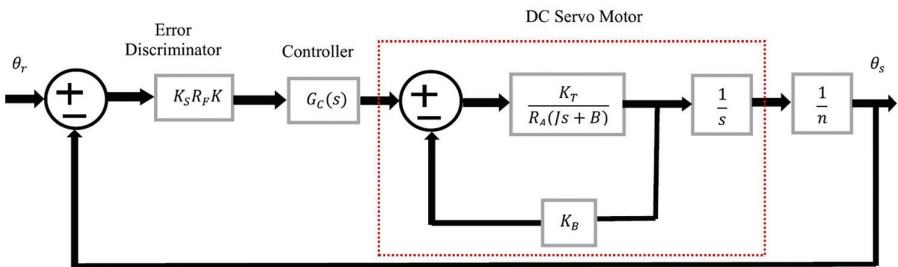


FIGURE 8.4
Block diagram representation of SSS.

functionality of the SSS can be unfavorably influenced by improper gain choice. Large artificial ingenious methods have been employed for tuning the PID controllers like Genetic Algorithm (GA), particle swarm optimization (PSO), and Teaching Learning-Based (TLB) optimization techniques. It is important to note that both PSO and GA are the standard PID parameter tuning methods, whereas Teaching Learning-Based Optimization (TLB-O) is the most advanced method to enhance the system's performance (Rawat et al., 2020).

In Figure 8.4, the controller supervises the position of the servomotor with respect to the error signal produced. The generated error signal is dependent on the variation between the sun's axis and the axis of the PV panel. Comprehensive modeling of the SSS system in practice is explained by Jha et al. (2014). The values employed for the system's parameters are given in Table 8.1 (Kuo and Farid, 2003). The open-loop transfer function (OLTF) of STS is presented in Figure 8.4 and it is described as given in eq. (8.9).

$$G_p(s) = \frac{\theta_s(s)}{\theta_r(s) - \theta_s(s)} = \frac{k_s R_F k_T K / n}{R_A J s^2 + K_T K_B S} \quad (8.9)$$

The main objective of the controller system is to reduce the error $\alpha(t) = \theta_r(s) - \theta_s(s)$, where sun's axis is the reference angle and is denoted by θ_r and angle θ_s describes the PV panel axis. A traditional PID controller is employed to reduce the variation between the sun's axis and the axis of the PV panel. The output of PID controller in expressions of error signal can be represented as in eq. (8.10) and its block diagram is shown in Figure 8.5.

$$U(s) = E(s) \left(K_p + \frac{K_I}{s} + sK_d \right) \quad (8.10)$$

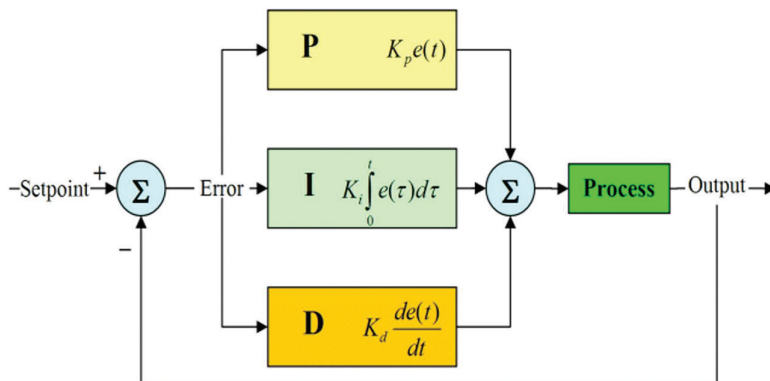


FIGURE 8.5

Block diagram representation of PID controller.

8.2.5 TLB Optimization-Based-Tuning of PID Controller

The TLB optimization method is devised by examining the impact of a teacher on the learner's performance for a given classroom (Rawat et al., 2020). This TLB method has two stages as teacher's phase and the learner's phase. The value of cost function (P) is expressed by consolidating Integral Square Error and Integral Absolute Error.

$$P = W_1 (\text{Integral Square Error}) + W_2 (\text{Integral Absolute Error}) \quad (8.11)$$

where W_1 and W_2 weights. The main objective is to reduce the objective function by choosing the proper value of design variables like K_p , K_i , and K_d in order to improve the dynamic response of the system. The flowchart for optimizing the SSS's controller gains is given in Figure 8.6.

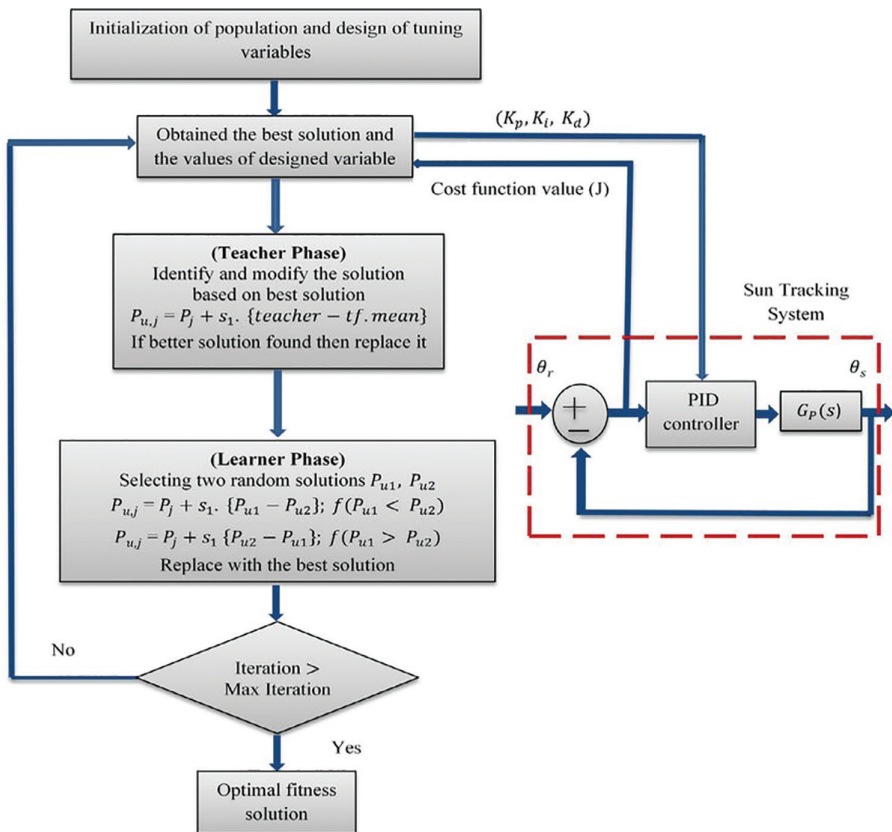


FIGURE 8.6

Flowchart for TLBO based the SSS's controller gains setting (Rawat et al., 2020).

8.3 Solar Tracker System

A solar tracking system as shown in Figure 8.7 tracks the position of the sun as it passes across the sky. When the solar PV panels are coupled with these tracking systems, the PV panels can track the pathway of the sun’s position and generate higher renewable energy output (Source: Renewable and Sustainable Energy Reviews, 2018). These tracking systems are normally joined with ground-mount PV systems; however, newly, the rooftop mounted solar trackers are emerging. Generally, the tracking devices will be attached to the set of solar panels. Hence, these panels move along with the passage of the sun. There are various configurations of solar tracking systems that are described in the following sections.

8.3.1 Components of a Solar Tracker System

The essential components of the solar PV mechanical tracking systems are drivers, tracker mount, sensors, controllers, motor, tracking algorithms, etc. (Juang and Radharaman, 2014). They are described as

- a. **Tracking mount:** It is used to hold the PV panel over which the panel is mounted at a suitable inclination.
- b. **Sensors and controllers:** They sense the related parameter values produced by the sun and the sensed measurements are further given to the controller.
- c. **Drives:** They are employed to regulate the shaft of the motor which is connected to the load.
- d. **Motor:** The motor transforms electrical energy into mechanical energy, and the controller guarantees that the accurate value of current is fed to the motor and microcontroller.
- e. **Tracker algorithm:** By using the time, date, and geographical data, these algorithms control the whole tracking system in order to attain maximum output.
- f. **Microcontroller:** It is an essential component of the tracking system. The microcontroller regulates all the actions. The PV panel is

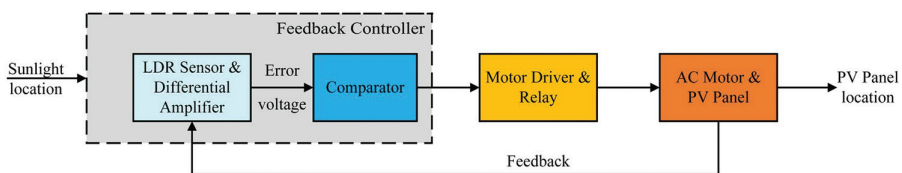


FIGURE 8.7
Block diagram of solar tracking system.

- adjusted according to sun’s position which works by an algorithm that is regulated by the microcontroller.
- g. **Relays:** Relays are employed wherever it is required to regulate a circuit by a less-power signal with total electrical separation between the controller and the regulated circuitry. The relays are employed to dc motors in the tracking system.
 - h. **Light-Dependent Resistor (LDR):** A photoresistor/LDRs/photocell is a resistor that operates on the electrical and optical phenomenon called photoconductivity in which the resistance reduces with growing incidence of the intensity of light.
 - i. **Battery:** A battery comprises electromechanical cells that deposit energy in chemical form and delivers it in the form of electricity in order to generate power.
 - j. **Battery Monitoring System:** The principal motto of the battery monitoring system is to raise the lifespan and energy storing capability of lithium polymer battery cells. In this, the continuous observation of SOC is needed. The system allows constant determination of both charging and discharging capacity of the battery.

8.4 Classification of Mechanical Tracking Systems

The mechanical solar tracking systems are majorly classified based on the (1) degree of freedom, (2) drives, (3) control strategies, and (4) tracking strategies (Seme et al., 2020) as shown in Figure 8.8.

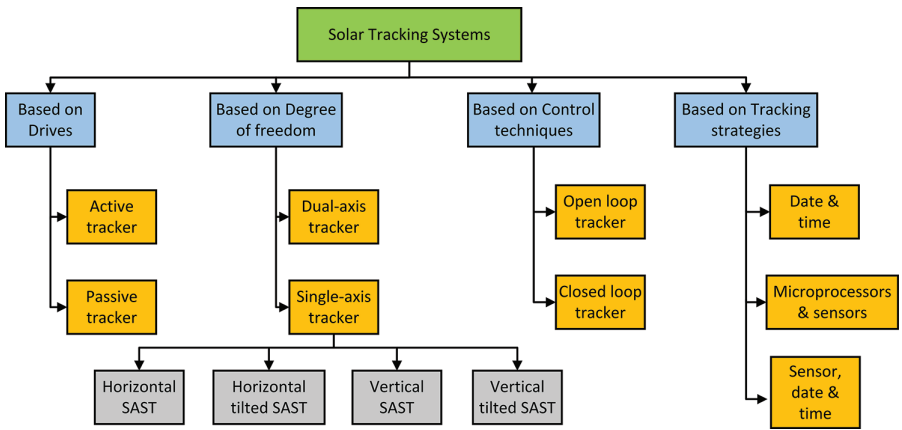


FIGURE 8.8
Classification of solar tracking systems.

8.4.1 Based on Driving Systems Employed

Based on the driving systems, the solar tracking systems are classified as follows.

8.4.1.1 Passive Solar Tracking (PST) System

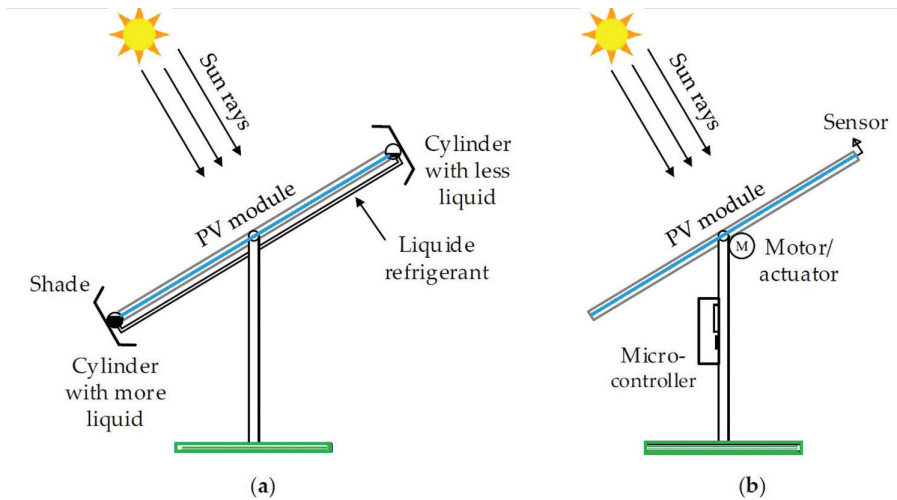
Passive solar tracking (PST) systems don't include mechanical driving systems to turn the PV panel aligning the radiation of the sun. Rather, it employs a shape-memory alloy as actuators, whereby undergoing unstable irradiation makes the PV panel experience some angular displacement to once again establish the irradiance equilibrium by causing thermal expansion in the alloys (Modified from Clifford and Eastwood, 2004). Whenever one side of liquid gas gets more heat energy compared to the other, the gas gets expanded and flows toward another side of the tracking system. It creates some unstable gravitational forces and makes the PV panel slide till a point of uniform illumination is attained. Even though it is slightly complicated and efficient, it cannot perform efficiently at lower temperature values.

8.4.1.2 Active Solar Tracking (AST) System

Active solar tracking (AST) systems employ electrical drivers plus mechanical gearing systems to face the PV panels toward the radiation of the sun. They use sensing systems, microprocessors, and motors for tracking, and further they are also accurate and effective compared to the PST systems (Hammoumi et al., 2018). However, conversely, they consume power for its operation and proper functioning. When the solar tracker is not aligned to the sun's direction, the installed sensors acquire varying illumination and generate a variation signal and are applied by a comparator in order to ascertain the suitable inclination in the proper orientation. The necessary signal is next transmitted to the motor to operate, respectively. This whole process terminates whenever the sensors get uniform illumination and PV panel is perpendicularly adjusted to the sun. AST systems are determined to enhance the performance by 40% when compared to the fixed ones. The schematic of PST and AST systems are shown in Figure 8.9a and b, respectively.

8.4.2 Based on the Degree of Freedom

It represents the total number of independent movements that can take place. Depending on this, the solar PV tracking systems are majorly categorized into single-axis solar tracking (SAST) systems and dual-axis solar tracking (DAST) systems (Mpodi et al., 2019). The various types of angles and axes that play a significant purpose in these systems are described as follows (Bhattacharjee and Bhattacharjee, 2020). In order to ascertain proper

**FIGURE 8.9**

(a) Passive solar tracking (PST) system and (b) active solar tracking (AST) system.

directions and locations, the following indices as shown in Figure 8.10 represent an important part:

- a. *Latitude*: It is the measurement of position on the surface of the earth ascertaining south or north corresponding to equator. It is estimated in angles.
- b. *Altitude angle*: It gives how distant the sun is in the sky. It is obtained by taking the angle between the horizontal axis and the line perpendicular to the sun.
- c. *Angle of incident*: It is the angle between the sun's ray incident and the line perpendicular to the surface of the plane.
- d. *Azimuth Angle*: It is azimuth angle of position of the sun.
- e. *Zenith angle*: It is the angle between the vertical axis and the sun (denoted by z).
- f. *Declination angle*: It is the angle between earth's equator and the orbit of the earth encompassing the sun and is symbolized by " δ ".
- g. *Tilt Angle*: It is the angle between the horizontal and the solar array.

Some parameters are very important and explicitly used in the calculation of the solar tracking system. Formulas for estimation of these parameters are given in Table 8.2.

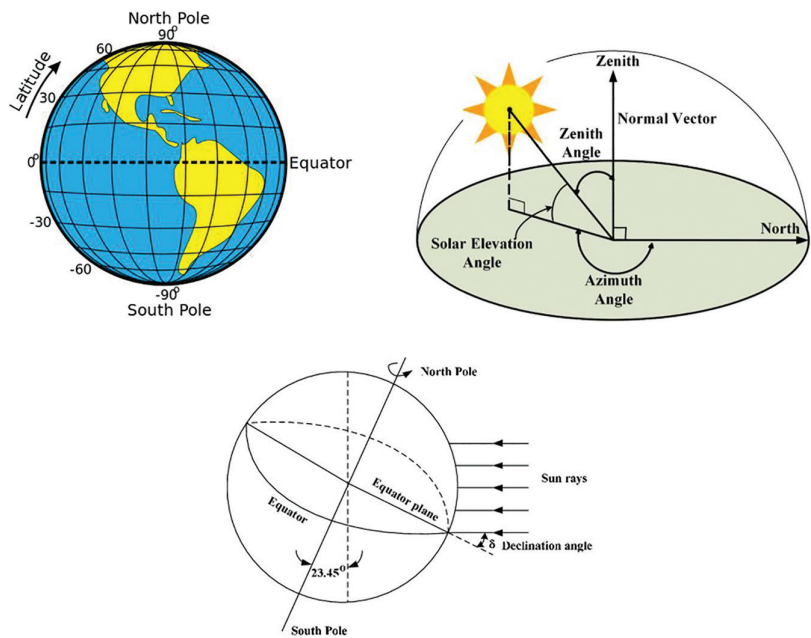


FIGURE 8.10
Description of various types of angles and axes.

TABLE 8.2

Parameters Employed to Determine the Tracking System Efficiency (Awasthi et al., 2020)

Parameter	Description	Formula
Azimuth angle	It is angle between north (estimated clockwise) about the horizon of an observer, and sun	$\gamma_s = \cos^{-1} \left[\frac{(\sin \Psi \sin \alpha) - \sin \delta}{\cos \Psi \cos \alpha} \right]$
Declination angle	It is angle between earth's equator and the orbit of earth encompassing the sun	$\delta = 23.45 \sin \left[2\pi \left(\frac{n + 284}{365} \right) \right]$
Zenith angle	It is angle between vertical and sun	$\beta = \left[\frac{\pi}{2} - \alpha \right]$
Maximum solar irradiation	It gives correlation between maximum and incident radiation	$H_n = \frac{H}{\cos \theta_z}$
Diffuse solar irradiation	Solar irradiation striking the surface of Earth	$H_n = H k_y$
Solar radiation ratio	Ratio of direct sun's irradiation to instantaneous sun's irradiation	$R_b = \frac{H_b}{H} = \frac{\cos \theta}{\cos \theta_z}$
Direct solar irradiation	Maximum irradiation is attained when the angle of incidence is zero	$H_f = H_n \cos \theta = H R_f$
Hour angle	Angular displacement of sun E/W about polar axis	$\omega = \frac{\text{minutes before noon}}{4}$
Total irradiation	Total radiation hitting the panel surface	$H_T = H_{gr} + H_s + H_{dp}$

8.4.2.1 Single-Axis Solar Tracking System

Several methods have been studied for tracking the sun's position. One of those techniques is a SAST system. SAST has one degree of freedom that functions as a rotation axis as shown in Figure 8.11a. In this, the rotation axis of the tracker system is adjusted along a geodetic North meridian (Chang, 2009). It is feasible to arrange them in all cardinal directions with sophisticated tracking algorithms. This system can track and trace the intensity of the sun to generate the highest possible power at the output irrespective of motor speed. These systems can be employed in the domestic sectors for alternative power production, particularly for noncritical and low-power apparatuses.

The various types of SAST systems are further classified as follows (Source: Sinovoltaics).

8.4.2.1.1 Horizontal SAST (HSAST) Systems

Horizontal SAST (HSAST) system revolves from east to west direction during the entire day on a single fixed axis positioned in parallel to the earth's surface. A typical HSAST is depicted in Figure 8.1a. It is commonly regarded as the cost-effective solar tracker arrangement in various PV schemes (Source: Sinovoltaics). This scheme needs fewer components for installation and its horizontal arrangement is highly favored compared to other tracking systems.

8.4.2.1.2 Horizontal Tilted SAST (HTSAST) Systems

It is quite similar to the HSAST systems which is placed at a particular angle. These are more complex than HSAST systems and are costly. These systems demand a solid base structure, appending to the cumulative system cost, and further, they are also not distinguished to be scalable.

8.4.2.1.3 Vertical SAST (VSAST) Systems

Vertical SAST systems can be installed in east/west and south /north orientation to track more movements of the sun. It is shown in Figure 8.12b. These

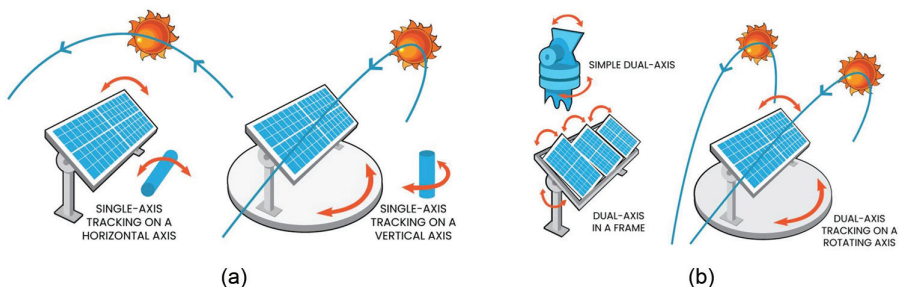
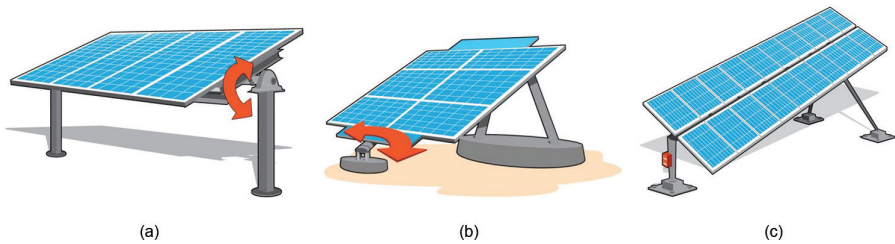


FIGURE 8.11

(a) Single-axis and (b) dual-axis solar tracking systems.

**FIGURE 8.12**

(a) Horizontal SAST, (b) vertical SAST, and (c) tilted SAST system. (Sinovoltaics.)

systems are most frequently noticed in high elevations, mountains, and those at greater latitudes.

8.4.2.1.4 Vertical-Tilted SAST (VTSAST) Systems

Vertical-Tilted SAST is very similar to HTSAST systems excluding that the tilt arranges to a parallel position and turns on the vertical axis. A tilted SAST system is shown in Figure 8.12c. These systems are more useful in generating power compared to HSAST systems. Nevertheless, their tilt is subjected to extended wind loads when compared to HSAST units. Additionally, they possess high structures and necessitate additional steel and concrete for establishing a firm basement.

Major Advantages of the SAST System:

The SAST systems hold a single degree of freedom that assists as a rotation axis, which is normally arranged along an N-S path. Some of the significant benefits of SAST systems encompass

- a. More reliability is ensured.
- b. SAST systems have a larger lifespan than DAST systems.
- c. SAST systems are more affordable than DAST systems as they hold a very manageable mechanism and works at an economical cost.
- d. These trackers are fitting for organizations with a more economical budget or frequently cloudy regions.
- e. These systems are approximately 20% effective when compared to a static solar tracking system-mounted PV panel.
- f. These systems track the sunlight from east to west, giving constant power yield the whole day.
- g. These tracker systems produce (15%–16%) higher power per year when compared to a fixed tracker system of identical capacity.
- h. SAST systems render the greatest density of PV module position per square.
- i. With SAST systems, the payback period is very less for the expense of the PV plant and yields a notable increment in savings.

Disadvantages of SAST System:

- a. Power output is lesser by SAST systems under sunshiny conditions when compared to DAST systems.
- b. It has very inadequate technological ascents.
- c. The establishment of these systems may necessitate some supplementary components and gears to append to the PV panel to the system, and they demand frequent monitoring and subsistence as well.

8.4.2.2 Dual-Axis Solar Tracking System

Dual-axis trackers track in contrast to single-axis trackers holds two degrees of freedom as shown in Figure 8.11b. They have both horizontal (east/west) and vertical (north/south) axis and hence can trace the entire position of the sun (Hafez et al., 2018). DAST systems have the ability to augment the output by properly orienting the PV array in direct sunlight for the most hours in a day. A solar panel with DAST systems produces 40% more power than the static ones; however, it costs 100% higher and holds larger maintenance expenses. Furthermore, it necessitates more complicated control systems and is more efficient than SAST systems. The parameters employed to determine the tracking system efficiency are shown in Table 8.1. DAST systems have two axes of rotation degrees, which are designated as the “primary and secondary axis.” The axis can actuate toward up or down to coordinate with sun angles during the entire day. DAST systems yield the most precise adjustment of the solar panel and are supposed to render 40% more extra output through energy consumption. Nevertheless, these systems are complicated and costly.

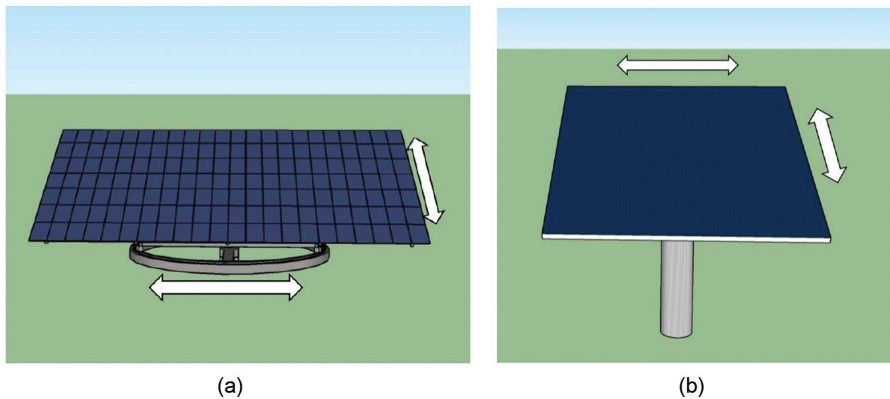
The DAST systems are employed for supplementary power gain. DAST systems are categorized as azimuth–altitude-based DAST and tip-tilt-based DASTs (TTDASTs) (Data from Hafez et al., 2018). Azimuth–altitude DAST (AADAST) systems and TTDAST are the prevalent dual-axis tracking systems exercised in different solar power applications.

8.4.2.2.1 Azimuth–Altitude DAST (AADAST) Systems

In AADAST systems as shown in Figure 8.13a, the solar collector needs to be available to revolve about altitude and azimuth axes. The azimuth axis needs to be parallel to the zenith axis, and the altitude axis (also known as the secondary tracking axis) should be constantly perpendicular to the azimuth axis and also parallel to the surface of the earth. The solar azimuth angle is the tracking angle around the azimuth axis and the solar elevation angle is the tracking angle around the altitude axis (Source: Researchgate).

8.4.2.2.2 Tip-Tilt-Based DAST (TTDAST) Systems

On the other hand, the TTDAST systems as shown in Figure 8.13b use the concept of turning the solar collector to track the rising of the sun in the east

**FIGURE 8.13**

(a) AADAST system and (b) TTDAST system (Melo et al., 2018).

and setting of the sun in the west from day to night and also adjusting the solar collector's tilting angle because of the annual variation of sun's pathway. Consequently, for the TTDAST system, one of its rotation axes is adjusted parallel with the polar axis of the earth which is directed toward the North Star. This provides it with a slope from the horizon corresponding to local latitude angle. And the other rotation axis is orthogonal to the polar axis. The tracing angle around the polar axis is identical to the hour angle of the sun and the tracing angle around the orthogonal axis is based on declination angle. With TTDAST systems, the tracking velocity is approximately consistent at 150/hour and consequently, the controller system is simple to devise.

Advantages of DAST systems

The main advantages of DAST systems include the following:

- a. Ensures 40% more power than a nonmoving or fixed PV panel
- b. Offers a greater degree of adaptability, providing greater energy yield on shining days
- c. Yields greater degree of precision in directional-pointing
- d. They necessitate less space and grant a possibility to utilize the unused space around for different supplementary purposes like car parking and cultivation.

Disadvantages of DAST systems

The major disadvantages of DAST systems include the following:

- a. Comprises many running parts that cause the system destined for the failure of devices and components.
- b. has very less lifespan and is also under reliable

- c. Undependable performance in overclouded or clouded climates.
- d. Extremely expensive. It produces 40% more power contrasted to fixed PV panels; however, it is additionally 100% more expensive.

Applications of DAST Systems:

- a. DAST systems can be employed for high and medium-scale energy generation systems.
- b. It can further be employed for energy generation in isolated areas.
- c. These are employed as residential auxiliary power systems.
- d. These are utilized in solar PV-based street lighting systems
- e. Furthermore, these are applied in solar heating and water-treatment technology-based systems.
- f. These systems continuously face the sun's path as they sway in two distinct directions. In general, the DAST systems are further categorized into altitude-based DAST systems, TTDAST systems, and azimuth–altitude-based DAST systems.
- g. Generally, DAST is employed to orientate a mirror and redirect the sun's rays along a fixed axis toward a stable receiver.
- h. These solar tracking systems trace the pathway of the sun horizontally as well as vertically and help in obtaining the highest solar power. The azimuth–altitude-based DAST systems can resolve both concerns. Notwithstanding, these systems are very costly and add approximately \$4,000–\$7,000 to the installation cost of the PV system.
- i. The functioning of DAST systems is dependent on horizontal and vertical pivots that are controller-guided related to special-purpose solar telescopes. These systems are very expensive, and their application is usually restricted to solar power systems of economic grade.
- j. The precise tracking of DAST systems is also employed in Concentrating Solar Power (CSP) technology applications, like mirrors that point to the sunlight receivers and transform the sunlight into heat.

8.4.3 Based on Control Technique

Based on the control techniques, the solar tracking systems are further categorized into open-loop solar tracking (OLST) systems and closed-loop solar tracking (OLST) systems (data from Awasthi et al. 2020).

8.4.3.1 Open-Loop Solar Tracking (OLST) Systems

In the OLST control technique, the tracker doesn't actively locate the position of the sun; however, it rather defines the sun's position for a selective locality.

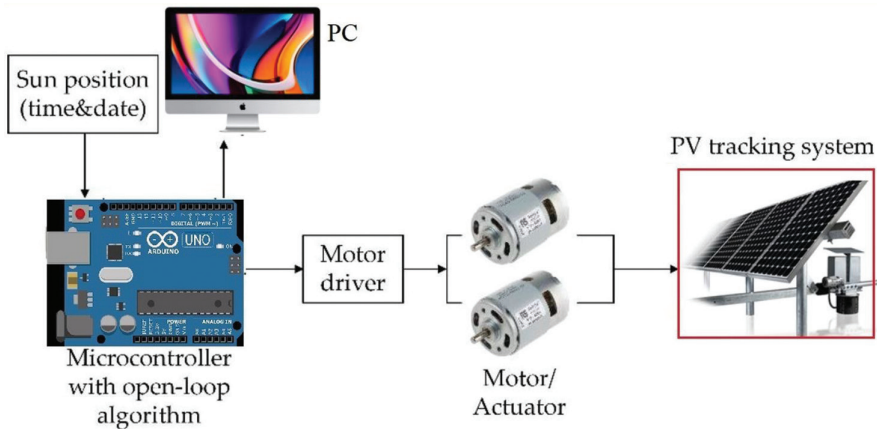


FIGURE 8.14
Open-loop solar tracking (OLST) systems.

The tracker system gets the present time, day, month, and year and later estimates the sun's position without employing any feedback. It regulates a stepper motor to trace the position of the sun without using a sensor while controlling. Hence, it is commonly termed an open-loop solar tracker system. The control strategy of the OLST system is shown in Figure 8.14.

8.4.3.2 Closed-Loop Solar Tracking (CLST) Systems

The CLST system is dependent on feedback regulation principles. In the CLST regulation approach, the position of the sun is identified during any time of the day; light sensors are employed and placed on the solar panel. Whenever the position of the sun is aligned with the PV panel precisely, there exists a variation in the intensity of light on one of the light sensors when compared to that of another sensor (Glilah et al., 2020). This variation can be applied to ascertain an inclination that the solar tracker system has to turn to be viewing the sun. The control strategy of the CLST system is shown in Figure 8.15. To discover the position of the sun, two light sensors are installed on the panel and are positioned at south and north or east and west; to sense the light intensity.

8.4.4 Based on Tracking Approaches

Based on the type of tracking approaches, the solar tracking systems are further classified (Glilah et al., 2020) as follows.

8.4.4.1 Using Date and Time

This system only employs a set of predefined algorithms that work on mathematical computations regarding the trajectory of the sun to ascertain its

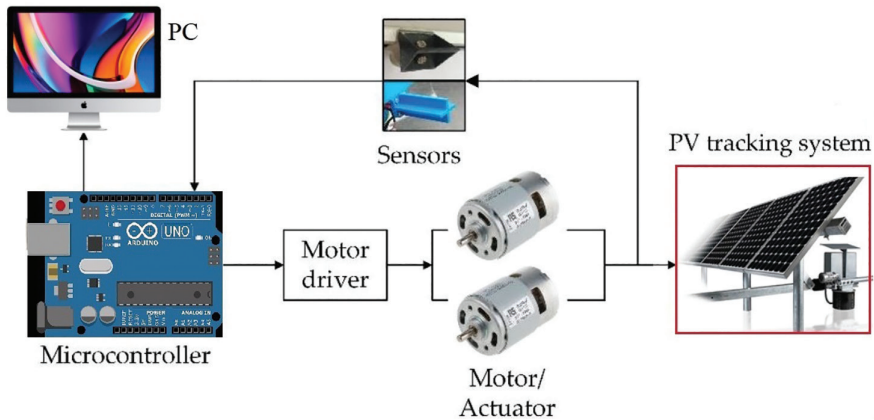


FIGURE 8.15
Closed-loop solar tracking (CLST) systems.

location at a specific time to orientate the PV array respectively. These systems don't employ any feedback or sensors for tracking. Therefore, the predefined algorithm is entirely accountable for proper functioning of system.

8.4.4.2 Employing Sensors, Date, and Time

Fundamentally, it operates on a predefined algorithm employing various sensors. They confirm the sun's position and orientate the PV array accordingly. A hybrid dual-axis tracking system employs both open-loop and closed-loop controls, which gives feedback signal in proportion to the generated power as obtained by sensors.

8.4.4.3 Employing Various Microprocessors and Electro-Optical Sensors

This tracking system includes various sensors to detect the position of the sun. Further, the signal is supplied to a microprocessor that further commands the motors or actuators for successful operation.

8.4.4.4 AI-Based Solar Tracking Systems

The solar plants have highly nonlinear behavior and are subject to perturbations (variation in the solar intensity, wind speed, humidity, and flow of air). Since they are characterized by long lifetime systems, it is expected that their parameters will be changed with that long time. For such systems, it is recommended to apply AI control techniques to control them (Chekired et al., 2011). A DAST system controlled by AI is proposed in Amelia et al. (2020) to track the sun's pathway and to hold the optimal point where maximum solar power can be obtained. This system comprises three cards, the primary

unit is acquisition/sensors card to give the data on sun’s position, the secondary unit is a regulation card in which the control algorithm is programmed which is accountable for constant controlling of the tracker’s position, and the last card is power card that functions as a mediator between regulation board and actuators. A PID algorithm is employed and subsequently, a practical inspection of the tracking system is determined in order to verify the proper regulation. However, these actuators absorb a lot of power to hold the optimal location; moreover, the data after the location shift is changed. Hence, the concept of AI is introduced by developing an algorithm based on sophisticated fuzzy logic (FL) with adaptable commands. This algorithm replaces the classical PID algorithm to regulate the passage of tracker axes and also determines the optimal location of maximum solar irradiation. This AI-based algorithm further records all the optimal locations observed throughout the day. The AI-based solar tracking system has enhanced performance where various information such as atmospheric conditions, climate, geographical characteristics, and solar radiation quantity at a given point of the earth are used.

8.4.5 Comparison of Solar Tracker Systems

An inclusive analysis of the comparison of solar tracker systems is given in Table 8.3.

8.4.6 Limitations of Solar Tracking Systems

Some of the major limitations of solar tracking systems are mentioned as follows (Chekired et al., 2011):

- a. **Cost-ineffectiveness:** When compared to fixed solar systems, the tracking systems are highly expensive. This is principally due to holding motor-driven and running parts.

TABLE 8.3
A Comparative Analysis of Different Solar Tracker Systems

Parameter	SAST System	DAST System
Degree of freedom	One degree of freedom	Two degrees of freedom
Rotation of surface	Around only one axis	Around two axes
Mechanism	Simple	Complicated
Measuring movement	Vertical	Horizontal and vertical
Efficiency	Low	High
Energy capture	20% high compared to fixed system	40% high compared to fixed system
Operating cost	Low	High
Setup cost	Cheap	Costly

- b. **Regular maintenance:** Possessing these movable and automated parts demands a periodic examination, regulations, and sometimes even replacements expected. They are not exactly “set and forget.”
- c. **Site preparation:** Every tracking system necessitates a big deal of locality preparation. Supplementary trenching for grading and wiring is needed additionally.
- d. **Financial challenges:** Funding tracking schemes are regarded as a complicated and high-risk investment from a financier’s perspective.
- e. **Environmental challenges:** Solar tracking systems are not favorable under wintry climates and are solely suited in sunny environments. On contrary, fixed solar systems are weather favorable than tracker systems.
- f. **Compatibility issues:** Fixed tracker systems are field-cooperative systems that can hold up to 20% slopes in the east/west direction. Whereas the tracker systems generally exhibit more limited slope accommodation around 10% in the north/south direction.

8.5 Conclusions

Solar energy is an abundant source of green energy which is mostly used in the form of electrical energy. In every 15 minutes, the sun’s position at a place on the earth changes about ten times due to its axial and orbital motion; hence, the solar radiation varies throughout the day. SPV panel output varies as it has different efficiency at different solar radiations. The overall efficiency of the SPV system can be enhanced by optimizing the tilt angle of the PV panels according to the sun’s position. PV panels are relatively expensive for power production in comparison to conventional power methods. Therefore, optimizing it to increase its production through auxiliary systems such as solar tracking systems and power electronics-based MPP tracking techniques is always encouraged. In this chapter, various solar tracking technologies to track the sun’s position are studied for harnessing green energy. A solar panel model and a typical sun tracking system model have been given for the basic understanding. As per the available research, AI-based solar tracking systems are the best way to efficiently track the sun’s path and enhance the performance of PV panels. Today cascaded control algorithms are used to track the sun movement with error of 1’ (1 minute). These solar tracking systems have rotating components, complex design, and control mechanism and also demand system maintenance.

References

- <https://iea-pvps.org/snapshot-reports/snapshot-2020/>.
- <https://sinovoltaics.com/learning-center/csp/hsat-trackers/>.
- <https://www.sciencedirect.com/topics/engineering/solar-tracking-system>.
- Amelia, A.R., Irwan, Y.M., Safwati, I., Leow, W.Z., Mat, M.H., Rahim, M.S.A. (2020). Technologies of solar tracking systems: A review, *IOP Conference Series: Materials Science and Engineering*, vol. 767, p. 012052.
- Awachie, L. (2003). *Solar Energy in Progress and Future Research Trends*. USA Addison Wesley Publishing, Boston, MA.
- Awasthi, A., Shukla, A.K., Manohar S.R.M., Dondariya, C., Shukla, K.N., Porwal, D., Richhariya, G. (2020). Review on sun tracking technology in solar PV system, *Energy Reports*, vol. 6, pp. 392–405.
- Bhattacharjee, R., Bhattacharjee, S. (2020). Performance of inclined heliostat solar field with solar geometrical factors, *Energy Sources, Part A: Recovery, Utilization, and Environmental Effects*. doi: 10.1080/15567036.2020.1784318.
- Canberra, S. (2004). Design of a traditional solar tracking system. In *AIP Conference Proceedings*, pp. 151–158.
- Chang, T.P. (2009). Output energy of a photovoltaic module mounted on a single-axis tracking system, *Applied Energy*, vol. 86, Issue 10, pp. 2071–2078.
- Chekired, F., Larbes, C., Rekioua, D., Haddad, F. (2011). Implementation of a MPPT fuzzy controller of photovoltaic systems on FPGA circuit, *Energy Procedia*, vol. 6, pp. 541–549.
- Clifford, M.J., Eastwood, D. (2004). Design of a novel passive solar tracker, *Solar Energy*, vol. 77, Issue 3, 2004, pp. 269–280. ISSN 0038-092X. doi: 10.1016/j.solener.2004.06.009.
- Glilah, I., Baraka, I.H., Amami, B. (2020). Introduce artificial intelligence in controlling a solar tracker. In: Ezziyyani, M. (ed.) *Advanced Intelligent Systems for Sustainable Development (AI2SD' 2019)*. Lecture Notes in Electrical Engineering, vol. 624. Springer, Cham. doi: 10.1007/978-3-030-36475-5_14.
- Hafez, A.Z., Yousef, A.M., Harag, N.M. (2018). Solar tracking systems: Technologies and trackers drive types – A review, *Renewable and Sustainable Energy Reviews*, vol. 91, pp. 754–782.
- Hammoumi, A.E., Motahhir, S., Ghzizal A.E., Chalh, A., Derouich, A. (2018). A simple and low-cost active dual-axis solar tracker, *Energy Science & Engineering*, vol. 6, pp. 607–620.
- ILO, F.U., Onoh, G.N., Eke, J. (2014). An artificial intelligent based solar tracking system for improving the power output of a solar cell, *International Journal of Engineering Research & Technology (IJERT)*, vol. 3, Issue 11, pp. 1203–1207.
- Jha, S.K., Yadav, A.K., Prerna, G., Parthasarathy, H., Gupta, J.R.P. (2014). Robust and optimal control analysis of sun seeker system. *Journal of Control Engineering and Applied Informatics*, vol. 16, Issue 1, pp. 70–79.
- Juang, J., Radharamanan, R. (2014). Design of a solar tracking system for renewable energy. In *Proceedings of the 2014 Zone 1 Conference of the American Society for Engineering Education*, pp. 1–8, doi: 10.1109/ASEEZone1.2014.6820643.
- Kuo, B.C., Farid, G. (2003). *Automatic Control System*, 8th ed. John Wiley and Sons (Asia) Pte Ltd, Singapore.

- Melo, K.B.D., Paula, B.H.K.D., Silva, M.K.D., Siqueira, T.G., Villalva, M.G. (2018). A study on the influence of locality in the viability of solar tracker systems. In *XXII Congresso Brasileiro de Automatica*, 2018.
- Mousazadeh, H., Keyhani, A., Javadi, A., Mobli, H., Abrinia, K., Sharifi, A. (2009). A review of principle and sun-tracking methods for maximizing solar systems output, *Renewable and Sustainable Energy Reviews*, vol. 13, Issue 8, pp. 1800–1818.
- Mpodi, E.K., Tjiparuro, Z., Matsebe, O. (2019). Review of dual axis solar tracking and development of its functional model, *Procedia Manufacturing*, vol. 35, pp. 580–588.
- Racharla, S., Rajan, K. (2017). Solar tracking system – a review, *International Journal of Sustainable Engineering*, vol. 10, Issue 2, pp. 72–81. doi: 10.1080/19397038.2016.1267816.
- Rawat, A., Jha, S.K., Kumar, B. (2020). Position controlling of sun tracking system using optimization technique, *Energy Reports*, vol. 6, Issue Supplement 2, pp. 304–309.
- Seme, S., Stumberger, B., Hadziselimovic, M., Sredensek, K. (2020). Solar photovoltaic tracking systems for electricity generation: A review. *Energies*, vol. 13, p. 4224.
- Suugur, B. (2007). A modified tracking algorithm for maximum power tracking of solar array. *Energy Conservation and Management*, vol. 45, pp. 911–925.
- Vinod, Kumar, R., Singh, S.K. (2018). Solar photovoltaic modeling and simulation: As a renewable energy solution, *Energy Reports*, vol. 4, pp. 701–712.
- Yatimi, H., Aroudam, E. (2018). MPPT algorithms based modeling and control for photovoltaic system under variable climatic conditions, *Procedia Manufacturing*, vol. 22, pp. 757–764.

9

Development of Solar Panel Models in Different Countries/Regions

Isa S. Qamber

University of Bahrain

CONTENTS

9.1 Introduction: Background	213
9.2 Literature Review.....	214
9.3 Proposed Developed Model and Methodology	220
9.4 Results and Discussion	224
9.5 Conclusion	228
Acknowledgment.....	228
References.....	228

9.1 Introduction: Background

Photovoltaic (PV) devices produce electricity directly from the sunlight through an electronic process that happens naturally. At the present time, photovoltaic devices have become the new objective of the energy sector that needs to be integrated into the electric grid for both distribution and transmission of power through electric systems. In these devices, the solar energy is captured and converted to electrical energy by transferring it through an electrical circuit, and then the electricity is sent to a grid.. In the next step, the DC output obtained from the solar panels is converted to alternating current (AC) before using in home or stepping down to the distribution grid. The standard PV panel capacity is calculated in direct current (DC), and watts is the unit of measure for power.

In 1839, Alexandre Edmund Becquerel discovered the PV effect which was the then topic of scientific inquiry. In 1954, Bell Labs introduced the first solar PV device that generated a useable amount of electricity. In 1958, solar cells were used in different small-scale commercial and scientific applications. In the 1970s, the major interest of using solar cells to produce electricity in both business and homes started. Then, the PV industry started to develop panels

increasingly which resulted in decrease of their cost. Thus, the price of producing solar power is also reduced simultaneously. This fall in price reached approximately 59% within a decade. The reason behind this drop might be that the industry has scaled up manufacturing by improving the PV technology with new types of materials. Moreover, the installation costs have also become less because of the availability of trained installers.

In the present time, the solar power has become an energy source that depends on the sunlight to generate electrical power. A question may arise in the reader's mind about the meaning of PV. The PV means that the panels can convert sunlight into electricity. The solar PV panels are comprised of many small PV cells. The DC electric current generated by the solar panel starts to flow through a series of wires to an inverter. It is well known that the function of the inverter is to convert the electricity from its DC form to AC form. The DC electricity should be converted to AC form because the equipment used in buildings needs AC electricity for functioning. The inverter transports the AC electricity to the electric panel known as breaker box. Then, the breaker box distributes the electricity throughout the building as needed. At this stage, the electricity is readily available to electrical devices such as lights and other appliances. It should be known that any electricity not consumed via the breaker box is sent to the utility grid through the utility meter. It is well known that there is a utility meter that measures the flow of electricity from the grid to your appliances and vice versa.

9.2 Literature Review

Converting the energy from the sunlight into electric power by the photovoltaic (PV) technologies is helping to get a clean energy away from pollution. There are several studies carried out on PV. In the present section, some of these studies are summarized.

Based on the results calculated by Qamber [1], the curve fitting is applied to form a suitable formula. Using a developed Adaptive Neuro-Fuzzy Inference System (ANFIS) method, Qamber [1] deals with the required design. The model developed in the study is formulated as a function of the number of units consumed per day in the Gulf Cooperation Council (GCC) region. It is well known that the GCC region has high consumption of energy influenced by several factors. The solar energy is helping to reduce the use of fossil fuels in the GCC countries to generate power. In conclusion, the results obtained encourage the GCC countries to use the solar energy through developments in the energy field. This means that their future vision is to increase the use of solar energy for power production. Also, the novelty of the study is to avoid using the gas to increase generation capacity. Furthermore, the model developed will help the economic development of the GCC countries.

The solar market nowadays has grown as demonstrated by Sheeja et al. [2]. This is carried out by installation of photovoltaic plants. Sheeja et al. [2] target a clean and efficient renewable energy generation that can produce uninterrupted flow of electricity. In their study, the focus was on two aspects: generating the electricity through solar energy, and establishing wireless communications to monitor the solar power inverter.

In their book chapter, Qamber and Al-Hamad [3] highlight some countries that have their own vision to direct their energy sector toward the renewable energy. The renewable energy is known as clean energy. This type of energy will help avoid the ill effects of global warming. The solar energy improves the sustainability levels of a country's energy sectors. The resources (VER) currently envisioned to be new energy resources are wind and solar powers. The PV generation is highly dependent on weather conditions. Factors that influence this type of energy generation differ in different regions. In their study, Qamber and Al-Hamad [3] used the artificial intelligence technique to estimate the required number of solar power panels to satisfy the estimated daily electric demand. This artificial intelligence technique plays an important role in modeling the renewable energy. At the same time, the main objective is to design a PV panel that helps reduce CO₂ emission. These panels are connected to a grid which is fed by the extra electricity generated through the solar power plant. Furthermore, the modeling and prediction help estimate the required estimated load in the future.

Moosa and Kazem [4] in their study concentrated on the central renewable energy resources in the GCC countries where more concentration will be in Oman. The study reported on both the solar and wind energy. In addition, it is mentioned that GCC countries, particularly Oman, receive high solar energy: 2.5–3.0 Wh/m²/day during the winter season and 5.5–6.0 Wh/m²/day in summer. In addition, in their study it was found that the GCC countries should look upon the future of renewable energy resources. Accommodating all future challenges are required in the coming future.

El idrissi et al. [5], in their research, suggest a maximum power point tracking (MPPT) method for a photovoltaic pumping system. This suggestion is based on a nonlinear robust method combining the backstepping and the sliding mode techniques. The system's power circuit comprises a solar panel, a step-up converter, and a DC motor feeding a water pump. The system can predict the desired optimal voltage quickly by using the Artificial Neural Network. In addition, the system's asymptotic stability is proven by Lyapunov's functions. It should be noted that the proposed method is compared with the hybrid technique.

Qamber and Al-Hamad [6], in their research, highlighted the need of solar energy to be connected to the grid. The GCC countries are located in a perfect place to receive high solar energy. Qamber and Al-Hamad [6], in their study, derived the model's design of solar cell under the same house specifications. The Panel Generation Factor (PGF) was considered in the research to satisfy the specification of the cells, where the specifications depend on the climate.

For the considered countries, the total capacity (in kWp) and number of PV panels needed for designing a 110 Wp PV module based on Solar Charge Controller Rating and PGF of each country are estimated.

Rufangura and Sabah [7], in their study, concentrated on the solar energy, which is one of the best sustainable energy resources, and considered a solar photovoltaic technology. This type of energy is used to generate electricity from solar radiation. The solar cell is one of the technologies that benefits from the metamaterial (MTM) technology, where an MTM serves as a perfect absorber in solar cells. The MTM technology improves the level of absorption. This design helps achieve approximately 99.94% absorption with a bandwidth of 23.4% in the visible spectrum.

Subashini and Ramaswamy [8], in their study, concentrated on solar PV which appears to be a vital source of renewable energy. They developed methods to improve the performance of a solar PV. Due to variation of irradiation supplied to the solar PV system, there is a fluctuation in generation of electricity and thus in the current fed to the converter. The outcome results exposed the behavior of the system through discrete time domain waveforms, phase portraits, and bifurcation diagrams. These outcomes help improve the efficacy of the study system.

Ajith et al. [9], in their article, present the designing and modeling of a Single-Ended Primary Inductance Converter (SEPIC) which is a DC-DC converter for photovoltaic applications. This SEPIC is a type of solar panel output. The designed panel varies with respect to solar radiation. In addition, this type of panel will have less radiation and does not meet the requirements of the load. For this reason, the authors [9] propose the SEPIC which helps as a step-up or step-down transformer to boost the voltage based on the level of solar radiation. At the same time, it acts as an impedance matcher and regulator between the source and the load. The effectiveness of the proposed system is shown in simulation using a MATLAB®/Simulink® environment, where the practical system was tested up to 15V solar panel, 12V lead acid battery 24V SEPIC converter module, and 230V inverter.

Qamber and Al-Hamad [10], in their study, considered renewable energy in both Bahrain and UK. Renewable energy provides many benefits to our environment, health, and economy. PV has become a new competitive technology for harnessing energy from renewable resources. Qamber and Al-Hamad considered the design of solar cells for both countries with the same considered specifications. The PGF is considered to satisfy the specifications of the cells. For both countries, the total capacity (in kWp) and number of PV panels needed for designing a 110 Wp PV module based on Solar Charge Controller Rating and PGF of each country were estimated.

The use of photovoltaic (PV) panels has already penetrated into the distribution system. Alboaouh [11] considered the rapid fluctuation of irradiance during the day. He also considered the bi-directional power flow in the distribution network. In addition, he proposed a control scheme to optimize PV output power. The design is optimized for the PV considering minimization

of power losses. The proposed model considers the uncertainty associated with irradiance and load demand. The proposed scheme was tested on the IEEE123 bus system.

Goyani and Patel [12], in their research, highlighted the renewable energy resources which are best to stand against the increasing risk of global warming. In their research, the wind energy conversion system two masse drive train-based wind turbine with zero pitch angles drives Doubly Fed Induction Generator (DFIG). Using the MATLAB simulation, a model of hybrid wind and PV system was developed.

Ma et al. [13], in their research, found that one of the possible solutions of renewable energy is the energy storage technology. In their research, a large-scale energy storage system that supports the power system and system frequency regulation was discussed. They present a new PV energy storage-coordinated dispatching method. The proposed system is helpful in reducing PV curtailment. In addition, the proposed system was validated based on the time-series production simulation. The results obtained indicate that the proposed method can effectively decrease the curtailment of solar power and help achieve the future vision. This vision is concentrated on large-scale solar power coordinated with energy storage system.

The solar panel installations are on the rise on Australian rooftops. Al-Saadi et al. [14], in their research, talked about such a phenomenon, where the distribution network operators and results by grid-connected solar panels were considered. In addition, the present study [14] presents a new model to estimate the total radiation incident on a sloped solar panel. The obtained model depends on the clearness index with a special concentration being paid for Australia, and the assessment of the model validity is achieved. In addition, high-resolution data of solar irradiations were adopted for the assessment.

Al-Hamad and Qamber [15], in their study, concentrated on the photovoltaic (PV) which became the new competitive technology for using energy resources of the planet. The objective of this study is to reduce the flow of load by approximately 20% using both distribution and transmission equipment. Many projects started to be organized to achieve maximum benefits in the power network. It is well known that the utilization of solar energy is an opportunity to create a sustainable energy resource for the GCC and many other regions. Therefore, the target of Al-Hamad and Qamber is to engage the PV technology to lower the load of equipment.

In PV system, different MPPT methods are used to obtain maximum power. Hassan et al. [16], in their article, provide an artificial intelligence-based fuzzy logic MPPT modeling. In addition, the model controls the PV system in a grid-connected hybrid power system under different weather patterns. Seven fuzzy sets are used with seven linguistic variables applied to a DC-DC converter. The system operates through the classical logic power management switching algorithm. The proposed method used the MATLAB simulation, where the results show better behavior in terms of load tracking and reliability.

Nowadays, solar energy is considered one of the principle renewable energy sources for generation of electric power. Gupta and Chauhan [17], in their study, highlighted the single-diode photovoltaic (PV) system and double-/bypass-diode PV system. These are designed in the MATLAB/Simulink environment based on their mathematical modeling. The design is valid on the commercial basis of available solar panels. Their study includes the effect of climatic conditions, wind speed, temperature, humidity level, and dust accumulation in the modeling of PV systems.

Al Badwawi et al. [18], in their research, integrated two types of renewable resources, namely, solar PV and wind energy, into an optimum combination. The impact of the variable nature of both solar and wind resources can be partially resolved, where the overall system becomes more reliable and economical to run. In the article, a review of challenges and opportunities/solutions of hybrid solar PV and wind energy integration systems are clarified and discussed. Voltage and frequency fluctuation, and harmonics can be resolved to a large extent by having a proper design and advanced fast-response control facilities. In addition, they can be considered as good optimization of hybrid systems. The study gives a review of the main research work reported in the literature and the state of the art of both grid-connected and stand-alone hybrid solar and wind systems.

Sharma et al. [19], in their study, proposed a solar PV array system. This system was proposed with and without grid connection. The MPPT algorithm was followed for extracting maximum available power from PV module. Two modes of operating control were followed: the unit-power control (UPC) and feeder-flow control (FFC) modes. In the UPC mode, the load variations are compensated by the main grid. In the FFC mode, the feeder flow is regulated to a constant. The main purpose of the operating strategy presented in their study was to find the control mode. In addition, the purpose was to minimize the number of mode changes, operate PV at the maximum power point.

Mengi and Altas [20], in their article, highlight the intelligent energy management system (IEMS). Their study concentrates on the maintenance of energy sustainability in renewable energy systems (RES). Mengi and Altas [20] their study consists of wind and photovoltaic (PV) solar panels which is established and used to test the proposed IEMS. The power generated by RES is collected on a common DC bus. This collection is considered as a renewable green power pool which can be used for supplying power to loads. In addition, the power requirement is supplied from either wind or PV or both. The decision about operating these systems is given by an IEMS with fuzzy logic decision maker [20].

El-Fergany [21], in his article, proposes an efficient tool to characterize the PV generating systems to define the parameters for commercial real PV cells, where the proposed tool is coupled with the mine blast algorithm. The objective of the study is to minimize the absolute errors between the experimental measurements and the calculated current values. The purpose of minimization of the absolute error is to find the accuracy of estimation for the targeted

photovoltaic parameters. Both single- and double-diode models of solar cells are targeted to certify the performance of the methodology used and proposed in the study [21]. Both calculated I-V and P-V characteristics are matching the measurement of the data, where the measurement will reach the insignificant absolute errors. In conclusion, the study finds that the single-diode equivalent circuit is adequate to exactly model the photovoltaic cells.

Almasoud and Gandayh [22], in their research, highlighted the continuing rise of electricity demand in Saudi Arabia. This rise demands power generation to be expanded. They tried to find an alternative way of generation to avoid environmental pollution and negative impacts on human health due to greenhouse gas emissions. Saudi Arabia is geographically suitable for solar power generation because it is in the Sun Belt. This has led the country to become one of the largest solar energy producers. Therefore, the solar energy is a good alternative to generate electricity without pollution. At the same time, harnessing solar energy via PV cells is considered as one of the methods to generate clean energy. Their study [22] proves that the cost of solar energy will be less than the cost of fossil fuel energy when the cost of the environmental and health damages is considered.

Eltawil and ElSbaay [23], in their research, concentrated on the solar photovoltaic (PV) pumping water to aeration of aquaculture in the reservoirs. In addition, the economic point of view and the effect of pump discharges on standard oxygen transfer rate are taken into consideration with standard aeration efficiency. The daily averages of PV energy output, PV efficiency, and load energy were investigated.

Bhoye and Sharma [24], in their research, utilized reasonably green energy such as PV. In their research, they concentrated on the sustainable development which is one of the most important challenging issues. They also aimed to build a suitable environmentally friendly PV power plant. In addition, they studied the way how to establish photovoltaic solar power plant design. Also, they calculated the power production to establish the green and sustainable development of solar PV power plant. This will help reduce the burden of state electricity boards.

Barua [25] highlights the power demand in industry and domestic areas which is sharply increasing day by day and results in the growing emission of harmful gases by diesel generators. In India, most of the power generation is based on coal. It is well known that this type of fuel emits lots of carbon dioxide. The carbon dioxide as a gas is one of the major sources of various environmental problems. Barua's [25] study discussed the power sharing by the solar photovoltaic (PV) panel of a microgrid and discussed the power quality of the system.

Mallika and Saravanakumar [26], in their research, presented a method based on the genetic algorithm. The presented method is used to perform a constrained tuning technique for the Proportional Integral Derivative parameters to optimize the power output of solar panel. Out of the study and as a dynamic model, the model is used to design the controller parameters

of the conventional proportional-integral-derivative (PID) controller. In the same way, the dynamics of the DC-to-DC converter is nonlinear. Therefore, it is hard to derive desirable performance. The genetic algorithm is used to optimize the control parameters of boost converter.

Bhakre et al. [27], in their study, discussed different designs of solar thermal absorber collectors and their development from the cooling system of PV panels point of view.

Wu et al. [28], in their study, set up an experimental platform of PV panel under linear light source and windy conditions. This setting was carried out in the laboratory. The experiments were performed on temperature distribution, convective heat dissipation, and output performance of PV panel.

Tripathi et al. [29], in their study, considered the effects of humidity on the solar radiation, output power of the panel, and the panel surface temperature. The increase of water droplets in the environment helps cool the panel surface temperature. The study [29] concluded that the humidity plays a two-fold role in the PV panel operation.

Protopapa et al. [30], in their research, investigated vibrational spectroscopy. They found that the vibrational spectroscopy is a suitable tool, where it recognized the structure and composition of the PVs in a rapid and cost-effective way.

The variable-speed wind energy conversion system (WECS) requires a power conversion unit to supply the rotor with a variable frequency voltage. This will keep the stator frequency constant irrespective of the wind speed through the study carried out by Manavalan [27], where the induction generator will be fed by rotor of a doubly and driven by a wind turbine which need rotor excitation. Therefore, the stator can supply a load or feed the grid. A set of photovoltaic (PV) panels depending on the availability of the solar power. In addition, the neutral point clamped multi-level inverter is applied to convert the rectified voltage from PV panels to a variable frequency voltage to supply the rotor.

9.3 Proposed Developed Model and Methodology

The combination of both fuzzy logic and Neural Networks will result in a neuro-fuzzy system which has a better advantage. The combination system will result in ANFIS, and the training of data will help obtain a better result. In addition, the input data is converted to a fuzzy value, where the output becomes the considered system model and finally the model estimated values are found. It should be noted that the process of defuzzification technique is an output set which should be mapped to a crisped value. At the same time, the present multi-layer study is applied as a rule-based neural

network structure. Therefore, to reduce the neuro-fuzzy weight, a vector update is needed:

$$w^x = \frac{w_r}{\sum_{i=0}^m w_i} \quad (9.1)$$

where w^x is the firing strength of fuzzy rules, w_i is the i th weight space, and w_r is the weight vector.

Newton's algorithm is used to find the size and direction of a step instead of weight space. The purpose of the size of step and direction at the weight space is to discover the cost function $J_N(\cdot)$ toward its minimum.

Using both Taylor's expansion and the cost function will find the approximation by the quadratic function:

$$J_N(w + \Delta w) = J_N(w) + \Delta w \frac{dJ_N(w)}{dw} + \frac{1}{2} \Delta w^T \frac{d^2 J_N(w)}{dw^2} \Delta w \quad (9.2)$$

Therefore, the updated weight vector is Δw which belongs to the weight vector w and T is defined as transpose. The $J_N(w)$ is the cost function which is a function of weight. The $J_N(w + \Delta w)$ is the cost function which is a function of updated weight vector Δw . Δw^T is the transpose of the updated weight vector. In addition, $\frac{dJ_N(w)}{dw}$ is the first derivative of the cost function and $\frac{d^2 J_N(w)}{dw^2}$ is the second derivative of the cost function.

Therefore, the updated weight vector Δw belongs to the weight vector w and T is defined as transpose. Finding the differentiation of eq. (9.2) and setting it to zero obtain the following results and minimize the equation:

$$\frac{dJ_N(w)}{dw} = \frac{d^2 J_N(w)}{dw^2} \Delta w \quad (9.3)$$

$$g = -H \cdot \Delta w \quad (9.4)$$

where

g is the gradient of $J_N(w_k)$,

H is the Hessian of $J_N(w_k)$.

The conjugate gradient algorithm illustrated in Figure 9.1 is truncated to find Newton's equation.

Both gradient and Hessian are needed for the cost function $J_N(w_k)$. The first and second derivatives of the cost function $J_N(w_k)$ are obtained:

$$\frac{\partial J_N(w)}{\partial w_p} = \frac{1}{N} \sum_{k=1}^N 2 \frac{\partial \hat{y}(w(k), w)}{\partial w_p} [y(k) - \hat{y}(w(k), w)] \quad (9.5)$$

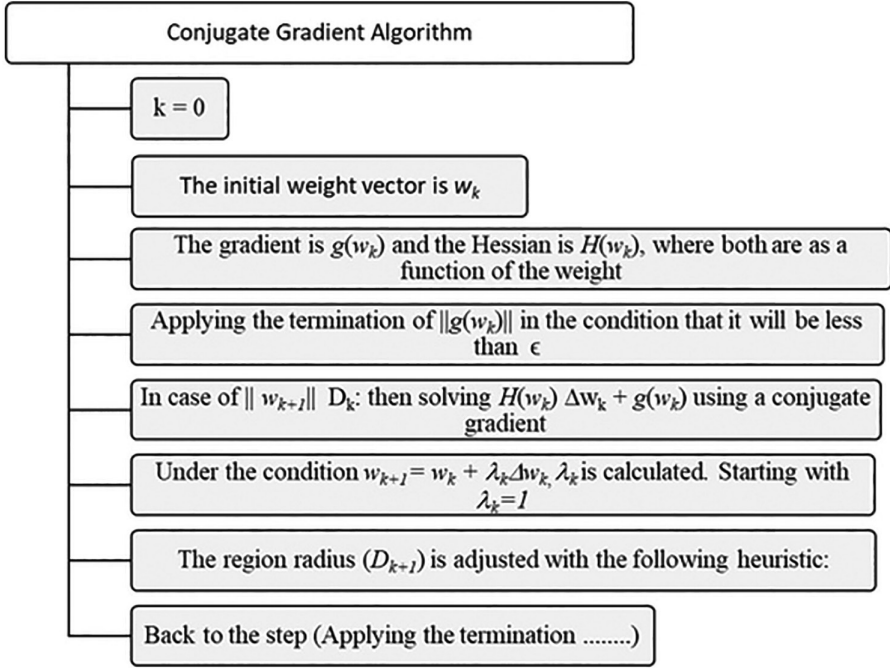


FIGURE 9.1

Conjugate gradient algorithm illustration.

where $\frac{\partial J_N(w)}{\partial w_p}$ is the first derivative of the cost function and $\frac{\partial \hat{y}(w(k), w)}{\partial w_p}$ is the first vector derivative of the cost function. In addition, $y(k)$ is the cost function and $\hat{y}(w(k), w)$ is the cost function vector.

$$\frac{\partial^2 J_N(w)}{\partial w_p \partial w_q} = \frac{1}{N} \sum_{k=1}^N 2 \frac{\partial \hat{y}(w(k), w)}{\partial w_p} [y(k) - \hat{y}(w(k), w)] \quad (9.6)$$

The gradient of the model output is obtained with respect to the weights:

$$\frac{\partial \hat{y}(x, w)}{\partial w_p} = \left\{ \begin{array}{c} \mu_{A^i}^u \\ \left[\prod_{u=1, u \neq k}^U \sum_{i=1}^{P_u} \mu_{A^i}^u w_i^u \right] \mu_{A^j}^k \end{array} \right\} \quad (9.7)$$

$$\frac{\partial^2 \hat{y}(x, w)}{\partial w_p \partial w_q} = \left\{ \left[\prod_{u=1, u \neq m \neq k}^U \sum_{i=1}^{P_u} \mu_{A^i}^u w_i^u \right] \mu_{A^j}^k \mu_{A^1}^m \right\} \quad (9.8)$$

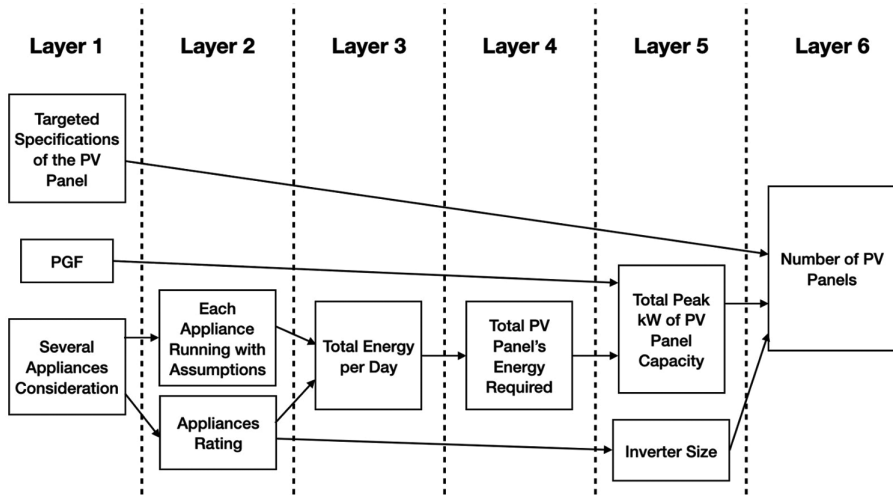


FIGURE 9.2
Developed ANFIS model.

where

w_p refers to the i th weight of the u th tensor model.

w_p refers to the j th weight of the k th tensor model.

$\mu_{A_i}^u$ on the input vector x_i has been dropped to reduce the notation.

In the present study, the ANFIS is followed and the Artificial Neural Network (ANN) is applied. This results in a developed ANFIS model which is shown in Figure 9.2. The number of PV panels is controlled by the ANFIS, where three inputs are cleared through the first layer. The first layer defines the several appliances considered, PGF, and the targeted specifications of the PV panel. The second layer is concentrates on each appliance running with assumptions and the considered appliances rating by the researcher. The third layer is becoming a continuity and the result of the second layer which is the total energy per day for the presented and considered system. The fourth layer is the output of the third layer which is the total energy of PV panels required and targeted. The fourth layer, first layer PGF will result in the fifth layer which is the total peak kW of the PV panel capacity. This is formed in the following equation:

$$\text{Total Peak kW of PV Panel Capacity} = \frac{\text{Total Peak kW Panel Capacity Required}}{\text{PGF}} \quad (9.9)$$

In addition, the inverter size is becoming an output of the second layer from the appliances rating:

$$\text{Inverter Size} = \text{Total number of Units per Day} \times 1.3 \quad (9.10)$$

The result of the present study is illustrated and presented in the following equation:

$$\text{Number of PV Panels Required} = \frac{\text{Total Peak kW of PV Panel Capacity Required} \times 1000}{110} \quad (9.11)$$

This is represented in the sixth layer as the output of the first and fifth layers (inverter size) as a second input in the fifth layer. The total peak kW of PV panel capacity is considered in the calculation of the number of PV panels required. This layer as the sixth one is the required output, and it is the targeted in the present study.

The GCC region is taken as an example to show the training data of the present study. Since the first layer is defined as the several appliances considered, the PGF of the region is 5.84. The second layer concentrates on the appliances running with assumptions and considered as 20.028 kW. The third layer is a continuity and result of the second layer which is the total energy of 407.51 kWhr/day. The fourth layer is the output of the third layer which is the total energy of PV panels required 529.763 kWhr/day. The sixth layer is the output of the first layer, and the fifth layer (Inverter size = 105.872 kW) is the second input in the fifth layer. The total peak kW of PV panel capacity (90.713 kW_p) is considered in the calculation of the number of PV panels required which is equal to 880 PV panels and is the targeted value in the present study.

In a PV solar system, the sunlight hits a solar panel to produce electricity. The usage of the solar energy in the living community has many benefits. The most important benefit is its renewable nature. In some regions such as GCC, the solar energy is available throughout the year. The solar energy is a better alternative to fossil fuels such as oil, coal, and natural gas. The latter can pollute environment by emitting dangerous toxins. In addition, the solar energy reduces a consumer's energy bills.

9.4 Results and Discussion

In the present study solar energy has been shown as an option to generate electricity. The rooftop PV system is considered as a small-scale solar power generation plant. This system can be fixed on the free roof surface of residential or commercial buildings. In addition, the system is connected to the main building of electric power system.

TABLE 9.1
PGF and the Number of PV Panels Results for Different Countries/Regions

Country/Region	PGF	No. of PV Panels
Europe	2.93	1,700
Thailand	3.43	1,450
India	4.32	1,170
GCC	5.84	880
Egypt	7.9	650

The study used fuzzy logic to obtain and assess the solar panel models in six layers, where the evaluation using fuzzy logic is based on different factors mentioned earlier.

In the present study, houses of five countries/regions that required load with several appliances were taken as examples. The following are taken in to consideration:

- a. types of appliances
- b. number of appliances (each type)
- c. average running time of each appliance which depends on the need.

The appliances rating is 20.028 kW, and the total number of units per day (in kWhr/day) is 407.51 kWhr/day. In addition, targeted specifications of the PV panel are $P_m=110\text{ W}$, $V_m=16.7\text{ V}$, $I_m=6.6\text{ A}$, $V_{oc}=20.7\text{ V}$, and $I_{sc}=7.5\text{ A}$. Furthermore, the inverter size (kW) is 105,872 W \approx 106 kW. These data belong to the GCC region.

The considered countries/regions are Thailand, India, Egypt, GCC, and Europe. Table 9.1 shows the PGF for each of them and the obtained results of the number of PV panels for the countries/regions mentioned earlier.

Figure 9.3 illustrates the histogram of the five considered countries/regions versus the number of PV panels.

The relationship between the PGF and the number of PV panels for the selected countries/regions is plotted in Figure 9.4.

The curve fitting technique is applied to find the mathematical relationship between the PGF and the number of PV panels results for the considered countries/regions using the polynomial quadratic regression. The mathematical expression becomes as follows:

$$\text{No. of PV Panels} = (a) + (b) \text{ PGF} + (c) \text{ PGF}^2 \tag{9.12}$$

Table 9.2 shows the coefficients of the mathematical expression and their errors.

Therefore, the final form obtained for the mathematical expression between the PGF and the number of PV panels becomes:

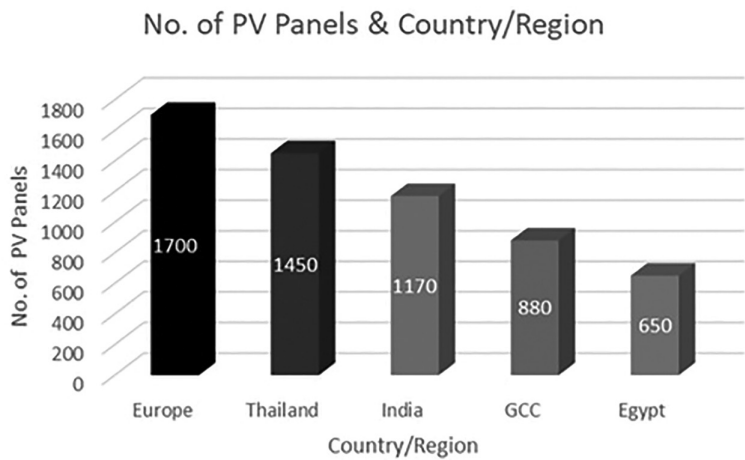


FIGURE 9.3
Histogram of the countries/regions versus the number of PV panels.

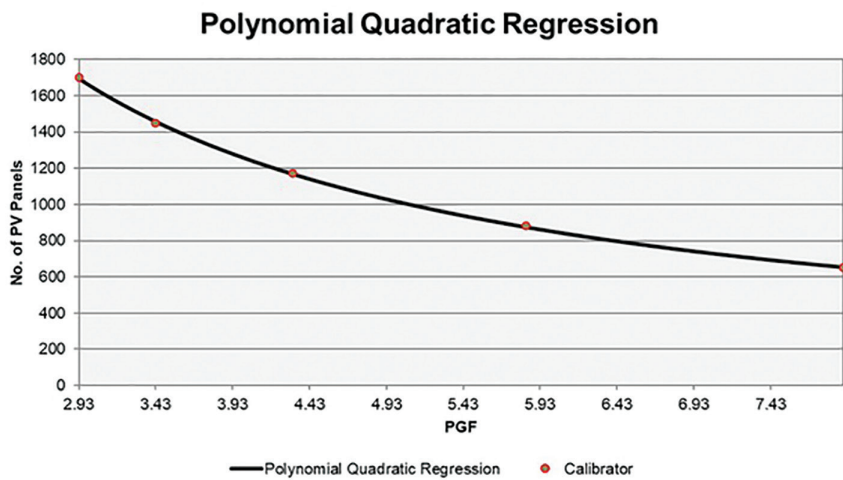
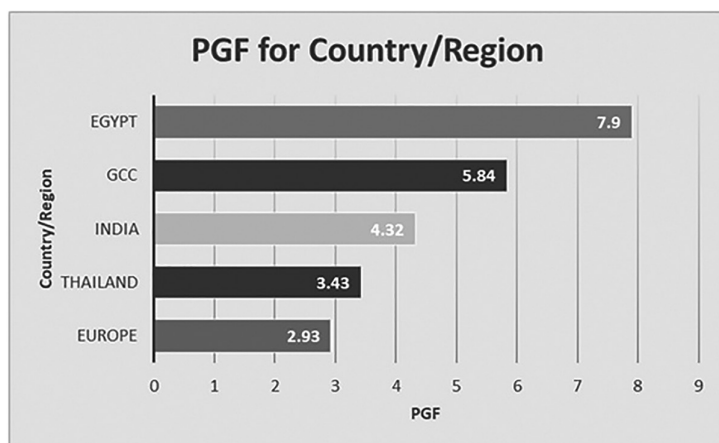


FIGURE 9.4
PGF and the number of PV panels results for the different countries/regions.

TABLE 9.2

The Coefficients of the Mathematical Expression and Their Errors

Coefficient	Value	± Error
a	3,147.84	209.348
b	−617.254	85.2445
c	38.2514	7.79416

**FIGURE 9.5**

PGF histogram for the different countries/regions.

$$\text{No. of PV Panels} = 3,147.8434 - 617.25415\text{PGF} + 38.251394\text{PGF}^2 \quad (9.13)$$

Figure 9.5 shows the PGF histogram for the considered countries/regions in the present study. It is found that the highest PGF is for Egypt and the lowest for Europe. As shown in the histogram for the same countries/regions in Figure 9.3, it is found that the highest number of PV panels is for Europe and the lowest belongs to Egypt. Based on the results, it is found that the relationship between the PGF and the number of PV panels is inverse. This means that the number of PV panels is inversely proportional to the PGF.

Solar energy is considered as a technology which collect thermal energy from the sun. This type of heat can also be used for water and space heating. In addition, solar space heating and cooling systems can circulate conditioned air or liquid throughout a building using existing HVAC systems, without using electricity.

The present study takes more regions and countries. The artificial intelligence technique is used to estimate the daily load for five countries by Qamber et al. [3]. They recommend estimating the required solar power panels to satisfy the estimated daily electric demand. Moosa and Kazem [4], in their study, highlighted both the solar and wind energy in the region of the GCC countries. At the same time, the authors concentrate on Oman. El idrissi et al. [5], in their research, used a nonlinear robust method combining the backstepping and the sliding mode techniques. It has been highlighted in the study of Qamber and Al-Hamad [6]. They concentrate on the six GCC countries. Qamber and Al-Hamad [6], in their study, derived the design of solar cell model. Goyani and Patel [12] carried out a study on the renewable energy resources. They used the MATLAB simulation, and also developed a model of hybrid wind and PV system.

9.5 Conclusion

One model to estimate the number of PV panels that help produce electricity in different countries/regions by photovoltaic modules of technologies under real operating conditions is developed and presented in this study. The obtained model does not consider the spectral distribution of incident radiation. The model developed in the present study assumes that the produced energy depends on the PGF, and this factor will be an affected factor that reached the results aimed to be obtained in the present study. The results obtained for the developed model of the five different countries/regions show its validity. Out of the obtained developed model for the five different countries/regions, where the number of PV panels are obtained, it can be concluded that the energy can be improved based on the targeted specifications of the PV panel. In addition, when any country with the same load obtaining the number of PV panels, the PGF can be obtained by applying the developed model equation. Furthermore, the obtained results show that the PGF is inversely proportional to the number of PV panels that the present research is targeted.

The predicted energy values from the machine learning algorithm track better along the current baseline approaches. Furthermore, additional work is still required to improve the predictions of the electricity using the PV panels, where the forecasted values might become better in future and match the measured values in our life. The present study demonstrates how machine learning can help and be used to improve photovoltaic performance modeling and the predicated energy values are calculated using ANFIS.

Acknowledgment

The author would like to thank Ms. Aysha Qamber for her excellent assistance in preparation of this chapter.

References

1. Qamber I., "Development model of the inverter size for the GCC countries", *Applications of Modelling and Simulation*, Vol. 5, pp. 1–6 (2021).
2. Sheeja N., Janvhi J., Muskaan F. K., "Smart solar power inverter", *Technium*, Vol. 2, No. 6, pp. 64–73 (2020).

3. Qamber I. S., Al-Hamad M. Y., "Photovoltaic design for smart cities and demand forecasting using a truncated conjugate gradient algorithm", *Optimization, Learning, and Control for Interdependent Complex Networks*, Part of the Advances in Intelligent Systems and Computing (AISC, vol. 1123), pp. 277–295. Springer, Cham (2020). doi: 10.1007/978-3-030-34094-0_12.
4. Moosa I., Kazem H. A., "Review of basic renewable energy in GCC countries: Current status and future vision", *International Journal of Computation and Applied Sciences*, Vol. 6, No. 1, pp. 397–406 (2019).
5. El idrissi R., Abbou A., Mokhlis M., Skik N., "Robust hybrid MPPT controller for PV pumping system", *International Journal of Innovative Technology and Exploring Engineering (IJITEE)*, Vol. 9, No. 2, pp. 1–8 (2019).
6. Qamber I. S., AL-Hamad M. Y., "Novel PV panels design modeling to support smart cities", *International Journal of Computing and Digital Systems (IJCDS)*, Vol. 8, No. 2, pp. 125–130 (2019). doi: 10.12785/ijcds/080204. ISSN: 2210-142X.
7. Rufangura P., Sabah C., "Perfect metamaterial absorber for applications in sustainable and high efficiency solar cells," *Journal of Nanophoton*, Vol. 12, No. 2 (2018). doi: 10.1117/1.JNP.12.026002.
8. Subashini M., Ramaswamy M., "Exploration of chaos and bifurcations in a solar PV MPPT SEPIC converter system", *IOSR Journal of Engineering (IOSRJEN)*, Vol. 08, No. 8, pp. 62–69 (2018).
9. Ajith K. U., Boobana M., Ramyaa M., Thangam A., Abinaya R., Seenivasan V., "Designing of single ended primary inductance converter for solar PV application using ARDUINO controller", *International Research Journal of Engineering and Technology (IRJET)*, Vol. 5, No. 4, pp. 1–5 (2018).
10. Qamber I. S., AL-Hamad M. Y., "A general methodology made cleaned PV energy panels for Bahrain and UK", *Smart Cities Symposium*, 22–23 of April 2018, IET and University of Bahrain, Zallaq, Kingdom of Bahrain.
11. Alboaouh K. A., "Optimization of PV response under the uncertainty of load and irradiance during the peak", *Engineering Press*, Vol. 1, No. 1, pp. 12–23 (2017). doi: 10.28964/EngPress-1-103.
12. Goyani C., Patel V.R., "Performance analysis of grid connected hybrid wind/PV system", *International Research Journal of Engineering and Technology (IRJET)*, Vol. 4, No. 4, pp. 1460–1463 (2017).
13. Ma S., Xu Y. P., Li X. F., Wang Y. F., Zhang N., Xu Y. R., "Research on reduction of solar power curtailment with grid connected energy storage system based on time-series production simulation", *Energy and Power Engineering*, Vol. 9, pp. 162–175 (2017).
14. Al-Saadi H., Zivanovic R., Al-Sarawi S., "Uncertainty model for total solar irradiance estimation on Australian rooftops", *World Renewable Energy Congress-17, E3S Web of Conferences* 23, p. 01004 (2017). doi: 10.1051/e3sconf/20172301004. (Al-Hamad M. Y., Qamber I. S., "Smart PV grid to reinforce the electrical network", *World Renewable Energy Congress-17, MATEC Web of Conferences* 023, 01002 (2017), E3S Web Conf., Volume 23, 2017, World Renewable Energy Congress-17, 2017. doi: <https://doi.org/10.1051/e3sconf/20172301002>, Published online 20 November 2017)
15. Hassan S. Z., Li H., Kamal T., Nadarajah M., Mehmood F., "Fuzzy embedded MPPT modeling and control of PV system in a hybrid power system", *2016 International Conference on Emerging Technologies (ICET)*, Islamabad, Pakistan, 18–19 Oct. 2016. doi: 10.1109/ICET.2016.7813236.

16. Gupta A., Chauhan Y. K., "Detailed performance analysis of realistic solar photovoltaic systems at extensive climatic conditions", *Energy*, Vol. 116, pp. 716–734 (2016).
17. Al Badwawi R., Abusara M., Mallick T., "A review of hybrid solar PV and wind energy system", *Smart Science*, Vol. 3, No. 3, pp. 127–138 (2015). doi:10.6493/SmartSci.2015.324.
18. Sharma K. D., Saroha S., Kumar S., "Active power control of grid connected hybrid fuel cell & solar power plant", *International Electrical Engineering Journal (IEEJ)*, Vol. 6, No. 5, pp. 1891–1897 (2015).
19. Mengi O. O., Altas I. H., "A new energy management technique for PV/wind/grid renewable energy system", *International Journal of Photoenergy*, Vol. 2015, p. 19, Article ID 356930 (2015). doi:10.1155/2015/356930.
20. El-Fergany A., "Efficient tool to characterize photovoltaic generating systems using mine blast algorithm", *Electric Power Components and Systems*, Vol. 43, No. 8–10, pp. 890–901 (2015).
21. Almasoud A. H., Gandayh H. M., "Future of solar energy in Saudi Arabia", *Journal of King Saud University – Engineering Sciences*, Vol. 27, pp. 153–157 (2015).
22. Eltawil M. A., ElSbaay A. M., "Utilisation of solar photovoltaic pumping for aeration systems in aquaculture ponds", *International Journal of Sustainable Energy*, Vol. 35, No. 7 (2016). doi: 10.1080/14786451.2014.928295.
23. Bhoje H., Sharma G., "An analysis of one MW photovoltaic solar power plant design", *International Journal of Advanced Research in Electrical, Electronics and Instrumentation Engineering*, Vol. 3, No. 1, pp. 6969–6973 (2014).
24. Barua A., "Load sharing and power quality improvement in solar PV connected microgrid", *International Research Journal of Engineering and Technology (IRJET)*, Vol. 4, No. 5, pp. 615–619 (2017).
25. Mallika S., Saravanakumar R., "Genetics algorithm based MPPT controller for photovoltaic system", *International Electrical Engineering Journal (IEEJ)*, Vol. 4, No. 4, pp. 1159–1164 (2013).
26. Manavalan R., "Analysis of hybrid renewable energy system using NPC inverter", *International Electrical Engineering Journal (IEEJ)*, Vol. 4, No. 1, pp. 864–868 (2013).
27. Bhakre S. S., Sawarkar P. D., Kalamkar V. R., "Performance evaluation of PV panel surfaces exposed to hydraulic cooling –A review", *Solar Energy*, Vol. 224, pp. 1193–1209 (2021).
28. Wu S.-Y., Guo H.-T., Xiao L., Chen Z.-L., "Experimental investigation on thermal characteristics and output performance of PV panel under linear light source and windy conditions", *Sustainable Energy Technologies and Assessments*, Vol. 43, p. 100918 (2021).
29. Tripathi A. K., Ray S., Aruna M., Prasad S., "Evaluation of solar PV panel performance under humid atmosphere", *Materials Today: Proceedings*, Vol. 45, pp. 5916–5920 (2021).
30. Protopapa M.L., Burrese E., Palmisano M., Pesce E., Schioppa M., Capodiecì L., Penza M., Sala D. D., Vincenti N., Accili A., Campadello L., "Optical methods to identify end-of-life PV panel structure", *Resources, Conservation & Recycling*, Vol. 171, p. 105634 (2021).

10

Performance Degradation in Solar Modules

Shabbir S. Bohra

Sarvajanik University

CONTENTS

10.1	Introduction.....	232
10.2	Causes and Rate of Degradation of Solar Panel	235
10.3	Degradation Types of Photovoltaic Modules.....	236
10.3.1	Corrosion of PV Module	236
10.3.2	Delamination of PV Module	237
10.3.3	Discoloration of PV Module	237
10.3.4	Breakage and Cracks in PV Modules.....	239
10.3.5	Potential-Induced Degradation (PID)	240
10.3.6	Hot Spots	240
10.3.7	Bubbles	241
10.4	PV Module Degradation Models.....	242
10.4.1	Pan Model	242
10.4.2	Exponential Model.....	243
10.4.3	Model of Degradation by UV Stress	244
10.4.4	Model of Degradation by Temperature Stress.....	245
10.4.5	Model of Temperature and Humidity Stress Degradation.....	246
10.5	Performance Assessment Techniques.....	247
10.5.1	Final Yield	247
10.5.2	Reference Yield	248
10.5.3	Performance Ratio	248
10.5.4	PVUSA Rating	248
10.5.5	Capacity Factor	248
10.5.6	System Efficiency	249
10.6	Degradation Rates of Various Cell Technologies	249
10.7	Conclusions.....	250
	References.....	251

10.1 Introduction

Solar energy has been considered one of the most promising candidates in today's clean energy economy; there is a long history behind photovoltaic (PV) technology. The cost of solar PV cells and the hence associated system has dropped significantly in the past decade or so. Let's have a look at major milestones achieved by solar energy and its industries; especially solar PV systems are illustrated in Table 10.1.

A solar PV-based generation system is installed at an appropriate location that offers various favorable parameters, such as sufficient irradiation and suitable temperature, number of sunny days, accessibility from transportation channels, and transmission line. Such utility-sized solar farm consists of a number of PV modules or sometimes referred to as PV panels in form of arrays in order to achieve the required voltage level and adequate power output. One such module or panel comprises a number of solar cells depending on power capacity, types of cell material, and manufacturer. Hence, PV modules are the building blocks and are often thought of as the most reliable component of a solar PV-based generation system. The various components of solar PV module are depicted in Figure 10.1.

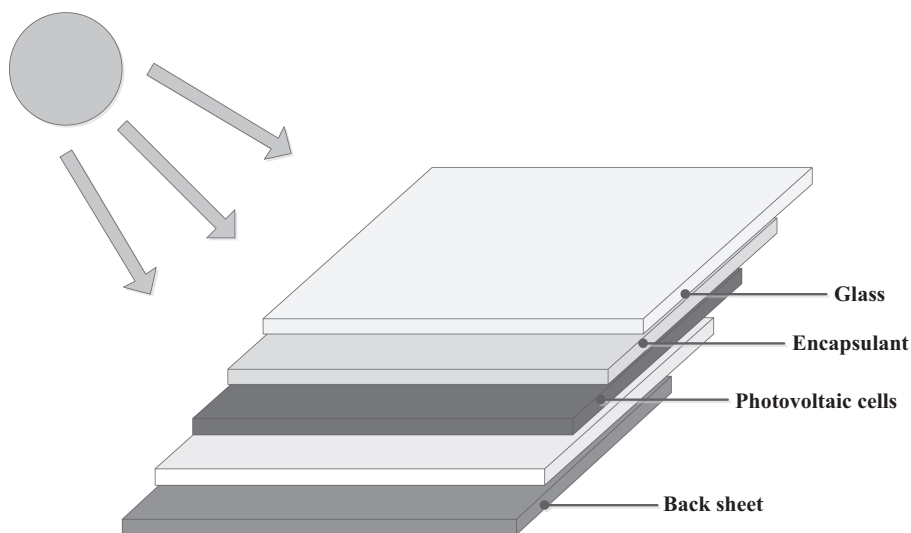
The typical power rating of solar PV panels are for rooftop and commercial installations are 250–400 W. For a region receiving sufficient insolation for 5 hours for around 300 days a year, one 300 W panel would generate 450 kWh in a full calendar year. And if 50 such premium panels are installed for utility-sized generation plant, approximately 22.5 MWh electrical units could have been generated.

The development of PV business is highly dependent on how precisely the installed system can deliver power over a specific period. This can be ensured by primarily two parameters: one is evidently the efficiency and the other how consistently the efficiency is maintained over a period. An accurate amount of power reduction over time is precisely known as degradation rate. It impacts significantly all the stakeholders such as utility companies, operators, investors, and manufacturers. From the economic perspective also, the degradation of a PV module is a crucial issue, because a higher degradation rate directly affects reduction in power production and revenue from energy supplied; hence, less future cash flows (Short et al., 1995). In addition to that, imprecision in determining degradation rates also escalates the chances of financial risk. Furthermore, techniques to accurately estimate degradation eliminate chances of failure to a great extent. A more efficient module with a degradation rate of as high as 50% might offer better efficiency than a non-degraded module with not as much of efficient one. The identification of the principal degradation technique performing experiments and modeling could result in prolonged life. Outdoor actual field testing has proved to be a vital exercise in measuring long-term behavior and lifetime for mainly two causes: it is the distinctive working environment for PV systems, and it is the

TABLE 10.1

Major Developments in PV Industry

Year	Development
1839	A 19-year-old French physicist named Edmond Becquerel discovered the effect of photovoltaic and observed potential differences when an electrolytic cell is exposed to light.
1876	Richard Evans Day and William Grylls Adams discovered and proved that Selenium can generate electricity under exposure of sunlight.
1883	An American researcher, Charles Fritts, developed the first 1% efficient solar cells made from selenium wafers.
1918	Polish scientist Jan Czochralski developed a process for growing single-crystal silicon which has been adopted by leading industries for extracting high-grade silicon.
1932	Stora and Audobert discovered the photovoltaic effect in cadmium sulfide (CdS).
1953	Dr. Dan Trivich, from Wayne State University, derived the theoretical expressions for the efficiencies for different materials and different band gaps according to the spectrum of the Sun first time.
1954	Daryl Chapin, Calvin Fuller, and Gerald Pearson developed the silicon PV cell at Bell Labs was remembered as first development of United States in Photovoltaic technology—the first solar cell converting the solar energy into electrical energy for commercial applications successfully. Bell Labs claimed efficiency of 4% for a silicon solar cell which later improved to 11%.
1957	8% efficient PV cells were developed by Hoffman Electronics.
1958	9% efficient PV cells were developed by Hoffman Electronics.
1959	Hoffman Electronics achieved 10% efficiency for commercial Solar PV cells.
1960	Hoffman Electronics achieved 14% efficient PV cells.
1963	Sharp Corporation produced silicon photovoltaic modules which are having field applications.
1973	The world's first (PV) powered residences were designed by the University of Delaware known as "Solar One".
1976	David Carlson with Christopher Wronski at RCA Laboratories fabricated the very first amorphous silicon photovoltaic cells.
1985	The University of South Wales broke the 20% efficiency barrier for silicon solar cells for 1-Sun conditions.
1986	ARCO Solar developed—the world's first commercial thin-film solar PV module.
1992	The University of South Florida succeeded to develop 15.9% efficient thin-film photovoltaic cell from cadmium telluride (Cd-Te), breaking the 15% barrier for the thin-film technology.
1994	Gallium indium phosphide (GInP) and gallium arsenide (GaAs) solar cells were developed by the National Renewable Energy Laboratory (NREL) with 30% conversion efficiency.
1999	Spectrolab, Inc. and the NREL jointly developed a PV solar cell of 32.3% at lab level. The higher conversion efficiency could be achieved by stacking multiple layers of PV materials forming single solar cell and can be incorporated into a concentrated PV system.
1999	The NREL crossed a new efficiency record for thin-film photovoltaic solar cells of 18.8% efficiency for the prototype solar cell.
2000	BP Solarex developed two new thin-film solar modules, breaking previous performance efficiency records. The 0.5 sq. mt ² module a conversion efficiency of 10.8%—the highest in the world for thin-film modules of its kind.

**FIGURE 10.1**

Structure of solar module (Short et al., 1995).

only option that can correlate indoor accelerated testing to outdoor results to predict field performance effectively. Extensive research is being conducted to estimate the degradation rate of PV module and overall system as well, for example, researchers have measured around 2,000 separate modules of systems, found median degradation rate of 0.5%/year (Jordan and Kurtz, 2013). It has also been perceived that the median rate for exposure length up to 10 years is considerably greater than for 10 years and longer, *i.e.*, 0.7%/year for 0–10 years, 0.46%/year for 10–20 years, and 0.43%/year for more than 20 years of exposure. The National Renewable Energy Laboratory (NREL) has identified that solar panels exhibit median degradation rate of 0.5%/year under normal environmental conditions but escalates for hotter climatic regions and rooftop PV installations.

The manufacturer guarantees for the performance of solar panels for 25–30 years, though it may be possible that the panel continues to produce electricity even after that period. Such a period of 25–30 years is known as the useful life of the panel. It has been evident that world's first commercial panel is still in operation after 50 years of its installation. Like other equipment, solar panels also do not offer the same efficiency throughout their lifespan from their first installation till the end of their useful life, *i.e.*, 25 or 30 years as mentioned by its manufacturer. Solar panel's conversion efficiency eventually decreases over the period or as it ages, though at a slower rate. This phenomenon is known as "Degradation." All solar panels slowly degrade over time, which means they are producing less electricity from the same amount of irradiation as it ages. A variety of external factors (like weather) cause such

negative impacts on their ability to produce electricity. Manufacturers typically guarantee 90% of the panels' production up to the end of the first ten years and then after ten years, that percentage falls to 80 for the remaining useful lifespan of 15–20 years. The solar modules may continue to convert sunlight into electricity. However, depending on financial perspective, one may decide to go for replacement of panels with the latest modules, offering better conversion efficiency.

Analysis of solar module degradation is a complex problem to solve because modules may get degraded in a number of ways due to a variety of influencing factors. Solar panel manufacturers are constantly evolving and coming up with solutions to reduce the degradation rate so that, solar panels can maintain their power output over their entire useful life. But in the meantime, panels are guaranteed to degrade at or below a particular rate, so one can rest being assured that the investment is a safe one.

10.2 Causes and Rate of Degradation of Solar Panel

Various aspects contribute to solar panel degradation, but many of them are impossible to control like the weather. During hot climatic conditions, the metal expands and contracts when it cools down. The solar panel undergoes such constant back-and-forth action a number of times throughout its life, which leads to considerable strain on it. Therefore, the atmosphere thermal cycling causes micro-cracks to develop in the silicon material of the solar cells. Such small cracks cause deterioration to electrical connections, breaking in fingers of cell, causing fewer paths for those electrons from the Sun to take, and thus a smaller amount of energy goes to the inverter that powers establishments like the rooftop of a house and commercial setups, solar farms or panels mounted on water bodies such as canal and floating systems. Other issues due to this thermal expansion and contraction are failures in junction box adhesion and discoloration.

Furthermore, strong winds can cause deformation in the panels because of the dynamic mechanical load experienced by such systems. But, as long as solar PV system is typically installed by skilled persons and taking into account the meteorological information of site and panels of premium quality, it could not be a key concern to degradation. However, extreme hot and cold weather, humidity, and snow and ice deposition or accumulation also gradually contribute to the degradation of solar modules, as solar system components experience different voltage potentials.

The established players in solar industry manufacture solar panels with ultraviolet (UV) blockers to protect the solar panels from most of the damages, but the sunlight received on these panels itself contributes significantly to the process of degradation. Typically, the solar modules degrade

at comparatively highest rates just hours after installation in the field when they are first exposed to the sunlight and hence UV rays irradiated from Sun. This phenomenon is known as light-induced degradation (LID). The degradation rate for solar panels could be of the order of 1%–3% in this initial small amount of time, but after that, degradation becomes sluggish.

It has been noticed from the field data available that solar modules degrade at a rate of 1% each year on an average. That is supported by the warranty assurance provided by the respective solar panel manufacturer. It guarantees 90% production in the initial span of ten years and 80% subsequently for next two to three decades down the line. Nevertheless, a study conducted by the NREL revealed a better projection of degradation of solar modules. This assessment has taken into account the degradation rates for almost 2,000 solar systems across the world in a variety of climates. They have observed that the mono-crystalline modules manufactured after the year 2,000 degraded at a rate of just 0.4%, which is less than half of the 1% rate used in the warranties. While degradation of solar modules plummeted by a few percentages right away due to the effect of LID, the degradation rate reduces noticeably for the rest of their lifetime.

10.3 Degradation Types of Photovoltaic Modules

Degradation is defined as the gradual deterioration of the characteristics of a component or of a system, which may affect its ability to operate within the limits of acceptability criteria and is greatly influenced by the operating conditions (Lannoy and Procaccia, 2005). According to the manufacturers, a PV module is claimed to be degraded when its power reaches a level below 80% of its initial power (Wohlgemuth et al., 2005b). The PV module's performance can be degraded due to several factors such as temperature, humidity, irradiation, mechanical shock (Quintana et al., 2002; Wohlgemuth et al., 2005a; Osterwald and McMahon, 2009; Munoz et al., 2011). The main kinds of solar PV module degradation are corrosion, discoloration, delamination, and breaking or cracking cells. Moreover, the degradations identified in crystalline silicon modules (Wohlgemuth and Kurtz, 2011; Bosco, 2010) are cracked interconnection, breakage in cells, sign of corrosion, delamination and discoloration of encapsulant, broken protecting cover glass, failure of bypass diode, and failure of welded ribbon.

10.3.1 Corrosion of PV Module

Corrosion, in general, is defined as the chemical or electrochemical reaction between a material—it could be a metal or alloy and its environment which initiates a deterioration of the material and its properties. Ingress of moisture

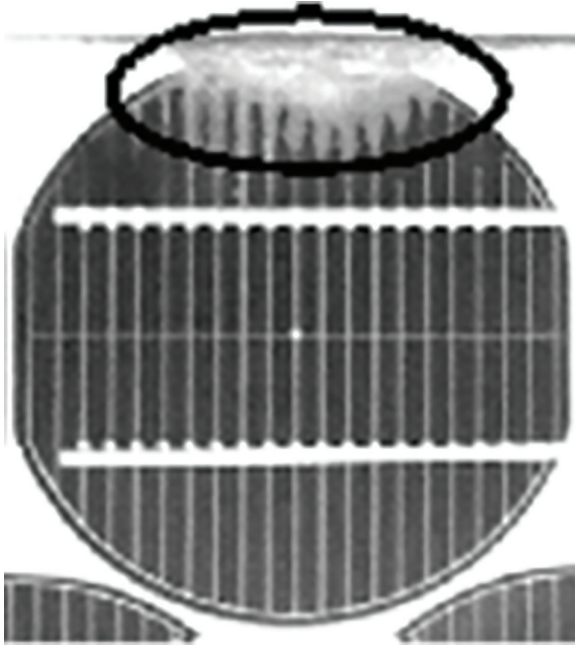
into a module via the laminated edges results in corrosion (Kemp, 2005). The chances of moisture retention in the casing of the module escalate electrical conductivity of the object. The corrosion affects almost all conducting metallic connections of PV cells and modules as well and causes a performance loss due to increased leakage currents. The effect of corrosion also damages the bonding between cells and metallic frames. An experiment was carried out according to IEC 61215 standard using accelerated testing techniques known as 85/85 ($T=85^{\circ}\text{C}/\text{RH}=85\%$) and it was observed that corrosion became noticeable after 1,000 hour of exposure of PV module under 85°C and 85% of relative humidity (Wohlgemuth and Kurtz, 2011). The reason for corrosion was identified as the presence of sodium in the glass. It reacts with moisture and causes corrosion of PV modules edges. Due to the water diffusion being relatively at a greater rate in the ethylene vinyl acetate (EVA), penetration of the moisture into the module becomes important during its lifetime even if the module is comprised of a double-glass structure. The moisture penetration can only be prevented by properly sealing through gaskets having low diffusivity containing a large quantity of desiccant was also mentioned (Kemp, 2005). Hence, it is more advisable to emphasize on methods to mitigate the corrosion processes, which is augmented because of substantial moisture content. An exhaustive survey of the field comprising of around 4,000 modules has been analyzed and observed that more than 90% of failures taking place in the field were caused by interconnecting breakage and corrosion (Wohlgemuth and Kurtz, 2011).

10.3.2 Delamination of PV Module

The loss due to adhesion or also known as delamination takes place between the cells and the forward-facing glass or encapsulating polymer and the cells. This characterizes the main problem because it originates two effects: (1) increases the reflection of light and (2) penetration of water into the module assembly (Munoz et al., 2011). Delamination becomes more dominant when it takes place on the sides of the module because along with the reduction in efficiency, it also causes electrical risks for the module and the complete installation. The delamination is more common in humid and hot climates. It causes moisture infiltration in the module and, therefore, leads to several chemical and physical degradations like corrosion of metal of the module structure often. The delamination may occur due to accumulation of salt and moisture infiltration into the PV module (Jansen and Delahoy, 2003). Figure 10.2 shows the PV module with delamination.

10.3.3 Discoloration of PV Module

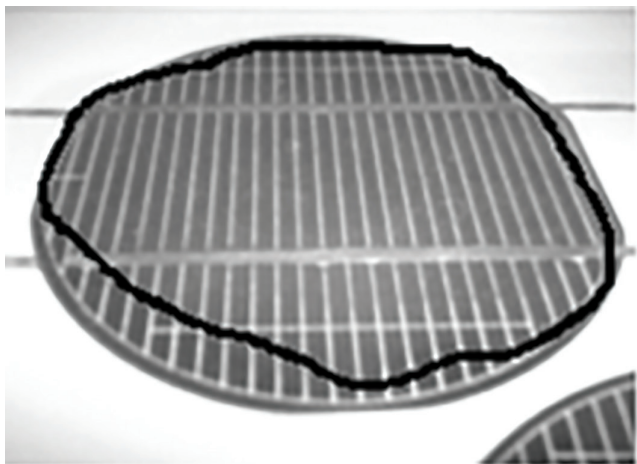
Module discoloration is defined as alteration in color of a material which turns into lighter yellowish to even brown in some worst cases. The degradation usually causes discoloration of the encapsulant module, EVA or adhesive

**FIGURE 10.2**

PV module with delamination (Jansen and Delahoy, 2013).

material between the PV cells and the glass. It changes the transmittance parameter of light imparting on solar PV modules and hence, due to lower irradiation received on it, the output power from the module decreases to some extent. The combining of UV rays with water at a temperature of more than 50°C is one of the main causes of EVA degradation. The discoloration could even start developing in other areas that are not nearby zones of an installed PV module or system (Oreski and Wallner, 2009).

The discoloration directly affects the reduction of the short-circuit current (I_{sc}) of PV module; this negative change in I_{sc} may vary from 6% to 8% and 10% to 13% below the nominal value for a partial discoloration and for wide-spread discoloration of PV module, respectively. The generation and collection of light-generated carriers establish I_{sc} and is the function of cell area, light intensity, spectrum of incident light, and optical properties. It varies linearly with the intensity of light, and discoloration directly affects the number of photons that reach the junction to create electron-hole pair. Maximum power extracted from a module is a function of open-circuit voltage, short-circuit current, and fill factor of it. Hence, it is evident that the module discoloration also disturbs the maximum power (P_{max}) available from the PV module. Realini (2003) reported a fall of 1.3% in I_{sc} and 4.5% in P_{max} for healthy (white) PV module discolored (yellow) (Realini, 2003). The solar cell discoloration observed is shown in Figure 10.3.

**FIGURE 10.3**

Solar cells discolored (Jansen and Delahoy, 2003).

10.3.4 Breakage and Cracks in PV Modules

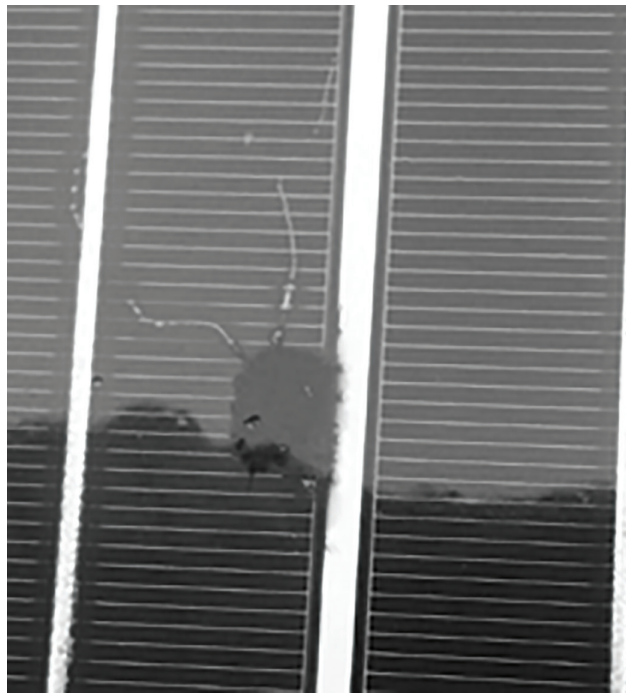
Another significant factor for PV modules degradation is glass breakage. There are a very few PV module manufactures across the globe, and installation sites are reasonably far from point of manufacturing or assembly. Transportation is inevitable in almost major renewable energy conversion devices as its installation demands large land size, adequate number of sunny days with enough irradiation as reasonable accessibility from rail or roads. Hence, the physical damage or breakage is likely to take place mainly during installation, maintenance, and during the transportation of modules to the generation site (Wohlgemuth and Kurtz, 2011). It has also been observed that modules with breakage or cracks may continue to work surprisingly without apparent change in their performance. But on the other hand, the chances of an electrical shock and moisture penetration increase. These degradations are typically followed by other degradation modes like discoloration, corrosion, and delamination (Quintana et al., 2002). Typically, the cost of cell and module is controlled by the volume of material, *e.g.*, silicon being used in it. Hence, the manufacturers are always interested in employing technology that saves silicon material and minimal manufacturing costs of PV cells. The cell manufacturers have started decreasing the thickness of silicon PV cells from 300 to 100 μm . The thinner and bigger cells 210 mm \times 210 mm are more fragile and more susceptible to breakage during handling. Optical methods are generally used to detect such defects in operational PV modules in the field (Rueland et al., 2005).

10.3.5 Potential-Induced Degradation (PID)

In large utility-scale solar plants, large numbers of PV modules are required to be connected in series. Such interconnection is an inevitable requirement in order to enhance system voltage of the order of hundreds of volts. From the safety perspective, all metallic structures of the system are grounded to protect personnel working on it. As a result, panels are often exposed to relatively higher potentials with respect to ground; much higher potential difference may lead to high-voltage stress (HVS). Due to such a high potential difference between panels and ground, it is very likely that a leakage current may find its way between these PV modules and grounded structures (Schutze et al., 2011). The adverse effect of HVS on long-term stability of solar panels is governed by the magnitude of leakage current flowing between solar cells and ground, which is observed by NREL in 2005 (del Cueto et al., 2005). Such persisted phenomenon initiates polarization effect, which may lead to degradation of the electrical characteristics of the PV cells. This degradation phenomenon is labeled as Potential-Induced Degradation (PID). The effect of PID is characterized by the progressive performance deterioration technique of *c*-Si PV modules, because of the existence of an electrical current that is induced in the PV module. The PID not only shifts the module's maximum power point (MPP) and its open-circuit voltage (V_{oc}) to a lower value but also decreases its shunt resistance as well. The severity of PID is governed by the solar plant and the surrounding environment it has been installed. Since the environmental control is beyond the scope, the only feasible option is to avoid PID damage to the panel and to buy a PV module with inbuilt PID resistance. Additionally, the selection of glass, its encapsulation, and used diffusion barriers have all been proved to have an influence on PID. It has been observed that the humid climate is promoting PID more than in hot and dry conditions because humidity accelerates leakage current (Hacke et al., 2011; Schutze et al., 2011; Schütze et al., 2011). The PID is observed not only on cell level but system and panel as well. An extensive review of PID on both *c*-Si and thin-film PV modules has been presented, the modeling of leakage current path in the module is explained. The temperature, humidity, and voltage dependency and acceleration modeling of PID are also examined. The preventive measures to be taken at cell, module, and system level against PID are also addressed by Luo et al. (2017). The system-level approach is to select the correct grounding scheme of the string poles which can minimize PID on system level and better encapsulation material that aids in the reduction of leakage current leading to PID of cells (Pingel et al., 2010).

10.3.6 Hot Spots

A small area of a PV module exhibiting a temperature higher than normal is known as the hot spot phenomenon. It could damage the cell which it has

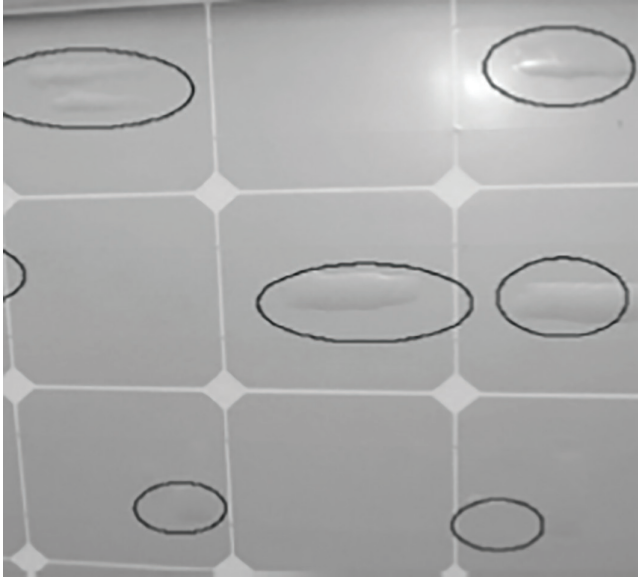
**FIGURE 10.4**

Hot spot developed on solar cell.

developed upon or other parts of that module. Partial shading, mismatch, or discontinuity between cells may turn in the development of the hot spot (Molenbroek et al., 1991). Consequently, this faulty cell starts behaving as electrical load for the rest of the cells of the module and becomes a reason for abnormal thermal stress and dissipation. The formation of a hot spot is illustrated in Figure 10.4.

10.3.7 Bubbles

This form of degradation is similar to the delamination type. The only difference is that the failure of EVA adhesion is affecting a smaller area and may show swelling on the surface. The release of gases from the PV module due to chemical reaction leads to the formation of bubbles. The presence of bubbles restricts the heat dissipation from cells and causes local overheating. It can be developed on the front and backside of the module as well. The bubble formation on the front side enhances the reflection of incident sunlight (Munoz et al., 2011) and could eventually reduce power output from the module as discussed previously. The bubbles developed on the backside of a PV module are illustrated in Figure 10.5.

**FIGURE 10.5**

Bubbles developed on the rear side of a PV module (Quintana et al., 2002).

10.4 PV Module Degradation Models

The phenomenon of degradation for PV module can be analyzed by measuring the output power, and therefore the reduction in power during its lifetime as compared to its output power when installed.

10.4.1 Pan Model

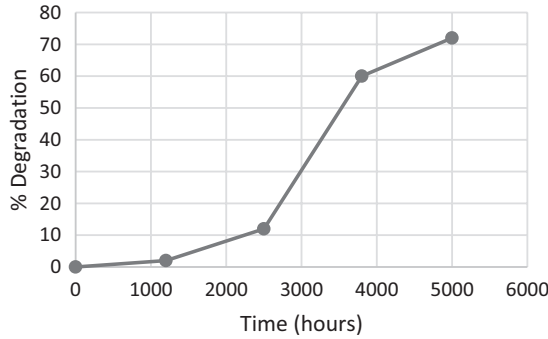
Pan (Jet Propulsion Laboratory) has developed a degradation model of the PV module output power which is explained by Pan et al. (2011):

$$D(t) = 1 - \exp(-y \cdot t^x) \quad (10.1)$$

where x and y are constants of the degradation model and can be computed from accelerated testing technique, and they depend on the degradation model being considered. They are derived using accelerated testing (Charki et al., 2013; Laronde et al., 2012). Hence, eqs. (10.2) and (10.3) illustrate the degradation model due to corrosion and discoloration, respectively:

$$D_{\text{corrosion}}(t) = 1 - \exp(-y_{\text{corrosion}} \cdot t^{x_{\text{corrosion}}}) \quad (10.2)$$

$$D_{\text{discoloration}}(t) = 1 - \exp(-y_{\text{discoloration}} \cdot t^{x_{\text{discoloration}}}) \quad (10.3)$$

**FIGURE 10.6**

Degradation of polycrystalline silicon PV module under test 85/85 (Pan et al., 2011).

The total degradation of the PV module is estimated as

$$D_{PV \text{ module}}(t) = 1 - \prod_{i=1}^n (1 - D_i(t)) \quad (10.4)$$

where n indicates the modes of degradation.

Degradation rate depends on relative humidity and temperature, and has been studied experimentally for PV after collecting history of them for multicrystalline solar cell over one year (Park et al., 2013). Pan et al. (2011) proposed a practical method that integrates weather information into the reliability prediction. After analyzing multiyear field data, the temperature was found to be a very significant parameter for PV performance degradation. It was suggested to carry out minimum two damp heat-tests like 85/85 ($T=85^\circ\text{C}/\text{HR}=85\%$) to determine $x_{\text{corrosion}}$ and $y_{\text{corrosion}}$ (Oreski and Wallner, 2009). It should be ensured that the temperatures during the test should be kept under the temperature of the PV modules' technological limit of 120°C . The limitation of the Pan model is that its accuracy depends upon degradation parameters x and y and testing time (Figure 10.6).

10.4.2 Exponential Model

In another model, module power (P) is taken as a reference in order to estimate degradation and performance analysis of PV module with respect to its original power (P_0) (Vazquez and Ignacio, 2008). The probability density function following Gaussian distribution for PV module power at a given time is given by Sakamoto et al. (2003):

$$P(p) = \frac{1}{\sqrt{2\pi}\sigma} \exp\left(-\frac{1}{2}\left(\frac{p-\mu}{\sigma}\right)^2\right) \quad (10.5)$$

where P refers to the power of PV module, and σ and μ are its standard deviation and mean value, respectively. The average power of PV module linearly reduces in time (Osterwald et al., 2002; Raghuraman et al., 2006).

$$\mu(t) = P_0 - At \quad (10.6)$$

where P_0 is the average or nominal module power at $t=0$, parameter A imitates reduction in module power annually, and t is the time (years). The limitation of this model, A , is assumed to be constant in time and linear degradation of PV module. Another model for exponential degradation is given below:

$$\mu(t) = P_0 e^{-\alpha t} \quad (10.7)$$

This aforesaid model facilitates to analyze the degradation of PV module during their useful life.

10.4.3 Model of Degradation by UV Stress

The UV radiation causes photodegradation in PV modules, which are exposed to direct sunlight. The discoloration would result due to UV exposure. It changes the encapsulating PV module transmittance and reduces in current supplied by PV module. This change or degradation factor can be quantified by taking the ratio of module short-circuit currents and is illustrated by Zimmerman (2008).

$$D(E) = \frac{I_{sc}(E)}{I_{sc}(E=0)} \quad (10.8)$$

where $I_{sc}(E)$ is the short-circuit current of the PV module and E is the dose of UV.

An analysis of unencapsulated and EVA encapsulated Si-cell in terms of I_{sc} degradation rates with UV exposure was carried out by Osterwald et al. (2005). The authors noticed up to 2% drop in I_{sc} when a UV dose of 1,056 MJ/m² (~3.8 years of outdoor exposure) is applied in unencapsulated cells (Osterwald et al., 2005). The relationship between UV dose and time of exposure t for solar spectrum $P(\lambda)$ is given by

$$E = ct \quad (10.9)$$

where

$$c = \int_0^{400} T_{cmx}(\lambda) P(\lambda) d\lambda \quad (10.10)$$

The integral is extended up to wavelength of 400 nm to represent a practical limit to UV photodegradation.

The UV degradation of PV module is given by

$$D(t) = 1 - n \ln(1 + a_{cmx}ct) \quad (10.11)$$

where a_{cmx} is the parameter of the material used for PV cell (Zimmerman, 2008).

This limitation of this model is that it involves the knowledge of the intrinsic characteristics of the materials utilized in the production of PV cells. Moreover, the sophisticated measurement techniques and instruments are essential to derive these characteristics.

10.4.4 Model of Degradation by Temperature Stress

A mathematical model constructed from the Arrhenius equation, a formula in physical chemistry for the temperature dependence of reaction rates is employed to determine the acceleration of temperature-dependent degradation processes that affects the performance of polymeric PV modules. The augmented temperature-dependent degradation processes following an Arrhenius behavior (Cocca et al., 2011; Haillant et al., 2011; Nehme et al., 2020) eq. (10.12) due to rise in temperature can be depicted as follows:

$$k_p = Ae^{-E_a/RT} \quad (10.12)$$

$$\frac{k_{p1}}{k_{p2}} = e^{E_a/RT \left(\frac{1}{T_2} - \frac{1}{T_1} \right)} = AF_T \quad (10.13)$$

where A represents an Arrhenius preexponential factor, k_p is the rate constant of the process, E_a indicates apparent activation energy (in J mol⁻¹), T is the absolute temperature (in K), R is the gas constant (8.314 J mol⁻¹ K⁻¹), and AF_T is the acceleration factor of test conditions 1 over test conditions 2 (ratio of rate constants). The Arrhenius equation-based model is one of the most widely used models for the temperature dependence of degradation processes. There are numerous assumptions and approximations necessary to apply Arrhenius equations.

- i. The rate constant k_p applies to a only change in performance or property.
- ii. The overall temperature-dependent process leads to a change in performance following an Arrhenius function.
- iii. In the given range of irradiances, the rate constant varies uniformly with irradiance.

- iv. Activation energies for weathering under accelerated testing conditions are only known for very few materials.
- v. The activation energy E_a remains constant over the considered temperature range for temperature-dependent process.
- vi. It is not possible to develop and predict the performance of the long-term degradation of PV modules using the Arrhenius-based model.

10.4.5 Model of Temperature and Humidity Stress Degradation

The Peck model (Escobar and Meeker, 2006) explains the acceleration model with the capability to take into account temperature (T) and relative humidity (HR), which is given by

$$\tau = A \cdot (HR)^n \cdot \exp\left(-\frac{E_a}{kT}\right) \quad (10.14)$$

where E_a represents the degradation process effective activation energy, k is Boltzmann's constant ($8.617 \cdot 10^{-5}$ eV/K), and A and n are the failure mode-dependent constants.

The accelerated factor is given by (Charki et al., 2013)

$$r(x_1, x_2, \gamma) = \exp\left(n \ln\left(\frac{RH}{RH^0}\right) - \frac{E_a}{k} \left(\frac{1}{T} - \frac{1}{T^0}\right)\right) \quad (10.15)$$

where x_1 and x_2 correspond to relative humidity (RH) and module temperature (T), $\gamma = (n, E_a)$, RH^0 and T^0 are reference relative humidity and temperature, respectively. The equivalent temperature, T_{eq} , can be estimated, which represents the degradation that would have occurred if the module had been operative for the same length of time but at a given constant temperature. The equivalent temperature T_{eq} can be determined using the below relation (Kurtz et al., 2011):

$$\exp\left(\frac{-E_a}{kT_{eq}}\right) = \frac{1}{t_2 - t_1} \int_{t_1}^{t_2} \exp\left(\frac{-E_a}{kT_{mod}(t)}\right) dt \quad (10.16)$$

where t is the time, $T_{mod}(t)$ is the time-dependent module temperature, and t_1 and t_2 are the start and end limits of integration, respectively. Using the same methodology, the equivalent of relative humidity H_{eq} can be estimated as given below:

$$(H_{eq})^n = \frac{1}{t_2 - t_1} \int_{t_1}^{t_2} (H(t))^n dt \quad (10.17)$$

where t is the time, $H(t)$ is the time-dependent environmental relative humidity, and t_1 and t_2 are the start and end limits of integration, respectively. The

module temperature $T_{\text{mod}}(t)$ and the relative humidity $H(t)$ are simulated hour by hour for a period of n years.

10.5 Performance Assessment Techniques

The key factors for performance evaluation of PV system as per IEC standards are (1) final yield (Y_F), (2) reference yield (Y_R), (3) performance ratio (PR), (4) PVUSA rating, (5) capacity factor (CF), and (6) system efficiency (η_{sys}).

10.5.1 Final Yield

Time series of yields and performance metrics are calculated according to recommendations mentioned in the IEC 61724:2017-1 standard.

The monthly in-plane irradiation (H_i in Wh/m^2) can be obtained as follows:

$$H_i = \sum_x^y G_{i,x} \cdot \tau_x \quad (10.18)$$

where $G_{i,x}$ (W/m^2) is the x -th recorded value of the in-plane irradiance, y is the number of instances recorded during a month, and τ_k (h) is the duration of the x -th recording interval. Measurements were taken at regular intervals, such as 15s then $\tau_k=1/240$ h or 30s then $\tau_k=1/120$ h or so. The monthly PV module AC output (E_{out} in Wh) was given by

$$E_{\text{out}} = \sum_x^y P_{\text{out},x} \cdot \tau_x \quad (10.19)$$

where $P_{\text{out},x}$ (W) is the x -th recorded value of the output AC power.

The monthly PV array energy yield (Y_A in Wh/W) was equal to E_A divided by the PV module ratings (P_{PVrated} in W):

$$Y_A = \frac{E_A}{P_{\text{PVrated}}} \quad (10.20)$$

The monthly final yield (Y_F in kWh/Watt) is defined as the ratio of total energy generated (E_{out}) by the installed PV system for a given period, to the rated output power P_{PVrated} . Similarly, it could be computed daily or yearly. The rated power is taken under standard test conditions (STC), i.e., irradiation of $1,000 \text{ W}/\text{m}^2$, ambient temperature of 25°C , and 1.5G air mass (AM).

$$Y_F = \frac{E_{\text{out}}}{P_{\text{PVrated}}} \quad (10.21)$$

10.5.2 Reference Yield

The ratio of entire in-plane solar irradiation (H_t , in kWh/m²) to the reference irradiation (G) (1,000 W/m²) is known as the reference yield (Y_R). This parameter considers equal number of hours under the reference irradiance and is depicted as below:

$$Y_R = \frac{H_t}{G} \quad (10.22)$$

The reference yield does not take into account the effect of temperature and humidity.

10.5.3 Performance Ratio

The ratio of final yield to reference yield is known as PR. It is a dimensionless quantity as it normalizes yield parameters with respect to solar irradiation. It facilitates to assess the performance of PV system over a long period. The yearly reduction in PR value indicates the degradation in the performance of PV system. It is one of the key indicators to assess the performance of PV system.

$$PR = \frac{Y_F}{Y_R} \quad (10.23)$$

10.5.4 PVUSA Rating

PVUSA rating method basically involves regression analysis for PV system. It takes into account the site-specific meteorological data to determine power at PVUSA test conditions, i.e., 1,000 W/m² plane-of-array irradiance at an ambient temperature of 20°C and wind speed of 1 m/s. The power can P computed as follows:

$$P = E(A + B \times E + C \times T_a + D \times W_s) \quad (10.24)$$

where P is AC power under specific test condition in kW, E represents plane-of-array irradiance (W/m²), T_a is ambient temperature (°C), W_s is wind speed (m/s), and A , B , C , and D are regression constants that are derived from operational data.

10.5.5 Capacity Factor

The ratio of actual annual energy supplied ($E_{AC \text{ actual}}$) of the PV system to the ideal energy output ($E_{AC \text{ ideal}}$) if operative for 24 hours a day is known as CF. It is a measure of how much energy a solar plant has produced compared to

the amount of energy it would have produced at full capacity. It is given as below:

$$CF = \frac{E_{AC\text{actual}}}{E_{AC\text{ideal}}} \times 8,760 \quad (10.25)$$

Solar energy is intermittent in nature; the irradiation varies with time of day and throughout the year as well. Moreover, it is available during the daytime only unlike wind energy. The estimated CF is around 25%–27% for plants installed where sites have more than 300 sunny days; and even as low as 15%–17% for some sites.

10.5.6 System Efficiency

System efficiency is defined as the ratio of energy available (E_{AC}) to product of incident irradiation (H_t) and module area (A_{module}).

$$\eta_{\text{sys}} = \frac{E_{AC}}{H_t \times A_{\text{module}}} \quad (10.26)$$

The value of system efficiency would always be little lower than the cell and module efficiency as it considers electrical losses taking place, which is negligibly smaller at cell and module levels.

10.6 Degradation Rates of Various Cell Technologies

From the various sources available, it is observed that the degradation rate has substantially reduced for cells/modules manufactured/installed before the year 2000 and after 2000. The typical value of degradation rate for various technologies is shown in Table 10.2.

A number of researchers are working to estimate the degradation rate of either field installed or laboratory PV modules. Such estimation requires the

TABLE 10.2

Typical Degradation Rates for Different Cell Technologies

	Before 2000	After 2000
a-Si degradation rate	1.85	1.15
Cd-Te	2.7	0.7
CIGS	1.85	1.4
Mono-Si	0.65	0.6
Multi-Si	0.71	0.7

TABLE 10.3
Degradation Rates with the Number of Modules and Exposure Time

Technology	No. of Modules/ Field Exposure In Years	Degradation Rate (%/year)	References
Crystalline Si	–/20	0.5 (module) 2.5 (system)	Quintana, et al. (2000)
	150/11	0.4	Reis, et al. (2002)
	–	0.5	Sakamoto and Oshiro (2003), King et al. (2000)
	4,000		Wohlgemuth et al. (2005b)
	–/12	1	Sanchez-Friera, et al. (2011)
	20/25	0.17%/year	Hedström and Palmblad (2006)
	–/30	1	Saleh, et al. (2009)
	3,000/–	0.5 and 1	Alonso-Abella, et al. (2005)
	9/10	1.05-1.46	Dhimish and Alrashidi (2020)
Amorphous	–/–	0.5 (on triple junction)	Dhere, et al. (2010)
	–/6	1 (on triple junction roof shingle)	Adelstein and Sekulic (2005)
		1	Osborn (2009)
		1 (single junction)	Apicella, et al. (2008)
		1 (dual junction)	Pietruszko, et al. (2009)
	–/5.5	10 (module) 0.6 (system)	Marion et al. (2001), Ross, et al. (2006)
		1	Foster, et al. (2006)

use of either modeling techniques or vigorous measurements on modules installed in the field. They have predicted different degradation rates based on the number of module samples considered, years of exposure, and the geographic locations they are installed at, such as hot and humid or cold ones. A few degradation rates along with the number of modules considered and field exposure in years are illustrated in Table 10.3.

10.7 Conclusions

The power generation from PV modules and hence PV system installed in the field does not remain the same throughout its lifespan but decreases though at a small rate and almost linearly. The causes of such degradation could be continuous outdoor exposure to temperature, humidity, UV exposure, thermal cycling, etc. The study indicates that the PV degradation rate varies between

–0.4% and –2.0%/year. The quantification tests may not be sufficient to predict PV module lifetime under field conditions. The researchers are making efforts in developing qualification tests more quantitatively by creating a comparative rating system for various conditions PV modules come across in the field worldwide. Many techniques are being developed by people to estimate the accurate degradation rate of PV module. But, due to nonavailability of information about power output from single module, failures due to module degradation are difficult to predict. Furthermore, such failures affect the economic structure of the project severely, and therefore, all associated stakeholders have started taking serious interest in reliability and lifetime of PV system. They both are dependent on energy contributed and degradation modes the PV modules are undergoing through. Evidences indicate discoloration of encapsulant and corrosion are key modes and temperature and humidity are observed to be the primary causes of degradation modes. In order to analyze and estimate degradation rate accurately, intelligent techniques such as artificial intelligence and machine learning could be incorporated into study and make it an entirely new arena for research in PV industry.

References

- Adelstein J. and Sekulic B., Performance and reliability of a 1-kW amorphous silicon photovoltaic roofing system. *Proceedings of the 31st PV Specialists Conference*, Lake Buena Vista, FL, pp. 1627–1630, 2005.
- Alonso-Abella M., et al. Toledo PV plant 1 MWp—10 years of operation. *Proceedings of the 20th European Photovoltaic Solar Energy Conference*, Barcelona, Spain, pp. 2454–2457, 2005.
- Apicella F., et al. Thin film modules: long term operational experience in Mediterranean climate. *Proceedings of the 23rd European Photovoltaic Solar Energy Conference*, Valencia, Spain, pp. 3422–3425, 2008.
- Bosco N. Reliability concerns associated with PV technologies. *Materials Science*, 2010.
- Charki A., Laronde R. and Bigaud D. Accelerated degradation testing of a photovoltaic module. *Journal of Photonics for Energy*, Vol. 3, p. 033099, 2013.
- Cocca M., D'Arienzo L. and D'Orazio L. Effects of different artificial agings on structure and properties of whatman paper samples. *Materials Science*, Vol. 2011, p. 7, 2011.
- del Cueto J.A., Trudell D. and Sekulic W. Capabilities of the high voltage stress test system at the outdoor test facility (Report). DOE Solar Energy Technologies Program Review Meeting, NRELICP-520-38955, 2005.
- Dhere N.G., Pethe S.A. and Kaul A. Photovoltaic module reliability studies at the Florida solar energy center. *IEEE International Reliability Physics Symposium (IRPS)*, pp. 306–311, 2010.
- Dhimish M. and Alrashidi A. Photovoltaic degradation rate affected by different weather conditions: A case study based on PV systems in the UK and Australia. *Electronics*, Vol. 9 (4), p. 14, 2020.

- Escobar L.A. and Meeker W.Q. A review of accelerated test models. *Statistical Science*, Vol. 21(4), pp. 552–577, 2006.
- Foster R.E., et al. Field testing of CdTe PV modules in Mexico. *Proceedings of the 35th American Solar Energy Society Annual Solar Conference*, Denver, CO, 2006.
- Hacke P., et al. System voltage potential-induced degradation mechanisms in PV modules and methods for test. *37th IEEE Photovoltaic Specialists Conference*, Seattle, WA, pp. 814–820, 2011.
- Haillant O., David D. and Allen Z. An Arrhenius approach to estimating organic photovoltaic module weathering acceleration factors. *Solar Energy Materials and Solar Cells*, Vol. 95, pp. 1889–1895, 2011.
- Hedström J. and Palmblad L. Performance of old PV modules: measurement of 25 years old crystalline silicon modules (Report). Elforsk Rapport 06:71, October 2006.
- Jansen K.W. and Delahoy A.E. A laboratory technique for the evaluation of electrochemical transparent conductive oxide delamination from glass substrates. *Thin Solid Films*, Vol. 423, pp. 153–160, 2003.
- Jordan D.C. and Kurtz S.R. Photovoltaic degradation rates — An analytical review. *Progress in Photovoltaics: Research and Applications*, Vol. 21, pp. 12–29, 2013.
- Kemp M.D. Control of moisture ingress into photovoltaic modules. *31st IEEE Photovoltaic Specialists Conference and Exhibition*, Lake Buena Vista, FL, 2005.
- King D.L., et al. Photovoltaic module performance and durability following long-term field exposure. *Progress in Photovoltaics: Research and Application*, Vol. 8, pp. 241–256, 2000.
- Kurtz S., et al. Evaluation of high-temperature exposure of photovoltaic modules. *Progress in Photovoltaics: Research and Applications*, Vol. 19, pp. 954–965, 2011.
- Lannoy A. and Procaccia, H. *Evaluation et maîtrise du vieillissement industriel*. Edition Lavoisier, Paris, 2005.
- Laronde R., Charki A. and Bigaud D. Lifetime estimation of a photovoltaic module subjected to corrosion due to damp heat testing. *Journal of Solar Energy Engineering*, Vol. 135, pp. 021010–021017, 2012.
- Luo W., et al. Potential-induced degradation in photovoltaic modules: A critical review. *Energy & Environmental Science*, Vol. 10, pp. 43–68, 2017.
- Marion B., et al. Performance summary for the first solar CdTe 1-kW system (Report). Lakewood, CO: NREL/CP-520-30942, October 2001.
- Molenbroek E., Waddington D.W. and Emery K.A. Hot spot susceptibility and testing of PV modules. *Conference Record of the 22th IEEE*, Las Vegas, NV, Vol. 1, pp. 547–552, 1991.
- Munoz M.A., et al. Early degradation of silicon PV modules and guaranty conditions. *Solar Energy*, Vol. 85, pp. 2264–2274, 2011.
- Nehme B., et al. Assessing the effect of temperature on degradation modes of PV panels. *REDEC'20the International Conference on Renewable Energy for Developing Countries*, Marrakech, Morocco, 2020.
- Oreski G. and Wallner G.M. Evaluation of the aging behavior of ethylene copolymer films for solar applications under accelerated weathering conditions. *Solar Energy*, Vol. 83, pp. 1040–1047, 2009.
- Osborn D.E. Long term field performance of amorphous silicon (a-Si) laminates in large scale photovoltaic deployments. *Proceedings of the 38th American Solar Energy Society Annual Solar Conference*, Buffalo, NY, 2009.

- Osterwald C.R., Pruett J. and Moriarty T. Crystalline silicon short-circuit current degradation study: Initial results. *Conference Record of the 31st IEEE Photovoltaic Specialists Conference*, Lake Buena Vista, FL, pp. 1335–1338, 2005.
- Osterwald C.R., et al. Degradation analysis of weathered crystalline-silicon PV modules. *Conference Record of the Twenty-Ninth IEEE Photovoltaic Specialists Conference*, New Orleans, LA, pp. 1392–1395, 2002.
- Osterwald C.R. and McMahon, T.J. History of accelerated and qualification testing of terrestrial photovoltaic modules: A literature review. *Progress in Photovoltaics: Research and Applications*, Vol. 17, pp. 11–33, 2009.
- Pan R., Kuitche J. and Tamizhmani G. Degradation analysis of solar photovoltaic modules: Influence of environmental factor. *Proceedings of the Annual Reliability and Maintainability Symposium*, Lake Buena Vista, FL, 2011.
- Park N.C., Oh W.W. and Kim D.H. Effect of temperature and humidity on the degradation rate of multicrystalline silicon photovoltaic module. *International Journal of Photoenergy*, Vol. 2013, p. 9, 2013. Article ID 925280.
- Pietruszko S.M., Fetlinski B. and Bialecki M. Analysis of the performance of grid connected photovoltaic system. *Proceedings of the 34th IEEE PV Specialist Conference*, Philadelphia, PA, pp. 48–51, 2009.
- Pingel S., et al. Potential Induced Degradation of solar cells and panels. *35th IEEE Photovoltaic Specialists Conference*, Honolulu, Hawaii, pp. 002817–002822, 2010.
- Quintana M.A., et al. Commonly observed degradation in field-aged photovoltaic modules. *Proceedings of the 29th IEEE Photovoltaic Specialists Conference*, New Orleans, LA, pp. 1436–1439, 2002.
- Quintana M.A., et al. Diagnostic analysis of silicon photovoltaic modules after 20-year field exposure. *Conference Record of the Twenty-Eighth IEEE Photovoltaic Specialists Conference*, Anchorage, AK, pp. 1420–1423, 2000.
- Raghuraman B., et al. An overview of SMUD's outdoor photovoltaic test program at Arizona State University. *IEEE 4th World Conference on Photovoltaic Energy Conversion*, Waikoloa, HI, pp. 2214–2216, 2006.
- Realini A. Mean time before failure of photovoltaic modules. Final Report (MTBF Project) (Report). Federal Office for Education and Science Technical Report, BBW 99.0579, 2003.
- Reis A.M., et al. Comparison of PV module performance before and after 11-years of field exposure. *Proceedings of the 29th PV Specialists Conference*, New Orleans, LA, pp. 1432–1435, 2002.
- Ross M., et al. Improvement in reliability and energy yield prediction of thin-film CdS/CdTe PV modules. *Proceedings of the 4th World Conference on Photovoltaic Energy Conversion*, Waikoloa, HI, pp. 2148–2151, 2006.
- Rueland E., et al. Optical I-crack detection in combination with stability testing for inline inspection of wafers and cells. *Proceedings of 20th EU PVSEC*, Barcelona, pp. 3242–3245, 2005.
- Sakamoto S. and Oshiro T. Field test results on the stability of crystalline silicon photovoltaic modules manufactured in the 1990s. *3rd World Conference on Photovoltaic Energy Conversion*, Osaka, pp. 1888–1891, 2003.
- Saleh I.M., Abouhdima I. and Gantrari M.B. Performance of thirty years stand alone photovoltaic system. *Proceedings of the 24th European Photovoltaic Solar Energy Conference*, Hamburg, Germany, pp. 3995–3998, 2009.

- Sanchez-Friera P., et al. Analysis of degradation mechanisms of crystalline silicon PV modules after 12 years of operation in Southern Europe. *Progress in Photovoltaics: Research and Application*, Vol. 19, pp. 658–666, 2011.
- Schütze M., et al. Laboratory study of potential induced degradation of silicon photovoltaic modules. *2011 37th IEEE Photovoltaic Specialists Conference*, Seattle, WA, pp. 000821–000826, 2011.
- Schütze M. et al. Investigations of potential induced degradation of silicon photovoltaic modules. *26th European Photovoltaic Solar Energy Conference*, Hamburg, Germany, 2011.
- Short W., Packey D.J. and Holt T. A manual for the economic evaluation of energy efficiency and renewable energy technologies (Report) / NREL. Report NREL/TP-462-5173, March 1995.
- Vazquez M. and Ignacio R.S. Photovoltaic module reliability model based on field degradation studies. *Progress in Photovoltaics: Research and Applications*, Vol. 16, pp. 419–433, 2008.
- Wohlgemuth J.H. and Kurtz S. Reliability testing beyond qualification as a key component in photovoltaic's progress toward grid parity. *IEEE International Reliability Physics Symposium Monterey*, Monterey, CA, 2011.
- Wohlgemuth J.H., Cunningham, D.W., Nguyen, A.M., Miller, J. Long term reliability of PV modules. *Proceedings of the 20th European Photovoltaic Solar Energy Conference*, Barcelona, Spain, pp. 1442–1446, June 6–10, 2005a.
- Wohlgemuth J.H., Cunningham, D.W., Nguyen, A.M., Miller, J. Long term reliability of PV modules. *Proceedings of the 20th European Photovoltaic Solar Energy Conference*, Barcelona, Spain, pp. 1942–1948, 2005b.
- Zimmerman C.G. Time dependent degradation of photovoltaic modules by ultraviolet light. *Applied Physics Letter*, Vol. 92, p. 241110, 2008.

Performance and Reliability Investigation of Practical Microgrid with Photovoltaic Units

**Burhan U Din Abdullah, Shiva Pujan Jaiswal,
Suman Lata, and Suman Dulal**

Sharda University

Vivek Shrivastava

NIT Delhi

CONTENTS

11.1	Introduction	256
11.2	Technological Development	257
11.3	PV Design.....	260
11.3.1	Maximum Power Point Tracking.....	260
11.3.2	Boost Converter.....	263
11.4	PV Unit	264
11.4.1	Grid-Connected PV Unit.....	264
11.4.1.1	Components.....	265
11.4.2	Stand-Alone PV Unit	266
11.4.3	Advantages of a Grid-Connected Unit	267
11.4.4	Disadvantages of a Grid-Connected PV Unit.....	267
11.5	Simulated PV Unit with Grid Connection	269
11.6	Simulation Results and Discussion.....	270
11.6.1	Input to PV Unit	270
11.6.2	Effect on PV Parameters by Varying Irradiation and Temperature.....	271
11.6.3	Dynamic Performance of Simulated PV Unit During Variation of the Solar Irradiance When Connected to the Grid	272
11.7	Improvements in the PV Unit Connected to Grid	276
11.7.1	Economic Aspect of Grid-Connected PV Unit	278
11.7.2	Reliability Associated with Grid-Connected PV Unit.....	279
11.8	Case Study	280
11.8.1	Reliability Data.....	283
11.8.2	Sensitivity Analysis	284
11.9	Conclusion	286
	References.....	287

11.1 Introduction

Owing to the sudden rise in environmental effects, such as greenhouse gas (GHG) pollution, thermal leaks, ozone layer degradation, climate change, noise, depletion of fossil resources, a sudden increase in electricity demand, and sudden change in fuel prices, the evaluation of a power grid has drawn public interest. On a daily basis, the global energy demand is growing at a faster rate than the world's population. As a consequence, the advent of sophisticated electronic gadgets that involve a constant power supply has resulted in a strong demand for a stable power supply. Currently, solar energy has been shown as the main source of renewable energy (RE) (Elizondo et al., 2017). There are several places on the planet which are not well connected to the electricity grid. Many areas are still linked to the grid, but they do not access power for around 10–12 hours a day, causing residents' economic activities to suffer as a consequence. Sources of RE like wind, solar, and biomass are abundant in all of these locations (Bhadoria et al., 2020).

Our society or industry is powered by energy, and its availability is a requirement for continued operation. During the last three decades, the Global Total Primary Energy Supply (GTPES) has expanded by about 70%, while the value of primary energy sources derived from fossil fuels has remained nearly constant. Because of two major factors, this energy situation appears to be unsustainable: oil and gas reserves are depleting and their usage is a threat to the environment and can't be ignored. Furthermore, many governments regard rising prices and external heavy reliance as major issues related to fossil fuels. In the countryside, there are a lot of properties or photovoltaic (PV) farmlands next to the roads. In comparison to stand-alone units, grid-connected PV units contribute to more than 99% of PV installed power (which uses batteries). Fuel cells are not needed in a grid-connected PV unit since the PV plant's entire output is transmitted to the grid for transmission, delivery, and use. As a result, the PV power-generated reduces the use of certain grid-feeding energy sources, such as hydro as well as fossil fuels, and the savings act as battery storage as in a unit, providing the same power regulatory oversight and backup as a rechargeable battery would in a stand-alone method. The power of the Sun has been unleashed thanks to this concept, as well as cost reductions, technological advancements, concern for the environment, and appropriate incentives and regulations. The complex modeling, architecture, and control mechanism of a grid-connected PV, power grid implemented via the main AC bus are investigated in this chapter. PV units use the Maximum Power Point Tracking (MPPT) technique to extract maximum electricity from their networks as solar irradiation changes; furthermore, various updated improvements in PV connected to the grid and their impacts on reliability and economy are also discussed.

11.2 Technological Development

Our civilization and business are propelled by energy, and its availability is a must for their continued operation. Over the last three decades, the GTPES has also increased by around 70%, although the proportion of primary energy supplies derived from fossil fuels has stayed nearly unchanged. Furthermore, several policymakers consider cost and global dependence to be major issues linked to fossil fuels. With the growing challenge of climate change and the loss of fossil fuel supplies, hybrid clean energy production is proving to be the most cost-effective way to fulfill our energy needs. According to World Energy Scenarios, global primary energy demand will begin to rise at a rapid pace until 2050. Meeting regional and global energy demands would be a major problem for the planet (Xu et al., 2019). There is no global solution to the energy shortage issue to achieve a prosperous future. Regional approaches must be created. Sustainable, reliable, and safe energy supply for everyone is a global target. The microgrid unit is capable of meeting the load requirements of a distant, isolated area for a few households.

Microgrid power units, which combine PV and wind energy with diesel generators, are being explored as a feasible energy source and an economically viable option (Diab et al., 2019). Energy is among the most important inputs for many daily tasks in the modern world. The most widely used fuels are oil, coal, shale gas, hydro, and nuclear power (Singh and Jaiswal, 2020). Only hydro may be called a green energy source, whereas the other forms are major sources of emissions on a local, regional, and global scale. Nuclear power is promoted as an RE alternative by nuclear lobbyists, but there are significant questions over its protection, as well as the handling of radioactive waste.

Grid-connected PV power sources are available in a variety of sizes and power levels to meet a variety of requirements and applications (Singh and Jaiswal, 2020), varying from a small PV module with a power rating of about 200 W to almost a billion modules for power units with a capacity of more than 100 MW (Sood and Abdelgawad, 2019). A unit of one or a few solar cells, an inverter, as well as many other devices and electrical parts that use sun's energy to generate electricity, is called a PV unit. PV units are available in a wide range of types, from small rooftops or portable units to massive utility-scale power plants. However, as off-grid PV units, PV units may function independently.

Over the last 5 years, PV generation has risen at a 60% annual pace, exceeding over 33% of total wind-generated electricity potential, and is rapidly turning into an integral component of the energy mix in some territories. The price of solar modules has decreased, which has fueled this trend. This expansion has prompted the development of traditional PV control units from a simple one-phase grid-connected unit toward a more advanced topology to

improve performance, power removal from modules, and consistency at no additional cost (Jenkins and Thornycroft, 2018).

Assessments of PV device output that are accurate and reliable are crucial for the PV industry's continued development. Benchmarks of consistency for current goods are established through performance assessments. They are a critical metric for technical staff in identifying potential requirements. They are critical instruments for assessing products and performance consistency to direct potential decision-making for unit integrators to end-users (Marion et al., 2005).

The world's most pressing question today is how to satisfy the world's ever-increasing need for oil. Furthermore, the accelerated decline of traditional power sources, as well as their inexhaustibility, has necessitated urgent research into alternative energy sources as alternate energy sources. PV and wind energy, among the alternative energy sources, have received a lot of recognition and are considered to be the most promising energy technologies for generating electricity (Jaiswal et al., 2019b). PV energy has proven to be a unit that could potentially help to replace fossil fuel as the major source of electricity across the world if harnessed efficiently.

The impact of shading (Rodriguez and Amaratunga, 2008) on the efficiency of PV modules has been extensively investigated. MPPT strategies may be used to mitigate shading losses by extracting the global peak power, unit structures, converter typologies, and PV array settings, among other things. Increased electricity consumption, increased understanding of global warming, and the loss of traditional energy supplies have contributed to the development of RE (Noureldeen and Ibrahim, 2018). With the aid of the sample regression function (SRF) principle and a proportional-integral (PI) controller, the suggested design is investigated for irradiance variance utilizing a decoupled power control. Specific PV modules used to create the PV array have performance characteristics that closely follow the manufacturer's curve, and inverter heat transfer coefficient at lower light intensity has harmonic distortion that is far inside the limits. This demonstrates that high-quality electricity is supplied to the unit. In addition, as opposed to other sophisticated and specialized controllers, SRF via PI controller needs less computing time.

Of all RE sources, PV is the most widely used and produced. Stand-alone units and grid-connected units are two types of PV power harnessing typologies. A suitable current controller is needed to inject high-quality power into the grid. In the literature, there are several models and controls for grid-connected PV units aimed at reducing power quality problems and delivering high-quality power. Grid-connected PV power units are available in a variety of sizes and power levels to meet a variety of requirements and uses, varying from a simple PV module with a power rating of about 220 W to over a thousand modules for PV plants with a capacity of over 110 MW (Kouro et al., 2015). During the last decade, the PV industry has grown at a breakneck pace, establishing itself as a viable option and an RE source in

several countries. PV matrix converters have been evolving in tandem with the decline in price and rise in performance of PV components, to meet more stringent specifications and standards. These rules are being updated to reflect a modern power unit situation in which RE sources play a significant role in the energy mix.

PV units have matured into a standard technology for electricity production, although they can have several detrimental consequences on the electricity grid. There have been studies on three of these types of impacts. In the RSCAD software, a solar array PV test method was found and simulated. At the point of common coupling (PCC), the harmonic material added by a 4MW PV device with a three-phase, two-level direct current/alternating current (DC/AC) inverter was found to be within acceptable limits. The effects of different load capacity factors and PV penetration rates on reactive power support were investigated. The antiislanding feature of the PV process is influenced, and it was discovered that for the unit under consideration, the vital islanding period of the said PV unit is 125 ms. In comparison to stand-alone devices that use batteries, grid-connected PV units account for almost all of the installed power around the world. Grid-connected PV units with no batteries are more cost-effective and need less maintenance. Grid-connected PV does not need batteries since the energy produced is submitted to just the grid for the transmitter, storage, and use. This reduces the load on other power sources that feed the grid (Jenkins and Thornycroft, 2018).

The study and creation of new DC-DC converter configurations for PV applications have made significant strides during the last decade. In the vast majority of instances, the recently developed typologies are full-power converters, which must process the entire sum of PV sheet (or PV string) power. PV energy has just recently been introduced into the construction unit. To begin with, units were made up of a large number of modules linked in series and parallel to a single large rectifier (central inverter). At this time, technology has progressed to architectures that consist of a set of parallel-connected panels as well as a PV inverter (Velasco-Quesada, 2009). The number of components per inverter is approximately 20–30, and there would be many more inverters as the activity needs (approximately 5kW per alternator). In contrast to a central inverter design, this architecture increases PV device stability in the face of unusual conditions. Since the amount of PV modules working under such a standard MPPT converter is decreased, mismatching and shadowing errors are reduced.

Other developments, including those that integrate modules with only a PV inverter and a DC–AC connector each (ac modules), are growing in popularity (Roman et al., 2006). Autonomous solar PV and wind energy units have been documented by several authors (Xu et al., 2019; Diab et al., 2019). However, an autonomous device with just one energy source necessitates a very broad storage capacity and related PE parts. A hybrid energy device, which combines two or more types of energy sources, may minimize battery energy storage (BES) requirements while still increasing efficiency. Wind and solar power are

perfect partners in the hybridization phase. Both have been seen to be comparable to one another in regular and annual behavior patterns.

Several researchers have proposed independent solar-fossil hybrid power units (Noureldeen and Ibrahim, 2018), recognizing the benefits of this mix. This generator is the most popular unit with small wind turbine applications. With PMSG, a gearless setup is feasible; however, it necessitates the use of a 100% microgrid-rated converter as well as a more expensive unit. Several scholars have also used a squirrel cage generator in conjunction with a wind-solar hybrid device (SCIG). Many scholars have also investigated doubly-fed induction generator (DFIG) for the production of electricity from the wind power plants.

11.3 PV Design

The PV cell is constructed with the help of criteria discussed in the above section. A PV module could be directly transferred to the unit; however, as we all understand, the generation of the panel varies during daytime because of the exposure to variable thermal radiations.

11.3.1 Maximum Power Point Tracking

The MPPT algorithm is a method for calculating the probability of the peak point of the panel. MPPT is a charge controller algorithm that extracts the maximum usable power from a PV module under some circumstances. Maximum power point (MPP) refers to the value at which a PV module will deliver the most power. Solar radiation, atmospheric temperature, and solar cell heat also affect maximum capacity. MPPT aims to keep the solar voltage level as similar as possible to MPP under different weather conditions (Jenkins and Thornycroft, 2018). They must run at their MPPT regardless of the homogeneous shift in environmental conditions to constantly gather the full power from the PV collection. Perturb and Observe (P&O) and Incremental Conductance (Inc-Con) are the two most widely used algorithms for PV applications since they are simple to introduce. The maximum power provided by PV panels is not necessarily constant and set at the very same operating conditions; it fluctuates depending on environmental factors such as solar radiation exposure, shadow, and temperature. To get the most power out of your unit, you'll need to use an MPPT algorithm that changes the power extraction dynamically. One of the most critical characteristics of all MPPT algorithms is convergence speed. Any variation in the MPPT increase time boosts the unit's stability and increases the power production and performance of the entire device (Marion et al., 2005). When the solar irradiance varies, the MPPT method is used to obtain the full production capacity from the PV collection.

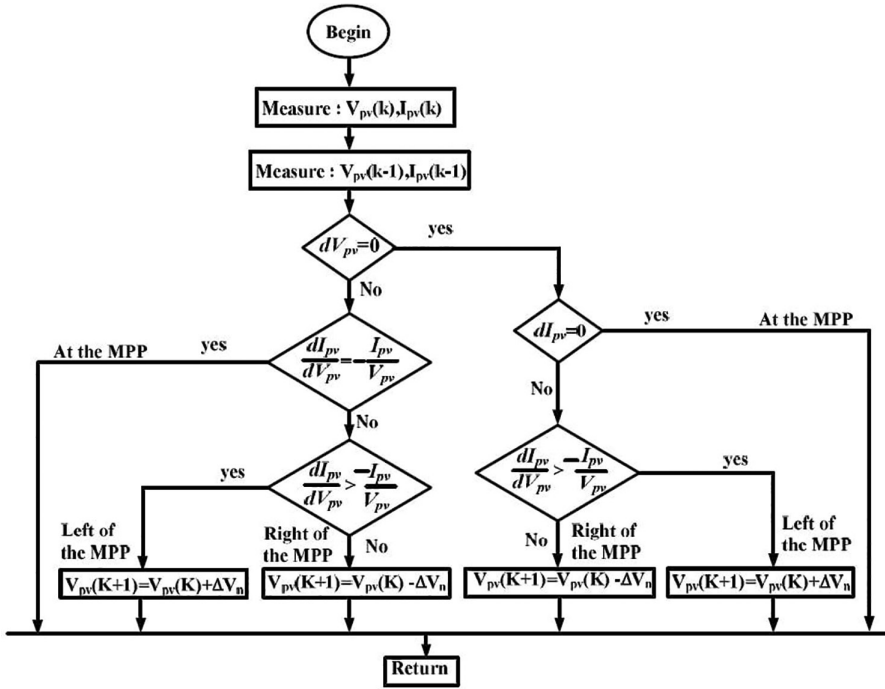


FIGURE 11.1
Flowchart of progressive conductance in MPPT method.

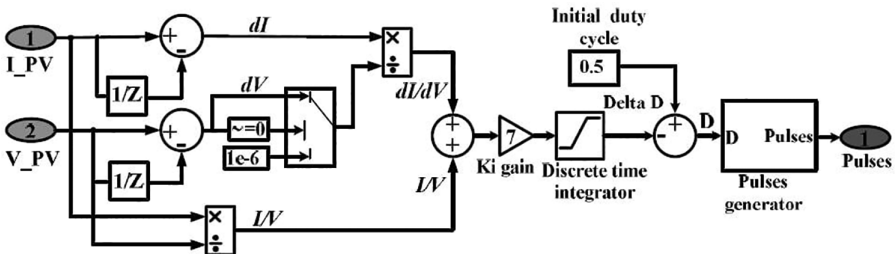
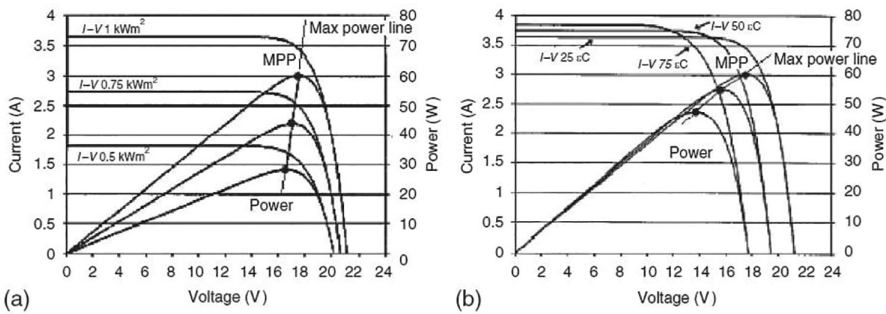


FIGURE 11.2
MATLAB/Simulink model of incremental conductance MPPT technique.

The gradual conductance MPPT technique is used in this paper to capture the full power since it has the tacit benefit of providing reasonable efficiency under rapid variations in solar irradiance. The related flowchart of the gradual conductance MPPT technique is shown in Figure 11.1. In addition, Figure 11.2 depicts the installation of this MPPT method in a MATLAB/Simulink model. The incremental conductance approach is based on the fact that at the MPP (Singh and Jaiswal, 2020), the slope of the P-V curves is zero.

**FIGURE 11.3**

P-V panel isolation: (a) temperature and (b) characteristics.

A PV array is usually installed in a fixed location and angled to the south to maximize energy generation at noon and during the day. To catch the most power for something like the season, perhaps for a year, the configuration of fixed panels should be carefully selected. As seen in Figure 11.3, PV arrays have had an optimal operating wise decision for the MPP. I-V characteristics show partly shaded conditions and P-V characteristics can also be obtained by the extraction method even under complex conditions (Bai et al., 2015). It's worth noting that electricity rises as voltage rises, hitting a peak value, and then drops as pressure rises, reaching a stage where current drops off. According to the peak voltage theorem, at a given temperature and insolation, this is the stage at which the load is suited to the solar panel's resistance. As seen in Figure 11.3, the I-V curve shifts as temperature or insolation levels shift and the MPP varies accordingly (Jaiswal et al., 2019a).

The MPPT improves the amount of energy that can be transmitted from the collection to a power device. The key role is on the way to change the panel's harvest voltage such that the load receives an extreme amount of electricity (Uzum et al., 2021). A switch-mode DC-DC adapter, a control unit, and a monitoring component are the three main components of most modern designs. And the energy drawn, which is retained as gravitational fields, is emitted at varying potential speeds, and the swap converter is at the heart of the whole supply. Voltage converters are programmed to have integrity as defined voltage or current, which corresponds to the highest PowerPoint, by arranging the switch-mode portion in different topologies including buck or boost converter. This allows the output resistance to balance the battery. A controller is needed to accomplish the abovementioned mechanism by continuously monitoring the PV device and ensuring that it operates at the maximum by observing this MPP. The controller's goal is to continuously calculate the currents and voltages provided by the PV and equate them to some threshold positions to use either a voltage-controlled process or a power response control unit. The benefits of wide-band-gap (WBG) tools are slowly being incorporated into inverters for PV units. Nonsilicon resources such as

silicon carbide (SiC) or gallium nitride (GaN) are used to build WBG devices. For string, multistring, and core, in addition to AC-module PV applications, there are a variety of PV converter typologies on the market. Multilevel converters, primarily the NPC, T-type, and H-bridge, have made one of the more significant appearances of all these converter typologies, not just for high-power application but correspondingly for domestic requests as in kilowatt and LV range. A brand new group of PV converters dependent on SiC voltage control is predicted to be produced in the not-too-distant future. (Some commercial PV converters are available, but they only use SiC diodes.) The next phase of power PV units will be enabled by these latest Silicon carbide PV converters and then the subsequent gain PV converters, which will diminish the balance between output and reliability.

11.3.2 Boost Converter

The DC-DC converter is a type of electrical circuit that is used to convert DC voltage from one level to another. It works in the same way as a converter in an AC source, allowing it to phase the power factor up or down (Sánchez et al., 2021). The average current (on-off duration of a switch) of the converter may be controlled to adjust the changing DC voltages. There are also many different types of DC-DC translators that may be used to change the reference voltage depending on the input or demand requirements. The boost converter's job is to raise the voltage level. The boost converter's circuit configuration is shown in Figure 11.4.

Mostly during the ON period of a proposed inverter, the power supplied by the inductor began to increase and energy is stored. The connection is considered to be in a condition of charging. In the OFF state, the inductor's stored electricity, together with the source, begins to dissipate further into demand. The inductor total current determines the waveform, which is higher than the input voltage. The load-side energy is calculated as the product of the changing device's source-side voltage and equivalent resistance.

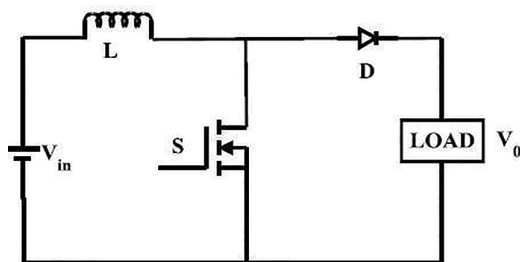


FIGURE 11.4

Circuit diagram of the boost converter.

11.4 PV Unit

The six single elements that make up the most PV units are the solar PV array, a recharge processor, battery reserve, conversion device, power meter, and the power infrastructure. The efficient installation of any of these components determines the effectiveness of the solar panels. Both elements of the grid-connected panels include a UPS, solar cells, energy storage, smart meters, a DC transit unit, and an AC bus.

On the other side, a converter and a fuel cell are not essential. While these two parts allow one to store and use your generated electricity more efficiently, they can also increase the total cost of the PV unit. Although solar PV arrays generate electricity when exposed to sunlight, additional components are needed for properly transmitting, and preserving the energy generated by the panels.

Stand-alone and grid-connected solar PV are two types of solar units.

11.4.1 Grid-Connected PV Unit

Grid-based PV units are made up of PV arrays that are associated with the grid by a power conditioning device that is planned to run analogous to the electric utility grid. The MPPT, inverter, grid interface, and control device required for efficient unit operation can all be included in the power conditioning unit. Scholars have focused on designing various electrical inverter topologies (Uzum et al., 2021) that meet the above mentioned criteria over the past two decades. Since solar cells are the gateway to a long-term PV business; further study is being done to maintain quality safety, efficiency, and inferior costs. Units that communicate with the utility network even without battery backup capabilities are the two main categories of electrical architectures for PV power arrangements (Figure 11.5).

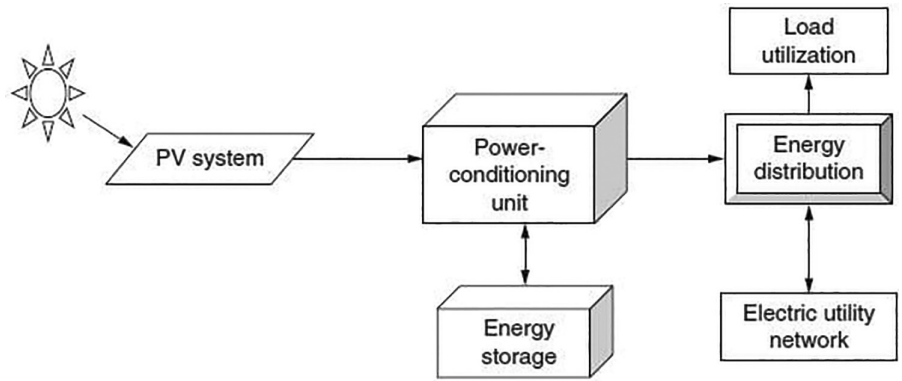


FIGURE 11.5
Major components of a photovoltaic unit.

11.4.1.1 Components

Power Conditioning Unit: The PCU selected has a significant influence on the unit's efficiency and economics. It is dependent on the type of waveform produced, which is dependent on the conversion method used, as well as the frequency filtering techniques used to remove unwanted frequencies. Whether choosing or constructing an inverter, many considerations must be taken into account: The reliability of the power conversion, specified output, and the duty rating of an inverter refers to the highest load it will provide over a given period, the voltage at the input, controlling the voltage security from high voltage, requirements for frequency, and the strength of the argument (Figure 11.6).

- Energy Storage (Battery)
- Energy Distribution
- Electric Utility Network
- Load Utilization

The PV array is connected to the MPPT to extract the maximum energy from the solar and to regulate the charging and discharging of the battery storage output concerning the load and also acts as a protective gear for the battery. The inverter used is a DC–AC, also known as the power conditioning unit, which is the most important feature of both units (PCU). The inverter is critical to the unit's performance, but it's perhaps the most difficult piece of hardware to understand. The inverter must be able to operate over a broad spectrum of voltages and current as well as provide controlled output voltage and frequency, while still delivering AC power for good power quality, such as lower total harmonic distortion and a strong power factor, as

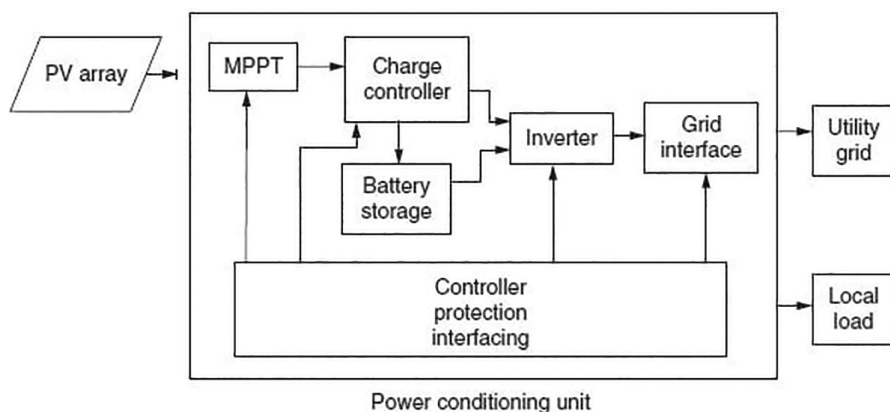


FIGURE 11.6

Block diagram of grid-connected photovoltaic system.

well as the maximum possible performance for all solar irradiance stages. Furthermore, the inverter can provide defensive devices that control the grid and, in the event of a fault, isolate the unit from both the utility grid and the PV unit.

11.4.2 Stand-Alone PV Unit

PV devices that are not connected to the grid are typically used as a backup source of electricity. They usually consist of solar loading modules, storage batteries, as well as controls or regulators. A mounting mechanism is needed for ground or roof-mounted units, and an inverter is also required if AC power is desired. They have also served as the main source in remotely accessible areas in 2009–2010 (Al-Sabounchi et al., 2013).

Batteries are also used for power storage in several stand-alone PV units, and they can help boost 40% of the total expense of a stand-alone PV device during its lifespan. Owing to a lack of time and resources to recharge the batteries, as well as inadequate battery care, these batteries trigger losses in the PV device. As a result, a battery charger is used to regulate the device and keep the battery from being overcharged or discharged. Overcharging reduces the life cycle of the battery and can cause gassing, while lowering can activate desulphurization and stratification, both reducing battery efficiency and lifespan. In PV units, batteries are widely used to store PV-generated energy all day long and then supply it with electricity whenever necessary. In particular, batteries are essential to have stable voltages for tracker units to operate on MPP (Liu et al., 2020). The tougher the plates and the more the battery could withstand deep discharges, the stronger the capacitor for defined group size (Figure 11.7).

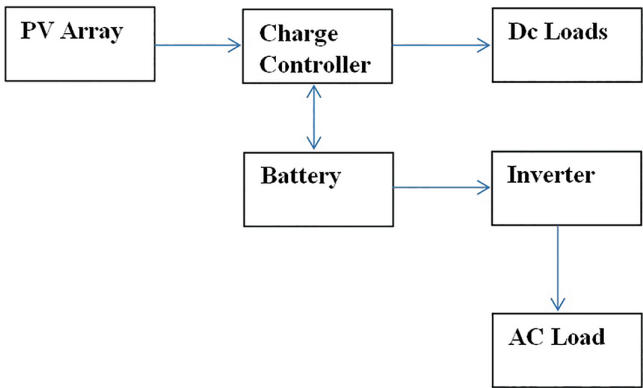


FIGURE 11.7 Stand-alone photovoltaic unit with battery and AC/DC load.

11.4.3 Advantages of a Grid-Connected Unit

The PV solar panels or collection in a PV unit, also known as a “grid-tied” or “on-grid” solar cell, are electrically attached or “tied” to the local main power electricity grid, which integrate electrical energy power into the unit (Jaiswal et al., 2021; Adefarati and Bansal, 2019). The key benefits of a grid-connected PV device include its ease of use, low operation and repair costs, and lower power bills. The downside is that to produce the necessary amount of surplus electricity, a substantial majority of solar panels must be mounted. Since grid-tied structures feed their energy from solar power into the unit, costly backup batteries are unnecessary and can be left out of most grid-tied designs. Furthermore, since this form of a PV device is permanently attached to the infrastructure, solar energy usage and solar panel sizing measurements are not necessary, allowing for a wide variety of choices, including a unit as small as 1.0kWh mostly on the rooftop to help minimize your energy costs, or a much larger floor-mounted installation big enough to practically eradicate your electricity bills.

Figure 11.8 shows how the grid-connected PV usually operates. The operation can be categorized into three sections.

1. Generation
2. Conversion
3. Supply.

In the generation section, the simple conversion of solar energy to electricity takes place by the PV panels. The electricity obtained is DC form and is very fluctuating because of various environmental issues like changing of solar radiations. To overcome this problem, charge controller is used which is mostly PWM or MPPT controllers and is used to regulate the charging and discharging of storage. Simultaneously, the DC power generated can be used to meet the local DC demand such as light bulbs, etc. The surplus power can then be transferred to the grid by the conversion process which is done with the help of a DC/AC inverter. As the transmission takes place in the AC form, protective measures such as isolators and circuit breakers are connected to overcome any unfavorable circumstances. A meter is also being installed to track the electricity supplied to the utility grid to receive rebates in the bill.

11.4.4 Disadvantages of a Grid-Connected PV Unit

Owing to the absence of batteries in on-grid solar units, they are unable to work or produce power during an outage for safety purposes. Since blackouts typically arise when the power unit is disrupted, if the power array continued to pump electricity through a damaged grid, it will jeopardize the protection of everyone working to restore the network's faults. Since the amount of PV modules working under a single MPPT converter is decreased, mismatching and shadowing errors are reduced (Roman et al., 2006). They can't generate RE

at night even when there's no sunshine, so they can't help you save money on your energy bill. They offer you less of an opportunity to save electricity. The issue with integrating RE sources with the traditional grid is power efficiency. Frequency fluctuation, flickering, unbalanced current and voltage harmonics, as well as voltage fluctuations, are all issues that may affect power efficiency. Switching modules used during power electronics applications, which are now an integral part of Renewable Energy Source (RES) technology, are the source of these challenges. In the case of solar PV, the severity of these problems is determined by the position of the PV module, the distributed device architecture, and the degree of solar PV penetration. When it comes to electricity, the form of the rotor, the density, and the strength of the wind all play a role. In all RES interconnected grids, power quality problems have been identified in the literature to exist at the delivery, storage, and transmission levels. Solar PV has intermittent characteristics due to rapid changes in sunlight and clouds, which induce voltage fluctuations and unbalance, while wind power production is affected by changing wind speed (Basit et al., 2020).

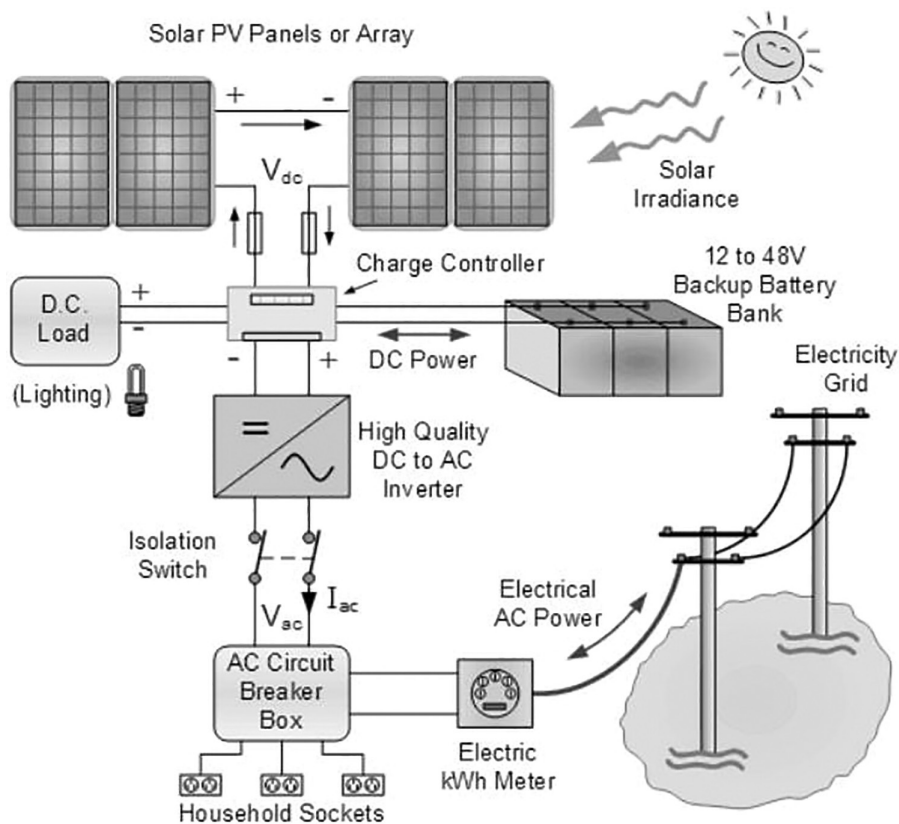


FIGURE 11.8

Operation of a grid-connected PV unit.

11.5 Simulated PV Unit with Grid Connection

The power unit consists of a 1MW PV plant and is connected to a grid at other sites. The PV plant is attached to the central PCC network to inject produced electricity and improve efficiency to provide the needed electricity production. The PV unit comprises several PV modules electrical coupled in parallel-series configurations. The PV unit also includes a DC/DC boost converter to enhance array emission voltage and an accumulated DC/AC inverter to transform produced DC power to AC power. The proposed control MPPT approach is used to get the most power out of a PV unit when the Sun irradiation changes. Additionally, the PV plant is linked to the PCC-bus via 260 V/25 KV/Y transformers (Figures 11.9 and 11.10).

The PV module is working on MPPT; through the incremental conductance method maximum power is being extracted from the solar PV panel.

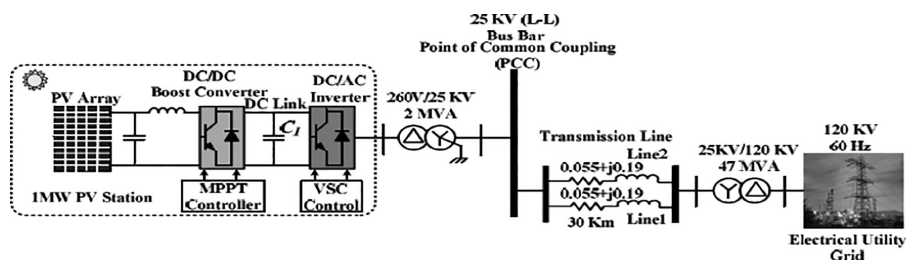


FIGURE 11.9

System configuration of studied PV connected to grid.

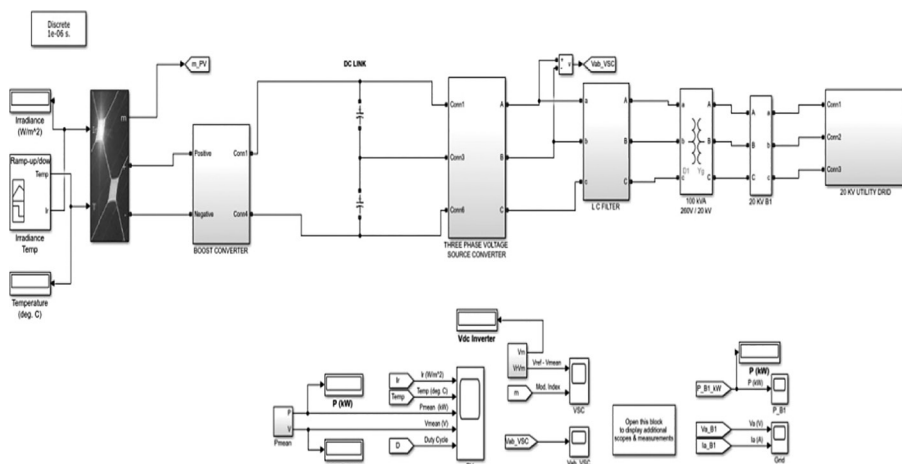


FIGURE 11.10

Simulink model (PV unit with grid connection).

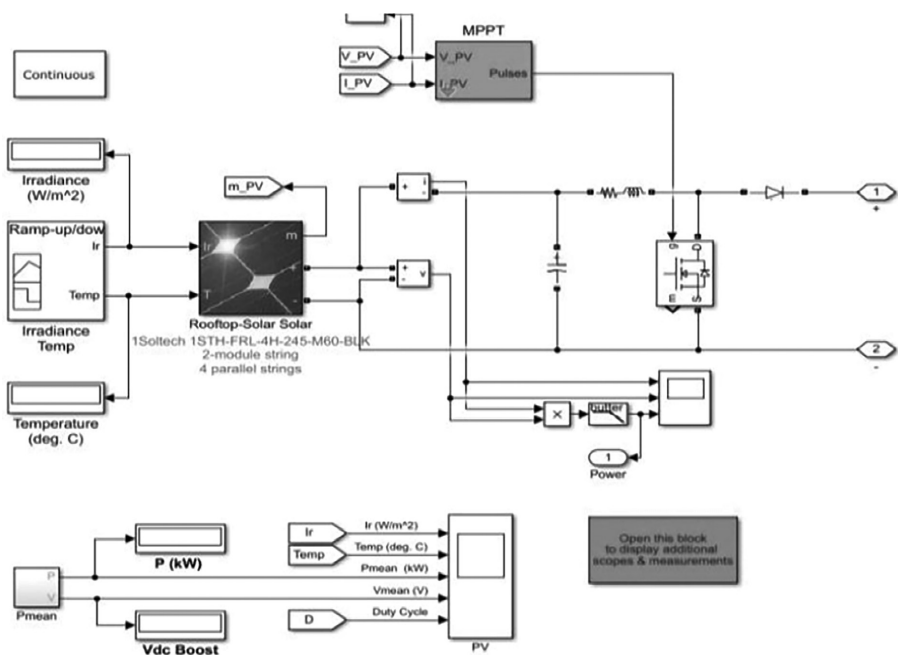


FIGURE 11.11
PV Array with MPPT.

A variable duty cycle is provided to the switch of the DC/DC boost converter, so that the output impedance matches with the input impedance (Figure 11.11).

11.6 Simulation Results and Discussion

The result of the PV power with and without MPPT is shown below; it is evident from the graphs that the power output of the model working on MPPT gives efficiently high power in comparison to the PV model working without MPPT. Hence it is advantageous for us to make the PV panel work on MPPT to draw maximum power output from the panel (Figure 11.12).

11.6.1 Input to PV Unit

The inputs to the PV unit are irradiance in “W/m²” and temperature in degree Celsius. In this work, variable irradiance and temperature has been used (Figure 11.13).

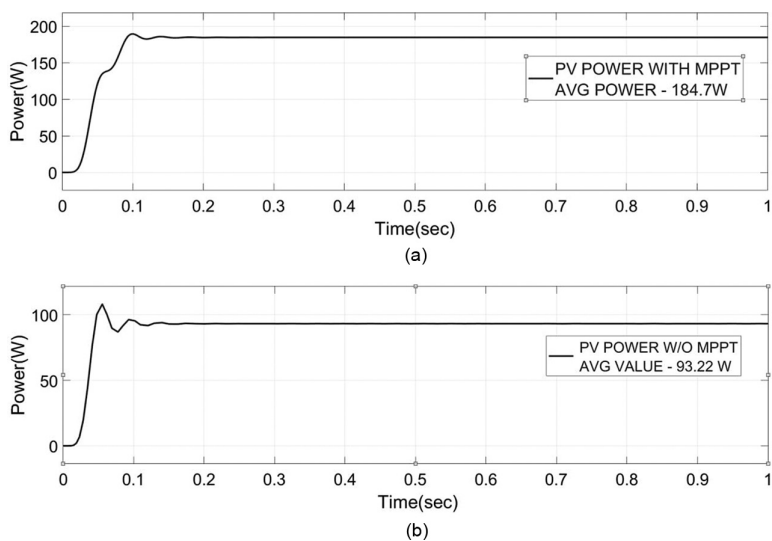


FIGURE 11.12
Comparison between PV power with and without MPPT.

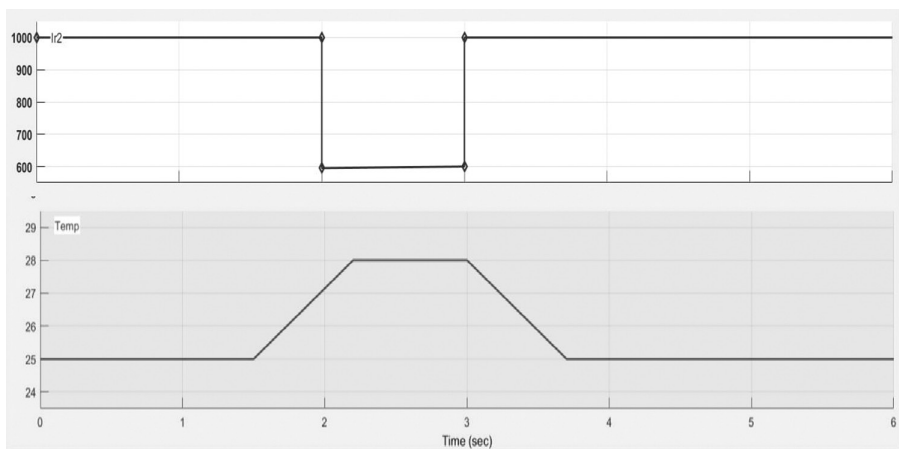


FIGURE 11.13
Irradiance and temperature input to the rooftop solar unit.

11.6.2 Effect on PV Parameters by Varying Irradiation and Temperature

From the below-shown tables, it is clear that current increases linearly with the increase in irradiation and decreases with the decrease in irradiation. The voltage on the other side increases logarithmically with the increase in irradiation. With the increase in temperature, the current increases, while the voltage decreases (Tables 11.1, 11.2, 11.3 and 11.4).

TABLE 11.1

Variable Irradiation

Time	Value	Type
0–02 seconds	1,000 W/m ²	Constant
02 seconds	999 W/m ² –599 W/m ²	Step decrease
02–03 seconds	600 W/m ²	Constant
03 seconds	599 W/m ² –1,001 W/m ²	Step increase

TABLE 11.2

Variable Temperature

Time	Value	Type
0–1.5 seconds	25°C	Constant
1.5–2.2 seconds	25°C–28°C	Linearly increasing
2.2–3 seconds	28°C	Constant
3–3.7 seconds	28°C–35°C	Linearly decreasing

TABLE 11.3Constant Irradiation (1,000 w/m² and Variable Temperature)

Irradiations (W/m ²)	Temperature (°C)	Time	Average Voltage (V)	Average Current (A)	Average Power (P)
1,000	25	0.1–1 seconds	24.96	7.40	184.4
1,000	30	0.1–1 seconds	23.63	7.64	180.5
1,000	35	0.1–1 seconds	23.33	7.56	176.2

TABLE 11.4Constant Irradiation (900 w/m² and Variable Temperature)

Irradiations (W/m ²)	Temperature (°C)	Time	Average Voltage (V)	Average Current (A)	Average Power (W)
900	25	0.1–1 seconds	24.96	6.56	159.7
900	30	0.1–1 seconds	24.34	6.88	167.5
900	35	0.1–1 seconds	24.15	6.79	163.6

11.6.3 Dynamic Performance of Simulated PV Unit During Variation of the Solar Irradiance When Connected to the Grid

The predictive response of the PV unit is explored in this portion as the solar irradiation varies. Throughout the experiment, the solar array's surface temperature was maintained constant at 25°C. The change in sun irradiation is shown in Figure 11.14. This variation, for example, depicts the shift in solar energy during the day and the shadow cast by a cloud. In Figure 11.15, the PV matrix output voltage closely follows the voltage at maximum power

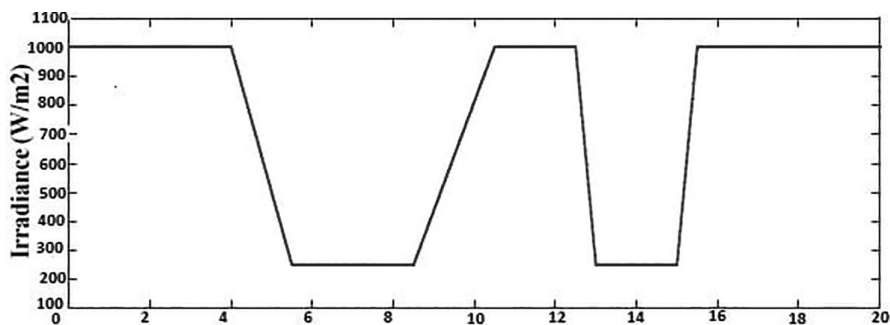


FIGURE 11.14

Solar irradiance variations on PV array.

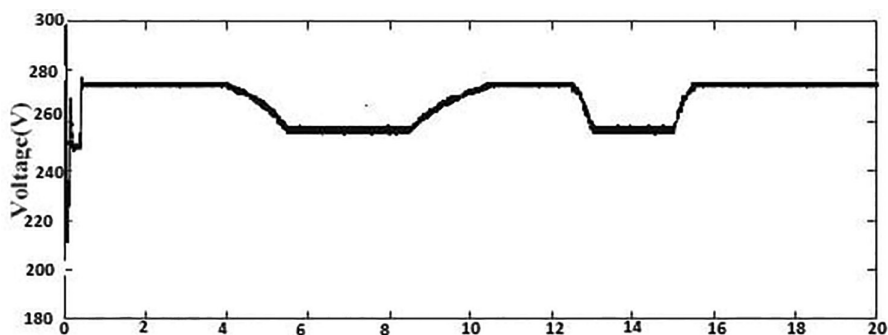


FIGURE 11.15

Voltage of PV array.

(V_{mp}) to harvest the maximum power from the PV panel when solar irradiation varies. The PV panel's maximum output power and output current is considered in the same scenario for the fluctuation of solar irradiation in Figure 11.16. In reaction to a change in solar irradiation from 1,000 to 250 W/m², the PV panel's output current drops from 367.7 to 87.2 A. The derivation of the power about the voltage is virtually zero ($dP_{pv} / dV_{pv} = 0$), as shown in Figure 11.17. As per results, the PV panel performs well at the MPP as the sun irradiation varies.

The PV unit's predictive response under daily solar change is next studied. The converter controls efficiently hold the DC link voltage constant at 500 V, independent of solar irradiation change, as shown in Figure 11.18. The reverse current axis (I_d) follows the fluctuation of solar irradiation, as shown in Figure 11.1. The inverter acts on the power factor of the unit. The active and reactive energy injected from the PV unit during the fluctuation of solar irradiation is depicted in Figure 11.20. It's worth noting that the injected active power varies with changes in solar irradiation. The PV unit's injected active power is equal to its nominal value when sun

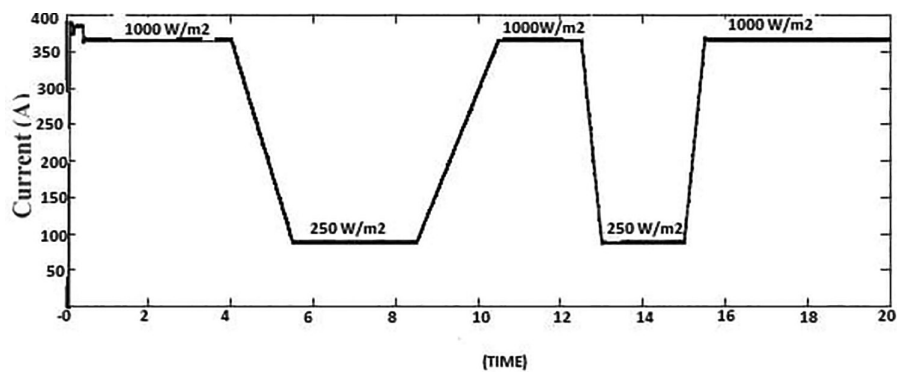


FIGURE 11.16
Current of PV array.

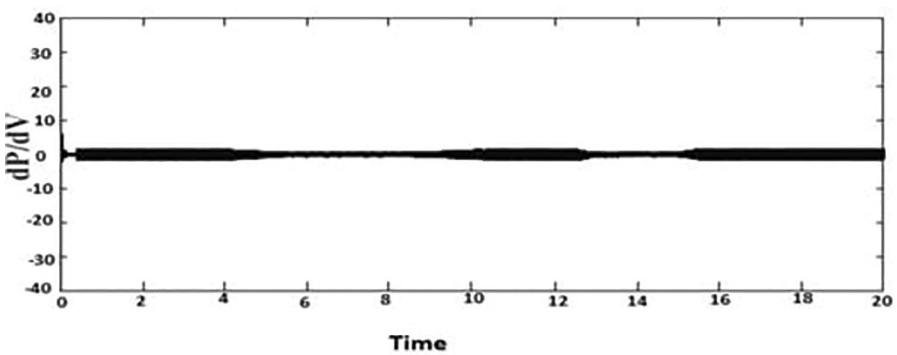


FIGURE 11.17
Derivative of PV power/voltage (dP/dV_{pv}).

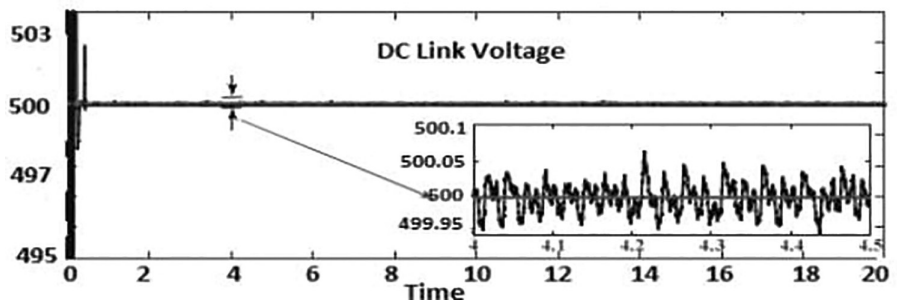


FIGURE 11.18
DC link voltage of the PV unit.

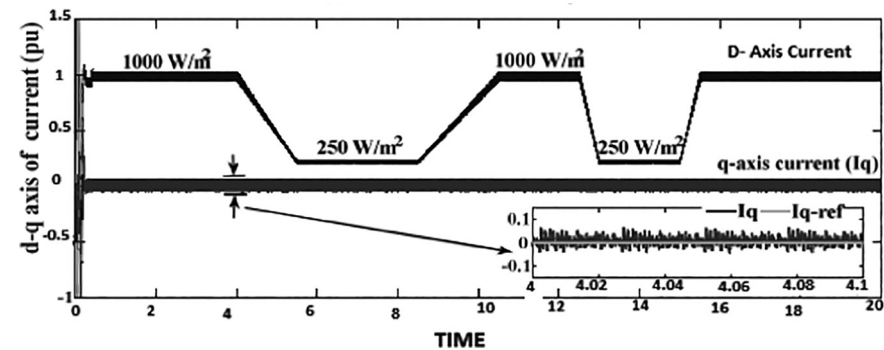


FIGURE 11.19
d-q axis components of injected current by the PV unit.

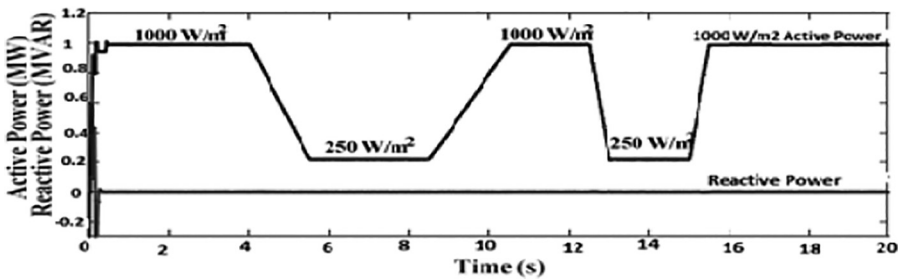


FIGURE 11.20
Active and reactive power injected by the PV unit.

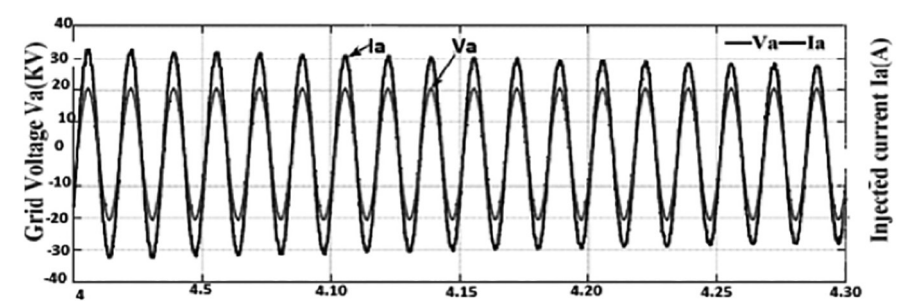


FIGURE 11.21
Grid V & I injected by the PV unit.

irradiation starts at $1,000\text{ W/m}^2$ (1 MW). When the solar irradiation falls below 250 W/m^2 , the active power injected lowers to 0.22 MW. As a result, the PV unit runs on the unit's power factor when the injected reactive power is zero. The PV unit's injected current is in phase with the mains voltage, as shown in Figure 11.21. Hence, by this suggested control method,

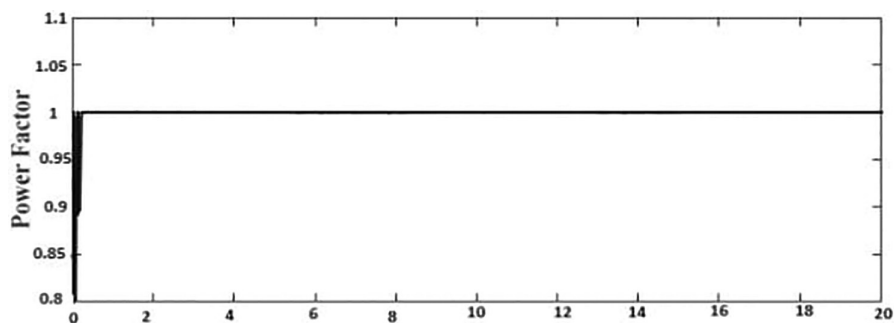


FIGURE 11.22
Power factor of the PV inverter.

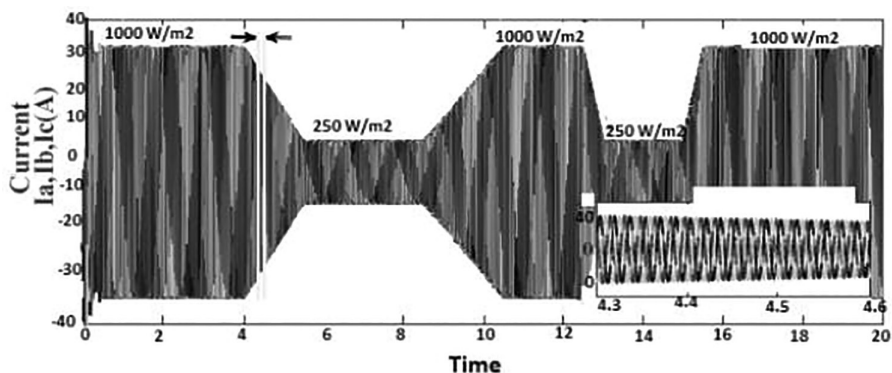


FIGURE 11.23
PV injected current to grid.

the PV unit can achieve the unit power factor illustrated in Figure 11.22, and the three-phase currents injected are depicted in Figure 11.23 under the waveforms obtained. It should be remembered that the inverter control adjusts the current amplitude based on the active power injected.

11.7 Improvements in the PV Unit Connected to Grid

In directive to increase the DC power production of a partially shaded solar array, multiple solutions are suggested: (1) the power conversion design or (2) the PV generation electrical behavior at the stage of the solar cell.

The solution that adapts a certain electricity production unit is defined by several individual PV generators pursuing the available PV modules. The PV units with equal climatic factors produce each PV variable to minimize the current string restriction. In addition, the generation of DC power is increased by a modified electronic infrastructure, which extends the full DC power supply among all cognitive models and independent PV generators. Whatever the number of PV generators, AC-module power converters (Marion et al., 2005) or full-bulb multidimensional topologies is one of the power electronic structures that allow for that method. It should be noted that this technique improves the power usage and reliability associated with PV units at the cost of increasing voltage and cost of comparison.

To avoid these flaws, other methods adjust the performance of the solar cell production company when imperfect shades are present and maintain the power conversion structure based on a single power converter (i.e., a single inverter in case of PO configuration). The most frequent is recognized by the PV module manufacturers who have the option of connecting bypass diodes with some types of saga solar cells built into the plate. The power of the PV module increases when these diodes switch on and allow the series relation limit when any of the cells are shaded. Once diodes are operated by the bypass, however, the PV generator's current/power diagrams display superfluous that one max. The maximum power mining thus includes the usage of specialized MPPT methods, which will neglect the local upper limits in comparison to the whole one. Sadly, these sophisticated algorithms seldom incorporate large inverters. A reconstruction strategy of PV generators is to increase the strength of PV-connected industrial PO-grid units now available, formed by standard PV modules and a centralized inverter supplied with a conventional MPPT algorithm. This technique is used by a survivable vector of flips, which rearchitects the PV arrays into a single line parallel, regulated by a power converter. A series of proof-of-concept experiments on a narrow grid-connected PV device with a capacity of 1.65 kWh demonstrated the viability of the solution as well as the increase in delivered power within a partial shade or in the event of panel failures. Although the drawbacks result from its greater sophistication and expense, this approach's power loss reduction may be useful for limited installation in municipal environments where even the PV generator may operate under extreme partial shadows cast by nearby obstacles.

PV generation was regarded as an energy supply (or current) that was pumped into the network, however, when the irradiance was permitted by the earliest regulations, several of which are still in use today. Metering, maintaining the voltage quality encountered by all other user groups (particularly mechanical distortion) was not breached, intrusion of DC, and lack of mains or ant grid-tie security were all covered by these regulations. As a result, PV generation was initially regarded solely as a source of negative load. As capacity increased, it became clear in certain countries that the impact of a vast number even for small generators was creating significant

effects in the power grid, and legislation was enacted to ensure PV power was consistent with current power unit practice. Reduced power production as network frequency increases, continuing operating if a short-circuit failure happens on the network and lowers the volt (known as Low-Voltage Fault Ride-Through), activity at nonunity, and varying power factor are some the steps implemented.

11.7.1 Economic Aspect of Grid-Connected PV Unit

While the solar PV industry has seen astronomical growth and reduced costs in recent years, several technical difficulties and value units must be prepared to accept order for DG tools such as Grid-Connected Photovoltaic System (GCPVS) to be competitive with conformist generation. To serve villagers in rural areas, micro grid-based RE sources may be used. PV plates, wind turbines, battery storage units, and diesel generators are all possible components of a microgrid (DG) (Fathy et al., 2020). It is critical to size these components correctly to create a microgrid that is both cost-effective and efficient. New technologies that enable the converters to do something more than having DC/AC transitions must be introduced for GCPVs to become widely adopted. Volt/VAR management (power aspect& voltage stabilizer), frequency management, storage, and new transportation protocols would all be required of modern grid-interactive inverters, all at a fair cost. Many papers have stated that the potential of the smart grid will consist largely of DG with several functional posts and well-installed Information and Communication Technology (ICT) frameworks which, aside from the revision of Distributed Network Protocols, use default supervisor control and data acquisition (SCADA) procedures such as IEC 60870-5-104 (DNP3.0). They often assert that the alternator serves as a multifunctional gate terminal, with many frameworks to enhance it to compensate for the control it introduces back into the unit. Microgrid power units, which combine PV and wind energy with diesel generators, are being explored as a promising source of energy and economically viable option. Isolated populations, in terms of energy supplies, are often seen on islands, in remote regions, and certain metropolitan areas in developed countries. Diesel generators typically meet the need for power in these countries, causing substantial concern due to the high cost of power and the high emission levels in the local atmosphere.

The dependability and performance of a PV microgrid are critical to its commercial success. The single-stage solutions, as well as the absence of ECs, are anticipated to improve reliability. After experimenting with various semiconductor configurations, a relatively good conversion performance of up to 97% was achieved. High performance is not only a selling point, but it also leads to increased stability by reducing internal thermal tension (Sahan et al., 2008).

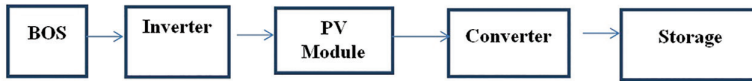
Inverters in forthcoming GCPVS designs will be required to track, respond to, and change their performance in response to real-time grid feedback.

In addition, the inverter would be able to store and exchange data with the facilities control scheme for trending, analytical, preventative, and corrective maintenance. These latest breeds of smart inverters would be able to record a variety of details, including usable battery storage times and capacity statistics, as well as provide routine power management data and alert on external events. Rethinking the function and capabilities of inverters will encourage widespread use of GCPVS while also assisting in the creation and maintenance of a more stable grid. GCPVS, unlike off-grid PV units, runs in parallel with the electronic utility grid and therefore does not need storage units. GCPVS helps in reducing GHG pollution by displacing the power used by the linked (local) load and adding additional energy to the grid when they provide surplus power (i.e., when produced power is larger than the home-grown load demand). As a result, fewer traditional generation plants are needed during maximum solar hours (maximum solar irradiance). GCPVS also lowers the losses of the distribution network (T&D) losses. T&D losses were 5.7% on average in the United States in 2010, although they were greater at peak hours. T&D losses for Southern California Edison & Pacific Gas & Electric, for example, were expected to be greater than 10% in 2010. The placement of DG properties near loads will help to offset these losses to some extent.

As the total cost of implementing and maintaining GCPVS units decreases, acceptance of this technology at the residential, industrial, and utility scales increases. While GCPVS has many advantages against fossil fuel power plants, such as a long operating life (25–30 years), lower construction and care costs, and apparent environmental benefits, they still have several challenges. Several academic studies have shown that widespread adoption or proliferation of GCPVS may put tremendous strain on the electric grid.

11.7.2 Reliability Associated with Grid-Connected PV Unit

The increased rate of growth of these devices drew the interest of investors, operators, and stakeholders looking to make a financial commitment, who could be harmed by unintended disruptions caused by prolonged downtime times. As a result, further concentrated measures are expected to ensure that somehow a PV device produces the projected amount of energy. To ensure a reliable forecast of PV energy generation, reliability, affordability, and maintainability (RAM) evaluation are conducted for grid-connected solar PV device planning. The second stage of RAM analysis is called reliability modeling. In recent years, some reliability mechanisms for RMA tests have been addressed. RBD is one of the most effective approaches for modeling solar-power units that are linked to the grid (Sayed et al., 2019). The device components in RBD are interpreted by concurrent or parallel blocks, which are linked together based on their impact on the whole unit. The failure or repair rates of each component's block are defined by the component's failure and repair rates. In recent years, some reliability mechanisms for RMA tests have been addressed. RBD is

**FIGURE 11.24**

Reliability block diagram of a grid-connected PV unit.

one of the most effective approaches for modeling solar-power units that are linked to the grid. The machine components in RBD are interpreted by sequential and parallel blocks, which are linked together based on their impact on the whole (Figure 11.24).

11.8 Case Study

For calculation of reliability evaluation, authors are taking the microgrid at Sharda University which is located in Greater Noida, Uttar Pradesh, India. As shown in Figure 11.27, the main power is supplied from NPCL, which is divided into three electric subunits (ESS)—ESS-1, ESS-2, and ESS-3—and DG are supplied to all ESS. DG connecting in the unit helps when if any interruption is occurring in the supply of NPCL then the power does not supply by NPCL to ESS then the DG fulfills the power of the unit. DG is a collection of small power of conventional energy of local. DG maintains stability and reduces the reactive power in the microgrid and also improves voltage stability.

The main power of an ESS is divided into two portions, each with a distinct voltage level, and these two powers are coupled together via a circuit breaker. If any sections of a segment are disrupted, the switch isolates the faulty parts while allowing the majority of the section undisturbed. Bus bars are connected through interconnection. Because if a fault occurs in the main power of an ESS, the switch isolates that fault and power is transferred to the fault ESS feeders or customers by other ESSs. Micro PV solar power is installed on the roof top of the building. In the microgrid, 10 micro PV solar-power units are employed, and when employing PV electricity in a microgrid, extra components for switching and controlling the microgrid are necessary (Figure 11.25).

The reliability of the microgrid is also affected by the micro PV solar-power units. Figures 11.26, 11.27, and 11.28 are single line diagrams of the electrical main panel of block-1, block-2, and block-3, respectively. For these blocks, the power is coming from DG sets and ESS-1 and also from micro PV solar-power units. The power of blocks goes for the customer through the feeder. In the feeder, many of their customers are connected. The number of customers for block-1 is 35, block-2 has 61, and block-3 has 37.

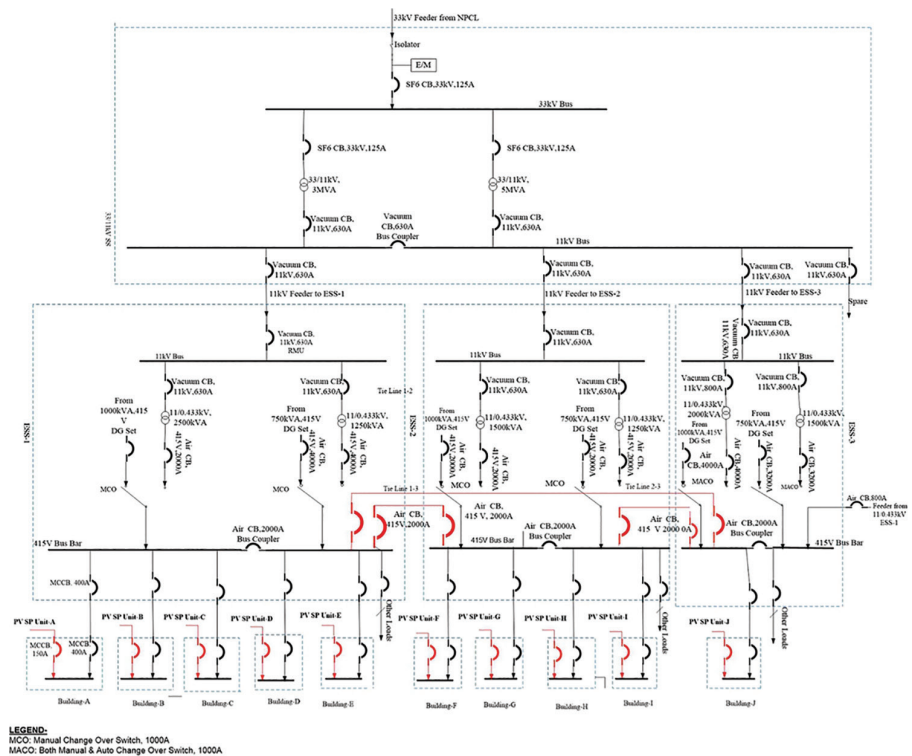


FIGURE 11.25
Single line diagram of the main power is a supply unit.

Single Line Diagram of Electrical Main Panel of Block-1, SET-1

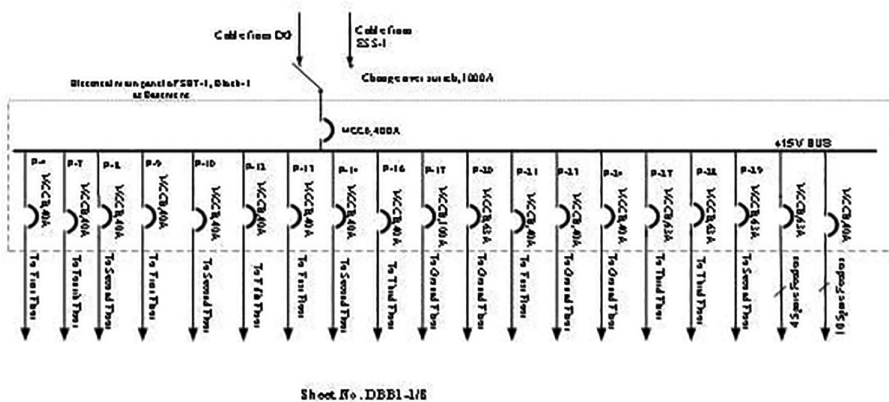


FIGURE 11.26
Single line diagram of the main panel of block-1.

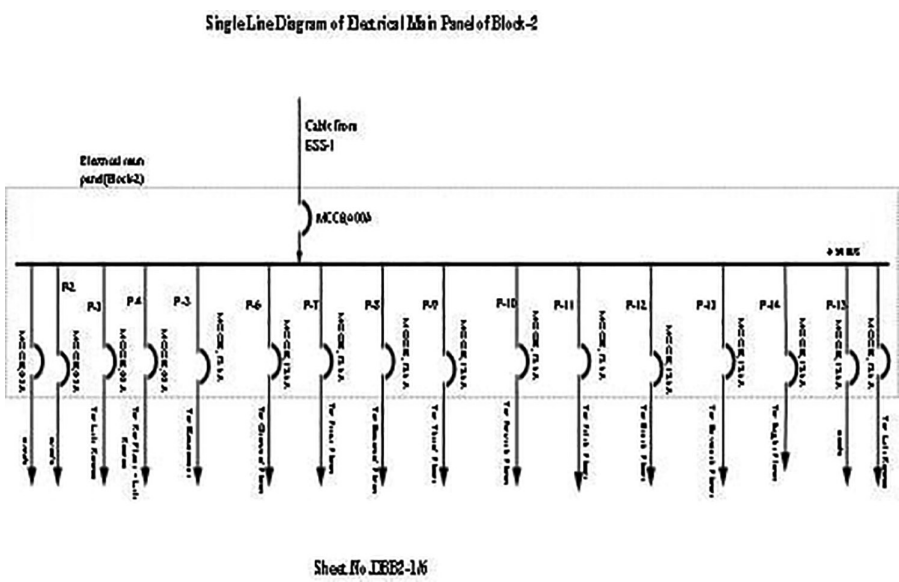


FIGURE 11.27
Single line diagram of the main panel of block-2.

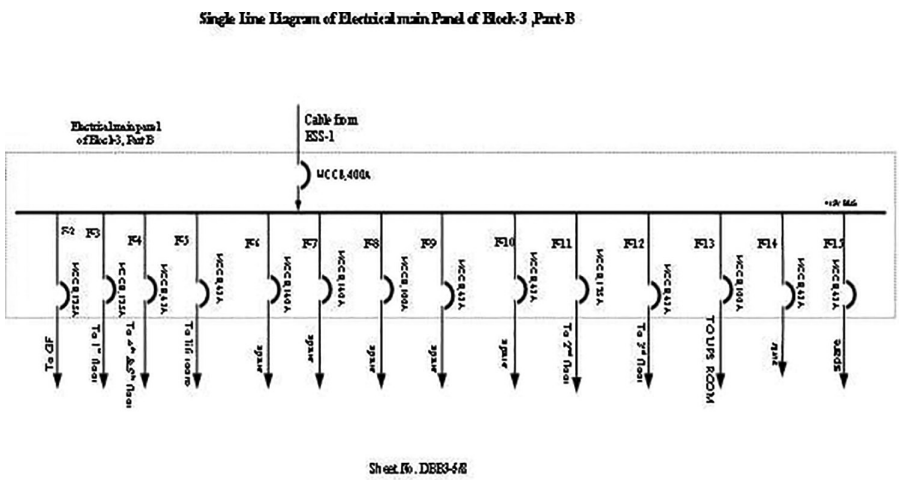


FIGURE 11.28
Single line diagram of the main panel of block-3.

To estimate the reliability of the units. It is compulsory to examine the interruption parts of the scheme. If we have to know the failure rate of the individual components and also know the repair time of the individual components, then the authors are finding the average outage time, average annual outage time, and average failure rate of the customers of the unit. For

fault isolation, an automatic switch and a manual switch are used. When a fault occurs in any part of the unit then an automatic or manual switch isolates those parts without any interruption of other part of the units, an automatic switch is controlled by the remote terminal units and a manual switch is controlled by remote terminal units otherwise human. The remote terminal units are controlled by the master terminal and the remote terminal unit activities status is monitored by using the SCADA.

For reliable evaluation of the microgrid, the following two cases are considered:

Case 1: Without PV solar power.

Case 2: With PV solar power.

First, the authors find the average failure rate, average annual outage, and average outage time up to the building unit.

Following that, the authors selected three building blocks to determine the unit's reliability: Block-1 has 35 customer numbers, Block-2 has 61 customer numbers, and Block-3 has 37 customer numbers.

Second, the authors find frequencies interruption, duration interruption, and customer's duration interruption in the customers or feeder side.

The interconnection in the microgrids improves the reliability and also supports the power when the main power supply cannot reach any of the ESSs due to fault. The customers or feeders are not interrupted by this because other ESSs are supplied to the customers or feeders.

11.8.1 Reliability Data

Before reliability analysis, we need to know the reliability characteristics of the individual components. The reliability data of the components are used in the analysis of the microgrids. The reliability data are taken from historical utility data of the unit and manufacturer, which are presented in Table 11.5. λ is component's failure rate and measured in failure per year. r is the component's mean-time-to-repair measured in an hour.

TABLE 11.5
Reliability Data of System Components

Components Type	λ (Failures/Year)	r (hours)
Transformer	0.015	15
Breaker	0.006	4
Bus bar	0.001	2
Photovoltaic	0.05	8
Automatic and manual switch	0.0001	2
Manual switch	0.0001	2

11.8.2 Sensitivity Analysis

The effective isolated action of the microgrid depends upon the effective action of the switches. The isolating action of the microgrid has a high possibility of achievement. The probability reserved to be an agreement, i.e., isolating action was always successful. Sensitivity analysis is achieved to the effect of reliability of micro PV solar-power units installed on microgrid indices. The reliability indices result of microgrids in four cases as shown in Table 11.6.

In reliability evaluation, three indices are calculated, such as Unit Average Interruption Frequency Index (SAIFI), Unit Average Interruption Duration Index (SAIDI), and Customer Average interruption Duration Index (CAIDI).

- **Unit average interruption frequency index (SAIFI):** The average number of outages that have been incurred, per year, over a given area per customer.

SAIFI=(Total numbers of customer disturbance)/(Total numbers of the customer)

$$= \left(\sum_i N_i * \lambda_i \right) / \sum_i N_i \quad (11.1)$$

- **Unit average interruption duration index (SAIDI):** The total duration of a client when equipment is closed down, i.e., prolonged experience by a customer.

SAIDI=(sum of customers duration)/(Total number of customers)

$$= \left(\sum_i U_i * N_i \right) / \sum_i N_i \quad (11.2)$$

TABLE 11.6

Reliability Indices of Customers

Block	Index	Case-1	Case-2
Block 1	λ (f/year)	0.019	0.0142
	r(hour)	3.8947	3.183
	U(hour/year)	0.074	0.0452
Block 2	λ (f/year)	0.019	0.0142
	r(hour)	3.8947	3.183
	U(hour/year)	0.074	0.0452
Block 3	λ (f/year)	0.019	0.0142
	r(hour)	3.8947	3.183
	U(hour/year)	0.074	0.0452

- **Customer average interruption duration index (CAIDI):** For all users who have faced prolonged the approximate duration of the outages.

CAIDI=(Sum of customer disturbance duration)/(Total number of customer disturbances)

$$= \frac{\sum_i U_i * N_i}{\sum_i N_i * \lambda_i} \quad (11.3)$$

λ_i =Frequency of disturbance for customer point i .

N_i =Number of customers in capacity point i .

U_i =Average annual when equipment is closed downtime at customers point i .

The result of the unit indicates an increase in reliability when micro PV solar-power units are installed in the microgrid. The values of failure rate, mean-time-to-repair, and unavailability of components are computed in Table 11.6. The failure rate of components in microgrid is reduced in both conditions with interconnection and without interconnection by installing micro PV solar-power units, and the frequency of components of fails will also reduce. Mean-time-to-repair of the components is reduced by installing micro PV solar-power units in both conditions with interconnection and without interconnection. The loss of power in the network for the customer's supply is reduced by reducing unavailability with the help of PV solar power in both conditions with and without the interconnection of the bus bar.

The SAIFI, SAIDI, and CAIDI values of customers are mentioned in Table 11.7. The values of all the indexes are reduced by the installation of micro PV solar-power units in a microgrid. The customer interruption per year is reduced so that the reliability of the microgrid is increased. By installing the micro PV units in the microgrid the reliability of the microgrid is improved. The results show that SAIFI is reduced by 30.36%, SAIDI is reduced by 44.66%, and CAIDI is reduced by 20.49%. The percentage reduction proves that by installing the micro PV units in the microgrid the reliability of the unit is more effective than without installing micro PV SP units. In the unit,

TABLE 11.7
Sensitivity Analysis

Case	SAIFI	SAIDI	CAIDI
Case-1	0.019	0.074	3.8947
Case-2	0.0142	0.0452	3.1831

TABLE 11.8

Expected Lifetime for Solar PV Panel

	BOS	Inverter	PV Module	Converter	Storage Unit	Overall Unit
MTTF (yr.)	19.22	8.2	42.72	30.72	10.9	3.09

TABLE 11.9

Case Descriptions for Simulation

Case	Statement	Temperature (C)	Irradiation (W/m ²)	Time (s)
1	MPPT control start	24	1,100	5
2	External condition change	21	850	7
3	External condition change	11	600	10

the outage duration per year is more improved than the frequency interruption per year and customer interruption per hour (Table 11.8).

The P&O and Inc-Con methods are superior to both the CVT approaches in terms of consistency and complex reaction times. Both techniques suffer from a lack of stable oscillation due to fluctuations. In comparison to the P&O and Inc-Con methods, the VSS approach has a faster dynamic reaction time and a higher overall power performance. Whenever the MPPT first begins at 5 seconds, it always takes a long time to reach a stable condition. In terms of reaction time and overall power output, the updated VSS approach, which employs the CVT method throughout the start-up phase, performs better (Table 11.9).

The simulation findings were also used to assess the benefits and disadvantages of current MPPT control methods. For engineers in the PV industry, an overview of MPPT strategies may be useful in interpreting the current MPPT control algorithms. The discussion and performance summary of various MPPT approaches may help determine which MPPT approach is best for complex PV structures in real-world applications.

11.9 Conclusion

In this chapter, dynamic modeling, design, and partial control strategy for a grid-connected PV are investigated. The power unit simulator comprises a PV unit connected to the grid through the main AC bus. An incremental conductance type of MPPT was used to extract the maximum power despite the changing solar radiations; this simulation validates the efficiency, the control strategy which maintained grid voltage constant even for the varying environmental condition, thereby maintaining the power factor unity. Thus, it can be suggested that in the future, if the energy demand increases, then more RE sources should be integrated to overcome the crisis and can generate more

clean energy with a more reliable and stable power unit. Various associated advancements and the impact of PV-connected grid on reliability and economy are also validated. Reliability is improved by installing micro PV units.

References

- Adefarati, T. and Bansal, R.C., 2019. Energizing renewable energy systems and distribution generation. In *Pathways to a Smarter Power System* (pp. 29–65). Academic Press. doi: 10.1016/B978-0-08-102592-5.00002-8.
- Al-Sabounchi, A.M., Yalyali, S.A. and Al-Thani, H.A., 2013. Design and performance evaluation of a photovoltaic grid-connected system in hot weather conditions. *Renewable Energy*, 53, pp. 71–78.
- Bai, J., Cao, Y., Hao, Y., Zhang, Z., Liu, S. and Cao, F., 2015. Characteristic output of PV systems under partial shading or mismatch conditions. *Solar Energy*, 112, pp. 41–54.
- Basit, M. A., Dilshad, S., Badar, R. and Sami urRehman, S.M., 2020. Limitations, challenges, and solution approaches in grid-connected renewable energy units. *International Journal of Energy Research*, 44(6), pp. 4132–4162. doi: 10.1002/er.5033.
- Bhadoria, V.S., Pachauri, R.K., Tiwari, S., Jaiswal, S.P. and Alhelou, H.H., 2020. Investigation of different BPD placement topologies for shaded modules in a series-parallel configured PV array. *IEEE Access*, 8, pp. 216911–216921.
- Diab, A.A.Z., Sultan, H.M., Mohamed, I.S., Kuznetsov, O.N. and Do, T.D., 2019. Application of different optimization algorithms for optimal sizing of PV/wind/diesel/battery storage stand-alone hybrid microgrid. *IEEE Access*, 7, pp. 119223–119245.
- Elizondo, M.A., Samaan, N., Makarov, Y.V., Holzer, J., Vallem, M., Huang, R., Vyakaranam, B., Ke, X. and Pan, F., 2017. Literature survey on operational voltage control and reactive power management on transmission and sub-transmission networks. In *2017 IEEE Power & Energy Society General Meeting* (pp. 1–5). IEEE.
- Fathy, A., Kaaniche, K. and Alanazi, T.M., 2020. Recent approach based social spider optimizer for optimal sizing of hybrid PV/wind/battery/diesel integrated microgrid in Aljouf region. *IEEE Access*, 8, pp. 57630–57645.
- Jenkins, N. and Thornycroft, J., 2018. Grid connection of photovoltaic systems: Technical and regulatory issues. In Kalogirou, S. (ed.) *McEvoy's Handbook of Photovoltaics* (pp. 847–876). Academic Press, Cambridge, MA.
- Jaiswal, S.P., Shrivastava, V. and Palwalia, D.K., 2019a. Impact of semiconductor devices on voltage stability of distribution system. *Materials Today: Proceedings*, 12, pp. 581–589.
- Jaiswal, S.P., Shrivastava, V. and Singh, S., 2019b, August. Economic viability solar PV power plant in distribution system. In *IOP Conference Series: Materials Science and Engineering* (Vol. 594, No. 1, p. 012010). IOP Publishing.
- Jaiswal, S.P., Shrivastava, V. and Palwalia, D.K., 2021. Opportunities and challenges of PV technology in power system. *Materials Today: Proceedings*, 34, pp. 593–597.
- Kouro, S., Leon, J.I., Vinnikov, D. and Franquelo, L.G., 2015. Grid-connected photovoltaic systems: An overview of recent research and emerging PV converter technology. *IEEE Industrial Electronics Magazine*, 9(1), pp. 47–61.

- Liu, H., Wang, S., Liu, G., Zhang, J. and Wen, S., 2020. SARAP algorithm of multi-objective optimal capacity configuration for WT-PV-DE-BES stand-alone microgrid. *IEEE Access*, 8, pp. 126825–126838.
- Marion, B., Adelstein, J., Boyle, K.E., Hayden, H., Hammond, B., Fletcher, T., Canada, B., Narang, D., Kimber, A., Mitchell, L. and Rich, G., 2005, January. Performance parameters for grid-connected PV systems. In *Conference Record of the Thirty-first IEEE Photovoltaic Specialists Conference*, 2005 (p. 1601).
- Noureldeen, O. and Ibrahim, A.M., 2018a, February. Modeling, implementation and performance analysis of a grid-connected photovoltaic/wind hybrid power system. In *2018 International Conference on Innovative Trends in Computer Engineering (ITCE)* (pp. 296–304). IEEE.
- Noureldeen, O. and Ibrahim, A.M., 2018b. Performance analysis of grid connected PV/Wind Hybrid power system during variations of environmental conditions and load. *International Journal of Renewable Energy Research*, 8(1), pp. 208–220.
- Nwaigwe, K.N., Mutabilwa, P. and Dintwa, E., 2019. An overview of solar power (PV systems) integration into electricity grids. *Materials Science for Energy Technologies*, 2(3), pp. 629–633.
- Rodriguez, C. and Amaratunga, G.A., 2008. Long-lifetime power inverter for photovoltaic AC modules. *IEEE Transactions on Industrial Electronics*, 55(7), pp. 2593–2601.
- Roman, E., Alonso, R., Ibañez, P., Elorduizapatrietxe, S. and Goitia, D., 2006. Intelligent PV module for grid-connected PV systems. *IEEE Transactions on Industrial Electronics*, 53(4), pp. 1066–1073.
- Sahan, B., Vergara, A.N., Henze, N., Engler, A. and Zacharias, P., 2008. A single-stage PV module integrated converter based on a low-power current-source inverter. *IEEE Transactions on Industrial Electronics*, 55(7), pp. 2602–2609.
- Sánchez, A.G., Pérez-Pinal, F.J., Rodríguez-Licea, M.A. and Posadas-Castillo, C., 2021. Non-integer order approximation of a PID-type controller for boost converters. *Energies*, 14(11), p. 3153.
- Sayed, A., El-Shimy, M., El-Metwally, M. and Elshahed, M., 2019. Reliability, availability and maintainability analysis for grid-connected solar photovoltaic systems. *Energies*, 12(7), p. 1213.
- Singh, S. and Jaiswal, S.P., 2020, December. Adaptive demand-side management in smart grid with plug-in electric vehicle. In *AIP Conference Proceedings* (Vol. 2294, No. 1, p. 040003). AIP Publishing LLC.
- Sood, V.K. and Abdelgawad, H., 2019. Power converter solutions and controls for green energy. In *Distributed Energy Resources in Microgrids*, pp. 357–387. doi: 10.1016/B978-0-12-817774-7.00014-4.
- Uzum, B., Onen, A., Hasanien, H.M. and Muyeen, S.M., 2020. Rooftop solar pv penetration impacts on distribution network and further growth factors—a comprehensive review. *Electronics*, 10(1), p. 55.
- Velasco-Quesada, G., Guinjoan-Gispert, F., Piqué-López, R., Román-Lumbreras, M. and Conesa-Roca, A., 2009. Electrical PV array reconfiguration strategy for energy extraction improvement in grid-connected PV systems. *IEEE transactions on industrial electronics*, 56(11), pp. 4319–4331.
- Xu, B., Chen, D., Venkateshkumar, M., Xiao, Y., Yue, Y., Xing, Y. and Li, P., 2019. Modeling a pumped storage hydropower integrated to a hybrid power system with solar-wind power and its stability analysis. *Applied Energy*, 248, pp. 446–462.

Index

Note: *Italic* page numbers refer to figures.

- activation function 110
- adaptive fuzzy logic controller
 - 107, 109, 112
- alternative energy 2, 258
- ANFIS 124, 214
- appliances 214
- applications 11
- artificial bee colony 107, 114, 120
- artificial intelligence 24, 215
- artificial neural network 33, 34, 131,
 - 164, 223

- bat algorithm 117, 121
- bio-inspired optimization 107, 111
- bridge link honey comb 162
- bridge link total cross tied 160, 169

- cat swarm optimization (CSO) 118
- charge controller 84
- cognitive constant 171
- contributing factors 39
- correlation matrix 35
- crossover 114

- datasheet for power foil 70
- degree of upgradation 55
- differential evolution 163
- diode current 166
- distribution system 216
- dragonfly-based optimization (DBO) 118, 121

- enhanced grey wolf optimizer (EGWO) 116, 121
- environmental conditions 5
- experimental validation 47

- firefly based MPPT algorithm (FB) 117
- fitness function 53
- fossil fuels 3

- GCC 214
- genetic algorithm 114–115, 120, 160, 176
- global best 112, 113, 117
- global maximum power point 106, 116,
 - 118, 163

- hill climbing/P&O algorithm 162
- hybrid-based MPPT 122–124

- ideality constant 49
- identity factor 166
- industrial application 11
- insolation level 167
- integral absolute error 196
- integral square error 196
- irradiance or insolation 26

- jelly fish optimization 119
- levy flight 116

- long-short term memory 33, 36

- mathematical modeling 47
- maximum power point 160
- maximum power point tracking 5
- mean absolute error 36
- mean absolute error 36
- metaheuristic approach 115, 122
- metaheuristic techniques 160
- monocrystalline 48
- multi-crystalline 3
- multijunction solar cell 9

- national solar mission 10
- neuro-fuzzy 123

- optimal solution 112, 113, 115, 140

- partial shading 113, 115, 119, 122, 123, 160
- particle swarm optimization 112, 120,
 - 160, 171

- Pearson correlation coefficient 34
- photovoltaic system 23, 39
- polycrystalline 3
- predicted solar power generation with LSTM 38
- predicted solar power generation with neural network 38
- predicted solar power generation with neural network without air temperature 40
- predicted solar power generation with neural network without zenith angle 40
- predicted solar power generation with random forest 37
- predicted solar power generation with SVR 37
- predicted solar power generation with XGBoost 38
- PV cell development 6
- PV panel capacity 223
- PV voltage 165
- random forest 32–33, 36
- ray tracing techniques 162
- renewable energy 2, 105
- residential application 11
- Roulette wheel method 176
- salp swarm optimization 114, 120
- semiconductor material 3
- shading 5
- social constant 171
- solar cooking 13
- solar desalination 12
- solar energy 3
- solar inverter 17
- solar irradiation level 5
- solar power prediction 30
- solar pumps 14
- solar PV system 3
- solar thermal 3
- solar water heating 12
- standard test condition
- Su-do-Ku 162
- support vector regression (SVR) 30–31, 36
- thin film/amorphous 3
- time control 120
- total cross tied 160, 169
- transportation 11
- two-diode model 47
- variable step size radial basis functional algorithm 107, 111–112
- whale optimization algorithm 119, 122
- wind energy 3
- XGBoost 31, 36